Metallic Nanoparticles Effects on Physical Properties of CuTl-1223 Superconductor

by

LIAQAT ALI

(37-FBAS/PhDPHY/F14)

DEPARTMENT OF PHYSICS,

FACULTY OF BASIC AND APPLIED SCIENCES,

INTERNATIONAL ISLAMIC UNIVERSITY ISLAMABAD,

PAKISTAN

(2019)

Superconductivity

Superconductors

Electronics--Materials

Metallic Nanoparticles Effects on Physical Properties of CuTl-1223 Superconductor

by

LIAQAT ALI

(37-FBAS/PhDPHY/F14)

Supervisor

Dr. Muhammad Mumtaz

(Associate Professor)

Co-Supervisor

Dr. Kashif Nadeem

(Associate Professor)

DEPARTMENT OF PHYSICS,

FACULTY OF BASIC AND APPLIED SCIENCES,

INTERNATIONAL ISLAMIC UNIVERSITY ISLAMABAD,

PAKISTAN

(2019)

Metallic Nanoparticles Effects on Physical Properties of CuTl-1223 Superconductor

by

LIAQAT ALI

(37-FBAS/PhDPHY/F14)

A thesis is submitted to

Department of Physics

For the award of the degree of

Doctor of Philosophy in Physics

Signature.....

(Chairman, Department of Physics)

Signature.....

(Dean FBAS, IIU Islamabad)

DEPARTMENT OF PHYSICS,

FACULTY OF BASIC AND APPLIED SCIENCES,

INTERNATIONAL ISLAMIC UNIVERSITY ISLAMABAD,

PAKISTAN

(2019)

Final Approval

It is certified that the work presented in this thesis having title "**Metallic Nanoparticles Effects on Physical Properties of CuTl-1223 Superconductor**" submitted by **Liaqat Ali**, Registration No. **37-FBAS/PhDDPHY/F14** is of sufficient standard in scope and quality for the award of degree of PhD Physics from International Islamic University, Islamabad, Pakistan.

COMMITTEE

Chairman

Dr. Wiqar Hussain Shah

Department of Physics,
FBAS, IIU, Islamabad, Pakistan .

External Examiner 1
Prof. Dr. Zakir Hussain
School of Chemical and Material Engineering
(SCME), NUST, H-12, Islamabad, Pakistan.

External Examiner 2
Prof. Dr. Sajid Qamar
Chairman, Department of Physics,
COMSATS, Islamabad, Pakistan.

Internal Examiner
Dr. Manzoor Ahmad
Assistant Professor, Department of Physics,
FBAS, IIU, Islamabad, Pakistan .

Supervisor
Dr. Muhammad Mumtaz
Assosciate Professor, Department of Physics,
FBAS, IIU, Islamabad, Pakistan .

Co-Supervisor
Dr. Kashif Nadeem
Assosciate Professor, Department of Physics,
FBAS, IIU, Islamabad, Pakistan .

A thesis submitted to

Department of Physics

International Islamic University Islamabad

As a partial fulfillment for the award of the degree of

Doctor of Philosophy

IN THE NAME OF ALLAH THE BENEFICENT THE MERCIFUL

DEDICATED

to

A great sacrifice in the history of humanity by Hazrat Syedna Imam Hussain (R.A), His beloved family and companions

DECLERATION

It is hereby declare that the work presented in this thesis has not been copied out from any source, neither as a whole nor a part. Furthermore, work presented in this dissertation has not been submitted in support of any publication other than those included in this thesis, any other degree or qualification to any other university or institute and is considerable under the plagiarism rules of Higher Education Commission (HEC) Pakistan.

Liaqat Ali

(37-FBAS/PhDPHY/F14)

CERTIFICATE

It is certified that **Liaqat Ali** Registration No. **37-FBAS/PhDPHY/F14** has carried out the research work related to this thesis having title, "**Metallic Nanoparticles Effects on Physical Properties of CuTl-1223 Superconductor**" under my supervision. This work fulfills all the requirements for the award of the degree of doctor of philosophy.

Dr. Muhammad Mumtaz

Associate Professor (TTS)
Department of Physics, (FBAS)
International Islamic University,
Islamabad, Pakistan.

ACKNOWLEDGEMENTS

I am very much thankful to **Almighty ALLAH**, who is the creator of the world and source of wisdom and knowledge. **ALLAH** has enabled me to complete my PhD thesis. I offer my humblest and sincere words of thanks to beloved **Holy Prophet Syedna Hazrat Muhammad (PBUH)** who is forever a source of guidance and knowledge for humanity. I am also satisfied that I have tried to obey the saying of our beloved **Holy Prophet Syedna Hazrat Muhammad (PBUH)** regarding the quest of knowledge.

Whole of my efforts would be a pack of garbage if I don't mention the name of my worthy supervisor **Dr. Muhammad Mumtaz** in this manuscript. It goes without saying that it was the undaunted and continuous struggle of my learned supervisor, which enabled me to understand the field of superconductivity. It is also pertinent to mention here that the instant thesis is also a reflection of efforts, hard work and affection of my respectable supervisor. I also feel myself a lucky student, who had the privilege to work with such a skilled and seasoned supervisor, who has got no parallel in his field. It would be a dishonest concealment if I do not jot down the extra ordinary help and guidance provided to me by my co-supervisor **Dr. Kashif Nadeem** in every project. He is an icon in his field and he left no stone unturned in the completion of my work. Definitely the persons mentioned above are the source of inspiration for me always. It will be un-just to mention the guidance provided by Dr. Muhammad Rahim in this difficult and crucial task. I am thankful to Chairman, Department of physics, to provide all possible facilities and full cooperation.

I want to thank **Dr. Nawazish Ali Khan** at Quaid-i-Azam University Islamabad, for providing me the chance to work under the congenial environment of his Materials Science Laboratory. I also say thank to **Prof. Qiu Xiang-Gang**, Beijing National Laboratory of Condensed Matter Physics, Institute of Physics (IOP), Chinese Academy of Sciences (CAS), Beijing, China, and **Dr. Nasir Khan** at PINSTECH for providing the characterization facilities.

Moreover, I would like to express my sincere thanks to all the devoted and respected faculty members of Department of Physics IIU Islamabad who blessed me with knowledge and guidance. I express my thanks to all staff in Department of Physics, IIUI, for their various services. I shall express my heartiest thanks to all of my research colleagues Abrar Ahmed Khan,

Waqas Rabbani, Dr. Faisal Zeb, Dr. Muhammad Kamran, Muhammad Imran, Muhammad Sohail, M. Amir Durani, Hur Abbas, Adnan Qurashi, Zareef Ahmed, Ghazanfar Ghaffar, Haris Abbasi, Mirza Hassan Baig, Hassan Shabbir, Tanzeel-ur-Rehman, M. Qasim and BS, MSc research fellows for being very supportive and co-operative throughout my research work. How can I forget to mention **Dr. Abdul Jabbar, Dr. M. Waqee-Ur-Rehman and Dr. Irfan Qasim** who have guided me always like my elder brother and helped me during my research. I acknowledge the efforts of my dearest research colleague **Mubasher Rajpoot**, whose friendship made me able to complete my thesis, who has facilitated me in various ways. Moreover, I would like to express my sincere thanks to Principal Sahib Raza Husnian Kharal, Dr. Tariq Masood Dr. Javeed Kasuar, as well as all the devoted and respected colleagues Prof. Zafar Hussain, Prof. Dr. Waqar Shah, Dr. Zakrya Khan Dr. Ejaz Abbasi, Prof Zafar Imran, Prof Zia Dogar, Prof. Azam, prof saqib, Prof. Aashiq Nawaz, Prof. Toqueer, Prof. Dr. Jamil, Dr. Haider Ali Bukahri, Prof. Malik Abdul Sattar and Qazi Tajdar Ahmed who blessed me with encouragement and guidance.

Finally, it will be an ornament in my thesis if I pen down the co-operation of my family in whole of this process. My loving and caring mother and respected father who are always praying for me, my elder brothers Mian Muhammad Waseem, Dr. M. Irshad Ali Chadhury, Bashrat Ali Chadhury, my beloved sister and their families who always helped me in any problem and guided me in a nutshell; all members of my family (especially Dr. waseeha, Maqdas, Sira, Dashab and all children of brothers and sister families) have contributed a lot in this achievement. It will be un-just if I do not mention the role of my beloved and caring wife Fozia Khalid and my beloved children Dua Fatima, Muhammad Ahmed and M. Hassan Ashraf who always wish, support, encourage, sacrifice time and pray for me and strengthened me during this difficult task. I could not wish for a more supportive, loving family, and for them I am deeply thankful and blessed. **ALLAH Kareem blessed them all.**

Liaqat Ali

Table of Contents

List of Figures

List of Tables

List of Publications

1. M. Mumtaz, **Liaqat Ali**, Mubasher, Ahmed Saleh, Y. Slimani, Irfan Qasim, Mehwish Hassan, Zubair Ahmad "AC-conduction mechanism via dielectric measurements of (Cr)x/(CuTl)-1223 nanoparticles-superconductor composites", Cryogenics **105** (2020) 103021.
2. M. Mumtaz, M. WaqeeUr-Rehman, **Liaqat Ali**, Waqas Ahmed Khan and K. Nadeem, "Infield Superconductivity in Au Nanoparticles Added $Cu_{0.5}Tl_{0.5}Ba_2Ca_2Cu_3O_{10-\delta}$ Phase" Physica C **559** (2019) 21-24.
3. **Liaqat Ali**, M. Mumtaz, Irfan Ali, M. Waqee-ur-Rehman, Abdul Jabbar,"Metallic Cu Nanoparticles Added $Cu_{0.5}Tl_{0.5}Ba_2Ca_2Cu_3O_{10-\delta}$ Superconductor", Journal of Superconductivity and Novel Magnetism **31** (2018) 561-567.
4. M. Mumtaz, M. Naveed, **Liaqat Ali**, Abrar A. Khan, M. Imran, M. Nasir Khan "Magneto-Transport Properties of $(Cu)_x$/CuTl-1223 Nanoparticles-Superconductor Composites", Cryogenics **95** (2018) 5-10.
5. M. Mumtaz, **Liaqat Ali**, Iftikhar Ahmad "Phase Formation, Activation Energy and Superconductivity of MgO Nanoparticles Added $(Cu_{0.5}Tl_{0.5})Ba_2Ca_2Cu_3O_{10-\delta}$ Phase", Physica C **551** (2018) 19-24.
6. M. Mumtaz, Zafar Iqbal, M. Raza Hussain, **Liaqat Ali**, M. Waqee-ur-Rehman, and M. Saqib "Study of $(DNPs)_x$/CuTl-1223 Nanoparticles-Superconductor Composites", Journal of Superconductivity and Novel Magnetism **31** (2018) 1315-1321.
7. Mustehsin Ali, Usama Tehseen, M. Ali , **Liaqat Ali** M. Mumtaz "Study of Un-coated and Silica-coated Hematite (α-Fe_2O_3) Nanoparticles", Journal of surfaces and Interface **13** (2018) 196-204.
8. M. W. Rabbani, **Liaqat Ali**, M. Mumtaz, and I. H. Gul "Infield superconducting properties of nano-sized Ag added $Cu_{0.5}Tl_{0.5}Ba_2Ca_2Cu_3O_{10-\delta}$", Progress in Natural Science: Materials International **27** (2017) 487-490.
9. F. Zeb, K. Nadeem, S. K. A. Shah, M. Kamran, I. H. Gul, **Liaqat Ali** "Surface spins disorder in uncoated and SiO_2 coated maghemite nanoparticles", Journal of Magnetism and Magnetic Material **429** (2017) 270–275.
10. M. Mumtaz, **Liaqat Ali**, M. Waqee-ur-Rehman, K. Nadeem, G. Hussain, G. Abbas, and Bilal

Majeed "Improvement in superconducting properties of $Cu_{0.5}Tl_{0.5}Ba_2Ca_2Cu_3O_{10-\delta}$ phase by addition of γ-Fe_2O_3 nanoparticles", Journal of Superconductivity and Novel Magnetism **30** (2017) 2741-2749.

11. **Liaqat Ali**, M. Mumtaz, M. W. Rabbani, "Flux pinning with addition of gold nanoparticles in CuTl-1223 superconductor", Journal of Superconductivity and Novel Magnetism **30** (2016) 325-329.
12. M. Mumtaz, **Liaqat Ali**, M. Nasir Khan, and M. Usman Sajid "Tuning of dielectric parameters of $(NiFe_2O_4)_x$/CuTl-1223 Nano-superconductor Composites by Temperature and frequency", Journal of Superconductivity and Novel Magnetism **404** (2016) 72-77.
13. M. Mumtaz, **Liaqat Ali**, A. Jabbar, M.W.Rabbani, M. Naveed, M. Imran, Badshah Amin, M. Nasir Khan, and M. Usman Sajid "Tuning of dielectric properties of $(ZnO)_x$-(CuTl-1223) nanoparticles-superconductor composites", Ceramics International **42** (2016) 11193-11200.
14. M. Mumtaz, **Liaqat Ali**, Shoaib Azeem, Saad Ullah, G.Hussain, M.W. Rabbani, A. Jabbar and K. Nadeem "Dielectric properties of $(Zn)_x$/CuTl-1223 nanoparticles-superconductor composites", Journal of Advanced Ceramics **5** (2016) 159-166.
15. K. Nadeem, **Liaqat Ali**, I. H. Gul, S. Rizwan, and M. Mumtaz "Effect of silica coating on the structural, dielectric, and magnetic properties of maghemite nanoparticles", Journal of Non-Crystalline solids **404** (2014) 72-77.

List of symbols and abbreviations

HTSCs	High-temperature superconductors
LTSCs	Low-temperature superconductors
LSCO	Lanthanum-based superconductor
YBCO	Yttrium-based
BSCCO	Bismuth-based
TBCCO	Thallium-based
CRL	Charge reservoir layer
BCS	Bardeen Cooper Schrieffer theory
SC	Superconductor
J_c	Critical current density
T_c	Critical temperature
H_c	Critical magnetic field
H_{irr}	Irreversibility field
SQUID	Superconducting quantum interference device
SEM	Scanning electron microscopy
XRD	X-ray diffraction
EDX	Energy dispersive X-ray spectroscopy
FTIR	Fourier transforms infrared spectroscopy
FWHM	Full width at half maximum
GB	Grain-boundaries

PPMS	Physical properties measuring system
APSs	Artificial pinning centers
FL	Lorentz force
FC	Flux creeps
FP	Pinning force
SNS	Superconductor normal metal superconductor junction
SMI	Semiconductor metal interface
MNPs	Metallic nanoparticles
GL	Ginzburg Landau
GO	Graphene oxide
FC	Flux creeps
FF	Flux flow
TAFF	Thermally activated flux flow
CENB	Carbon encapsulated nano-boron
GnPs	Graphene nano-platelets

ABSTRACT

Metallic (i.e. Cu, Ag and Au) nanoparticles (MNPs) were synthesized by sol-gel method and $(CuTl)_{0.5}Ca_2Ba_2Cu_3O_{10-\delta}$ (CuTl-1223) superconducting phase was synthesized by solid-sate reaction method. Different wt. % of these MNPs were added in CuTl-1223 superconducting phase to obtain $(D)_x$/(CuTl)-1223; (x = 0 ~ 4 wt.% and D = Cu, Ag and Au) nanoparticles-superconducting composites and their physical properties were investigated. X-rays diffraction (XRD), scanning electron microscopy (SEM) and X-rays dispersive spectroscopy (EDX) were utilized for structural, morphological and compositional analysis of these composites. Superconducting transport properties were investigated by resistivity versus temperature (R-T) measurements with the help of Physical Property Measurement System (PPMS). The role of these MNPs on flux pinning strength in (CuTl)-1223 superconducting phase was investigated by thermally activated flux flow (TAFF) model. The broadening of superconducting transition regions in R-T curves was decreased with the inclusion of these MNPs in (CuTl)-1223 superconducting matrix, which was increased with the increase of applied magnetic field due to TAFF. Activation energy (U_o) was increased with the inclusion of these MNPs up to certain optimum level in (CuTl)-1223 superconductor, indicating strong flux pinning abilities of these MNPs. Transition widths (ΔT) were suppressed by inclusion of these MNPs in (CuTl)-1223 superconducting matrix, while it was increased with the increase of external applied magnetic field. The reduction in ΔT and enhancement in U_o demonstrated the enhancement in flux pinning ability of CuTl-1223 superconducting phase with the inclusion of MNPs. The broadening in ΔT with external applied magnetic field obeyed the power law ($\Delta T = \Delta T_o + CH^n$). The value of upper critical magnetic field (H_{c2}) of (CuTl)-1223 superconductor was enhanced with the inclusion of MNPs up to some optimum level, which was suppressed with external applied magnetic field. The zero resistivity critical temperature (T_c), infield critical current density (J_c) were increased and normal state resistivity ρ (Ω-cm) was decreased with the inclusion of MNPs in (CuTl)-1223 superconducting phase. Over all superconducting properties of (CuTl)-1223 superconducting phase were improved due to enhanced inter-grain connectivity by filling up the pores and voids with the inclusion of these MNPs. The superconducting transport properties were enhanced due to enhanced mobility of carriers with improved inter-grain connections. These superconducting

properties were suppressed after certain optimum level of these MNPs inclusion as result of suppression of superconducting volume fraction.

Chapter No. 1

Basics of superconductivity and literature review

1.1 Superconductivity; Historical background

Class of materials characterized by zero electrical resistance is known as superconductors and mechanism is called superconductivity. In 1911, H. K. Onnes along with his co-workers discovered superconductivity while studying resistivity of mercury on temperature dependence just three years later after liquefaction of Helium [1]. They found that at specific temperature of 4.2 K, resistivity disappeared in mercury. This temperature is known as critical temperature T_c, which is the characteristic of any material. H. K. Onnes was bestowed Noble prize for liquefaction and breakthrough in superconductivity in 1913 [2]. Several metals like aluminum, tin, lead, niobium, some alloys and inter-metallic compounds have shown superconductivity phenomena, soon after breakthrough in superconductivity of mercury. Fig. 1.1 represents the graphical sketch of resistance (R) against temperature (T) for mercury (Hg) and platinum (Pt).

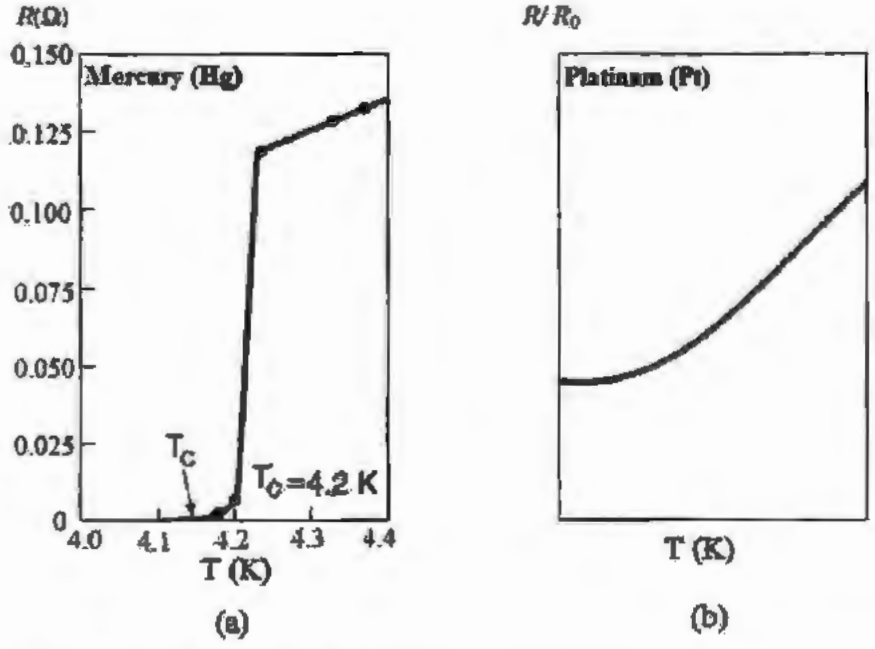

Fig.1.1: Graphical sketch of variation in resistance against temperature of (a) Mercury (Hg) and (b) Platinum (Pt).

Materials with critical temperatures ($T_c \leq 30K$) are called low temperature superconducting materials (LTSCs). Some low temperature superconducting materials with their critical temperatures are shown in Table 1.1. The highest value with $T_c \geq 23K$ for conventional LTS is observed in Nb_2Ge compound [3].

Table 1.1: Some low superconducting materials with their critical temperatures [4]

Elements	T_c (K)	Elements	T_c (K)
Hf	0.128	Al	1.175
Be	0.026	Hg	4.2
La	4.88	Ir	0.113
Cd	0.517	Ti	0.40
Ga	1.083	Pb	7.196
In	3.408	Zn	0.850
Mo	0.915	Nb	9.25
Os	0.66	Th	1.38
Pa	1.4	V_3Si	17.10
W	0.0154	Nb_3S_4	18.05
Zr	0.61	Nb_3Ge	23.30

It is observed that superconductivity is destroyed not only by application of heat as well as applied magnetic fields. Superconductors oppose the flux lines from their interior surfaces with application of applied external field, which was detected by R. Ochsenfeld and W. H. Meissner in year 1933 [5]. Meissner effect opened new era in the field of superconductivity. In 1935 ontological theory was developed by two London brothers Fritz and Heinz [6]. The microscopic theory of superconductivity was developed by J. Bardeen, L. Cooper and R. Schrieffer in 1957 [7]. New types of oxides superconductors with T_c around 35 K was invented in year 1986 by J. G. Bednorz and K. A. Muller which renewed the research of superconductivity [8]. M. K. Wu in

1987 discovered $YBa_2Cu_3O_{7-\delta}$ superconductors with critical temperature (T_c =93K) above liquid nitrogen temperature [9]. $Tl_2Ca_2Ba_2Cu_3O_y$ (Tl-based superconductors) was reported with higher T_c 125 K in 1988 [10]. HgBaCaCuO (mercury based cuprates superconductors) was reported with T_c 133 K [11] and T_c 138 K [12] in 1993 and 2000, respectively, and observed to enhance critical temperature 164 K by using 30 GPa high pressures [13]. Fig. 1.2 represents superconducting materials history with critical temperature and years.

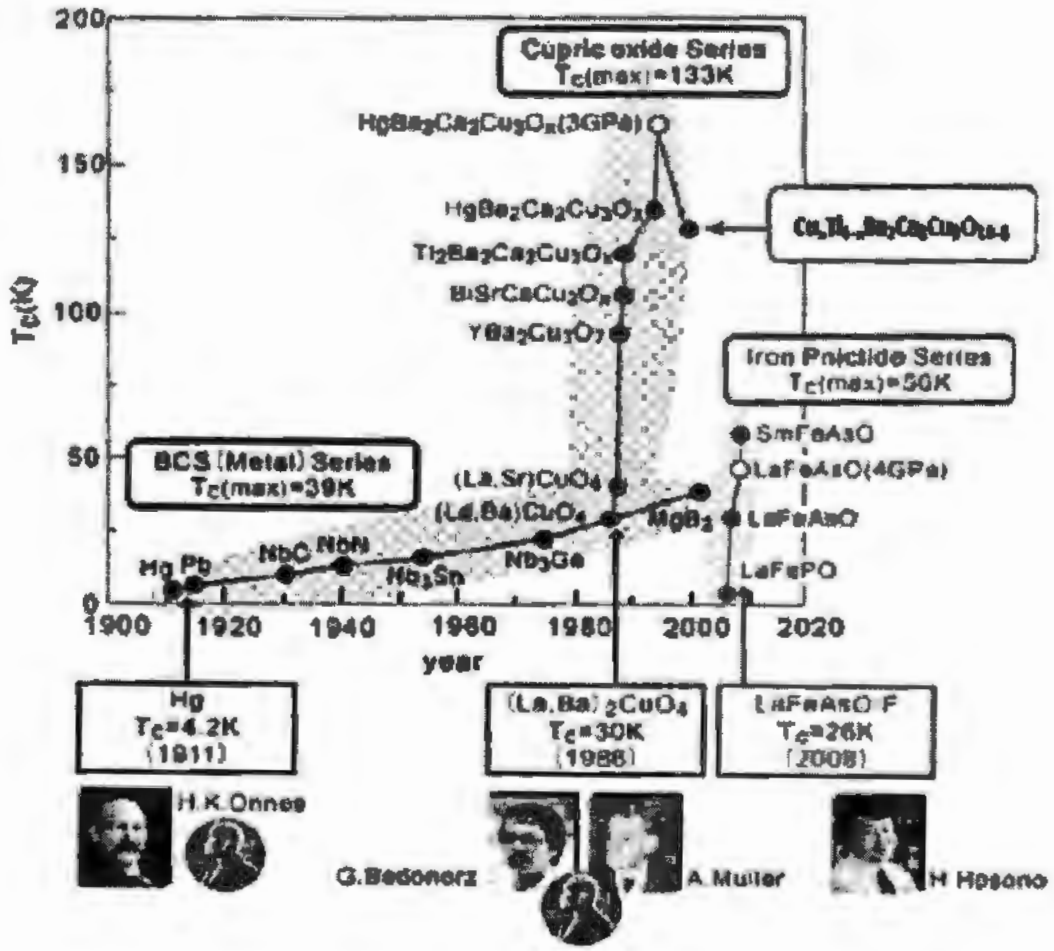

Fig.1.2: Critical temperature versus years of discovery for superconducting materials [14]

1.2 Characteristics and critical parameters of superconductors

Superconductivity depends upon some critical parameters and these parameters are basically characteristics of any materials.

1.2.1 Zero electrical resistance

Resistance is opposition to flow of charge carriers, which depends upon the size and nature of the materials and resistivity of material is given by the formula;

$$\rho = \frac{RA}{L} \text{----------} (1.1)$$

where L is length, A is area and R is Resistance of the material. Resistance and resistivity in different materials such as conductors, semiconductors and superconductors depend upon the behavior of charge carriers flowing through them. Resistance and flow of charge carriers according to Ohm Law ($R=\frac{V}{I}$) are inversely proportional to each other, so current approaches to infinity, when resistance falls to zero or close to zero in superconducting materials. Latest data indicated that resistivity below 10^{-27} Ω cm has been observed in superconductors [15]. Resistivity in some materials decreases by lowering of temperature due to slow down of charge carriers flow. Table 1.2 represents resistivity of some materials at room temperature.

Table 1.2: Room temperature resistivity (Ω. cm) of some common substances [16, 17]

Substance	Resistivity ρ (Ω. cm) at room temperature
Pure Copper	1.75×10^{-6}
Lead	21.1×10^{-6}
Silver	1.59×10^{-6}
Mercury	95.8×10^{-6}
Manganin	48.2×10^{-6}
Aluminum	2.8×10^{-6}
Amber	1.0×10^{18}
Tungsten	5.6×10^{-6}
Rubber	4.0×10^{23}

1.2.2 Perfect diamagnetism

Another important property of every superconducting materials is perfect diamagnetism i.e., B=0 and magnetic flux are expelled from inside the materials surface. When superconductor material are cooled down to transition temperature in applied magnetic field then relation is given by

$$B = \mu_o H \text{----------(1.2)}$$

where μ_0 is free space permeability and H is strength of magnetic fields. Susceptibility of material is given by

$$\chi = \frac{M}{H} \text{----------(1.3)}$$

also

$$B = \mu_o (H+M) \text{----------(1.4)}$$

and

$$B = \mu_o H(1+\chi) \text{----------(1.5)}$$

For perfect superconductors, B= 0, χ= -1 and M= -H [18], which shows perfect diamagnetism in superconducting materials.

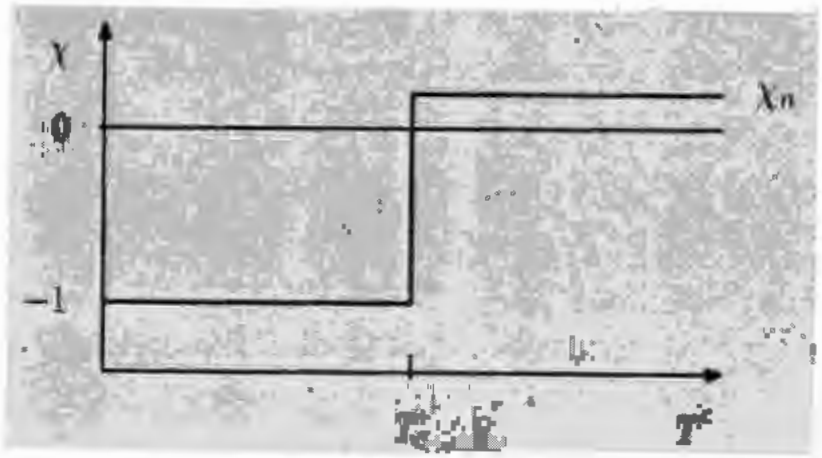

Fig.1.3: Graphical representations of perfect diamagnetism in superconducting materials.

1.2.3 Coherence length and penetration depth

Maximum distance associated with electrons of cooper pair from state of superconductivity to normal conductor state is called coherence length (ξ). The coherence length depends upon temperature as well as nature of material [19] and is given by the equation;

$$\xi = \left(\frac{\hbar^2}{2m\alpha T}\right)^{\frac{1}{2}} \text{----------(1.6)}$$

Also

$$\xi(T) = \begin{cases} \xi_o\left(\frac{T}{Tc} - 1\right)^{-\frac{1}{2}} & when\ T > T_c \\ \xi_o\left(1 - \frac{T}{Tc}\right)^{-\frac{1}{2}} & when\ T < T_c \end{cases} \text{---(1.7)}$$

where ξ_o is the coherence length at temperature T= 0 and also known as Pippard coherence length. For purest form and defect free system of superconductor, it depends upon Fermi velocity (V_F) and critical temperature (T_c) [20- 22] and is given by an equation;

$$\xi_o = \frac{0.18\hbar V_F}{K_B T_c} \text{----------(1.8)}$$

Pippard empirical relation between Pippard coherence length or intrinsic coherence length (ξ_o) is given by;

$$\frac{1}{\xi} = \frac{1}{\xi_o} + \frac{1}{\alpha l} \text{----------(1.9)}$$

where ℓ is mean free path between Cooper pair and α is empirical constant, having unity value.

Metal superconductors have large values whereas un-conventional superconductors have very small size of coherence length. The characteristic length by which magnetic flux lines penetrates from normal region to superconducting region of material is called as penetration depth (λ). Magnitude of penetration depth is also material as well as temperature dependent and towards core of superconductors; it decreases exponentially as indicated in Fig. 1.4. It indicates that

outside superconductor (Normal conductor) penetration depth shows a constant value whereas inside it decreases exponentially with applied magnetic field and approaches to zero. Magnitude of penetration depth for pure metal is found from 10 nm to 100 nm [23].

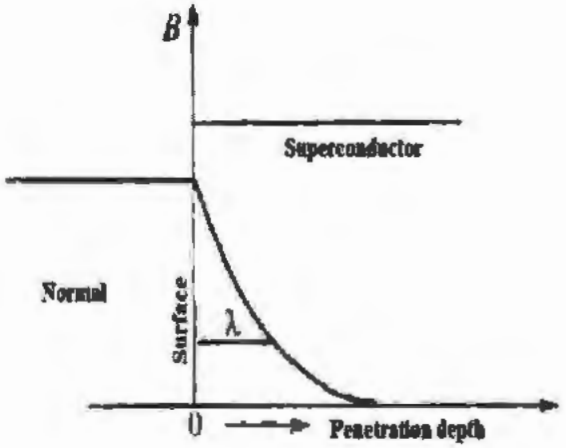

Fig.1.4: Schematic representation of penetration depth with applied magnetic field for superconductors.

Temperature dependent penetration depth ($\lambda(T)$) is given by

$$\lambda^2(T)=\left[\frac{mc^2}{4\pi n_s(T)e^2}\right]^{\frac{1}{2}} \text{----------(1.10)}$$

where, c is the speed of light, density of superconductor is represented n_s and charge on electron is represented by e. It is cleared from above equation that penetration depth is inversely related to number density of superconductors. The temperature dependent penetration depth and coherence length are related with each other and is given by an equation [24];

$$\lambda(T)\xi(T)=\frac{\varphi_o}{2\pi}\sqrt{2\mu_o H_c(T)} \text{----------(1.11)}$$

1.2.4 Critical Temperature (T_c)

Transition temperature by which material is transformed from normal conductor state to state of superconductivity is called critical temperature and is denoted by T_c. Material resistivity drops to zero suddenly at this transition temperature [24]. Resistance of material becomes zero at transition temperature with formation of cooper pair due to shrink of molecular motion. When

temperature is increased above transition temperature then cooper pair breaks due to oscillating thermal motion of molecules and superconducting material is transforms into normal materials [25] as shown in Fig. 1.5. Critical temperature (T_c) depends upon nature of materials so, it is different for different materials.

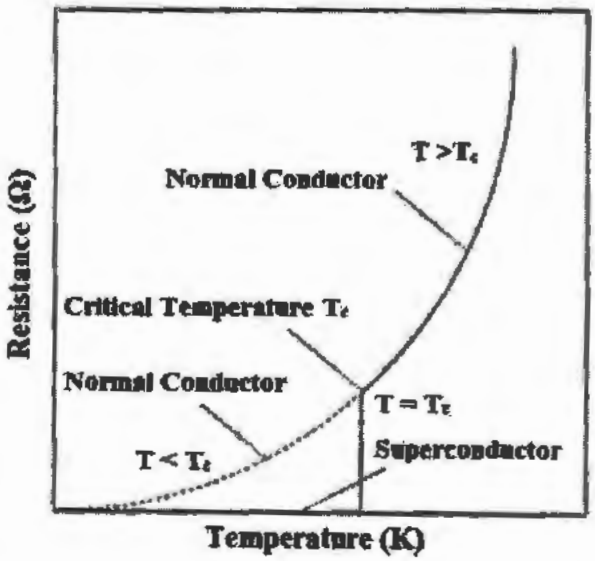

Fig.1.5: Behavior of material at different temperatures.

1.2.5 Critical magnetic fields (H_c)

Magnitude of applied H_c used to convert material in state of superconductivity to normal state (conductor) is known as critical magnetic field (H_c). Value of this field depends upon temperature and it decreases with increase of temperature below T_c. Empirical relation is given by formula [26],

$$H_c(T) = H_c(0)\left(1-\left(\frac{T}{T_c}\right)^2\right) \text{----------(1.12)}$$

Graphical sketch of dependence of critical magnetic field (H_c) is represented in Fig. 1.6. It is cleared that inside the region material is in state of superconductivity and outside the region the state is destroyed.

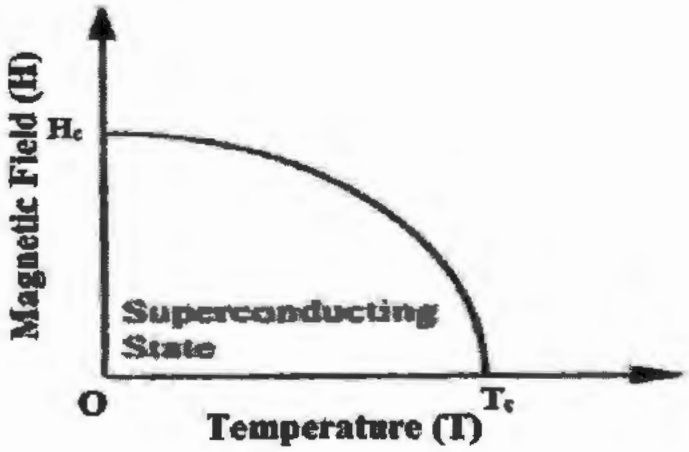

Fig.1.6: Temperature dependence of critical magnetic field (H_c).

1.2.6 Critical current density (J_c)

Critical current (I_c) per unit area of material is known as critical current density (J_c) and magnitude of critical current density is required to transform material from superconducting state into normal state. Critical current (I_c) and critical current density (J_c) are important parameters for synthesis of material used in wire technology [27]. According to Francis Silsbee's ruler [28, 29], a connection between I_c and H_c is

$$I_c = \frac{2\pi r H_c}{\mu_o} \text{----------(1.13)}$$

where r is radius of wire, μ_o is permeability of free space having value $4\pi\times10^{-7}$ Hm^{-1}. Magnitude of critical current density is represented as

$$J_c = \frac{I_c}{A} = \frac{2\pi r H_c}{\mu_o \pi r^2} = \frac{2H_c}{\mu_o r} \text{----------(1.14)}$$

1.2.7 Relation between critical variables

All critical parameters, i.e., T_c, H_c and J_c are dependent on each other. In order to sustain materials in state of superconductivity, the magnitude of these three variables are kept smaller than critical (transition) values. Variation in values of all these variables is graphically shown in Fig. 1.7.

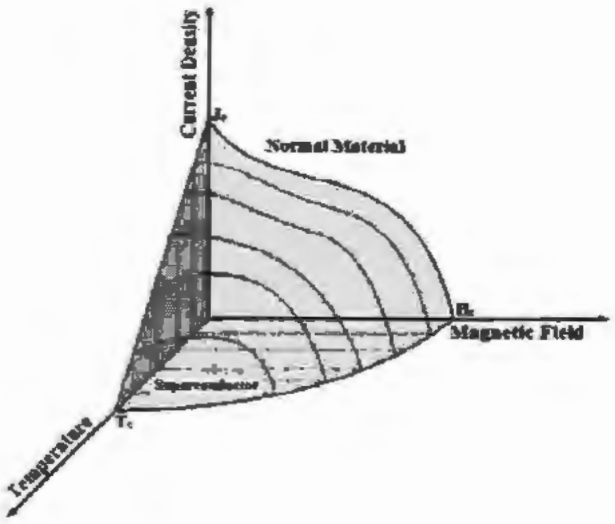

Fig. 1.7: Inter-dependence of three critical variables indicating state of superconductivity inside and normal state (conductor) beyond of shaded portion.

Fig.1.7 indicates inter-dependence of these critical parameters (H_c, T_c and J_c). Material is in state of superconductor within confine of these critical parameters and changes into normal state (conductor) with exceeds of any one of these critical parameters. Mathematically these parameters (H_c, T_c and J_c) are related by equation 1.14 and placing value of H_c from equation 1.12

$$J_c = \frac{2H_c(0)\left[1-\left(\frac{T}{T_c}\right)^2\right]}{\mu_o r} \qquad (1.15)$$

1.3 Types of superconductors

It is not necessarily for pure metals containing zero impurities to show zero electrical resistance by cooling it to absolute zero. However materials with superconducting nature essentially show definite phase transition (Meissner effect) near or at critical temperature and transforms from paramagnetic to diamagnetic material [26]. The superconductors are divided into two main types dependent on applied magnetic fields [30, 31]. Later it was discovered by A. A. Abrikosv that superconductivity exists in material with partial diamagnetic nature and this type of superconductor is known as mixed state of superconductor [30].

1.3.1 Type-I superconductors

That type which shows completely Meissner effect below transition temperature is called type-I superconductor. Pure metals and metalloids are characterized by type-I superconductors. Magnetic flux lines are expelled by materials with values of applied magnetic field is less than critical magnetic fields. As magnetic fields lines start to penetrate inside materials with $H > H_c$, superconductivity is destroyed and material is transformed into normal material. Superconductivity in type-I superconductors is vanished not only for temperature $T > T_c$ but also for applied magnetic field $H > H_c$ and critical current density $J > J_c$. This type of superconductor is also called soft superconductors. Graphical representation of type-I superconductor is represented in Fig.1.8 (a, b and c).

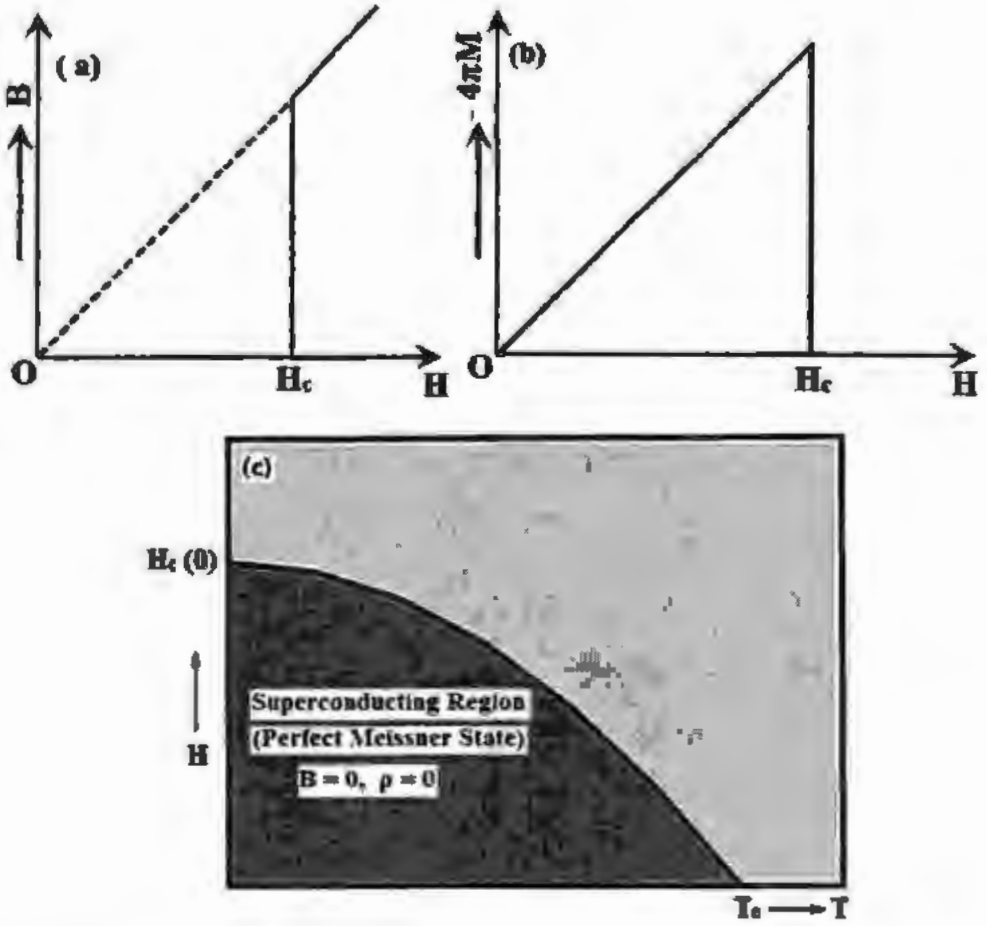

Fig.1.8: Graphical representation of type-I superconductor between (a) B versus H, (b) M versus H and (c) H versus T.

Type-I superconductor can be represented in term of Ginzberg-Landau parameters (κ), penetration depth (λ) and coherence length (ξ)

$$\kappa = \frac{\lambda}{\xi} \text{----------(1.16)}$$

If $\kappa \ll \xi$ and $\kappa \ll 1 (\kappa < 1/\sqrt{2})$ material will be type-I superconductors. Surface energy equation is given by

$$\sigma_s = \frac{(\xi - \lambda)\mu_o H_c^2}{2} \text{----------(1.17)}$$

As in case of type-I class of superconductors ξ is greater than λ, so these materials have positive surface energy [32].

1.3.2 Type-II superconductors

A new class of material called type-II class of superconductors (also known as mixed state of superconductors) and prepared by using alloys and metallic compounds in 1930. These types of material possessed two critical fields known as lower (Hc_1) and upper critical (Hc_2) fields. Response of type-II superconductor with applied magnetic fields is quite different from type-I superconductor. At lower critical field (H_{c1}) magnetic flux are excluded from internal surface as in case of type-I superconductors. When field is increased from lower critical field (H_{c1}) to upper critical field (H_{c2}) then field lines starts to penetrate inside material partially. Above H_{c2} material is transformed from superconductor to normal and shows no diamagnetic behavior [32]. If $\kappa \gg \xi$ and $\kappa \gg 1 (\kappa > 1/\sqrt{2})$ material will be type-II superconductors. It is also known as hard superconductors. As in case of type-II superconductors coherence length (ξ) is smaller than penetration depth (λ), so these materials have negative surface energy [33]. Fig. 1.9 (a, b) indicates representation between magnetization versus applied field and temperature versus applied field for type-II superconductors.

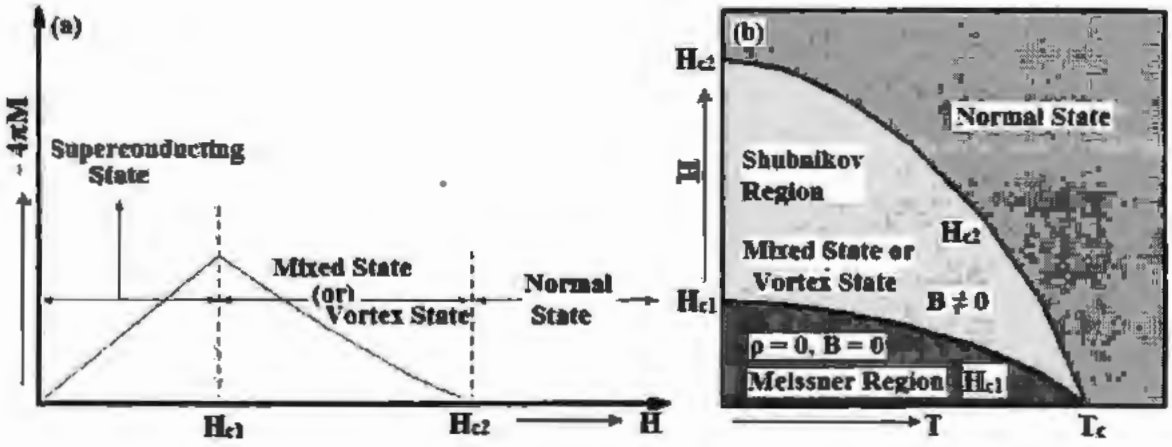

Fig.1.9: Schematic representation of type-II superconductor with (a) M versus H, (b) H versus T [34].

Demagnetizing effect in case of mixed state superconductor or intermediate state is given by an expression [34]

$$H_i = \frac{H}{1-n} \text{----------(1.18)}$$

where n is called demagnetizing factor or shape factor and depends upon the shape of material as well as magnetic field orientation [23]. For example n= 0, 1/2 when cylinder is placed in parallel and perpendicular field orientation respectively. Similarly n is observed 1/3, 1 for sphere and thin plate with perpendicular field orientation [35]. Formation of triangular vortex as observed in intermediate state or mixed state is shown in Fig. 1.10. Temperature dependent critical fields of some modern superconductors are represented in Fig.1.11.

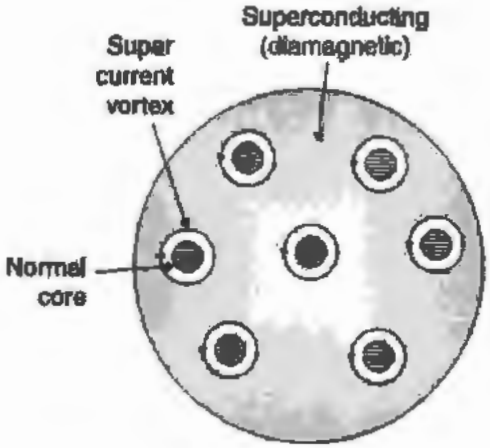

Fig.1.10: Formation of triangular vortex in type-II superconductor (mixed state)

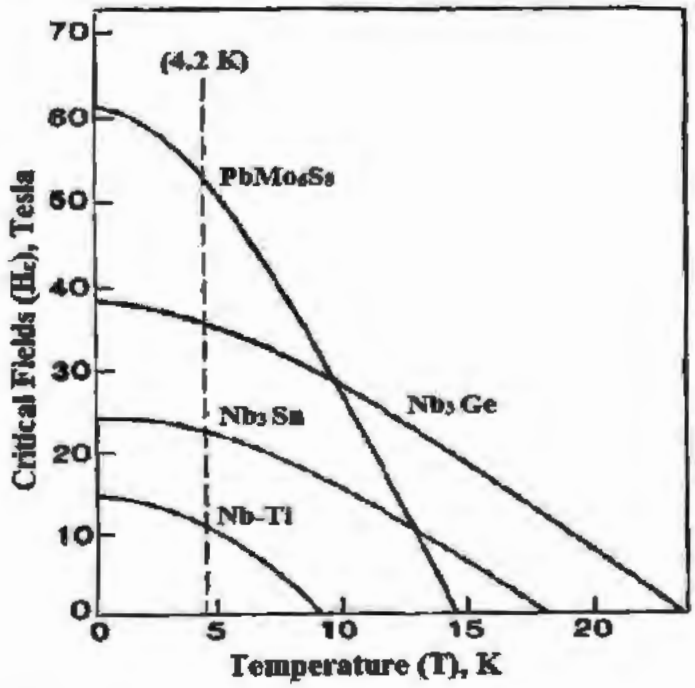

Fig.1.11: Temperature dependent critical fields of some modern superconductors [36]

1.4 Meissner effect

Exclusion of magnetic field lines from internal surface (inner core) of material is familiar as Meissner effect. This important phenomenon was noticed by German professor W. Meissner and his student R. Ochsenfeld in 1933 [37]. Materials manifest diamagnetic property (B=0) due to

exclusion of magnetic flux from surface. Diamagnetism is an intrinsic property which is used to observe superconductivity in materials [38, 39].

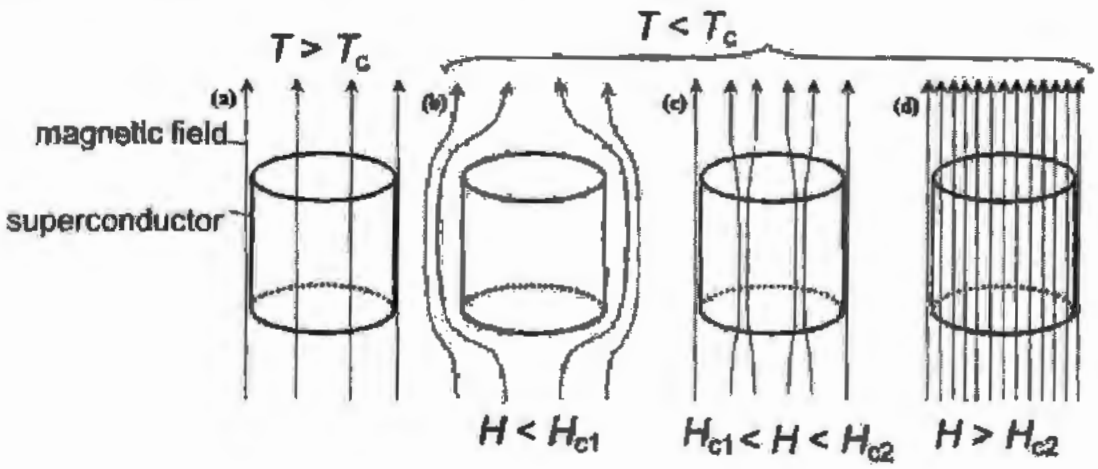

Fig.1.12 (a-d): Meissner effect representation in material with $T > T_c$ and $T < T_c$.

When superconducting material with and without applied magnetic field is positioned in external magnetic field with $T > T_c$ then field lines are entered inside material and material behaves as conductor, as shown in Fig. 1.12 (a). When superconducting material is placed in magnetic field ($H < H_{c1}$ with $T < T_c$) then all field lines are expelled from surface and behaves as superconductor (type-I, in diamagnetic state with B=0) as shown in Fig. 1.12 (b). Again superconductor is placed in magnetic field ($H_{c1} < H < H_{c2}$ with $T < T_c$) then lines are partially expelled from surface and material behaves as superconductor (mixed state, type-II) as shown in Fig. 1.12 (c). When superconductor is inserted in magnetic field ($H > H_{c2}$ with $T < T_c$) then all field lines are again invaded inside core of material and it behaves as normal material (conductor) as shown in Fig. 1.12 (d).

1.5 London's equation

Maxwell equations cannot explicate why magnetic field lines are expelled from internal surface of superconductors. London brothers Fritz and Heinz formulated basic phenomenological theory for superconductors by using idea of Gorter and Casimir two-fluid model in 1935 [40, 41]. These two London equations are used to relate microscopic electric and magnetic fields of superconductors. It was proposed by London brothers that field lines are not removed from surface and these lines remain trapped within thin surface called penetration depth. According to

two-fluid model total number density (n_o) is $n_o = n_s + n_o$, where n_s, n_n represent the number density of superconductor and normal electron respectively. Equation of motion for super-fluid electron is

$$\frac{m\,dv_s}{dt} = -eE \text{----------(1.19)}$$

and current density is

$$J_s = -en_s v_s \text{----------(1.20)}$$

Equation (1.19) and (1.20) yield

$$\frac{dJ_s}{dt} = \frac{n_s e^2 E}{m} \text{----------(1.21)}$$

Equation (1.21) is called London first equation. Taking curl of equation (1.21)

$$\nabla \times \left(\frac{dJ_s}{dt}\right) = \frac{n_s e^2}{m} \times (curlE)$$

By using Max-well equation, above equation can be written as

$$\nabla \times \left(\frac{dJ_s}{dt}\right) = \frac{n_s e^2}{m}\left(\frac{\partial B}{\partial t}\right)$$

Integrating above equation yield

$$\nabla \times J_s = -\frac{n_s e^2 B}{m} \text{----------(1.22)}$$

Equation (1.22) is known as London 2nd equation. By using Max-well equation, Meissner effect can be drawn from London 2nd equation

$$\nabla \times B = \mu_o J_s \text{----------(1.22)}$$

By getting curl of above equation yield

$$\nabla(\nabla.B)-\nabla^2 B=\mu_o(\nabla\times J_s)$$

as $(\nabla.B)=0$, one can get

$$\nabla^2 B=\frac{1}{\lambda_L^2}B \text{----------(1.24)}$$

Where $\lambda_L=\sqrt{\frac{m}{\mu_o n_s e^2}}$ is known as London's penetration depth

The explication of Eq.1.24 is given by

$$B(x)=B_o e^{-\frac{x}{\lambda}} \text{----------(1.25)}$$

Penetration depth and number density are temperature dependent quantities and given as

$$\lambda_L(T)=\lambda_L(0)\sqrt{1-\left[\frac{T}{T_c}\right]^4}$$

$$n_s=n_0\left(1-\left[\frac{T}{T_c}\right]^4\right)$$

Temperature dependent penetration depth and number density of superconductor is shown in Fig.1.13. Penetration depth and coherence length in nanometer range is given in Table 1.3.

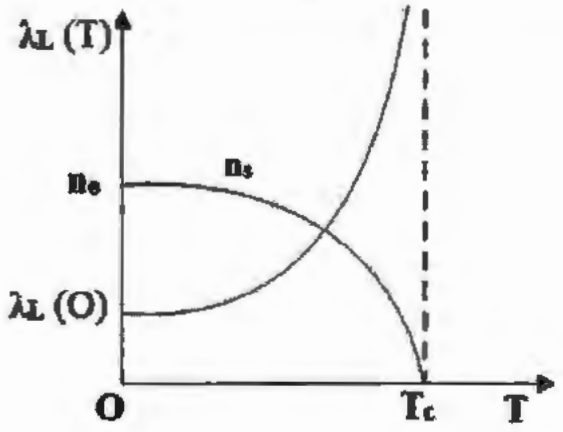

Fig.1.13: Temperature dependent London penetration depth and number density of superconductor.

Table 1.3: Penetration depth and coherence length (in nm) at various critical temperature of some superconducting materials [42].

Superconducting Material	T_c (K)	Penetration Depth λ (nm)	Coherence Length ξ (nm)
Nb	9.2	45	38
NbN	16	200	5
MgB_2	39	85	3.7
Nb_3Sn	18.4	80	3.5
UPt_3	0.5	780	20
$LuNi_2B_2C$	11	76	7
$YBa_2Cu_3O_7$	93	145	1.3
$Ba_{0.6}K_{0.4}BiO_3$	31	220	3.5
Rb_3C_{60}	30	420	3
$HgBa_2Ca_2Cu_3O_{10}$	135	177	1.3

1.6 Ginzberg-Landau Theory

Quantum effects did not take into account in theory of superconductivity developed by London brothers. First phenomenological theory of superconductivity with quantum effects was given by Ginzberg-Landau [43]. Advantages of introducing quantum effects in theory is that superconducting state becomes more order than normal state and, secondly that transition from one state to another state (without magnetic field) behaves as 2^{nd} order phase transition [44]. Ginzburg and Landau introduced effective wave function Ψ (r) for superconducting electrons. According to GL theory, free energy for superconducting state near transition state can be measured by this order parameters Ψ (r). Ginzberg Landau theory implies that it is valid only at temperature close to $T_c - T \ll T_c$ (Transition Temperature). Let us assume that wave function of superconducting electrons with effective wave function Ψ (r) is the order parameters. One can get density of cooper pair by normalization of wave function Ψ (r)

$$|\Psi(r)|^2 = \frac{n_s}{2} \text{----------(1.26)}$$

Free energy density of a homogenous superconductor without applied external magnetic field near critical temperature is given by

$$F' = F_n + \alpha|\Psi|^2 + \frac{\beta}{2}|\Psi|^4 + \left|\frac{1}{2m}(-i\hbar\nabla - 2eA)\psi\right|^2 + \frac{|\beta|}{2\mu_o} \text{----------(1.27)}$$

where F' and F_n are free energies in superconducting state without applied magnetic field and in normal state conductor respectively, whereas α and β are phenomenological expansion coefficients, which are characteristic of materials. Here A, m, e and B are vector potential, effective mass, charge on electron and applied magnetic field, respectively. Let us find value of $|\Psi|^2$, for which the free energy of homogeneous superconductor, the F' has minimum value. This value $|\Psi|^2$ is solution of equation (1.27) by taking its derivative; i.e.,

$$\frac{dF'}{d|\Psi|^2} = 0 \quad \text{and} \quad |\Psi_o|^2 = -\frac{\alpha}{\beta} \text{----------(1.28)}$$

By putting equation (1.28) into equation (1.27), one gets difference in energy

$$F_n - F' = \frac{\alpha^2}{2\beta} \text{----------(1.29)}$$

Free energy in case of applied magnetic field is

$$F_n - F' = \frac{H_c}{8\pi}$$

By comparing above both equations one gets a new equation

$$H_c = \frac{4\pi\alpha^2}{\beta} \text{----------(1.30)}$$

It is cleared from equation (1.28) that $\alpha = 0$ at $T = T_c$ and $\alpha < 0$ at $T < T_c$.

Equation (1.29) indicates that coefficient β is positive and also independent of temperature. Indeed as follows by an equation (1.28), at $T < T_c$ with $\alpha < 0$, $|\Psi|^2$ can be positive only if $\beta > 0$. On the other hand if $T > T_c$ with α, β are positive then energy F' reaches its minimum values $|\Psi|^2 = 0$. This means that there is no superconducting state at $T > T_c$. Thus we have $\beta > 0$ both at $T < T_c$ and $T > T_c$.

1.7 BCS theory of superconductors

Superconductivity is phenomenon up to transition temperature of ~ 10^{-5} K in which large number of conduction electrons takes part. There are two major drawbacks in phenomenon of superconductivity. Firstly conduction electrons behave as fermions and follow Fermi-Dirac distributions with two electrons cannot occupy same energy and quantum states. Secondly these electrons observe Coulomb repulsive force due to their same nature, and therefore cannot combine with each other due to this repulsive force. The idea of attractive force between these electrons with lattice malformation was given first time in 1950 by Frohlich [45]. It was argued by Frohlich that new superconducting state developed by electron-phonon interaction with absorption and emission of these phonons, thus behaving as Bosons and forms a bound pair which obeys Bose-Einstein distributions. Later, isotopes effect was observed in many superconductors via conformation of these electron-phonon interactions [46, 47]. J. Bardeen, L. Cooper and J. R. Schrieffer in1957 published a theory (known as BCS theory, pair produced are called cooper pair) by using key idea and argument of Frohlich [48, 49]. If an electron is considered passing through 2-D lattice, distorts the lattice by attracting positive ion and the lattice distortion produced by moving electron in shown in Fig. 1.14.

$$d = \frac{2\pi V_F}{\omega_D} \text{----------(1.31)}$$

where ω_D = Debye frequency and d is observed to be 100-1000 nm.

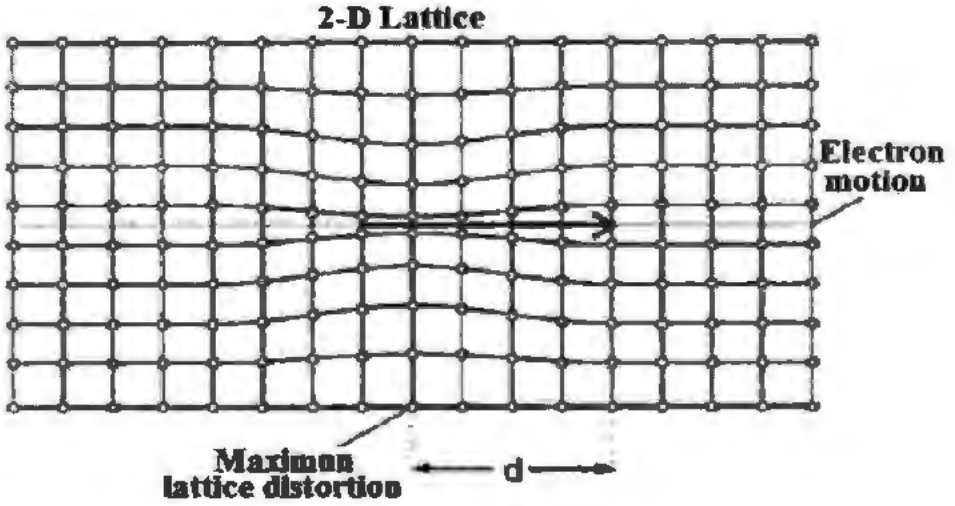

Fig.1.14: Deformation produced in lattice by motion of electron.

By acquisition of positive charge due to lattice distortion, attracts another negative electron passing through region. The maximum distortion is observed through distance d when electrons move opposite to each other in lattice site. This attractive force persists much more time in lattice region than coulomb repulsive force. Cooper proposed [50] these two electrons with opposite momentum having greater values than Fermi momentum and these two electrons have 10^{-3}~ 10^{-4} eV binding energy. It is necessary to keep temperature low in order to maintain binding energy of these opposite electrons. These electrons have strongest binding energy only if they have same magnitude and opposite momentum (total momentum must be equal to zero) and behave as singlet wave function. Size of Cooper pair can be calculated by the expression as,

$$r = \frac{\hbar V_F}{E_b} \text{----------(1.31)}$$

where V_F = Fermi velocity and its value is 10^8 m/sec, E_b = Binding energy and its value is 10^{-3}~10^{-4} eV and one can get same value as that of d = 100-1000 nm.

J. Bardeen, L. Cooper and J. R. Schrieffer proved that with phase coherence, the energy of system has lowest value if they have same and opposite momentum. Comparison between energy level of normal metal and superconductor at different temperature is shown in Fig. 1.15.

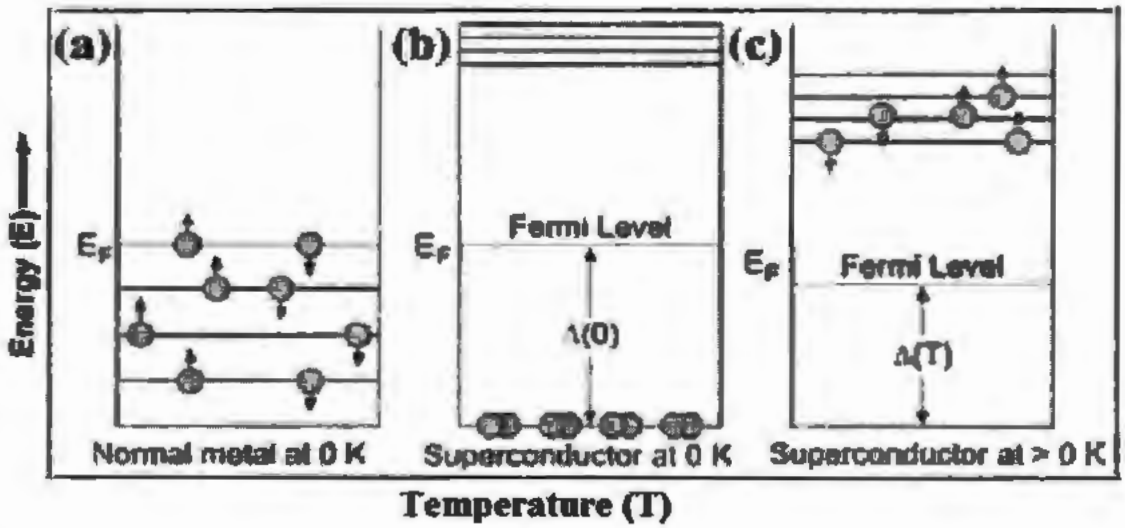

Fig.1.15: Comparison of energy spectrum between metal and superconductor at different temperatures.

It is seen from above Fig 1.15 (a) that Fermi levels are filled but empty above Fermi level in case of metals. In case of superconductors all electrons are in bound pair state with energy gap equal to 2Δ at T= 0 K and same amount of energy is required to break this bound pair of superconductor. Fig. 1.16 (a, b) represents the Cooper pair formation and mechanism of the Cooper pair in superconductor.

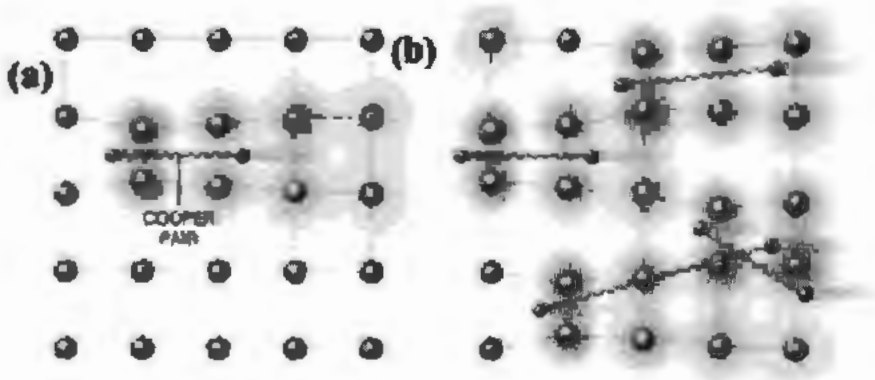

Fig.1.16: Schematic representation of (a) Cooper pair and (b) mechanism of Cooper pair in superconductor [51].

Relation between number density state of electron and transition temperature in weak coupling limit as suggested by BCS theory is given by;

$$K_B T_c = 1.14\hbar\omega e^{-\frac{1}{N_o V}} \text{----------(1.33)}$$

where V is called electron-phonon interaction parameter, k_B Boltzmann constant. ħ is plank constant, ω angular frequency and N_o is the density states of electron. Above equation indicates that phonon frequency ħω is proportional to critical temperature. It is also cleared from above equation that transition temperature is strongly dependent on electron concentrations, so one can conclude that by alloying or applying pressure transition temperature may change. BCS theory also predicted relation between energy gap and critical temperature [51]

$$2\Delta = 3.5 K_B T_c \text{----------(1.34)}$$

The relationship between temperature and energy gap close to critical temperature (T_c) is given by

$$2\Delta = 3.2 K_B T_c \left[1 - \frac{T}{T_c}\right]^{\frac{1}{2}} \text{----------(1.35)}$$

1.8 Different groups of superconductors

Superconductors are categorized into various groups on principle of their variegated properties and crystal structures. More than seven thousands superconducting materials have been discovered [42]. These materials can also be differentiated into certain categories based on mechanism of superconductivity. Mechanism in these different superconducting materials is different. So these materials are divided into three major types depending on superconductivity mechanism [52]. These materials are in form of low dimensional magnetic materials, some metals and their alloys as well as low dimensional non-magnetic materials. Solid materials show process of superconductivity when these materials are in the form of poly-crystalline ceramic, single crystal and in thin film. Some materials show mechanism of superconductivity at high pressure when they are irritated. Superconducting state is observed in some unconventional superconductors when they are subjected to applied magnetic field.

1.8.1 First group of superconducting materials

First group of superconducting materials is explained completely on BCS theory. This group includes classical, conventional, non-magnetic elemental superconducting materials and their

alloys [42]. Majority of these materials are type-I superconductors and their critical temperature cannot exceed 10 K. First group of superconducting materials is not desirable for practical application due to low T_c and critical magnet fields [42]. Cesium, chromium, lithium, silicon etc are some examples of first group of superconducting materials. Their superconducting properties and critical temperatures can be enhanced by manufacturing them in the form of films.

1.8.2 Second group of superconducting materials

Second group of superconducting materials can be characterized with help of two superconducting sub-systems interactions. Some materials can be described and some materials cannot be described on BCS theory. So, half of these materials are called half un-conventional and alternatively half of them are known as conventional superconductors [42]. This group involves low dimensional and non-magnetic materials. These compounds are type-II superconducting materials and their critical temperature cannot exceed to 40 K and critical magnetic fields cannot exceed to 10 T. Some materials of this group are suitable for practical applications. A-15 superconductors, Metal oxide superconductors, MgB_2, Binary compounds (Nitrides, carbides and laves phases) and semiconductors are members of this group.

1.8.3 Third group of superconducting materials

Materials in this group are called unconventional superconductors and include low dimensional and magnetic materials. This group of materials has very short coherence length, very large penetration depth and large upper critical magnetic fields [42]. Superconductivity can be explained on mechanism of electron-phonon interaction and this interaction is considered non linear and strong. Materials in this group are normally called high temperature superconductors. These materials are used at large scale in different field of practical applications. Chevrel phase superconductors and copper oxides superconductors (LSCO, NCCO, Bismuth based and YBCO) are members of third group of superconductors.

1.9 High temperature superconducting cuprates

Superconducting materials with T_c larger than 30 K are termed as high temperature superconductors (HTSCs). Lanthanum based oxide compound with critical temperature of 30 K was first discovered in IBM, Zurich research laboratory by Bednorz and Muller [53] in 1986. Critical temperature of $(La_{0.85}Ba_{0.15})CuO_{4-x}$ superconducting compound was raised from 36 K to 40 K with 13 K bar pressure by Chu et al. [54] and obtained T_c from 36.5 K to 38.5 K by

replacing smaller ion strontium with Lanthanum by Cava et al. [55], immediately after discovery of first HTSC. Now large number of different families with oxides and copper (Cu-O layers) called cuprates with T_c greater than boiling point of liquid nitrogen (77 K) has been discovered. Critical temperature (T_c) of these HTSCs families with double CuO_2 layer per unit cell is always greater than single CuO_2 layer and so on. These HTSCs are in form of perovskite structure [56], have large number of structural phase transitions and coherence length much larger than penetration depth. Superconductivity is taken place in copper oxide planes and these cooper oxides planes mainly affect critical temperature of materials. CuO_2 layers in cuprates have tetragonal structure and each cooper ion is attached with four O ions and detached with length of 1.9 Å [42].

Chemical formula for high temperature supereonductors is much lengthy and difficult, so their structures are represented by four digits schemes. First digit is used for representation of insulating layer among neighboring conducting blocks. Second digit is used for spacing layer between copper oxides blocks. Number of CuO_2 layer inside of conducting blocks is represented by third digit and CuO_2 layer within conducting blocks is depicted by fourth integer [57]. HTSCs have superconducting as well as charging blocks and superconducting block is separated by two charge blocks. CuO_2 is considered as common elements in these HTSCs [58-60]. HTSCs have highest T_c at optimum level due to its stable structure and are decreased in over-doped and under-doped regions [61, 62].

1.10 Major families of cuprates based HTSCs

More than hundred families of high temperature superconductors are well known today. CuO_2 planes are essential part of these families and also responsible for superconductivity in these HTSCs. Charge carriers flow through these conduction planes in normal state as well as superconducting states in them. The copper oxide planes are sandwiched among multilayer of TlO, LaO, SrO and BaO, which are considered of insulating nature and are used for charge neutrality and crystal structure stabilizations [63]. Lanthanum, Yttrium, Bismuth, Mercury, Thallium and Copper thallium based superconductors are major families of high temperature superconductors. Some of above liquid nitrogen boiling point high temperature superconductors along with their critical temperatures are given in Table 1.4

Table 1.4: Some of high temperature superconducting families with critical temperature greater than boiling point of liquid nitrogen [64- 83].

Family	T_c (K)	Family	T_c (K)	Family	T_c (K)
$YBa_2Cu_3O_{7-\delta}$	93	$LaBa_2Cu_3O_{7-\delta}$	98	$Bi_2Ca_{0.8}Sr_{0.8}La_{0.4}CuO_{6+\delta}$	80
$EuBa_2Cu_3O_{7-\delta}$	95	$Bi_{1.7}Pb_{0.3}Sr_2Ca_2Cu_3O_{10}$	116	$Bi_{2.14}Sr_{1.77}Ca_{0.92}Cu_2O_{8-\delta}$	93
$GdBa_2Cu_3O_{7-\delta}$	94	$Bi_2Sr_2CaCu_2O_8$	87	$TlBa_2Cu_2O_x$	110
$NdBa_2Cu_3O_{7-\delta}$	96	$Tl_2Cu_2O_{6+\delta}$	93	$Tl_2Ba_2Cu_2O_{6+\delta}$	93
$Bi_{1.8}Pb_{0.4}Sr_{1.72}Ca_2Cu_3O_{10+\delta}$	111	$Bi_{2.2}Sr_2Ca_{0.8}Cu_2O_{8+\delta}$	84	$Tl_2Ba_2Cu_3O_{10-\delta}$	128
$Tl_{0.5}Pb_{0.5}Sr_2Ca_2Cu_3O_9$	122	$Tl_{1.7}Ba_2Ca_{1.06}Cu_{2.32}O_{9+\delta}$	108	$Tl_2Ba_3Cu_4O_{12+\delta}$	114
$Tl_{1.1}Ba_2Ca_{1.9}Cu_3O_{9.7}$	110	$TlBa_2Ca_3Cu_4O_{11+\delta}$	114	$Tl_{1.64}Ba_2Ca_{1.87}Cu_{3.11}O_{10+\delta}$	125
$Hg_{0.8}Tl_{0.2}Ba_2Ca_2Cu_3O_{8+x}$	138	$HgBa_2CaCu_2O_{6+\delta}$	123	$HgBa_2CuO_{4+\delta}$	93
$HgBa_2Ca_4C_5O_{12+\delta}$	110	$HgBa_2Ca_2Cu_3O_{8+\delta}$	135	$AlSr_2Ca_3Cu_4O_{11}$	110
$PbSr_2Ca_2Cu_3O_x$	122	$GaSr_2Ca_3Cu_4O_{11}$	107	$BSr_2Ca_3Cu_4O_{11}$	110
$Cu_{0.5}Tl_{0.5}Ba_2Ca_3Cu_4O_{12-\delta}$	126	$CuBa_2Ca_2Cu_3O_{8+\delta}$	117	$Cu_{0.5}Tl_{0.5}Ba_2Ca_2Cu_3O_{10-\delta}$	132
$Cu_{0.5}C_{0.5}Ba_2Ca_3Cu_4O_{11+\delta}$	117	$HgBa_2Ca_3C_4O_{10+\delta}$	126	$HgBa_2Ca_5C_6O_{14+\delta}$	107

1.11 Crystal structure and physical properties of HTSCs

Copper oxide superconductor with perovskite structure having critical temperature of above 39 K was discovered in late 1986, which revolutionized all future work [84]. The importance of this structure was that it had superconducting and non-superconducting region. These classes of superconductors have very short coherence length, flux creep affects and anisotropic physical properties. Copper oxidation states and oxygen variations play an important role in the structure, critical temperatures and other properties of these HTSCs. There are many cuprate based superconducting families with different critical temperature and other physical properties. First high temperature superconducting family (LSCO) with two CuO_2 planes and critical temperature of 90 K was synthesized under high pressure. $YBa_2Cu_3O_{7-\delta}$ with orthorhombic structure having critical temperature of 90 K was discovered. $YBa_2Cu_3O_{7-\delta}$ structure was not stable and $YBa_2Cu_4O_8$ with 80 K critical temperature was stable through high pressure [85]. Fig. 1.17 presents the layered structure along with bond length of La_2CuO_4 and $YBa_2Cu_3O_7$. Sheng and Hermann in 1988 discovered thallium based HTSC with T_c of 90 K [86-88] and T_c of 120 K in this type of family was discovered later by other researchers [89]. Fig.1.18 presents the layer diagram along with bond length of $Tl_2Ba_2Ca_{n-1}Cu_nO_{2n+4}$. Layered crystal structure of $Bi_2Sr_2Ca_{n-}$

$_1Cu_nO_{2n+4}$ is obtained with substituting barium by strontium and thallium by bismuth, respectively.

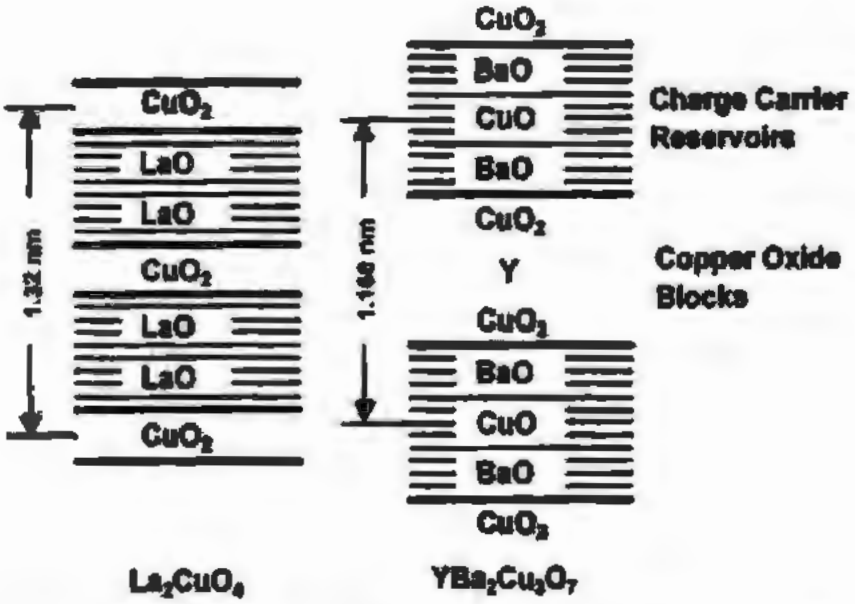

Fig.1.17: Crystal structure of La_2CuO_4 and $YBa_2Cu_3O_7$ along with their layers [86, 87].

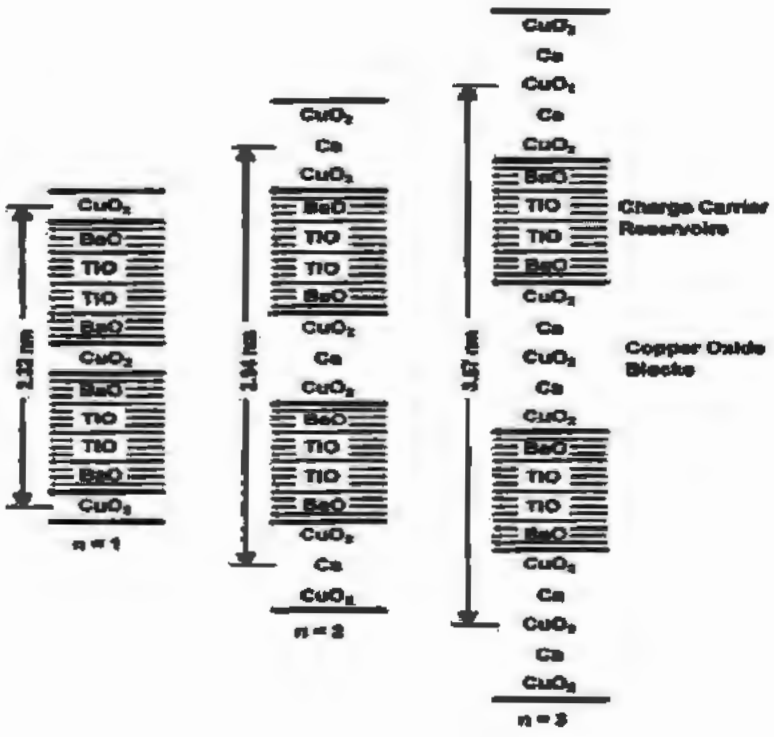

Fig.1.18: Layered crystal structure of $Tl_2Ba_2Ca_{n-1}Cu_nO_{2n+4}$ and $Bi_2Sr_2Ca_{n-1}Cu_nO_{2n+4}$ is obtained by replacing Ba with Sr and Tl by Bi respectively [90, 91].

Thallium based superconductors have tetragonal structure along with n Cu-O layers as well as two Tl-O layers. The critical temperatures of 80 110 and 125 K are obtained in case of Tl-based superconductors with n= 1, 2 and 3, respectively. It was noticed that critical temperature enhanced with number of Cu-O layer up to 3 and found to decrease with further increase of Cu-O layer [91]. Mercury based high temperature superconductors with empirical formula $HgBa_2Ca_{n-1}Cu_nO_{2n+2+\delta}$ having critical temperature of 94 K were discovered. Multi-phase Hg based superconductors with n= 1~3 were discovered with T_c around 130 K by Schilling et al. [92], and $HgBa_2Ca_2Cu_3O_{8+\delta}$ with T_c of 135 K was synthesized. Hg-based superconductors have tetragonal structure and their c-axis length increased with increase of CuO_2 layers. Critical temperature increased with increase of pressure due to hole conductivity in these HTSCs. Hg-1223 with T_c =153 K with pressure of 150 Kbar by Chu et al. was reported [93]. Critical temperatures of Hg- (1201, 1212 and 1223) compounds were increased from 118 K, 154 K and 164 K, respectively with pressure of 45 GPa and was observed by Gao et al. [94].

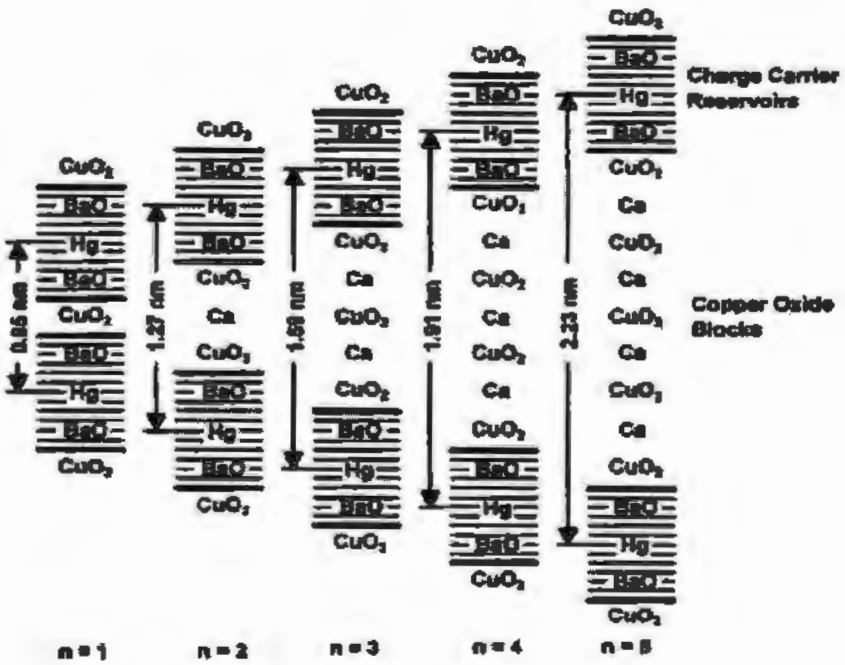

Fig.1.19: Layered crystal structure of $HgBa_2Ca_{n-1}Cu_nO_{2n+2+\delta}$ with different number (n) [91].

Structure of $HgBa_2Ca_{n-1}Cu_nO_{2n+2+\delta}$ with different number of CuO_2 layers is shown in Fig. 1.19. The synthesis of Hg compound is much difficult because of toxic and decompositions of HgO into Hg and O.

1.12 (Cu, Tl)BaCaCuO superconducting family

CuTl based is another promising family of high temperature superconductors due to its highest critical temperature after Hg based superconductors. This family has long c-axis coherence length, low anisotropy, higher transition temperature and has highest critical temperature (132 K) among Cu based superconducting families [95, 96]. This superconducting family has superconducting copper-oxide layer, separated by insulating Ca atom and semi-insulating charge reservoir layer. Thallium executes as reaction accelerator and stabilizer of structure in CuTl based superconductors [97].

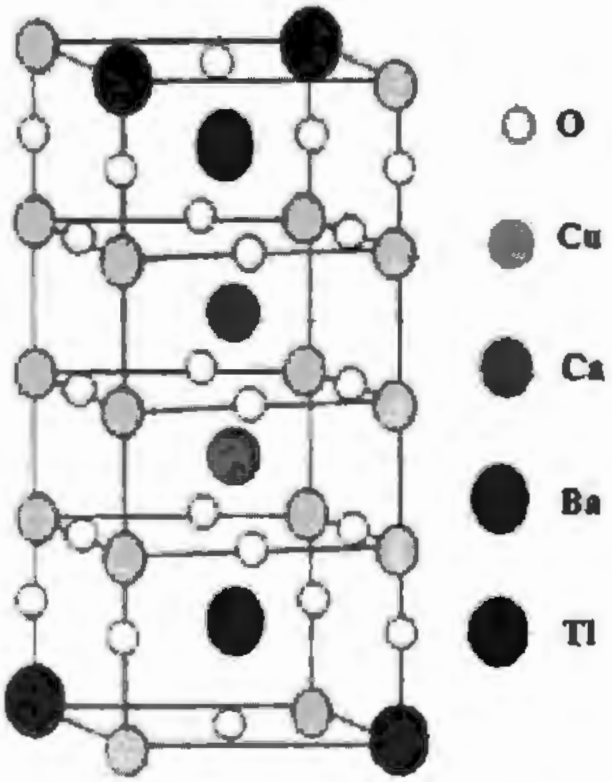

CuTl-1223 Superconductor

Fig.1.20: CuTl-1223 superconductors with its crystal structure.

General chemical formula of this superconducting family is $(Cu_{1-x}Tl_x)Ba_2Ca_{n-1}Cu_nO_{2n+4-\delta}$ (where x= 0.5 and n= 2,3,4……..). We have preferred $(Cu_{1-x}Tl_x)Ba_2Ca_{n-1}Cu_nO_{2n+4-\delta}$ (where x= 0.5

and n= 3), i.e., CuTl-1223 due to highest critical current density and critical temperature among this CuTl family and can be prepared at ambient and high pressure [98]. The (CuTl)-1223 superconductor with its unit cell and different atoms [99] is shown in Fig. 1.20. (CuTl)-1223 family shows tetragonal structure with P4/mmm symmetry. Copper-oxide planes connected with Ba atoms are recognized by p-planes and Cu-O layer between p-planes are recognized by s-planes. Usually p-planes are over-doped and s-planes are optimally doped [99]. Charge carriers are transferred in these superconducting families from p-planes to s-planes. Barium atoms also play vital double role in cuprates based superconductor i.e., for copper oxidation Ba behaves as strong catalyst as well as promoter of layered structure [100]. Barium is also considered as effective ingredient for tuning of oxygen contents and to increase hole carriers for optimal values of critical temperatures [101]. Another important factor in HTSCs is number of CuO_2 planes in copper oxide blocks, which plays vital role for critical temperature enhancement. Maximum possible T_c for different cuprates superconducting families is attained for three CuO_2 planes and this behaviour is shown by different families such as Tl-22(n-1)n [102-104], Bi-22(n-1)n [105, 106] and (Hg, Tl)-22(n-1)n [101]. Critical temperature is further decreased with number of CuO_2 layers greater than four. Lattice imperfections, voids, grain-boundaries and defects are behaved as natural pinning centers in HTSCs. In order to enhance superconducting properties and to avoid thermal flux in these superconductors, a large number of different techniques are introduced for artificial pinning centers.

1.13 Role of in-homogeneities in superconductivity

Conduction electrons are scattered by structural in-homogeneities, twinning planes, grain and surface boundaries which affect the superconducting properties and ordered parameters [107]. Impurity atoms and superconductors have different electronic structure so, their conduction electrons interact with each other via Coulomb force. There are two kinds of impurities, one is static and other is dynamic impurities [108]. Magnetic impurities in conventional superconductors give drastic effect while non-magnetic impurities give small effect on T_c and both impurities have opposite effect in magnetic fluctuations. Conventional superconductors have very large coherence length so impurity effects on micro level and macro level are same. However it is not true in case of cuprates superconductors due to short coherence length. In cuprates superconductors at macroscopic level, magnetic and non-magnetic in-homogeneities have similar effects [42]. The effect on T_c by partial substitution of Zn, Ni and Fe for Cu was

observed same except Zn substitution in YBCO, where T_c was suppressed three times faster by Zn substitution than Ni. The reason for suppression of T_c was occupancy of Zn atoms by Cu sites in CuO_2 planes in which chain location and phase coherence were interpreted by Zn atoms [42].

Phonon and spin fluctuations are responsible for superconductivity in un-conventional and cuprates superconductors. Local spin fluctuations do not change so much by magnetic impurity while it affects the pairing greatly. Non-magnetic impurities do not alter pairing so much but affects locally the spin fluctuations. It was shown by tunneling measurements that Zn impunities situated in CuO_2 planes created voids in it, which resulted the suppression in superconducting state. Ni atoms in contrast to Zn have small effect on local environment so that superconductivity is not interpreted so much by Ni atoms. In electron-doped NCCO or hole-doped cuprates, non-magnetic Zn produces magnetic moments of 0.8 μ_B and does not destroy local antiferromagnetic correlations. In electron-dopped NCCO, magnetic Fe and Ni atoms produce magnetic moments of 2.2 and 2 μ_B respectively. In hole-doped cuprates both magnetic atoms produce magnetic moments of 4.9 and 0.6 μ_B respectively [42]. Mean free path of charge carriers is reduced by presence of different types of in-homogeneities in superconducting materials. Also mean distance of these electrons in cooper pair is decreased, which produce two results in superconductors (i.e.) increase of penetration depth and decrease in coherence length. Ginzburg Landau parameter is increased by change of above parameters. So by the addition of these impurities or in-homogeneities, type-I superconductor is changed into type-II superconductors [109].

1.14 Weak-links and grain-boundaries

When two superconducting regions are combined with each other so that the value of J_c in contact region is smaller than that of single component (region) of superconductor, is called weak-link. These weak-links are known as grain-boundary junction or bi-crystal junctions. It was predicted by Josephson in 1962 that this weak-link junction had new and unexpected properties [110]. According to Josephson, this junction sustains supercurrent without voltage application. When this junction is driven by external source, critical current is increased which produces high frequency electromagnetic waves. A large number of defects are produced along length of grain-boundaries by grain-boundaries forces in superconductors. The transport J_c in sintered poly crystalline HTSCs are observed low due to its granularity nature. Magnetization measurement shows that values of J_c in individual grain are much greater than transport critical current

densities. Cuprates superconductors have small coherence length so that grain-boundaries can behave as barriers for flow of supercurrent. Many superconductors have different types of low angle grain-boundaries. Orientation dependence of J_c in case of artificial grain-boundaries was studied by Dimos and his co-workers for $SrTiO_3$ single crystal grown on Y-123 films [111, 112]. They slowly cooled this film in oxygen atmosphere in order to get highest T_c. Their result indicated that values of J_c across grain-boundaries were found to decrease with increase of angle θ. The values of J_c for tilt grain-boundary of [001] in Y-123 film were observed 2×10^7 Acm^{-2} at 4.2 K with θ= 6.3° and 6×10^6 Acm^{-2} at 26 K with θ= 5° in case of Bi-2223, respectively [113, 114]. The rapid drop in values of J_c across grain-boundaries was observed with increase of angle θ for Y-123 bi-crystal [115].

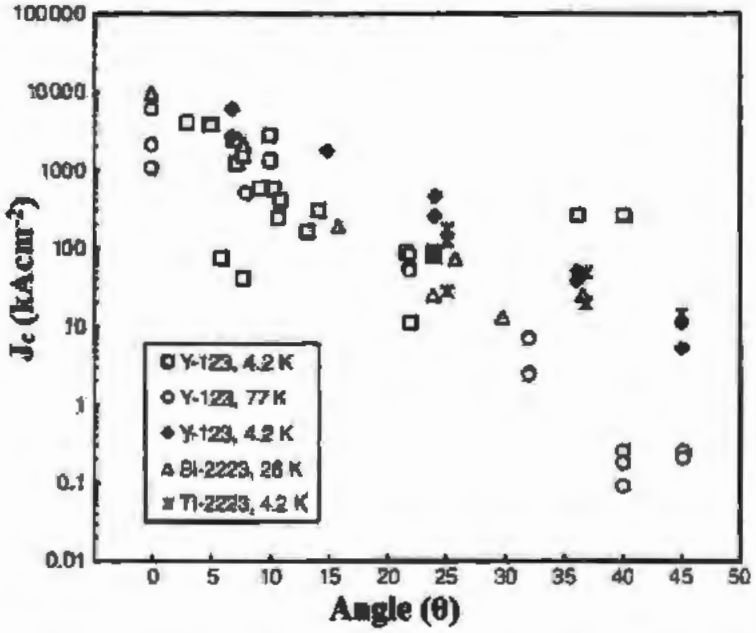

Fig.1.21 : Relation between values of J_c across artificial grain-boundaries versus angle (θ) of some HTSCs [111-115].

Relation between J_c across grain-boundary as function of angle of some HTSCs is shown in Fig. 1.21. The figure indicates that values of J_c across artificial grain-boundaries are decreased with increase of angle in HTSCs. Possible reason of weak-links in these HTSCs with high angle grain-boundaries was due to structural defects as a results of segregations and variation of oxygen vacancies across grain-boundaries [116].

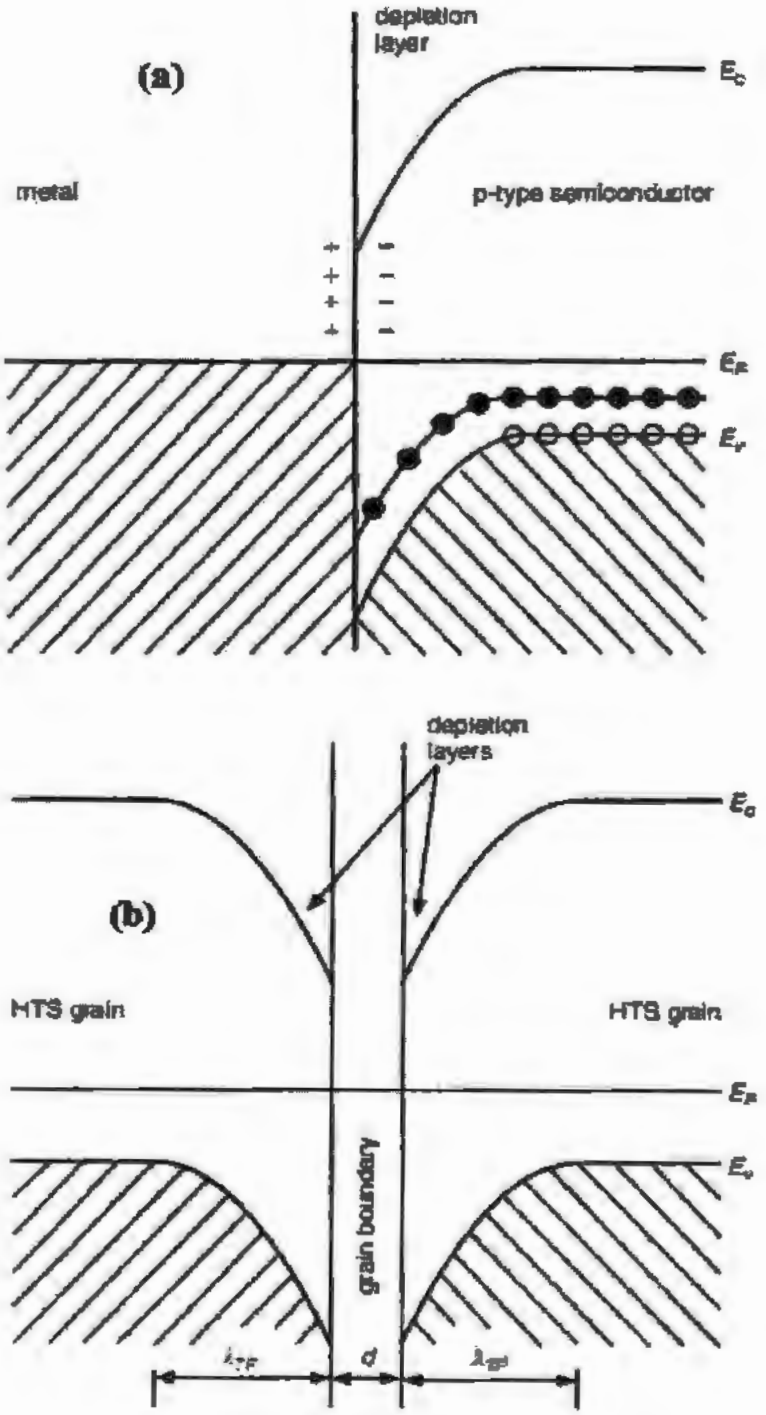

Fig.1.22: Space charge effects leading to band bending at (a) semiconductor metal interface and (b) grain-boundaries of cuprates HTSCs [116, 117]

Similarities between grain-boundaries in HTSCs and semiconductor metal interface (SMI) were identified by Hilgenkamp and Mannhart [117, 118]. Fig. 1.22 (a, b) represents bond bending space charge effects in case of SMI and grain-boundary in cuprates HTSCs. Fig 1.22 (a) shows bond bending at interface of p-type semiconductor with metal having low work function. Charge carriers moves from metal to semiconductors with excess of negatively charge ions. Space charge region enlarges with decrease of number of holes in interfacial region and negligible amount of current enters from metal to semiconductor. Band bending effects can occur in HTSCs at grain-boundaries due to small carrier concentrations and large dielectric constant ($\varepsilon \approx 10$) and grain-boundaries behaves as doubled Schottky barrier as shown in Fig.1.22 (b). Cuprates HTSCs have Thomas-Fermi screening length (λ_{TF}), which lies between 0.5 to 1 nm [117]. Fig. 1.23 indicates graphical sketch between critical current density and hole concentration for $Y_{0.7}Ca_{0.3}Ba_2Cu_3O_{7-\delta}$ superconductor.

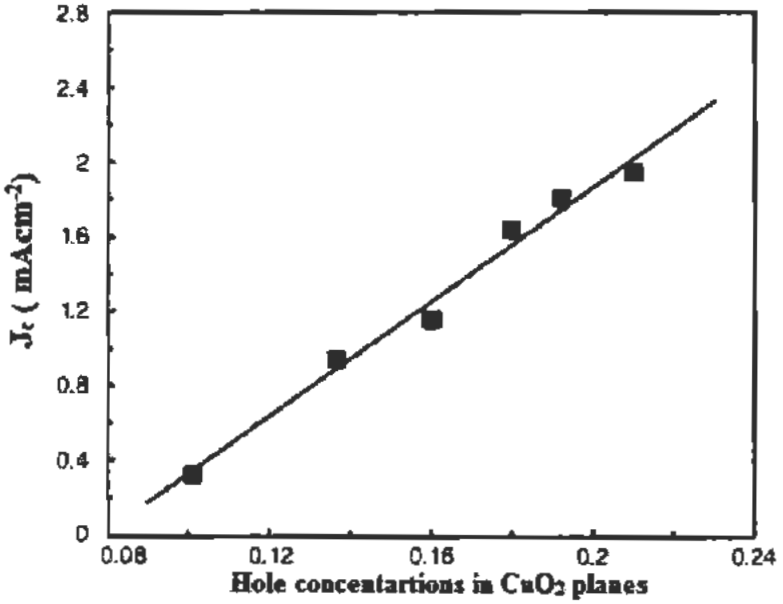

Fig.1.23: Graphical sketch between hole concentrations and J_c of $Y_{0.7}Ca_{0.3}Ba_2Cu_3O_{7-\delta}$ [118].

1.15 Vortex mechanism in HTSCs

Vortex is derived from Latin word vertex which means whirlpool [119]. Vortex mechanism is studied in HTSCs when they are subjected to applied external magnetic fields. This mechanism is observed in mixed state superconductor also called Shubnikov phase, where density of flux is

between H_{c1} and H_{c2}. Flux vortices are kind of quantized flux tube surrounded by supercurrent and its value is given by [120]

$$\varphi_o = \frac{h}{2e} \text{----------(1.36)}$$

where e = charge on electron and h = Plank's constant. The experimental verification of flux quantization was given by Doll & Nabauer at Munich and Fairbank & Deaver at Stanford in 1961 [121, 122]. The number of vortices and vortex density are directly proportional to magnetic field, i.e., vortices increase with increasing strength of magnetic field, so also increase in vortex density of superconductors [122]. We make simple approximation that B(r) and n_s (r) vary exponentially from central axis to understand vortex motion in HTSCs [123].

$$B(r) = B_{center} \frac{e^{-r}}{\lambda} \text{----------(1.37)}$$

and

$$n_s(r) = n_{s\infty}\left(1 - e^{-\frac{r}{\xi}}\right) \text{----------(1.38)}$$

also

The schematic representation of single vortex with function of super-electron density (n_s) and magnetic field (B) is indicated by Fig. 1.24.

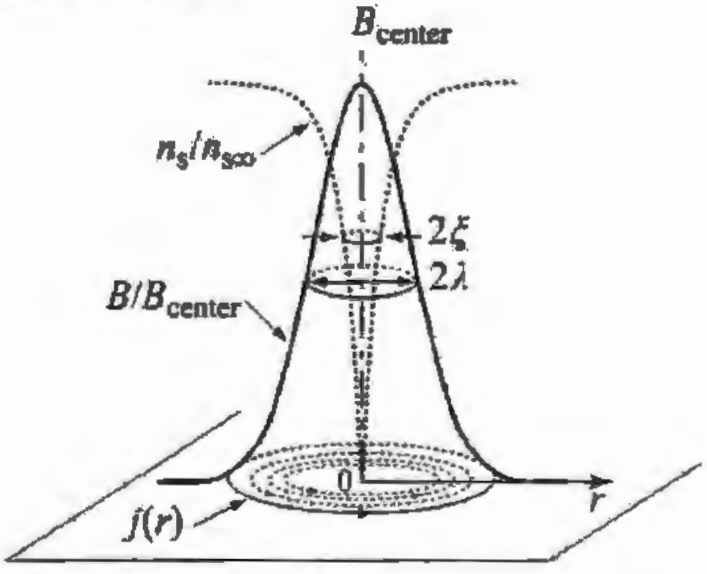

Fig.1.24: Schematic description of spatial variation in characteristic parameters of single vortex.

This figure indicates maximum value of magnetic field at centre with super-current which decreases with characteristic distance λ. Density of super-electron increases from zero to bulk values $n_{s\infty}$ over ξ. At vortex centre, the magnetic field varies little due to small density of current at core region. The interaction between two vortices is repulsive due to same direction and same nature of these vortices. These vortices arranged themselves in triangular form due to repulsive forces and are known as Abrikosov lattice. Distance between two consecutive flux lattices is given by

$$a=1.075\sqrt{\frac{\phi_0}{B}} \qquad \text{----------(1.39)}$$

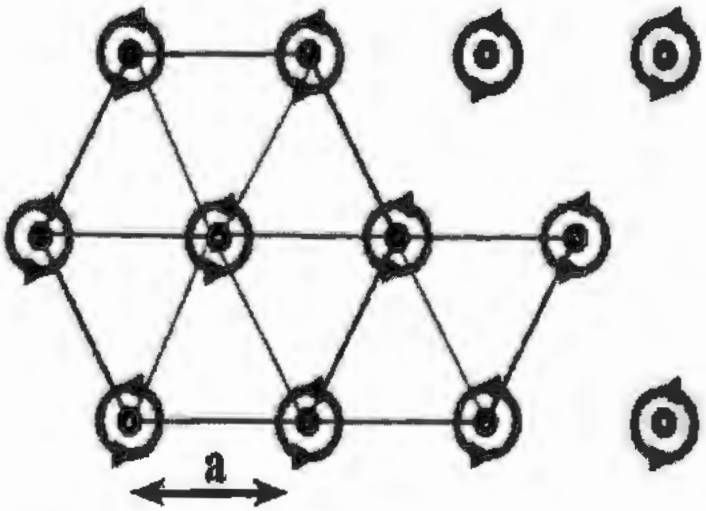

Fig.1.25: The Abrikosov triangular lattice representation in type-II HTSCs.

1.16 Pancake vortices

Superconductivity is taken place in CuO_2 planes in cuprates layered SCs which are superposed on each other with separation of insulating layer known as Josephson junctions. This phenomenon was first reported by Lawrence- Doniach (LD) in their model of anisotropy layered superconductors [124]. These theories in case of specific superconductors depend upon dimensional-less ratio, given as

$$r_a=\frac{2\xi_c^2(0)}{d} \qquad \text{----------(1.40)}$$

The c-axis coherence length and distance among CuO_2 planes are represented by ξ_c and d respectively. When r_{cr} is greater than 1, then GL model must be preferred and if r_{cr} smaller than 1 then LD model will be preferred. LD model explicates that when insulating region between superconducting regions is thick then cross over from 3D to 2D behaviour of SC takes place at characteristic temperature known as cross over temperature (T_{cr}). When HTSCs obeying LD model are subjected to magnetic field then flux vortices are shortened to 2D flat discs familiar as Pancake vortices [124]. The vortices interact with each other in different layered superconductors and net interaction between them is attractive only. The reason of attractive force between these vortices is Josephson coupling between them.

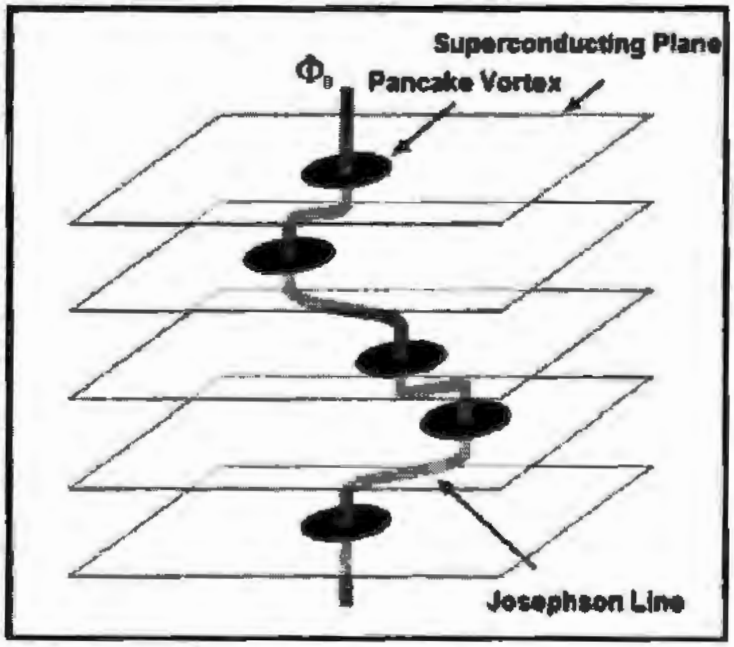

Fig.1.26: Pancake vortices illustrative diagram liked with Josephson coupling [125].

1.17 Vortex dynamics

The dissipation less current sustaining capability can be significantly abolished due to interaction among flux vortices and supplied current in type-II superconductors. It is anticipated that as long as vortices regions do not lap over, the materials consistently yield path to supply current. The current abstains passing through non-superconducting domains as $\lambda > \xi$, the current has to ravine

through the domains having magnetic fields. Vortices experience Lorentz force due to interaction of magnetic field and electronic current which is given as

$$\vec{F}_L = \varphi_{(o)} \vec{J} \times n \text{----------(1.41)}$$

where F_L = Lorentz force acting on vortices, J= current density and n= is unit vector in applied magnetic field direction.

Vortices start to accelerate due to Lorentz force and this F_L is equitable by resistive force acting on vortices which is given as

$$\vec{F}_v = -\eta \vec{v} \text{----------(1.42)}$$

where $\vec{v}$ is vortex average velocity and η is coefficient of viscosity

Electric field is induced as results of motion of vortices in superconductors, which is parallel to current and directly proportional to velocity.

$$\vec{E} = \vec{B} \times \vec{V} \text{----------(1.43)}$$

Energy is dissipated as a result of induced of electric field. Free flux flow resistivity is observed as a result of friction coefficient, which can be calculated as,

$$\rho_{FFF}(T) = \frac{\rho_o B}{\mu_o H_{c_2}(T)} \text{----------(1.44)}$$

Where μ_o is free space permeability and ρ_o is extrapolated normal state resistivity

Upper critical magnetic field and magnetic field resistance were increased with increase of temperature [126]. Vortex dynamics must be ceased in order to obtain dissipation less flow of super-electrons through superconductors. So, flux pinning in vortices is mandatory in vortex-state SC for several infield practical applications such as MRI machines and particles-accelerators [127, 128]. There are different methods in order to pin the flux vortices inside superconductors by introducing precipitates such as impurity phases, lattice imperfections and crystal defects [129]. As type-II superconductors have poly-crystalline in nature and have universal pinning centers in shape of grain-boundaries and crystal imperfection which resist flux vortex motion [130]. In order to cease the motion of flux vortices in cuprates HTSCs, artificial pinning centers are inserted along with natural pinning centers [131]. There are three different types of flux dynamics in HTSCs such as flux creep (FC), flux flow (FF) and thermally assisted flux flow (TAFF) [132,133]. These dynamics depends upon temperature and current density. The resistivity and applied current density schematic illustration is shown in Fig. 1.27. The vortices

flux flow starts at higher temperature when magnetic vortices thermal activation energy dominates the pinning potential. The liquid phase vortex is converted to solid phase by decreasing temperature. The process of TAFF is taken place when pinning potential energy dominates by thermal activation energy. The process of TAFF and flux creep appear with $J< J_c$ and $J= J_c$, respectively. The process of FF is occurred when vortices will not be influenced by pinning barriers at $J>J_c$.

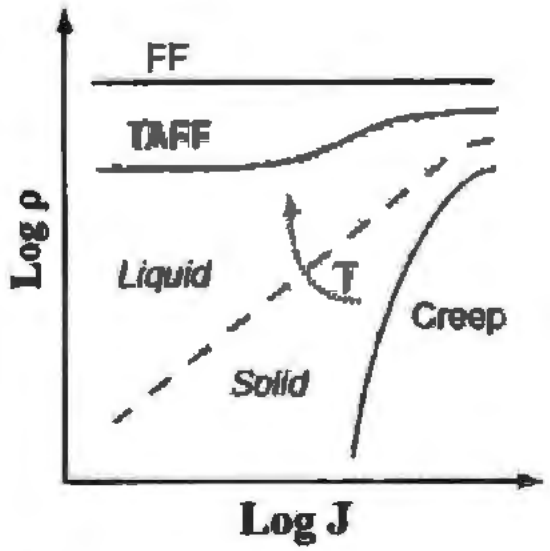

Fig.1.27: The resistivity versus current density schematic illustration for HTSCs.

1.18 Flux pinning mechanism

Pinning force (F_P) is produced in superconductors due to attractive force in between defected sites and core of vortices. Vortices dynamics can be ceased with Lorentz force (F_L) < F_P and when $F_L > F_P$, the vortices started to move due to dislodging from their sites. The resistance is induced by motion of vortex due to dragging of core through superconducting matrix and affect values of J_c. Its value depends upon temperature and magnetic field. Maximum value of J_c is observed when $F_L = F_P$, and its value is decreased with increase of T and H. Critical current density is observed to zero at temperature dependent value of H known as irreversibility field (H_{irr}). Irreversibility lines are appeared when graph is drawn between H_{irr} and T as indicated in Fig. 1.28. Cuprates HTSCs have different types of defects namely 0-D point defect, (1D and 2D) correlated and 3D spherical defects. Fig. 1.29 (a) represents the defects free sample of superconductor in the absence of F_P (clean superconductors) and (b, c, d and e) parts of this

figure represents different defects like atomic or point defects, linear or columnar defects, twin boundaries or planar defects and cluster or large random defects respectively.

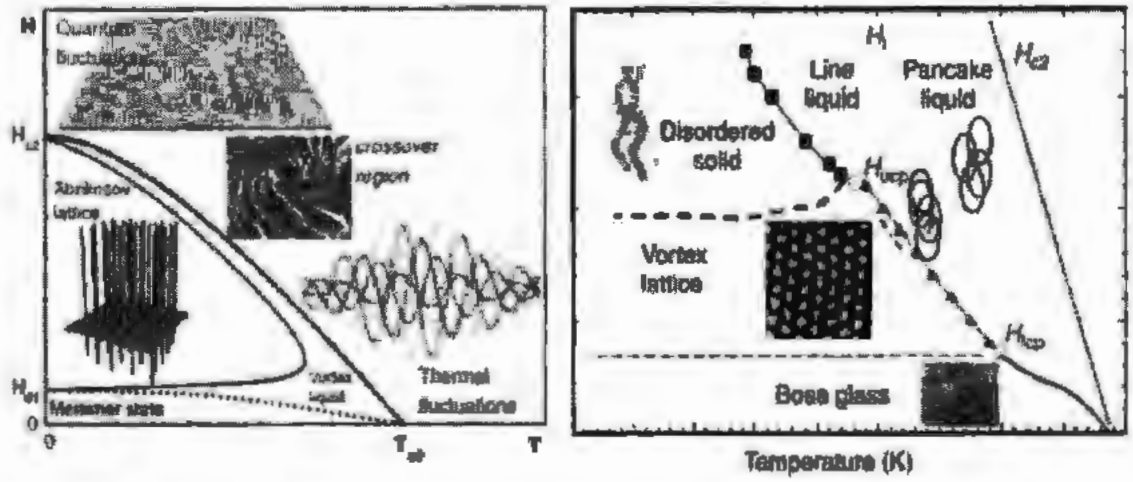

Fig.1.28: Vortex phase representation of HTSCs [134].

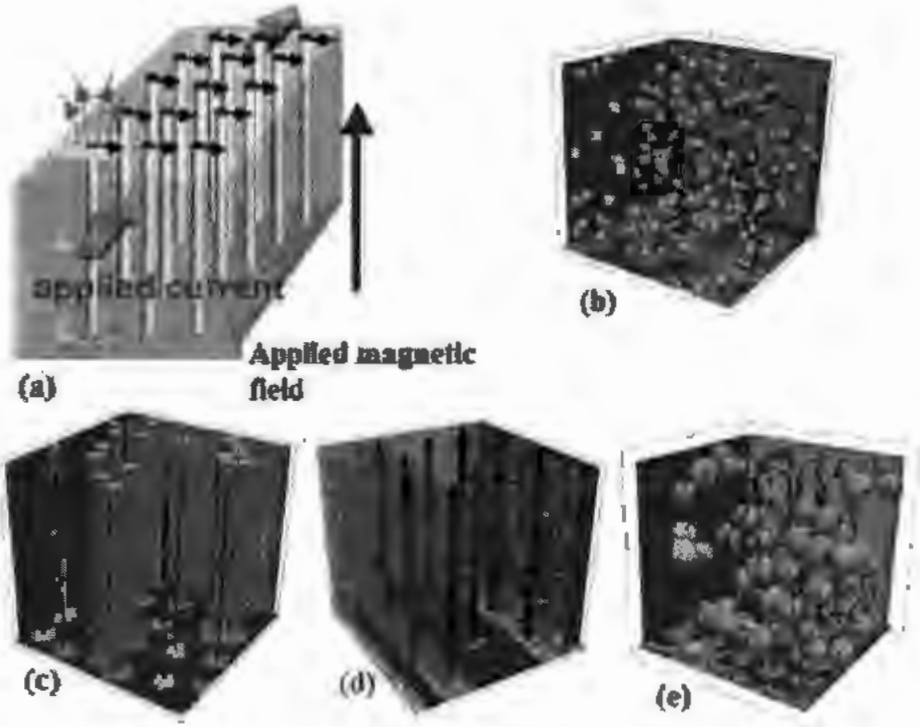

Fig.1.29: Vortex matter 3D illustrations of HTSCs with (a) defects free samples (b) Random atomic or point like defects (c) Linear or columnar defect (d) Planar defects and (e) Large random or cluster defects [135].

Different artificial defects along with natural defects are introduced to pin the vortex motion and these defects are known as artificial pinning centers (APCs). Different additives, ion irradiation, chemical doping, addition of different sizes and shapes of nano-structures are types of APCs as studied in literature [134-140].

Novel and facile technique in HTSCs in order to induce APCs is inclusion of nano-structures. The main idea and objective of this research work is to investigate physical properties (infield, superconducting and magneto-resistance) of CuTl-1223 by inclusion of metallic nanoparticles (MNPs).

1.19 Vortex creep and thermal de-pinning

The mechanism in which vortex pinning is influenced by temperature is known as thermal de-pinning. Thermal de-pinning has two major parts involved in its mechanism.

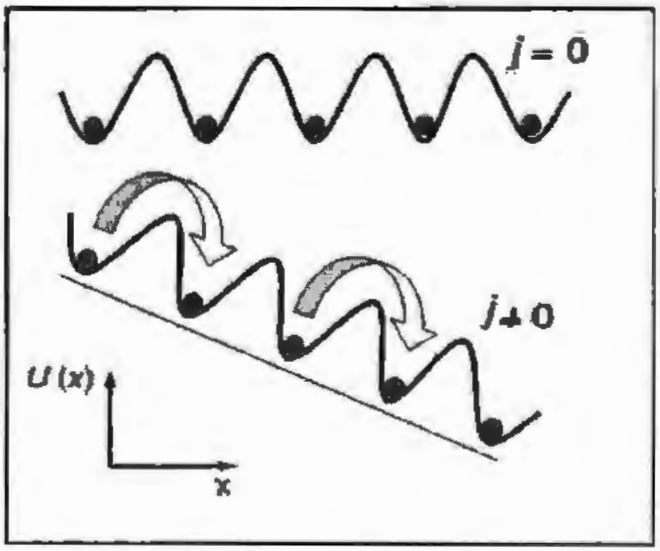

Fig.1.30: Schematic representations of flux flow with J=0 and flux jumping of flux creep with J≠0.

First step involves vibration of flux vortices about their equilibrium position and these flux vortices started to move freely from their pinning sites after getting enough energy. Second part of mechanism involves jumping of flux vortices from one pinning site to another pinning site as result of thermally activated vortices, known as vortices or flux creep. Flux motion of vortices and flux creep with different values of J is shown in Fig.1.30. A single vortex is shown with two different conditions with free energy potential having randomly distributed defects. Creeps in

flux vortices are possible in superconductors only with application of current. When current is not applied the plausibility of flux creep over activation energy barrier is uniform in every direction so, there will be no net flux flow. Net flux takes place in specific direction due to probability of distribution of potential barriers with application of current ($J \neq 0$) to superconducting materials. There is increase of probability of flux hooping bundles in applied current direction, which increase in resistivity. The hooping in flux vortices is possible when $J_o > J$ and flux creep is altered in flux flow with greater J_o due to flatten out potential energy barriers. In 1962, Anderson asserted that vortices can move and they are not static even with driven forces are smaller than pinning forces [141]. Theory of flux creep was developed by Anderson and Kim after two years later [142]. As a result of thermal activation, the vortices can jump between adjacent pinning sites as suggested by flux creep theory of Anderson and Kim. Vortices jumping rate can be expressed as;

$$\upsilon = \upsilon_o e^{\left[\frac{U_o}{k_B T}\right]} \text{----------(1.45)}$$

Here activation energy is expressed by U_o and υ_o is the characteristic frequency and having a value 10^{-8} to 10^{-10} sec^{-1} [143]. In the absence of current, the vortices jumping rate is equal in either direction due to equal potential barriers in both directions. The above reason is true for static vortices without application of current. Potential barrier's height decreases on either side by an amount of ($UL = JBVcd$), for superconducting material in the presence of applied current and same amount of potential height increase on either side. So, net flux creep is of the form;

$$\upsilon_{net} = \left\{\upsilon_o e^{-\frac{U_o}{k_B T}}\right\}\left\{e^{\frac{U_L}{k_B T}} - e^{-\frac{U_L}{k_B T}}\right\}$$

and

$$\upsilon_{net} = 2\upsilon_o e^{\left(-\frac{U_o}{k_B T}\right)} \sinh\left(\frac{U_L}{k_B T}\right) \text{----------(1.46)}$$

where υ_{net} is the flux creep rate and is also known as flux creep velocity. So average flux creep velocity is given by;

$$E = B \times \upsilon$$

So, electric filed induced by vortices flux creep is

$$E=2\upsilon_o Bd e^{\left(\frac{U_o}{k_B T}\right)} \sinh\left(\frac{U_L}{k_B T}\right) \text{----------(1.47)}$$

where d is the average effective jump distance.

1.20 Thermally activated flux flow (TAFF)

In case of J_{app} has a very minute quantity as compared to critical current density then

$$\frac{U_L}{k_B T} \ll 1$$

So, equation 1.47 can be written as

$$E=\frac{2\upsilon_o B^2 f V_c d^2}{k_B T} e^{\left(\frac{U_o}{k_B T}\right)} \text{----------(1.48)}$$

This is known as thermally activated flux flow (TAFF) region. As U_o is comparable to $K_B T$ so, thermal fluctuation is more observable in compound of HTSCs. TAFF model has more thermal effects than flux creep model. We can get resistivity due TAFF by division of E with J, which is given as;

$$\rho=\rho_o e^{\left(\frac{U_o}{k_B T}\right)} \text{----------(1.49)}$$

where $\rho_o=\frac{2\upsilon_o B^2 V_c d^2}{k_B T}$ is called characteristic resistivity, usually represented by normal state resistivity [144-146]. The activation energy U_o is function of temperature, and magnetic field and is given by;

$$U_o(T, H) = f(T)\, U(H) \text{----------(1.50)}$$

and $f(T)$ is given as

$$f(T)=\left(1-\frac{T}{T_p}\right)^m \text{----------(1.51)}$$

where T_p is mean field critical temperature [147], m is normally taken as 1.5 for cuprates HTSCs according to Yeshurun-Malozemoff model but later dissimilar amount were found for various cuprates HTSCs. The values of m dependent on synthesis condition of superconductor [148,

149]. From linear portion's slope of graph between $\ln(\rho/\rho_o)$ and $1/K_BT$, the field dependent activation energy can be extracted [150, 151]. Field dependent activation energy follows various power laws but it commonly abide by $U_o = \beta H^{-\alpha}$ [152-155]. Transition width ($\Delta T = T_c^{onset} - T_c(0)$) can be used for estimation of pinning ability of superconductors in TAFF regime. Suppression observed in pinning potential with enhancement in values of ΔT and vice versa. ΔT also obeys various power laws like activation energy and it is given by [156, 157];

$$\Delta T - \Delta T_o = CH^n \text{----------} (1.51)$$

Here C is dependent on critical current density (J_c).

1.21 Various vortex phases

Abrikosov lattice is regular triangular lattice which arrange vortices in mixed state through repulsive forces. HTSCs have various types of disorder and defects due to its highly anisotropic nature. Fig. 1.30 represents various vortex phases in HTSCs. These vortex types are produced due to exchange of various energies such as vortex-vortex, thermal, coupling and vortex pinning energies respectively. The vortex lattice or solid lattice is produced by vortex-vortex energy. Thermal energy contributes in de-pinning the vortices and as a result vortex liquid appears. The pancake vortices are formed by coupling energy and vortex pinning energy turns the vortex lattice to vortex glass phase. The vortices are initially split into two types, solid vortex state and liquid vortex phase. The effect of disorder and thermal energy on Abrikosov lattice is shown in Fig.1.31 and 1.32. When weak random defects are imported in HTSCs in vortex glass state and long range lattice translational and rotational symmetry are destroyed. The vortex lattice phase is transferred to Bose glass state by induction of 1-D columnar defects such as tracks generated by heavy ion irradiation or 2-D planar twin boundaries. Thermal energy prevail the energy barriers due to vortex-vortex and vortex- pinning interplay, when temperature is increased and as result vortex solid diffuses into vortex liquid. Fluctuations are enhanced in HTSCs due to small coherence length, large anisotropy and temperature. In HTSCs, vortex liquid is considerd as unique state as comparison to vortex solid in which mechanical properties are explained with shear viscosity in place of shear modulus.

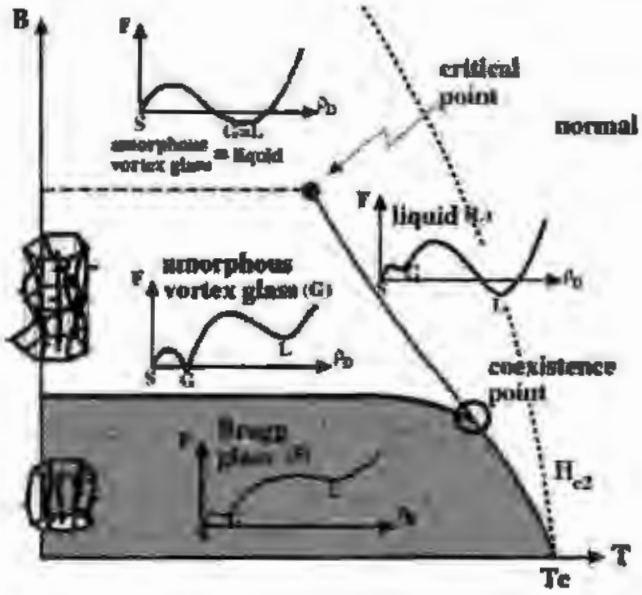

Fig.1.31: Magnetic phase description of HTSCs with numerous types of vortex phases [158].

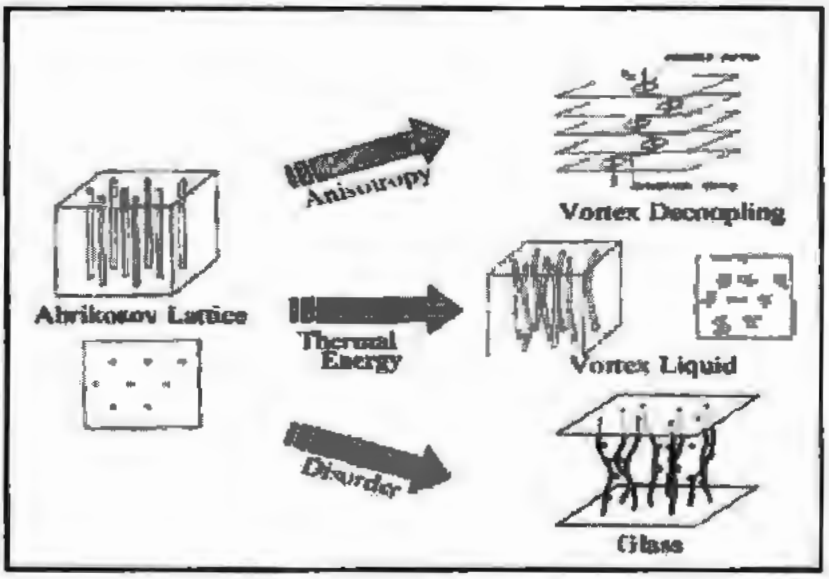

Fig.1.32: Representation of effects on Abrikosove lattice by anisotropy, thermal energy and disorder [159].

1.22 Magnetic hysteresis loop and critical current

Magnetic hysteresis loop gives information about magnetic properties of superconductors. Loop drawn among adapted magnetic field and induced magnetic field of magnetic material is known as M-H loop of materials. Different models are used to calculate the J_c from M-H loop of

superconductors. It also gives clue about magnetic losses of superconductors. Information about retantivity, residual magnetic flux, coercive forces, reluctance and permeability can be obtained by experimental M-H loop of superconductors. Current without resistance in superconducting material can flow when flux lines are pinned and cannot move, called supercurrent. In cuprates HTSCs, grain-boundaries can act as barriers to flow of supercurrent.

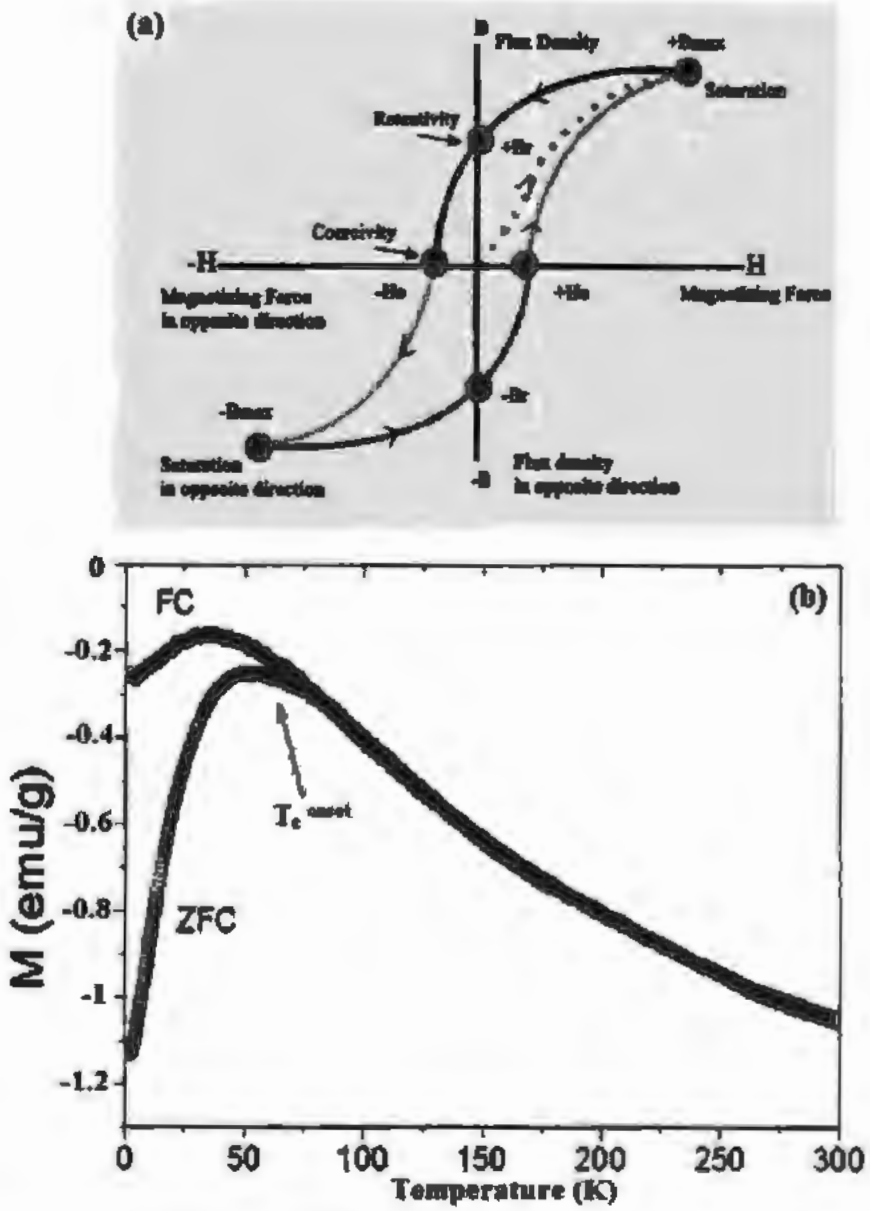

Fig.1.33 (a, b): Schematic representation of M-H loops and FC, ZFC versus temperature curves of superconductors.

Magnetization measurements indicate that J_c in sintered cuprates HTSCs in individual grain is larger than transport critical current density as result of weak-link of these grain-boundaries [63]. It was proposed with simple model by Evetts and Glowacki that at low magnetic field flux enter into materials due to weakly coupled grains [160]. Flux lines cannot pass through materials due to strong coupled grains. When strength of magnetic field is increased then flux has started to penetrate into superconducting materials. The flow of screening current near to surface of individual grain reduced the magnetic field inside grain while it increased near grain-boundaries. Schematic representation of M-H loops and FC, ZFC versus temperature curves of superconductors are represented by Fig. 1.33 (a, b).

1.23 The Bean model

C.P. Bean in 1962 manipulated idea to calculate critical current density by using hysteresis loop and irreversible magnetization [161, 162]. We know that high applied field obeys the condition $H_{app} >> H^*$ so, average internal field H varies in between $(H_{app} + \frac{1}{2}H^*)$ and $(H_{app} - \frac{1}{2}H^*)$ and magnetization of superconducting material is $\mu_o M = H - H_{app}$, also

$$H^* = \mu_o J_c a \text{----------(1.52)}$$

Magnetization difference ($\Delta M = M_+ - M_-$) with high values of hysteresis loop is given by;

$$M_+ - M_- = J_c a \text{----------(1.53)}$$

Equations of upper and lower magnetization are given by;

$$\mu_o M_+ = \frac{H^*}{2} \text{----------(1.54)}$$

$$\mu_o M_- = \frac{H^*}{2} \text{----------(1.55)}$$

According to Bean model formula, the J_c in term of measured magnetization value is given by

$$J_c = \frac{2(M_+ - M_-)}{d} \text{----------(1.57)}$$

Also

$$J_c = \frac{1.59 \times 10^6 \mu_o \Delta M}{d} \text{----------(1.58)}$$

where d = diameter of grain in meter, J_c is in A/m^2, $\mu_0\Delta M$ is in tesla. The Eq.1.58 indicated high field Bean model formula and such an indirect method for J_c measurement using hysteresis loops is widely used. In electromagnetic or cgs unit above equation reduces to

$$J_c = \frac{20\Delta M}{d} \text{----------(1.59)}$$

where d = diameter of grain in cm, J_c is measured in Acm^{-2} and ΔM is measured in emu.

1.24 Nanostructure insertion in HTSCs

Colossal values of J_c and H_{c2} are crucial parameters of HTSCs, which assemble them suitable for practical purposes like permanent magnetic, energy storage articles and solenoids etc. It is therefore essential to exalt flux pinning capabilities of HTSCs with addition of APCs. The consequence of APCs is colossal when size of nanostructure is equal with ξ of superconductors, so these textures may be useful tool as APCs. Profuse researchers have explored the inclusion effects of different (sizes and shapes) structures on physical properties (micro-structural, superconducting, infield, mechanical and dielectric) properties of HTSCs. Few features of various researchers' work in this concern are extracted here.

Crystallization and connectivity between grains were found in order to improve properties by increasing concentration of Ag nanoparticles in $YBa_2Cu_3O_{7-\delta}$ superconductor. The values of I_c and J_c were enhanced with increasing size of Ag NPs till 700 nm and then found to decrease with further increasing size of Ag NPs. The value of J_c observed to be greater in higher concentration samples of Ag nanoparticles than lower concentration of Ag nanoparticles in superconductor [163]. The electrical and mechanical properties of CuTl-1223 superconductor were investigated by inclusion of Ag nanoparticles with different concentration. Crystal structure was un-altered with addition of Ag NPs up to 2 wt. % and phase was found to change to CuTl-1212 with further increasing concentrations. T_c and J_c were improved up to 1.5 wt. % due to increase of volume fraction and was decreased with further increase content of Ag NPs due to phase change or trapping of mobile carriers. The flux pining capability enhanced due to increase of critical current density [164]. Ag NPs with different concentrations were introduced in (Bi, Pb)-2223 superconductor for inspection its properties. Phase formation of (Bi, Pb)-2223 superconductor was reduced with increasing concentration of Ag NPs. Values obtained from E-J curves and J_c were enhanced up to 0.6 wt. % by inclusion of Ag NPs due to NPs refinement among inter-grain connectivity and settlement of these NPs at twin and grain-boundaries [165]. Transport and

micro-structural properties of YBCO SC were elaborated by inclusion of different contents of various metallic oxides NPs. Better superconducting properties were obtained in case of magnetic NPs than non-magnetic NPs [84]. Different concentrations of carbon base nanostructure such as C_x SiC and CNT were used for investigation of $YBa_2Cu_3O_{7-\delta}$ superconductor. T_c was enhanced due to addition of CNT while decreased by addition of C and SiC. The J_o was increased by inclusion of CNT while degraded due to presence of SIC and C in superconductor [166].

Nickel (Ni) NPs encapsulated in carbon were used to investigate different properties of MgB_2 superconductor. Small variation was observed in critical temperature due to homogenous distribution of NPs and carbon within grain. Transport properties enhanced due to better grain connectivity and pinning centers by addition of Ni NPs [167]. YBCO based graphene nanocomposite was studied by using different techniques and degradation in properties were observed in this nanocomposite material [168]. Physical properties of Bi-2212 phase were explored at low temperature by addition of Pr_2O_3 nanoparticles. Different parameters and electrical properties were enhanced up to 0.6 wt. % by addition of these NPs [169]. Average grain size was decreased with increasing contents of Au NPs in YBCO superconductor. This was probably presence of Au NPs among grains, which restricted the growth of samples. I-V measurements were carried out with magnetic field in ranging from 0.3 to 0.7 T and values of J_c were decreased with increasing applied magnetic field due to moving of vortices. The J_c was found highest in all samples which indicated improvement of weak-links [170]. CNTs were used inY123 superconductor to study its properties under normal and high pressure. Electronic properties of Y123 were enhanced with addition of CNTs and increasing rate of normal state resistivity in undoped sample was four times larger than doped samples under pressure. Critical temperature was increased with increase of pressure in Y123 superconducting samples with inclusion of CNTs [171]. Magnetoresistance study was carried out with inclusion different contents of $BaZrO_3$ (BZO) in $YBa_2Cu_3O_{7-\delta}$. Increase in residual resistivity and room temperature resistivity was increased with BZO NPs inclusion in YBCO superconductor. H_{c2} (0) was enhanced to some optimum levels (2 wt. %) in YBCO superconductor with insertion of BZO NPs. Also activation energy (U_o) and glass transition temperature (T_g) were increased to some optimum level which showed increase of grain connectivity with addition of BZO NPs [172].

$BaCeO_3$ (BCO) nanoparticles embedded within $YBa_2Cu_3O_{7-\delta}$ and BiFeO3 (BFO) within single crystals $YBa_2Cu_3O_{7-\delta}$ were fabricated, explored their superconducting properties. Smaller grain size was observed in these samples due to reduction of growth rate of superconductors. Enhanced superconducting properties as well as magnetic levitation force observed due to these NPs acted as multi-source pinning centers in these samples [173, 174]. Normal state resistivity was suppressed and hence critical temperature increased with addition of graphene oxide (GO) NPs in YBCO superconductor. Maximum value of J_c was obtained as result of reduced porosity and enhanced pinning properties at optimum of 0.7 wt. % of GO NPs [175]. Different properties of $GdBa_2Cu_3O_{7-\delta}$ (Gd123) thin film and superconducting phase were investigated by insertion of $BaSnO_3$ (BSO) nanoparticles, single and multi-wall carbon nanotubes (SWCNTs and MWCNTs) [176, 177] respectively. Enhanced pinning properties were observed in thin film with inclusion of BSO NPs. Critical temperature was increased with certain optimum level in case of SWCNTs (0.06 wt. %) and MWCNTs (0.08 wt. %) and was further decreased with increasing concentration of these CNTs. Also mechanical properties were enhanced up to above mentioned optimum values of these CNTs structures in Gd123 superconductor. Flux pinning properties examined with inclusion of Ni NPs in MgB_2 superconductor. The value of critical current density was suppressed due to weak-links and greater flux penetration in grain-boundaries as a result of addition of Ni in MgB_2 superconductor [178]. Superconducting properties and flux pinning mechanism of YBCO superconductor and multi-layer film were investigated with addition of Al_2O_3, BCO nanodots and BZO nanorods [179, 180]. Superconductivity was degraded with increase contents of Al_2O_3 NPs and T_c was decreased due to agglomerizations and forming larger structure of samples, so unable to pin most of fluxes. On the other hand BCO nanodots and BZO nanodots improved pinning capabilities of superconducting film.

Transport and superconducting properties were explored in YBCO superconductor with CNTs and TiO_2 NPs insertion [181, 182]. Connectivity was improved among superconducting grain by small amount of TiO_2 NPs addition. Conduction mechanism in superconductor was improved with inclusion of these NPs. Maximum values of J_c and hence pinning properties were observed for 0.1 wt. % of TiO_2 NPs. So electrical, magnetization and critical current densities were enhanced remarkably in YBCO superconductor with small amount of TiO_2 NPs insertion. On the other hand T_c was decreased with CNTs up to 0.6 wt. % and was increased with further increase of CNTs contents. Samples with CNTs displayed more values of J_c than pristine sample.

Highest value of J_c found optimum for 0.2 wt. % additions on CNTs due to formation of pinning centers and enhanced flux pinning properties. Critical current density was enhanced with different thickness of ZnO seed impurity in MgB_2 superconducting film and proved that this ZnO impurity served as effective pinning centers [183]. Magnetoresistance measurements were examined in Bi2223 superconductor by Ni impurity with different sintering temperatures. It was observed that properties enhanced up to temperature of 700 °C and then decreased with further increase of temperature. Also flux pinning properties were improved by inclusion of Ni impurity optimum level of 700 °C [184]. Superconducting properties and T_p were suppressed with addition of K_2CO_3 as a result of carbon doping and pinning properties were decreased with co-doped of Al & SiC in MgB_2 superconducting phase [185, 186]. Mechanical, superconducting and magnetic properties were investigated for BSCCO superconductor by addition of carbon encapsulated nano-boron (CENB). Hardness as measured by mechanical properties was increased with CENB addition. The J_c was enhanced optimum level of 0.1 wt. % and was further decreased with increasing contents of CENB in BSCCO superconductor as result of aggregation of CENB in grain-boundaries. Also amount of J_c were lessened with increasing strength of magnetic field [187]. Crystalline size, stress, lattice strain and T_c were suppressed with increasing contents of Ag & CNT in YBCO superconducting phase [188]. On the other hand lattice strain was increased with insertion of GO NPs in YBCO superconductor. T_c, J_c and pinning energy were enhanced remarkably with inclusion of GO in YBCO superconductor [189]. Superconducting transport properties were studied with addition of graphene NPs with different concentrations in Tl-1212 superconductor. The amount of T_c and J_c were lessened with raising contents of graphene NPs [190]. The Ni NPs with x= 0~ 10 wt. % were added in CuTl-1223 superconductor for investigation of superconducting and flux pinning properties [191]. $T_c(0)$ and T_c^{onset} were decreased with Ni addition in CuTl-1223 superconductor. London penetration depth, inter-layer coupling and coherence length along c-axis were decreased with increasing contents of Ni NPs. However J_c was increased to some extent and proved that Ni nanoparticles could be served as effective pinning centers.

CNTs and different sizes nano-wires as well as NPs of TiO_2 were added in YBCO superconductor for investigation of superconducting properties [192, 193]. Superconducting properties enhanced by nano-entities of TiO_2 up to 0.1 wt. %. The T_c was increased with these nano-entities of TiO_2 as result of improvement in grain connectivity while T_c^{onset} was decreased

for low contents and increased for higher concentrations of CNTs. Values of J_c were observed higher in case of TiO_2 nanoparticles than nano-wires, so TiO_2 NPs were considered as better pinning sites than TiO_2 nano-wires. On the other hand the values of J_c were enhanced optimum level of 0.8 wt. % by inclusion of CNTs and found 12 times larger than pristine sample. Crystal size as well as lattice strain were reduced and fluctuation induced conductivity of these nano-composites was suppressed by addition of CNTs. Transport properties of MgB_2 round wires were studied by Au NPs at different sintering temperatures and in the presence of Dc test currents of 50 mA as well as 500 mA with magnetic strength of 3T and 7T. The T_c was observed greater in Dc current of 500 mA than 50 mA and showed significant improvement of almost 10 times in infield measurements in a sample with 7T than 3T magnetic field [194]. Microstructure and superconducting properties of CeO_2 doped YBCO film were explored and found that critical current was increased first and then decreased with temperature [195]. Al_2O_3 and Al_2O_3 along with nano-carbon were inserted in YBCO and MgB_2 superconductors separately [196, 197]. Crystal structure was affected and hence superconducting as well as thermal properties changed by nano-alumina in YBCO superconductor. T_c was suppressed due to lattice strain by inclusion of nano C and Al_2O_3 in MgB_2 superconductor. Activation energy was reduced as result of decrease in J_c and weakens of flux pinning properties by nano-entities in MgB_2 superconductor. Superconducting transport properties were studied with graphene nano-platelets (GnPs) and Ni NPs in YBCO superconductor [198, 199]. Elastic modulus was improved up to 2.5 wt. % and then decreased with further increasing contents of Ni NPs in YBCO superconductor. Porosity was decreased due to better connectivity among grain and superconducting properties were enhanced due to GnPs addition with optimum level of 0.07 wt. %. Transition width was decreased; hence T_c and J_c were enhanced by inclusion of GnPs in YBCO superconductor. Structural, morphological and flux pinning properties were explored by insertion of WO_3 nano-wires and particles in YBCO superconductor [200, 201]. Single sharp transition in ρT curve was observed which indicated better connectivity and dominance of YBCO phase. Magnetic properties were enhanced with WO_3 nano-wires added than pure samples. H_{irr} was observed greater in WO_3 nano-wires as compared of pure sample indicating strong pinning capability. The J_c was enhanced by a factor of 4.3 in the absence of applied magnetic field and by a factor of 21.9 in the presence of applied magnetic field with WO_3 nano-wires addition. Flux pinning properties improved optimum level of 0.10 wt. % by insertion of WO_3 nano-wires. Average

grain size was lessened with additional content of WO_3 NPs. Resistivity was found to increase up to 0.1 wt. % due to disorder, defects and in-homogeneities and T_c was slight decreased with increasing contents of WO_3 NPs. Magnetization, J_c, intra-grain characteristic and pinning properties were enhanced in samples with added WO_3 NPs than un-added sample. Values of J_c were enhanced by a factor of 3.2 for pristine sample and by a factor of 17.3 at 1T magnetic field for WO_3 NPs added samples. The (CuTl)-1223 superconducting phase was explored by insertion of gold (Au) NPs with different contents [202]. As a whole superconducting properties as well as grain size were improved with Au NPs insertion. Numerous nano-structures like In_2O_3 and Fe_2O_3 were inserted in (CuTl)-1223 superconductor while depreciation in porosity and enhancement of superconducting properties were noticed by inclusion of these nano-additives [203, 204]. Suppression in superconducting parameters was noticed in (CuTl)-1223 by insertion of nano Al_2O_3, which was assigned to insulating behaviour of these nanoparticles [205]. Superconducting parameters like critical temperature and current density were enhanced till 0.5 wt. % by insertion of Cr_2O_3 NPs in (Bi, Pb)-Sr-Ca-Cu-O superconductor [206]. The nano Al_2O_3 was inserted in $YBa_2Cu_3O_y$ and decrement in superconducting parameters like T_c and field dependent J_c was witnessed [207]. The $(Cu_{0.5}Tl_{0.25}Pb_{0.25})$-1223 superconducting phase was investigated via addition of ZnO nanoparticles in order to see impact on physical and superconducting properties. Volume fraction, melting point critical temperature and density current were enhanced till 0.8 wt. % while these parameters were lessened on further higher concentrations of ZnO NPs [208]. Various nanoparticles like Fe_3O_4 and CO_3O_4 are inserted in $YBa_2Cu_3O_{7-\delta}$ and (Bi, Pb)-2223 superconductors for investigation of infield superconducting properties and these properties were enhanced until certain optimum level [209, 210]. The Bi-Sr-Ca-Cu-O superconductor was studied by inclusion of Fe_3O_4 NPs and improvement in flux pinning mechanism as well as current carrying property was reported [211]. The peculiar contents of Yb NPs were added in $Bi_2Sr_2Ca_1Cu_2O_y$ to study superconducting properties and suppression in these properties were pointed out after inclusion of these NPs [212].

1.25 Applications of HTSCs in various fields

Oxides based high temperature superconductors are vastly used due to their potential applications in different fields. The utilization of HTSCs for generation, storage, transmission and transformation of electrical power in electronic industry is being estimated all over the world. In order to develop power industry, major efforts are continuously being enhanced and

improved the three critical parameters like T_c, J_c and H_c. SQUIDs and PPMS are important instruments which are being widely used with application of magnetic fields and operated by liquid He (4.2 K) as well as nitrogen (77 K) temperature. In very large scale integration (VLSI) technology, these HTSCs will be utilized extensively in telecommunications and high speed computers in near future. These HTSCs are vastly utilized in medical fields as magnetic resonance imaging (MRI) and in magnetically elevated trains. Some salient applications of superconductivity in various major fields are given below [15];

- ✓ Magnets for variety of devices and passive microwave devices
- ✓ Microelectronics interconnects and electrical energy transport by cables
- ✓ In PPMS and SQUIDS
- ✓ Medicine (Nuclear medicine resonance tomography)
- ✓ Electrical power industry and computers
- ✓ Plasma confinement (High energy physics), microwave detectors and mixtures
- ✓ Transport mechanism (Ships and levitation trains) and in hybrid technology

1.26 Motivation

High temperature superconductors are important for purpose of practical application, so in order to optimize superconducting parameters by modification of grain-boundaries as conducting medium for utilizations in technology and industrial field.

1.26.1 Problem statement

As HTSCs have layered structure with weak links at grain-boundaries and when external magnetic field is applied, the vortex dynamics causes energy dissipation that may vary oxygen contents and carrier densities, resulting the suppression of superconducting properties.

1.26.2 One of the possible solutions

As metallic nanoparticles have conducting nature and can serve as conducting medium as well as artificial pinning centres, which can facilitates the movement of charge carriers to improve superconducting properties and parameters such as, H_c, T_c and J_c.

1.27 Scope of thesis

High temperature superconductors are salient materials to overcome energy crisis of the world. Vortex motion begins among superconductor when temperature is increased which causes

deterioration of fluxes and causes energy dissipation in superconducting materials. So, the challenging milestone for researches, working in era of superconductivity is enhancement in flux pinning of HTSCs. It is required to introduce effective pinning artificial defects along with natural defects in HTSCs. Dislocation, twin boundaries, stacking fault and oxygen deformity can be served as artificial defects. The utmost appropriate and easiest scheme for effective pinning centers is inclusion of various nanostructured materials. In current research, metallic nanoparticles (MNPs) such as Cu, Ag and Au with different concentrations are added in CuTl-1223 superconductor, which are expected to behave as conducting medium among grain to facilitate the movement of charge carriers. Some of crucial specks of scope of this dissertation are indexed below;

- ✓ To investigate response of metallic NPs on physical and infield transport superconducting properties of (CuTl)-1223 SC
- ✓ To examine structural variations in (CuTl)-1223 superconductors by addition of MNPs
- ✓ To investigate flux pinning mechanism of MNPs in superconductor on basis of the TAFF model
- ✓ To evaluate magneto-resistance of superconductor composite by Bean model, Anderson and Kim model
- ✓ To find proper nanostructured material with appropriate concentration and optimum level, this can strengthen flux pinning capability of superconductor composite.

1.28 References

[1] H. K. Onnes, "The superconductivity of mercury", Commun. Phys. Lab. Uni. Leiden, 122 (1911) 122.

[2] C. Kittel, "Introduction to solid state physics", 7th Ed. John Wiley & Sons, U. K. (1996).

[3] D. Safarali, "Theory of conventional and unconventional superconductivity in the high-T_c cuprates and other systems", Nova Science Publishers, Inc. New York (2013).

[4] S. Nakajima,M. Kikuchi, Y. Syono, K. Nagase, T. Oku, N. Kobayashi, D. Shindo, and K. Hiraga, "Improvement in superconductivity of $TlBa_2CaCu_2O_y$ system", Physica C 170 (1990) 443.

[5] J. R. Castellanos, Y. Matsui, E. T. Muromachi, and M. Isobe, "Microstructural characterization of $GaSr_2Ca_2Cu_3O_{9+\delta}$, n=3 member of the homologous series of superconductors $GaSr_2Ca_{n-1}Cu_nO_{2n+3}$, Physica C 251 (1995) 279.

[6] F. London, and H. London, "The electromagnetic equation of superconductor", Proc. Roy. Soc. Lond. A 149 (1935) 71.

[7] J. Bardeen, L. N. Cooper and J. R. Schrieffer, "Theory of superconductivity", Phys. Rev. 108 (1957) 1175.

[8] I. G. Bednorz, and K. A. Mueller, "Possible high Tc superconductivity in the Ba-La-Cu-O system", Zeit. fur Phys. B 64, (1986) 189.

[9] M. K. Wu, J. R. Ashburn, C. J. Torng, P. H. Hor, R. L. Meng, L. Gao, Z. J. Huang, Y. Q. Wang and C. W. Chu, "Superconductivity at 93 K in a new mixed-phase Y-Ba-Cu-0 compound system at ambient pressure", Phys. Rev. Lett. 58 (1987) 908.

[10] S. S. P. Parkin, V. Y. Lee, E. M. Engler, A. E. Nazzal, T. C. Huang, G. Gorman, R. Savoy, and R. Beyers, "Bulk Superconductivity at 125 K in $Tl_2Ca_2Ba_2Cu_3O_x$", Phys. Rev. Lett. 60 (1988) 2539.

[11] A. Schilling, M. Cantoni, J. D. Guo, and H. R. Ott, "Superconductivity above 130 K in the Hg–Ba–Ca–Cu–O system", Nature, 363 (1993) 56.

[12] S. N. Putilin, E. V. Antipov, A. M. Abakumov, M. G. Rozova, K. A Lokshin, D. A. Pavlov, A. M. Balagurov, D. V. Sheptyakov, and M. Marezio, "Effect of fluorination and high pressure on the structure and properties of the Hg-bearing superconducting Cu mixed oxides", Physica C 338 (2000) 52.

[13] S. N. Putilin, E. V. Antipov, O. Chmaissem, and M. Marezio, "Superconductivity at 94 K in $HgBa_2CuO_{4+\delta}$", Nature 362 (1993) 226.

[14] G. Blatter, V. B. Geshkenbein, and A. I. Larkin, "From isotropic to anisotropic superconductors: A scaling approach", Phys. Rev. Lett. 68 (1992) 875.

[15] A. K. Saxena, "High temperature superconductors", Springer, Verlag, Berlin, Germany (2010).

[16] V. L. Ginzberg and E. A. Andryushin, "Superconductivity", World Sci. Pub. U.K. (1994).

[17] C. G. Goincoli "Physics", 4th Ed. Prentice Hall (1995).

[18] F. J. Owens and C. P. Poole, Jr., "Electromagnetic absorption in the copper oxide superconductors", Kluwer, Acad. Pub. U. S. A (2002).

[19] V. L. Ginzberg and D. A. Kirzhnits, "High temperature superconductivity", Cons. Bur. Pub. Corp. New York (1976).

[20] D. M. Buczek, L. J. Masur, P. K. Miles, F. Sivo, D. Marlowe, E. R. Podtburg, D. R. Parker, S. Fleshler, and J. D. Scudiere, "Manufacturing of HTS composite wire for a superconducting power transmission cable demonstration", IEEE Trans. Appl. Supercond. 7 (1997) 2196.

[21] T. Hasegawa, T. Koizumi, Y. Hikichi, T. Nakatsu, R. M. Scanlan, N. Hirano, and S. Nagaya, "HTS Conductors for Magnets", IEEE Trans. Appl. Supercond. 12 (2002) 1136.

[22] A. P. Malozemoff, W. Carter, S. Fleshler, L. Fritzemeier, Q. Li, L. Masur, P. Miles, D. Parker, R. Parrella, E. Podtburg, G. N. Riley JR., M. Rupich, J. Scudiere, and W. Zhang, "HTS wire at commercial performance levels", IEEE Trans. Appl. Supercond. 9 (1999) 2469.

[23] R. G. Sherma, "Superconductivity: Basics and applications to magnets", Springer Int. Pub. Switzerland (2015).

[24] M. A. Omar, "Elementary solid state physics", 3rd Ed. Addison-Wesley Pub. Comp. (2007).

[25] L. N. Cooper, "Bound electron pairs in a degenerate fermi gas", Phys. Rev. 104 (1956) 1189.

[26] J. F. Annett, "Superconductivity, super-fluids and condensates", Oxford Uni. Press (2004).

[27] J. Bardeen, L. N. Cooper, and J. R. Schreiffer, "Theorey of superconductivity", Phys. Rev. **108** (1957) 1175.

[28] A. G. Lebed, "The Physics of organic superconductor and conductors", 1st Ed. Springer Series Mat. Sci. (2008).

[29] M. Tinkham, "Introduction to superconductivity", 2nd Ed. McGraw-Hills, New York, NY: (1996).

[30] A. A. Abrikosove, "On the magnetic properties of superconductors of the second group", Soviet Phys. JETP 5, (1957) 1174.

[31] D.R. Tilley, and J. Tilley, "Super-fluidity and superconductivity", 3rd Ed. IOP Pub. (1990).

[32] J. B. Kettereson, and S. N. Song "Superconductivity", Cambridge Uni. Press (1999).

[33] V. V. Schmidt, "The Physics of Superconductors", Springer-Verlag,Berling, Heidelberg (1997).

[34] I. I. Mazin and V. P. Antropov, "Electronic structure, electron–phonon coupling, and multiband effects in MgB_2", Physica C **385** (2003) 49.

[35] H. J. Choi, M. L. Cohen, and S. G. Louie, "Anisotropic Eliashberg theory of MgB_2: T_c, isotope effects, superconducting energy gaps, quasiparticles, and specific heat", Physica C **385** (2003) 66.

[36] F. R. Fickett, "Standards for measurement of the critical fields of superconductors", J. Res. Nat. Bure. Stand. **90** (1985) 95.

[37] D. D. Hughes, "Flux pinning mechanisms in type II superconductors", Phil. Mag. 30 (1974) 2.

[38] A. M. Campbell, and J. E. Evetts, "Flux vortices and transport currents in type-II superconductors", Adv. Phys. **50** (2001) 1249.

[39] A. M. Campbell, J. E. Evetts, and D. D. Hughes, "Pinning of flux vortices in type- II superconductor", Phil. Mag. **18** (1968) 313.

[40] C. A. C. Passos, M. T. D. Orlando, J. L. Passamai, Jr., E. V. L. de Mello, H. P. S. Correa, and L. G. Martinez, "Resistivity study of the pseudogap phase for (Hg, Re)-1223 superconductors", Phys. Rev. B **74** (2006) 094514.

[41] A. L. Solovjov, H. U. Habermeier, and T. Haage, "Fluctuation conductivity in $YBa_2Cu_3O_{7-y}$, $YBa_2Cu_3O_{7-y}$ films with different oxygen content. II. YBCO films with $T_c \approx 80$ K", Low Temp. Phys. **28** (2002) 99.

[42] A. Marouchkine, "Room-temperature superconductivity", 1st Ed. Cambridge Int. Sci. Pub. U.K. (2004).

[43] V. L. Ginzburg, and L. D. Landau, "On the theory of superconductivity", Zh. Eksp. Teor. Fiz. **20** (1950) 1064.

[44] L. D. Landau, and E. M. Lifshitz, "Statistical physics", 3rd Ed. Pergamon Press, Oxford, U. K. (1980).

[45] H. Frohlich, "Theory of the superconducting state. I. The ground state at the absolute zero of temperature", Phys. Rev. **79** (1950) 845.

[46] E. Maxwell, "Isotope effect in the superconductivity of mercury", Phys. Rev. **78** (1950) 477.

[47] C. A. Reynold, B. Serin, W. H. Wright, and L. B. Nesbitt, "Superconductivity of isotopes of mercury", Phys. Rev. **78** (1950) 487.

[48] B. Betlogg, "Cuprate superconductors: Science beyond high T_c", Solid State Commun. **107** (1998) 639.

[49] H. Ibach, and H. Luth, "Solid state physics", 2nd Ed. Springer, Berlin, (1996).

[50] C. M. Varma, "High-temperature superconductivity: Mind the pseudogap", Nature 468 (2010) 184.

[51] G. Baskaran, and P. W. Anderson, "Gauge theory of high-temperature superconductors and strongly correlated Fermi systems", Phys. Rev. B 37 (1988) 580.

[52] A. Mourachkine, "Quasi-one-dimensional topological-excitation liquid in $Bi_2Sr_2CaCu_2O_{8+x}$ from tunnelling spectroscopy", Supercond. Sci. Technol. 14 (2001) 329.

[53] G. Baskaran, "Principle of valence bond amplitude maximization in cuprates: Superconductivity and spin and charge ordering", Phys. Rev. B 64 (2001) 092508.

[54] B. D. Josephson, "Possible new effects in superconductive tunnelling", Phys. Lett. 1 (1962) 251.

[55] V. Emery and S. Kivelson, "Importance of phase fluctuations in superconductors with small superfluid density", Nature 374 (1995) 434.

[56] C. P. Poole, T. Datta, and H. A. Farach, "Copper oxide superconductors" John Wiley and Sons Inc. New York, NY; (1988).

[57] A. Iyo, Y. Ishiura, Y. Tanaka, P. Badica, K. Tokiwa, T. Watanabe, and H. Ihara, "Effects of residual carbon on phase formation of $TlBa_2Ca_{n-1}Cu_nO_y$ (n=3 and 4) superconductors", Physica C 370 (2002) 205.

[58] X. Zhang, C. R. A. Catlow, S. C. Parker, and A. Wall, "Simulation study of pressure-induced structural changes in La_2CuO_4 and in $La_{1.83}Sr_{0.17}CuO_4$", J. Phys. Chem. Solids 53 (1992) 761.

[59] P. Millet, O. Seeger, R. Enjalbert, and J. Galy, "Preferential crystallographic site substitution and oxygen migration in $Bi_2\{Sr, Ca, Ln\}_3Cu_2O_8$ related to rare earth ion size (Ln= La, Yb)", J. Solid State Chem. 90 (1991) 344.

[60] S. Sato, I. Nakada, T. Kohara, and Y. Oda, "Structure of high-T_c superconducting tetragonal $Ba_2YCu_{3-x}O_{7-y}$ at 298 and 120 K", Acta Cryst. C 44 (1988) 11.

[61] E. Dagotto, "Correlated electrons in high-temperature superconductors", Rev. Mod. Phys. 66 (1994) 763.

[62] J. Ruvalds, "Theoretical prospects for high-temperature superconductors", Supercond. Sci. Technol. 9 (1996) 905.

[63] R. Wesche, "Physical properties of high temperature superconductors", 1st Ed. John Wiley & Sons Ltd. U. K. (2015).

[64] F. A. List, D. M. Kroeger, and V. Selvamanickam, "Hysteresis of the transport critical current of (Tl,Pb)-(Sr,Ba)-Ca-Cu-O and Bi–Sr–Ca–Cu–O conductors: Effects of temperature and magnetic field", Physica C 275 (1997) 220.

[65] L. Cesnak, T. Melisek, P. Kovac, and I. Husek, "Magnetic field hysteresis of critical currents in Bi(2223)/Ag tapes and a way to overcome it", Cryogenics 37 (1997) 823.

[66] K. Kimura, M. Morita, M. Tanaka, S. Takebayashi, L. Trouilleux, K. Miyamoto, M. Hashimoto, K. Watanabe, S. Awaji, and N. Kobayashi, "Transport critical current density of melt-processed (QMG) $YBa_2Cu_3O_x$ bulk superconductors", Cryogenics 33 (1993) 506.

[67] M. Lepropre, I. Monot, M. P. Delamare, M. Hervieu, Ch. Simon, J. Provost, G. Desgardin, B. Raveau, J. M. Barbut, D. Bourgault, and D. Braithwaite, "Critical currents up to 71000 Acm^{-2} at 77K in melt textured YBCO doped with $BaSnO_3$", Cryogenics 34 (1994) 63.

[68] H. Ikuta, T. Yamada, M. Yoshikawa, Y. Yanagi, Y. Ytoh, B. Latha, and U. Mizutani, "Melt processing of (rare earth)-Ba-Cu-O bulk superconductors", Supercond. Sci. Technol. 18 (2005) S119.

[69] K. Iida, N.H. Babu, Y.H. Shi, D.A. Cardwell, and M. Murakami, "Gd-Ba-Cu-O bulk superconductors by a seeded infiltration growth technique under reduced oxygen partial pressure, Supercond. Sci. Technol. 19 (2006) 641.

[70] M. Muralidhar, M. Jirsa, and M. Tomita, "Flux pinning and superconducting properties of melt-textured NEG-123 superconductor with TiO_2 addition, Physica C 470 (2010) 592.

[71] P. Diko, V. Antal, K. Zmorayova,M. Sefcikoa, X. Chaud, J. Kovac, X. Yao, I. Chen, M. Eisterer, and H.W. Weber, "The influence of post-growth thermal treatments on the critical current density of TSMG YBCO bulk superconductors", Supercond. Sci. Technol. 23 (2010) 124002.

[72] S. Elschner, J. Bock, and S. Gauss, "Development of HTSC-rings for inductive fault current limiters, Advances in superconductivity VII," Springer-Verlag, Tokyo (1995).

[73] J. F. Fagnard, S. Elschner, J. Bock, M. Dirickx, B. Vanderheyden, and P. Vanderbemden, "Shielding eficiency and E(J) characteristics measured on large melt cast Bi-2212 hollow cylinders in axial magnetic fields", Supercond. Sci. Technol. 23 (2010) 095012.

[74] R. Wesche, "Temperature dependence of critical currents in superconducting Bi-2212/Ag wires", Physica C 246 (1995) 186.

[75] L. H. Allen, P. R. Broussard, J. H. Claassen, and S. A. Wolf, "Temperature and field dependence of the critical current densities of Y–Ba–Cu–O films", Appl. Phys. Lett. 53 (1988) 1338.

[76] D. P. Norton, A. Goyal, J. D. Budai, D. K. Christen, D. M. Kroeger, E. D. Specht, Q. He, B. Safian, M. Paranthaman, C. E. Klabunde, D. F. Lee, B. C. Sales, and F. A. List, "Epitaxial $YBa_2Cu_3O_7$ on bi-axially textured nickel (001): An approach to superconducting tapes with high critical current density", Science 274 (1996) 755.

[77] P. Schmitt, L. Schultz, and G. S. Ischenko, "Electrical properties of $Bi_2Sr_2CaCu_2O_x$ thin films prepared in situ by pulsed laser deposition", Physica C 168 (1990) 475.

[78] J. T. Kucera, D. G. Steel, D. W. Face, J. M. Graybeal, T. P. Orlando, and D. A. Rudman, "Critical current densities in textured thin films of Bi–Sr–Ca–Cu-oxide", Physica C 162–164 (1989) 671.

[79] J. E. Tkaczyk, J. A. DeLuca, P. L. Karas, P. J. Bednarczyk, D. K. Christen, C. E. Klabunde, and H. R. Kerchner, "Enhanced transport critical current at high fields after heavy ion irradiation of textured $TlBa_2Ca_2Cu_3O_z$ thick films", Appl. Phys. Lett. 62 (1993) 3031.

[80] A. A. Gapud, J. Z. Wu, L. Fang, S. L. Yan, Y. Y. Xie, M. P. Siegal, and D. L. Overmyer, "Supercurrents in $HgBa_2CaCu_2O_{6+\delta}$ and $TlBa_2CaCu_2O_7$ epitaxial thin films", Appl. Phys. Lett. 74 (1999) 3878.

[81] S. H. Jun, J. Z. Wu, S. C. Tidrow, and D. W. Eckart, "Growth of $HgBa_2Ca_2Cu_3O_{8+\delta}$ thin films on $LaAlO_3$ substrates using fast temperature ramping Hg-vapor annealing", Appl. Phys. Lett. 68 (1996) 2565.

[82] S. H. Jun and J. Z.Wu, "Superconductivity above 130 K in high-quality mercury-based thin films, Appl. Phys. Lett. 68 (1996) 862.

[83] S. Tonies, H. W. Weber, G. Gritzner, O. Heiml, and M. H. Eder, "Tl-1223 thick films – A competitor for Y-123 coated conductors?", IEEE Trans. Appl. Supercond. 13 (2003) 2618.

[84] C. Stolzel, M. Huth, and H. Adrian, "c-axis oriented thin $Bi_2Sr_2CaCu_2O_{8+\delta}$ films prepared by lash-evaporation", Physica C 204 (1992) 15.

[85] V. S. Dang, P. Mikheenko, A. Sarkar, M. M. A. Kechik, J. S. Abell, and A. Crisan, "Increased critical current density and pinning in thick $Ag/YBa_2Cu_3O_{7-x}$ multilayers", Physica C 470 (2010) 1238.

[86] F. London, and H. London, "Supraleitung und diamagnetismus", Physica 2 (1935) 341.

[87] C. P. Poole, H. A. Farach, and R.I. Creswick, "Supercoductivity", Acad. Press, San Diego (1995).

[88] L. K. Elbaum, C. C. Tsuei, and A. Gupta, "High current densities above 100K in the high temperature superconductor $HgBa_2CaCu_2O_{6+\delta}$", Nature 373 (1995) 679.

[89] Y. Tsabba and S. Reich, "Giant mass anisotropy and high critical current in Hg-1223 superconducting films", Physica C 269 (1996) 1.

[90] R. Hott, H. Rietschel, and M. Sander, "Hoch-T_c-Supraleiter: Wie steht es mit den Anwendungen?", Phys. Bl. 48 (1992) 355.

[91] A. Maignan, C. Martin, V. Hardy, Ch. Simon, M. Hervieu, and B. Raveau, "A crystal study of the 128 K superconductor $Tl_2Ba_2Ca_2Cu_3O_{10-\delta}$ synthesis and anisotropic magnetic properties", Physica C **219** (1994) 407.

[92] P. Monthous, A.V. Balatsy, and D. Pines, "Weak-coupling theory of high-temperature superconductivity in the antiferromagnetically correlated copper oxides", Phys. Rev. B **46** (1992) 14803.

[93] P. Monthoux, D. Pines, and G. G. Lonzarich, "Superconductivity without phonons", Narture **450** (2007) 1177.

[94] H. Monien, M. Takigawa, and D. Pines, "Application of the antiferromagnetic-Fermi-liquid theory to NMR experiments on $YBa_2Cu_3O_{6.63}$", Phys. Rev. B **43** (1991) 258.

[95] H. Ihara, "How to achieve the best performance superconductor based on Cu-1234", Physica C **364-365** (2001) 289.

[96] J. Y. Juang, J. H. Horng, S. P. Chen, C. M. Fu, K. H. Wu, T. M. Uen, and Y. S. Gou, "Enhancement of critical current density in direct-current-sputtered $TlBa_2Ca_2Cu_3O_{9\pm\delta}$ superconducting thin films", Appl. Phys. Lett. **66** (1995) 885.

[97] J. Kortus, "Current progress in the theoretical understanding ofMgB_2", Physica C **456** (2007) 54.

[98] T. Watanabe, S. Miyashita, N. Ichioka, K. Tokiwa, K. Tanaka, A. Iyo, Y. Tanaka and H. Ihara, "Carrier doping and superconducting properties in Cu-1234 and CuTl-1223 superconductors", Physica B **284–288** (2000) 1075.

[99] A. Brinkman, A. A. Golubov, H. Rogalla, O. V. Dolgov, J. Kortus, Y. Kong, O. Jepsen, and O. K. Andersen", "Multiband model for tunneling inMgB_2 junctions", Phys. Rev. B **65** (2002) 180517.

[100] P. G. Vassilev, "Superconducting and normal properties of $Y_{1-x}Ba_2Cu_3O_{7-y}$, $YBa_{2(1-x)}Cu_3O_{7-y}$ and $YBa_2Cu_{3(1-x)}O_{7-y}$", Physica C **153-155** (1988) 868.

[101] S. S. P. Parkin, V. Y. Lee, A. I. Nazzal, R. Savoy, T. C. Huang, G. Gorman, R. Beyers," Model family of high-temperature superconductors: $Tl_mCa_{n-1}Ba_2Cu_nO_{2(n+1)+m}$ (m=1,2; n=1,2,3)", Phys. Rev. B **38** (1988) 6531.

[102] R. Hott, H. Rietschel, and M. Sander, "Hoch-T_c-Supraleiter: Wie steht es mit den Anwendungen?", Phys. Bl. **48** (1992) 355.

[103] R. S. Liu, J. L. Tallon, and P. P. Edwards, "An efficient and reproducible approach for attaining superconductivity at 128K in $Tl_2Ba_2Ca_2Cu_3O_{10-\delta}$", Physica C **182** (1991) 119.

[104] A. Maignan, C. Martin, M. Huve, J. Provost, M. Hervieu, C. Michel, and B. Raveau, "The "2201" thallium cuprate: T_c's up to 92 K can be achieved by "hydrogen" annealing", Physica C **170** (1990) 350.

[105] J. Hejtmanek, M. Nevriva, E. Pollert, D. Sedmidubsky, and P. Vasek, "Superconductivity and transport of $Bi_{2+x}Sr_{2-y}CuO_{6+\delta}$ single crystals", Physica C **264** (1996) 220.

[106] T. Schweizer, R. Muller, and L. J. Gauckler, "A wet chemistry method to determine the Bi and Cu valencies in Bi–Sr–Ca–Cu-O (2212) high-temperature superconductors, Physica C **225** (1994) 143.

[107] H. Alloul, J. Bobroff, M. Gabay, and P. J. Hirschfeld, "Defects in correlated metals and superconductors", Rev. Mod. Phys. **81** (2009) 45.

[108] M. Tachiki and S. Takahashi, "Effect of intrinsic pinning on critical current in cuprate superconductors", Cryogenics **32** (1992) 923.

[109] P. Mangin, and R. Kahn, "Superconductivity: An introduction", Springer, Int. Pub. AG, Switzerland (2017).

[110] A. Salama, M. El-Hofy, Y. Rammah and M. Elkhatib, "Effect of magnetic and nonmagnetic nano metal oxides doping on the critical temperature of a YBCO superconductor", Adv. Nat. Sci. **6** (2015) 045013.

[111] D. Dimos, P. Chaudhari, J. Mannhart, and F. K. LeGoues, "Orientation dependence of grain-boundary critical currents in $YBa_2Cu_3O_{7-\delta}$ bicrystals", Phys. Rev. Lett. **61** (1988) 219.

[112] D. Dimos, P. Chaudhari, and J. Mannhart, "Superconducting transport properties of grain boundaries in $YBa_2Cu_3O_7$ bicrystals", Phys. Rev. B 41 (1990) 4038.

[113] A. Schmehl, B. Goetz, R. R. Schulz, C. W. Schneider, H. Bielefeldt, H. Hilgenkamp, and J. Mannhart, "Doping-induced enhancement of the critical currents of grain boundaries in $YBa_2Cu_3O_{7-\delta}$", Euro. Phys. Lett. 47 (1999) 110.

[114] A. Attenberger, J. Hanisch, B. Holzapfel, and L. Schultz, "Electrical transport properties of Bi(2223) [0 0 1] tilt grain boundary junctions", Physica C 372–376 (2002) 649.

[115] V. R. Todt, X. F. Zhang, D. J. Miller, M. S. L. Weber, and V. P. Dravid, "Controlled growth of bulk bicrystals and the investigation of microstructure-property relations of $YBa_2Cu_3O_x$ grain boundaries", Appl. Phys. Lett. 69 (1996) 3746.

[116] Q. Li, Y. N. Tsay, Y. Zhu, M. Suenaga, G. D. Gu, and N. Koshizuka, "Large T_c depression at low angle [1 0 0] tilt grain boundaries", Appl. Phys. Lett. 70 (1997) 1164.

[117] J. Mannhart and H. Hilgenkamp, "Interfaces involving complex superconductors", Physica C 317–318 (1999) 383.

[118] H. Hilgenkamp and J. Mannhart, "Superconducting and normal-state properties of $YBa_2Cu_3O_{7-\delta}$-bicrystal grain boundary junctions in thin films", Appl. Phys. Lett. 73 (1998) 265.

[119] M. Mittag, R. Job, and M. Rosenberg, "Magnetic relaxation and flux creep in ceramic (Bi, Pb)-2223 HTSC", Physica C 174 (1991) 101.

[120] B. Maruszewski, A. Drzewiecki, and R. Starosta, "Anomalous features of the thermomagnetoelastic field in a vortex array in a superconductor: Propagation of love's waves", J. Therm. Stresses 30 (2007) 1049.

[121] B. S. Deaver Jr., and W. M. Fairbank, "Experimental evidence for quantized flux in superconducting cylinders", Phys. Rev. Lett. 7 (1961) 43.

[122] R. Doll, and M. Nabauer, "Experimental proof of magnetic flux quantization in a superconducting ring", Phys. Rev. Lett. 7 (1961) 51.

[123] G. Ireson. "Discovering superconductivity", 1st Ed. John Wiley & Sons, Ltd. U. K. (2012).

[124] G. Blatter, M. F. Man, V. Geshkenbein, A. Larkin and V. M. Vinokur, "Vortices in high-temperature superconductors", Rev. Mod. Phys. 66 (1994) 1125.

[125] V.A. Kashurnikov , A. N. Maksimova, I. A. Rudnev, and D. S. Odintsov, "The critical current density in the layered superconductors with ferromagnetic nanorods", Physica C 528 (2016) 17.

[126] J. Bardeen and M. Stephen, "Theory of the motion of vortices in superconductors", Phys. Rev. 140 (1965) A1197.

[127] S. Kutuk, S. Bolat, C. Terzioglu and S. Altintas, "An investigation of magnetoresistivity properties of an $Y_3Ba_5Cu_8O_y$ bulk superconductor", J. Alloys Compd. 650 (2015) 159.

[128] K. Ma, Y. Postrekhin and W. Chu, "Superconductor and magnet levitation devices", Rev. Sci. Instrum. 74 (2003) 4989.

[129] I. Guillamon, H. Suderow, P. Kulkarni, S. Vieira, R. Cordoba, J. Sese, J. D. Teresa, M. Ibarra, G. Shaw, and S. Bannerjee, "Nanostructuring superconducting vortex matter with focused ion beams", Physica C 503 (2014) 70.

[130] E. Nazarova, A. Zaleski, K. Nenkov, and A. Zahariev, "Intergranular flux pinning in underdoped and overdoped $R_{1-x}Ca_xBa_2Cu_3O_z$ (R=Y, Gd; x=0, 0.2) samples", Physica C 468 (2008) 955.

[131] J. Trastoy, V. Rouco, C. Ulysse, R. Bernard, G. Faini, J. Lesueur, J. Briatico, and J. Villegas, "Nanostructuring of high-T_c superconductors via masked ion irradiation for efficient ordered vortex pinning", Physica C 506 (2014) 195.

[132] R. Arpaia, D. Golubev, R. Baghdadi, M. Arzeo, G. Kunakova, S. Charpentier, S. Nawaz, F. Lombardi, and T. Bauch, "Resistive state triggered by vortex entry in $YBa_2Cu_3O_{7-\delta}$ nanostructures", Physica C 506 (2014) 165.

[133] S. Naqib, and R. Islam, "Field-dependent resistive transitions in $YBa_2Cu_3O_{7-\delta}$ thin films: Influence of the pseudogap on vortex dynamics", Chinese Phys. B 24 (2015) 017402.

[134] S. Ito, Y. Ichino, and Y. Yoshida, "Comparison of flux motion in type-II superconductors including pinning centers with the shapes of nanorods and nanoparticles by using 3D-TDGL simulation", Physica C **518** (2015) 40.

[135] T. Naito, H. Yamamoto, K. Konishi, K. Kubo, T. Nakamura, and H. Mayama, "Critical current density of superconductors with different fractal dimensions", Adv. Mater. Sci. 1 (2016) 15.

[136] Y. Zalaoglu, M. Pakdil, G. Yildirim, M. Dogruer, C. Terzioglu and O. Gorur, "Enhancement of local microstructural distortions, boundary weak-interactions and crucial defeats performed via Bi^{+3}/La^{+3} partial substitution in the Bi-2212 matrix", J. Alloys Compd. **658** (2016) 732.

[137] I. Guillamon, H. Suderow, P. Kulkarni, S. Vieira, R. Cordoba, J. Sese, J. M. De Teresa, M. R. Ibarra, G. Shaw and S. S. Banerjee, "Nanostructuring superconducting vortex matter with focused ion beams", Physica C **503** (2014) 70.

[138] J. Trastoy, V. Rouco, C. Ulysse, R. Bernard, G. Faini, J. Lesueur, J. Briatico and J. E. Villegas, "Nanostructuring of high-T_c superconductors via masked ion irradiation for efficient ordered vortex pinning", Physica C **506** (2014) 195.

[139] M. Shahbazi, X. Wang, S. Ghorbani, M. Ionescu, O. V. Shcherbakova, F. S. Wells, A. V. Pan, S. Dou and K. Choi, "Vortex-glass phase transition and enhanced flux pinning in C^{4+}-irradiated $BaFe_{1.9}Ni_{0.1}As_2$ superconducting single crystals", Supercond. Sci. Technol. **26** (2013) 095014.

[140] A. Park, S. Pyon, T. Tamegai and T. Kambara, "Flux pinning in $Ba_{1-x}K_xFe_2As_2$ superconductor with splayed columnar defects", Physica C **530** (2016) 58.

[141] P. W. Anderson, "Theory of flux creep in hard superconductors", Phys. Rev. Lett. **9** (1962) 309.

[142] P. W. Anderson and Y. Kim, "Hard superconductivity: theory of the motion of Abrikosov flux lines", Rev. Mod. Phys. **36** (1964) 39.

[143] K. Fossheim and A. Sudbo "Superconductivity: Physics and application", John Wiley & Sons, Ltd. U. K. (2004).

[144] S. L. Liu, G. J. Wu, X. B. Xu, J. Wu and H. M. Shao, "The effective activation energy Ueff(T,B,J) in Hg-1223 single phase superconductors", Solid State Commun. **133** (2005) 615.

[145] Y. Tokura, H. Takagi, and S. Uchida, "A superconducting copper oxide compound with electrons as the charge carriers", Nature **337** (1989) 345.

[146] I. A. Ansari, M. Shahabuddin, N. S. Alzayed, A. Vajpayee, V. Awana and H. Kishan, "Enhancement of activation energy in nano diamond doped MgB_2 superconductor", Physica C **470** (2010) 369.

[147] J. Dyson, D. Rinaldi, G. Barucca, G. Albertini, S. Sprio and A. Tampieri, "Flux Pinning in Y-and Ag-Doped MgB_2", Adv. Mater. Phys. Chem. **5** (2015) 426.

[148] M. Rupp, A. Gupta, and C. C. Tsuei, "Magnetic field induced broadening of resistive transition in epitaxial c-axis-oriented $HgBa_2CaCu_2O_{6+\delta}$ films, Appl. Phys. Lett. **67** (1995) 291.

[149] Y. Yeshurun and A. Malozemoff, "Giant flux creep and irreversibility in an Y-Ba-Cu-O crystal: An alternative to the superconducting-glass model", Phys. Rev. Lett. **60** (1988) 2202.

[150] H. Frank, J. Lethen, L. Buschmann, B. Decker, J. Wiesener, G. Wirth, P. Wagner, H. Adrian, P. Lemmens, and G. Guntherodt, "Dimensional crossover in the pinning of heavy-ion irradiated Bi-2212 films", Physica C **259** (1996) 142.

[151] A. Snezhko, T. Prozorov and R. Prozorov, "Magnetic nanoparticles as efficient bulk pinning centers in type-II superconductors", Phys. Rev. B **71** (2005) 024527.

[152] J. Jaroszynski, F. Hunte, L. Balicas, Y. J. Jo, I. Raicevic, A. Gurevich, D. Larbalestier, F. Balakirev, L. Fang and P. Cheng, "Upper critical fields and thermally-activated transport of $NdFeAsO_{0.7}F_{0.3}$ single crystal", Phys. Rev. B **78** (2008) 174523.

[153] A. Sidorenko, V. Zdravkov, V. Ryazanov, S. Horn, S. Klimm, R. Tidecks, A. Wixforth, T.

Koch and T. Schimmel, "Thermally assisted flux flow in MgB_2: strong magnetic field dependence of the activation energy", Philos. Mag. **85** (2005) 1783.

[154] X. L. Wang, S. R. Ghorbani, S. I. Lee, S. X. Dou, C. Lin, T. Johansen, K. H. Muller, Z. Cheng, G. Peleckis and M. Shabazi, "Very strong intrinsic flux pinning and vortex avalanches in (Ba, K) Fe_2As_2 superconducting single crystals", Phys. Rev. B **82** (2010) 024525.

[155] T. Palstra, B. Batlogg, R. V. Dover, L. Schneemeyer and J. Waszczak, "Dissipative flux motion in high-temperature superconductors", Phys. Rev. B **41** (1990) 6621.

[156] A. A. Khurram, S. Ahmad and N. A. Khan, "Flux pinning in $Tl_{1-x}C_xBa_2Ca_3Cu_4O_{12-\delta}$ superconductor", Physica C **480** (2012) 19.

[157] M. Tinkham, Resistive transition of high-temperature superconductors", Phys. Rev. Lett. **61** (1988) 1658.

[158] S. Senoussi, M. Oussena, and S. Hadjoudj, "On the critical fields and current densities of $YBa_2Cu_3O_7$ and $La_{1.85}Sr_{0.15}CuO_4$ superconductors", J. Appl. Phys. **63** (1988) 4176.

[159] H. Yamasaki, K. Ohki, I. Yamaguchi, M. Sohma, W. Kondo, H. Matsui, T. Manabe, and T. Kumagai, "Strong flux pinning due to dislocations associated with stacking faults in $YBa_2Cu_3O_{7-\delta}$ thin films prepared by fluorine-free metal organic deposition", Supercond. Sci. Technol. **23** (2010) 105004.

[160] J. Evetts and B. A. Glowacki, "Relation of critical current irreversibility to trapped flux and microstructure in polycrystalline $YBa_2Cu_3O_7$", Cryogenics **28** (1988) 641.

[161] C. P. Bean. "Magnetization of hard superconductors", Phys. Rev. Lett. **8** (1962) 250.

[162] C. P. Bean. "Magnetization of high-field superconductors", Rev. Mod. Phys. **36** (1964) 31.

[163] M. Farbod, and M. R. Batvandi "Doping effect of Ag nanoparticles on critical current of $YBa_2Cu_3O_{7-\delta}$ bulk superconductor", Physica C **471** (2011) 112.

[164] W. Abdeen, N. H. Mohammed, R. Awad, S. A. Mahmoud, and M. Hasebbo, "Influence of nano-Ag addition on the mechanical properties of $(Cu_{0.5}Tl_{0.5})$-1223 superconducting phase", J. Supercond. Nov. Magn. 26 (2013) 3235.

[165] R. Mawassi, S. Marhaba, M. Roumie, R. Awad, M. Korek, and I. Hassan, "Improvement of superconducting parameters of $Bi_{1.8}Pb_{0.4}Sr_2Ca_2Cu_3O_{10+\delta}$ Added with Nano-Ag", J. Supercond. Nov. Magn. 27 (2014) 1131.

[166] S. Dadras, and M. Ghavamipour, "Investigation of the properties of carbon-base nanostructures doped $YBa_2Cu_3O_{7-\delta}$ high temperature superconductor", Physica B 484 (2016) 13.

[167] Q. Zhao, C. Jiao, Z. Zhu, Z. Chen, and S. Cui, "In-situ synthesis of carbon capsulated Ni nanoparticles and their cooperative doping effects on superconducting properties of MgB_2", J. Alloys Compd. 682 (2016) 441.

[168] M. Colie, D. Mihaiescu, A. Surdu, R. Trusca, B. Vasile, D. Istrati, A. Ficai, C. Plapcianu, and E. Andronescu, "High temperature superconducting materials based on Graphene / YBCO nanocomposite", Mater. Today, Proceed. 3 (2016) 2628.

[169] A. Miura, D. Oikawa, H. Andoh, T. Sughura, and T. Tsukamoto "Effect of Pr additions to Li-doped Bi2212 bulk superconductors sintered at low temperature", Phys. Proced. 8 (2016) 37.

[170] S. Dadras, and Z. Gharehgazloo, "Effect of Au nano-particles doping on polycrystalline YBCO high temperature superconductor", Physica B 492 (2016) 45.

[171] S. Dadras, N. Manivannan, V. Daadmehr, A. T. Rezakhani, and K. H. Kim "Pressure effects on the carbon nano-tube embedded Y-123 superconductors", Physica B 487 (2016) 42.

[172] B. A. Malik, K. Asokan, V. Ganesan, D. Singh, and M. A. Malik "The magnetoresistance of YBCO/BZO composite superconductors", Physica C 531 (2016) 85.

[173] E. Solano, F. Geenen, T. Puig, X. Obradors, C. Mocuta, and C. Detavernier, "Axiotaxy in oxide heterostructures: Preferential orientation of $BaCeO_3$ nanoparticles embedded in superconducting $YBa_2Cu_3O_{7-\delta}$ thin films", Thin Solid Films 638 (2017) 105.

[174] G. Z. Li, S. Y. Wang, J. W. Li, and W. M. Yan, "Introducing multi-source pinning centers into Y–Ba–Cu–O superconductor through addition of $BiFeO_3$ nano-particles", Scripta Materialia 132 (2017) 22.

[175] S. Dadras, S. Dehghani, M. Davoudiniya, and S. Falahati, "Improving superconducting properties of YBCO high temperature superconductor by graphene oxide doping", Mater. Chem. Phys. 193 (2017) 496.

[176] B. Kang, D. H. Tran, and W.N. Kang, "Scaling of pinning forces in $BaSnO_3$-added $GdBa_2Cu_3O_{7-x}$ superconducting thin films", Thin Solid Films 624 (2017) 16.

[177] M. Anas, S. Ebrahim, I. G. Eldeen, R. Awad, and A. I. Abou-Aly, "Effect of single and multi-wall carbon nanotubes on the mechanical properties of Gd-123 superconducting phase", Chem. Phys. Lett. 686 (2017) 34.

[178] Q. Zhao, C. Jiao, E. Zhu, and Z. Zhu, "Refinement of MgB_2 grains and the improvement of flux pinning in MgB_2 superconductor through nano-Ni addition", J. Alloys Compd. 717 (2017) 19.

[179] M. S. M. Suan, and M. R. Johan, "Synthesis of $Y_{1-x}Al_xBa_2Cu_3O_{7-\delta}$ via combustion route: Effects of Al_2O_3 nanoparticles on superconducting properties", Physica B 506 (2017) 178.

[180] M. Malmivirta, H. Rijckaert, V. Paasonen, H. Huhtinen, T. Hynninen, R. Jha, V. S. Awana, I. V. Driessche, and P. Paturi, "Enhanced flux pinning in YBCO multilayer films with BCO nanodots and segmented BZO nanorods", Sci. Report 7 (2017) 14682.

[181] N. A. Khalid, M. M. A. Kechik, N. A. Baharuddin, C. S. Kien, H. Baqiah, N. N. M. Yusuf, A. H. Shaari, A. Hashimb, and Z. A. Talib, "Impact of carbon nanotubes addition on transport and superconducting properties of $YBa_2Cu_3O_{7-\delta}$ ceramics", Ceram. Int. 44 (2018) 9568.

[182] E. Hannachi, Y. Slimani, F. B. Azzouz, and A. Ekicibil, "Higher intra-granular and inter-granular performances of YBCO superconductor with TiO_2 nano-sized particles addition", Ceram. Int. 44 (2018) 18836.

[183] D. Pham, H. V. Ngoc, S. G. Jung, D. J. Kang, and W. N. Kang, "Enhanced critical current density of MgB_2 thin films deposited at low temperatures by ZnO seed impurity", Current Appl. Phys. **18** (2018) 762.

[184] G. Yildirim, "Formation of artificial flux pinning centers in Bi-2223 cuprate superconductor with Ni impurities and enhanced resistant to thermal fluxon motions of correlated 2D pancake vortices in new matrix", J. Alloys Compd. **745** (2018) 100.

[185] J. C. Grivel, "Critical current density improvements in MgB_2 superconducting bulk samples by K_2CO_3 additions", Physica C **550** (2018) 1.

[186] N. S. Kia, S. R. Ghorbani, H. Arabi, and M. S. A. Hossain, "Effect of magnetic field on the flux pinning mechanisms in Al and SiC co-doped MgB_2 superconductor", Solid State Commun. **275** (2018) 48.

[187] H. Ozturk, and S. Safran, "Effects of carbon-encapsulated nano boron addition on superconducting parameters of BSCCO", J. Alloys Compd. **731** (2018) 831.

[188] S. Dadras, and M. Davoudiniya, "Analysis of YBCO high temperature superconductor doped with silver nanoparticles and carbon nanotubes using Williamson–Hall and size–strain plot", Physica C **548** (2018) 116.

[189] S. Dadras, S. Falahati, and S. Dehghani, "Effects of graphene oxide doping on the structural and superconducting properties of $YBa_2Cu_3O_{7-\delta}$", Physica C **548** (2018) 65.

[190] W. Kong, I. Kong, M. M. A. Kechik, and R. Abd-Shukor, "Effect of graphene addition on the transport critical current density of bulk $(Th_{0.85}Cr_{0.15})$ $Sr_2CaCu_2O_{7-\delta}$ superconductor", Mater. Today: Proceed. **5** (2018) 3176.

[191] N. A. Khan, A. Saleem, S. Q. Abbas, and M. Irfan, "Ni nanoparticle-added $Ni_x/(Cu_{0.5}Tl_{0.5})Ba_2Ca_2Cu_3O_{10-\delta}$ superconductor composites and their enhanced flux pinning characteristics", J. Supercond. Nov. Magn. **31** (2018) 1013.

[192] B. Sahoo, S. R. Mohapatra, A. K. Singh, D. Samal, and D. Behera "Effects of CNTs blending on the superconducting parameters of YBCO superconductor", Ceram. Int. **45** (2019) 7709.

[193] Y. Slimani, E. Hannachi, A. Ekicibil, M. A. Almessiere, and F. Ben Azzouz, "Investigation of the impact of nano-sized wires and particles TiO_2 on Y-123 superconductor performance", J. Alloys Compd. **781** (2019) 664.

[194] A. T. Ulgen, F. Karaboga, M. Karakaya, R. Podila, A. M. Rao, and I. Belenli, "Improved transport properties of MgB2 superconducting round wires via minute addition of gold nanoparticles", Ceram. Int. **45** (2019) 1031.

[195] W. Wang, L. Liu, T. Zheng, S. Liu, and Y. Li, "Superconducting properties and microstructures of CeO_2 doped $YBa_2Cu_3O_{7-\delta}$ films fabricated by pulsed laser deposition", Ceram. Int. **45** (2019) 1998.

[196] V. Antal, V. Kavecansky, D. Volochova, and P. Diko, "Thermal reactivity of $YBa_2Cu_3O_{7-\delta}$ with Al_2O_3 addition in air atmosphere", Ceram. Int. **45** (2019) 2866.

[197] I. A. Ansari, "Study of ac-susceptibility for co-doped MgB_2 superconductor with nano-Al_2O_3 and nano-C at low magnetic field", Intermetallics **106** (2019) 100.

[198] B. Sahoo, K. L. Routray, D. Samal, and D. Behera, "Effect of artificial pinning centers on YBCO high temperature superconductor through substitution of graphene nano-platelets", Mater. Chem. Phys. **223** (2019) 784.

[199] H. A. Afifi, I. Z. Hager, N. S. A. Aal, and A. M. Abd El-Aziz, "Study of the effect of Ni additive in $YBa_2Cu_3O_{7-\delta}$ superconducting composite employing ultrasonic measurement", Measurements **135** (2019) 928.

[200] Y. Slimani, M. A. Almessiereb, E. Hannachi, A. Baykal, A. Manikandan, M. Mumtaz, and F. Ben Azzouz, "Influence of WO_3 nanowires on structural, morphological and flux pinning ability of $YBa_2Cu_3O_y$ superconductor", Ceram. Int. **45** (2019) 2621.

[201] Y. Slimani, M. A. Almessiere, E. Hannachi, M. Mumtaz, A. Manikandan, A. Baykal, F. Ben Azzouz, "Improvement of flux pinning ability by tungsten oxide nanoparticles added in $YBa_2Cu_3O_y$ superconductor", Ceram. Int. **45** (2019) 6828.

[202] A. Jabbar, I. Qasim, K. M. Khan, Z. Ali, K. Nadeema, and M. Mumtaz, "Synthesis and superconducting properties of $(Au)_x$/CuTl-1223 composites", J. Alloys Compd. **618** (2015) 11.

[203] N. H. Mohammed, A. I. Abou-Aly, I. H. Ibrahim, R. Awad, and M. Rekaby, "Effect of nano-oxides addition on the mechanical properties of $(Cu_{0.5}Tl_{0.5})$-1223 Phase", J. Supercond. Nov. Magn. **24** (2011) 463.

[204] N. H. Mohammed, A. I. Abou-Aly, R. Awad, I. H. Ibrahim, M. Roumie, and M. Rekaby, "Mechanical and electrical properties of $(Cu_{0.5}Tl_{0.5})$-1223 phase added with nano-Fe_2O_3", J. Low Temp. Phys. **172** (2013) 234.

[205] A. Jabbar, I. Qasim, M. Zaman, K. Nadeem, and M. Mumtaz. "Structural and superconducting properties of $(Al_2O_3)_y$/CuTl-1223 Composites", J. Electron. Mater. **44** (2015) 110.

[206]. H. Abbasi, J. Taghipour, and H. Sedghi. "Superconducting and transport properties of (Bi-Pb)-Sr-Ca-Cu-O with Cr_2O_3 additions", J. alloys Compd. **494** (2010) 305.

[207] A. Mellekh, M. Zouaoui, F. B. Azzouz, M. Annabi, and M. B. Salem, "Nano-Al_2O_3 particle addition effects on $YBa_2Cu_3O_y$ superconducting properties", Solid Stat. Commun. **140** (2006) 318.

[208] M. M. Ebkr, R. Awad, A. A. El-Ghany, A. A. Shama, and A. A. El-wanis, "Effect of nano-sized ZnO on the physical properties of $(Cu_{0.5}Tl_{0.25}Pb_{0.25})Ba_2Ca_2Cu_3O_{10-\delta}$", J. Supercond. Nov. Magn. **24** (2011) 1345.

[209] S. N. Abd-Ghani, R. Abd-Shukor, and W. Kong, "Effects of Fe_3O_4 nano particles addition in high temperature superconductor $YBa_2Cu_3O_{7-\delta}$", Adv. Mater. Res. **501** (2012) 309.

[210] A. N. Jannah, R. Abd-Shukor, and H. Abdullah, "Effect of Co_3O_4 nanoparticles addition on (Bi, Pb)-2223 superconductor", World Acad. Sci. Eng. Technol. **7** (2013) 3.

[211] R. Abd-Shukor, and W. Kong, "Magnetic field dependent critical current density of Bi–Sr–Ca–Cu–O superconductor in bulk and tape form with addition of Fe_3O_4 magnetic nanoparticles", J. Appl. Phy. **105** (2009) 07E311.

[212] H. Gundogmus, B. Ozcelik, B. Ozkurt, A. Sotelo, and M. A. Madre, "Physical, mechanical and magnetic properties of the Yb substituted $Bi_2Sr_2Ca_1Cu_2O_y$ textured superconductor", J. Supercond. Nov. Magn. **26** (2013) 111.

Chapter No. 2

Samples preparation and characterization techniques

The preparation of $(D)_x$/CuTl-1223 nanoparticles-superconductor composites (D= Cu, Ag and Au) is described in this chapter. Different experimental characterization techniques are also explained which have been opted for characterization of nanoparticles superconductor composites.

2.1 Preparation strategy

Sol-gel procedure is used for the synthesis of NPs while solid state reaction technique is utilized for HTSC preparation. The description and advantages of these methods are demonstrated here.

2.1.1 Sol-gel method for nanoparticles preparation

Sol-gel procedure is a multifaceted technique for the preparation of NPs. This synthesis method is utilized to produce variety of nano-materials with novel and pre-defined properties in simple manner with low cost. It consists of metallic organic compound and inorganic metal salts as starting materials. A sol consists of deferment of solid entities in liquid whereas gel means of solid nexus having liquid phase. Sol-gel is commonly utilized for synthesis of different nanostructures due to wide range of precursors and can be performed at low temperature as well. Sol-gel method is preferred over other techniques due to its large number of advantages [1, 2]

- ✓ Morphological control and getting better size of nanoparticles
- ✓ Low cost and low temperature synthesis technique
- ✓ High purity and uniform phase distribution as compared to other techniques

2.1.2 Solid state method for HTSCs preparation

Different techniques have been opted for HTSCs since their discoveries but most suitable and effective technique is solid state reaction method. HTSCs have layered, granular and polycrystalline structure so, it is immense to get command single phase manufacture and free of impurities structure of HTSCs [3-7]. Powder in form of oxides or carbonates in appropriate amount are mixed with each other and this method is required high temperature treatment with 24 to 48 hours. This procedure is also known as two steps solid state reaction mechanism

because of heat treatment is given twice to sample in order to get homogenous precursor. This mechanism has its own advantages and disadvantages. A few demerits are listed below:

- ✓ Difficult to control the size of product or composites in required technique
- ✓ There is no direct and simple way to monitor this synthesis method
- ✓ High temperature ~ 2000 °C in this method is involved in some cases so that large electrical energy is expend to acquire such colossal temperature
- ✓ Chemical homogeneity is difficult to attain in product at molecular level
- ✓ There is chance of addition of impurities during grinding process via grinding media

Solid state reaction procedure is often utilized for synthesis of HTSCs despite all these restrictions. Some facts should be kept in mind for synthesis of HTSCs by using solid state reaction method, which are listed below

- ✓ Heating, temperature and cooling rates must be monitored during synthesis process
- ✓ Purity levels of initial chemical powder must be very high
- ✓ In order to enhance homogeneity in grinding purpose, the grinding must be carried out for long period and intermediate grinding is also required between two heat treatments

2.1.3 Preparation of nanoparticles superconductor composites

To execute objective of our research work, we prepared $(D)_x$/ (CuTl)-1223; (D= Cu, Ag and Au) nanoparticles superconductor composites with help of solid state reaction method accomplished in two steps. For synthesis of nanopartioles, we have taken respective nitrates of these required nanoparticles in appropriate ratios and mixed them in calculated amount of ethanol by mixing in one beaker with continuous stirring. The calculated amount of citric acid and distilled water are mixed in another beaker and placed on magnetic stirrer for continuous stirring. The solution of second beaker is placed in first beaker drop by drop. Ammonia is poured drop by drop to get required pH and then heat is started to get gel. This gel is placed in oven for 15 hours at 100 °C to dry this gel. This dry powder is ground and placed in furnace at different temperature for 2~4 hours to get required NPs. Flow chart for nanoparticle synthesis is shown in Fig. 2.1. Copper cyanides $\{Cu(CN)\}_2$, calcium and barium nitrates $\{Ca(NO_3)_2$ and $Ba(NO_3)_2\}$ are blended with appropriate quantity and crushed for 3 hours in agate motor and pestle.

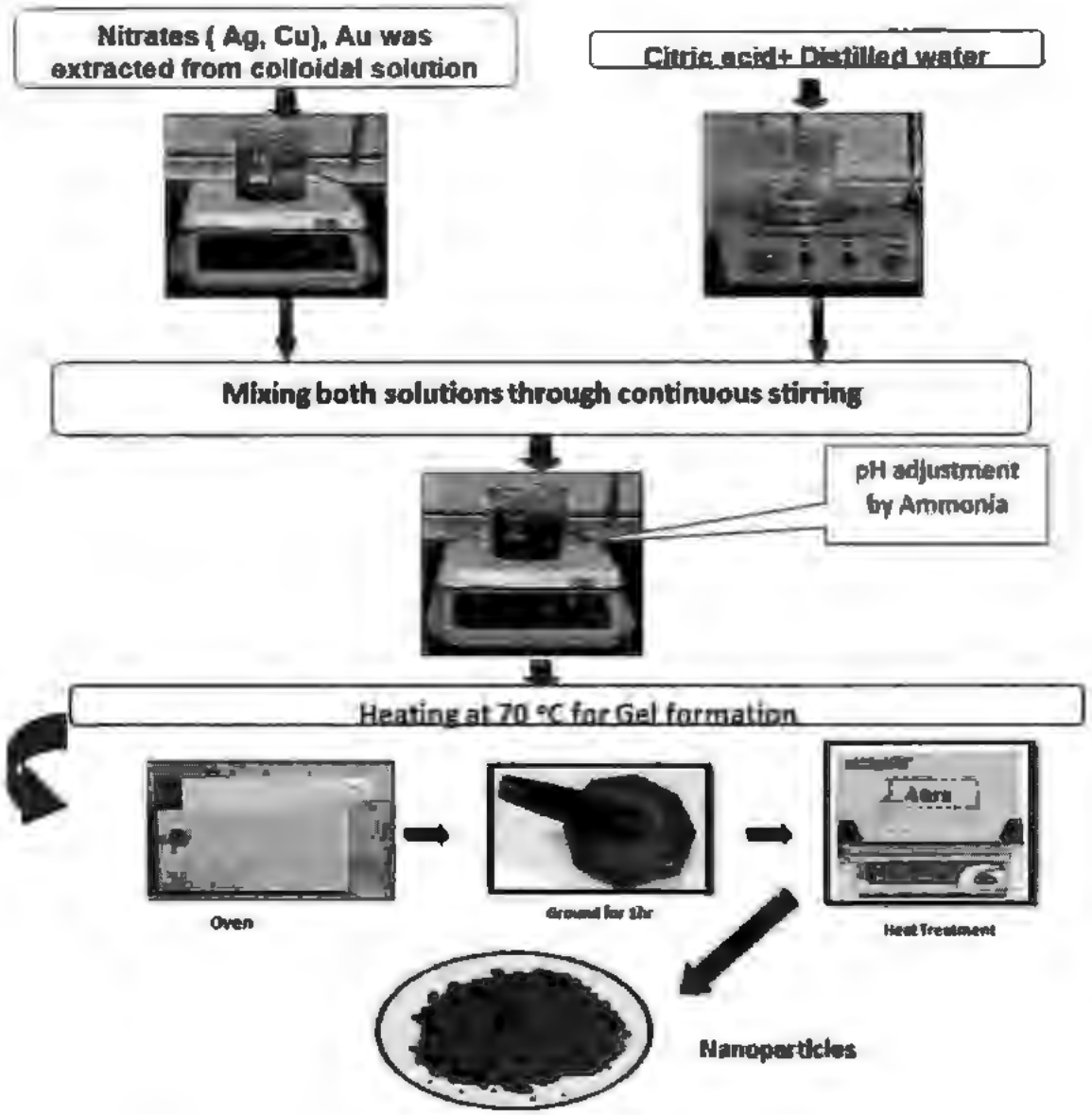

Fig. 2.1: Flow chart of preparation of NPs by sol-gel

The pellets are formed by using 3.8 ton cm^{-2} by hydraulic pressures and sintered in a gold capsule at 860 °C for ten minutes in chamber furnace to get $(D)_x$/ CuTl-1223; (D= Cu, Ag and Au) nanoparticles superconductor composites. Flow chart of NPs superconductor composites is represented by Fig. 2.2.

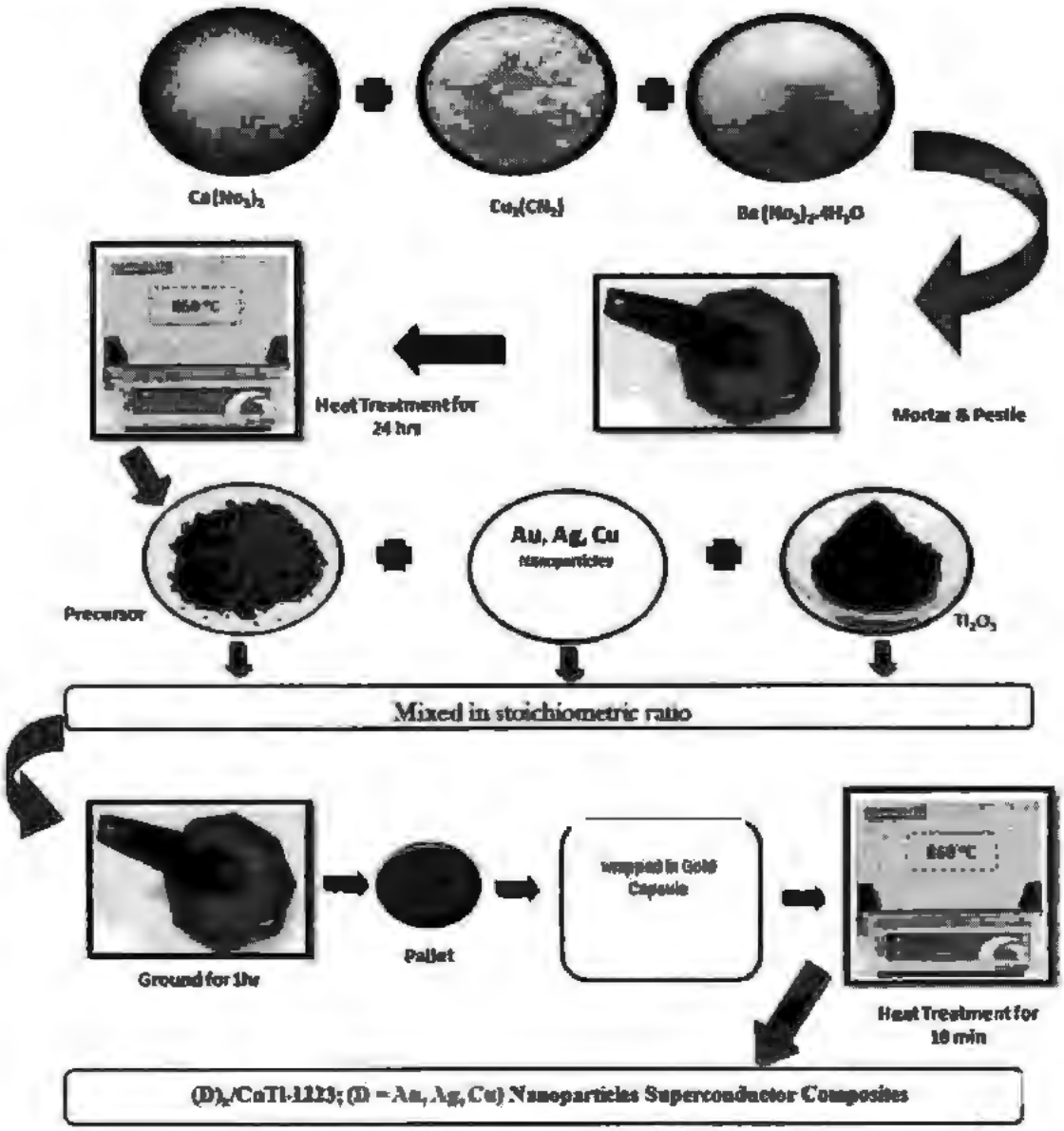

Fig. 2.2: Schematic representation of synthesis of NPs superconductor composite

2.2 Experimental tools

We have used various experimental techniques for the investigation of different properties of $(D)_x$/ CuTl-1223; (D= Cu, Ag and Au) nanoparticles superconductor composites.

2.2.1 X-ray diffraction (XRD) analysis

In 1895 Roentgen rays were discovered by German physicist Wilhelm Roentgen and called X-rays due to its unknown nature at that time. These rays are of electromagnetic nature having

shorter wavelength. X-rays have invisible but have more penetration power than ordinary light [8]. Discovery of X-rays opened new era for different material characterization in different fields. X-rays are electromagnetic radiations having shorter wavelength of around 1 Å produced with declaration of higher energy electrons to inner shells of atom [9]. XRD is a special technique to study crystal symmetry of material. The diffraction pattern will be produced by the interaction of crystalline material with X-rays. These diffraction patterns are helpful to identify various materials on the basis of their mono or multiphase structure identification. It is also used for measurements of crystal structures, degree of crystallinity, stacking faults, phase transitions, particle size, stress, strain and impurity in structures [10- 17].

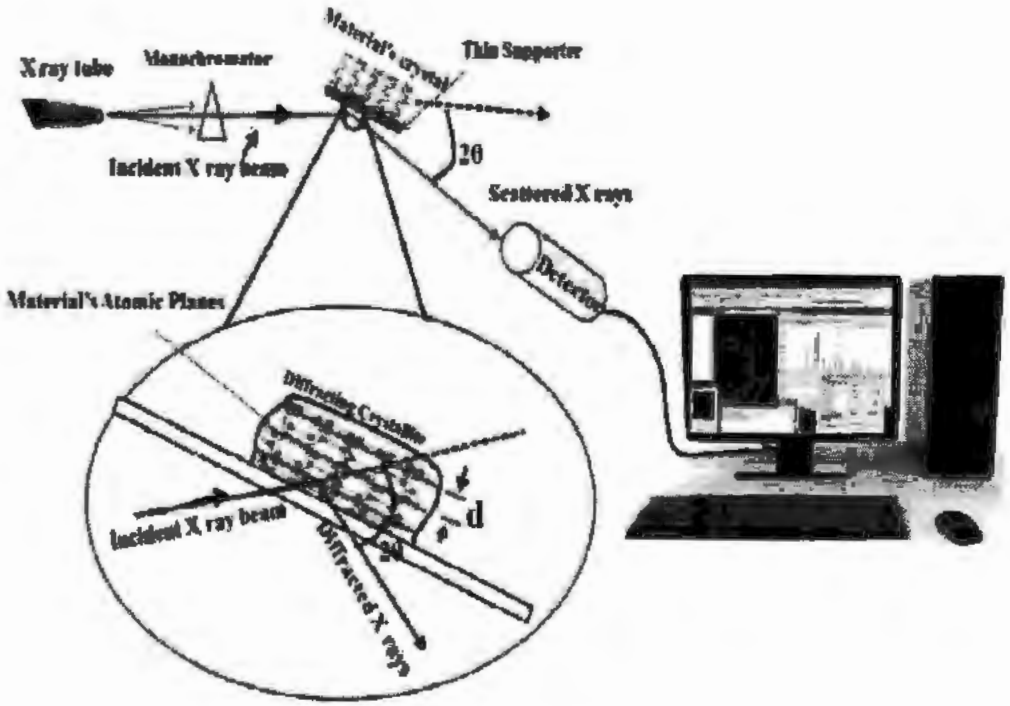

Fig. 2.3: Schematic representations of basic principle of X-ray diffraction (XRD) [17].

Every material has its own structure and fingerprint, which can be identified by comparing these structures with allusion (reference) database in JCPDS library. Purity and impurity present in a sample can be identified on the basis of diffraction peaks. Basic principle of XRD is shown in Fig. 2.3. Generally materials are formed of repeated atomic planes which make up crystal structure of any material. Polychromatic cathode rays are usually produced in a special tube and focused these beams of rays by making into monochromatic rays on materials. So, these rays are diffracted, absorbed or transmitted in order to give pattern of materials. A diffraction pattern is

formed by the inference of diffracted waves at various atomic planes. Arranged or periodic atoms yield diffraction patterns having sharp interference peaks. XRD obeys following Braggs law as [18];

$$m\lambda = 2d\sin\theta \text{----------(2.1)}$$

where distance of lattice planes is represented by d, m is order of diffraction peak and λ is wavelength of incident rays. Geometrical representation of Bragg's law is shown in Fig. 2.4.

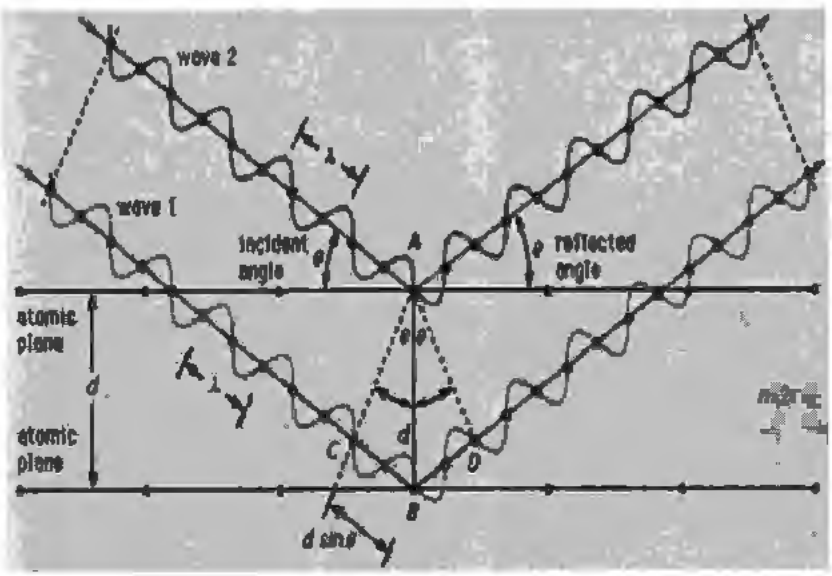

Fig. 2.4: Bragg's law geometrical representations with crystal planes [19].

The production of XRD patterns consists of following stages:

- ✓ High energy electron beam production
- ✓ Their bombardment at target
- ✓ Interaction of material and X-rays
- ✓ Production of diffracted beams

In X-rays tube, electrons are produced at cathode which is accelerated towards target (anode) through accelerating voltage across electrodes. Due to collection of these electrons, some of the energy is converted into X-rays by inner shell transition. Special information in the form of diffraction patterns at atomic level can be gathered due to X-rays wavelength. Such kind of information cannot be obtained by longer wavelengths in visible and ultra-violet range. When

monochromatic X-rays having wavelength λ incidents on the material at an angle θ, constructive interference occurs only when the distance travelled by the rays reflected from successive planes differs by *n* wavelengths.

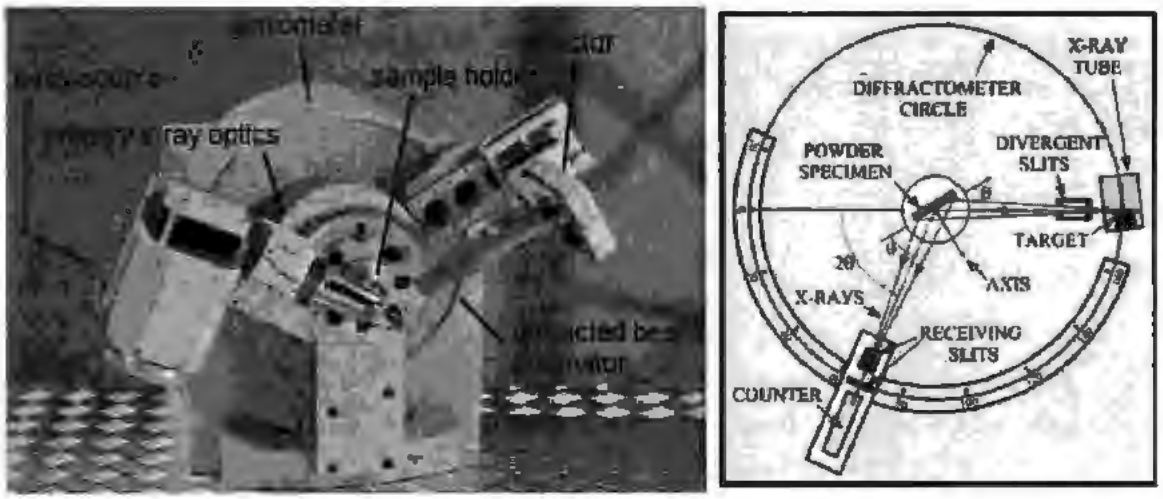

Fig. 2.5: Components of modern X-rays diffraction machine and production of X-rays from X-rays diffractometer [20].

Components of modern X-rays diffraction machine and production of X-rays from X-rays diffractometer are shown in Fig.2.5. Computer programme MDI-jade and Chekcell are used for analyzing and indexing the spectra of nano-composite materials obtained by XRD. Average size of crystal is estimated by using Debye Scherrer formula as inured below;

$$t = \frac{k\lambda}{\beta \cos\theta} \text{----------(2.2)}$$

where t= Crystallite size, K= Shape factor dependent on material's shape, β= Full width at half maximum of material's peak and θ= diffraction or Bragg angle [21, 22]. XRD is used in different fields for various structure measurements. Various uses of XRD in era of nano-composite, material science, medical etc is indicated by Fig. 2.6.

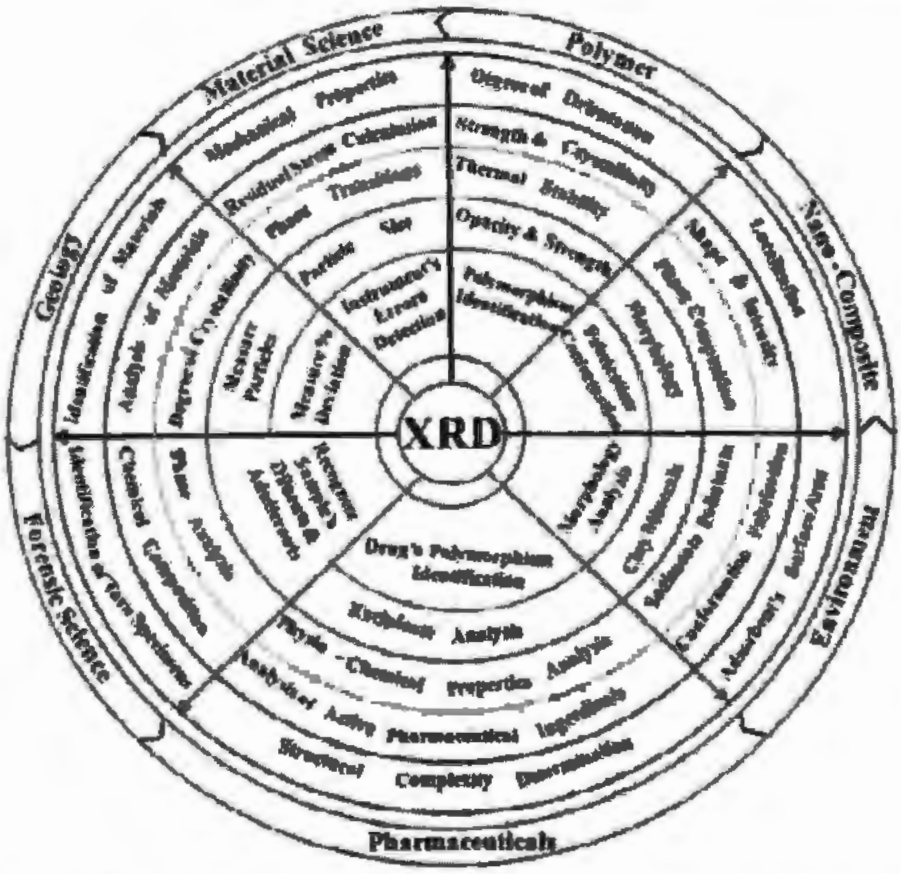

Fig. 2.6: The illustration of different application of XRD in various fields [20].

2.2.2 Scanning electron microscopy (SEM)

The morphology of the prepared material is investigated by surface probing technique known as scanning electron microscope (SEM) which uses intense beam of electron. To generate intensified image of materials, wave nature of electrons are used in SEM instead of light. The magnetic lenses are utilized in SEM to target the beam of electrons on sample species despite of spherical mirrors that are utilized in optical microscope. The SEM is preferred due to greater magnification than optical microscope for material characterizations. Electron gun, scanning coils, electron detectors, anode, stage and magnetic lenses are main components of SEM. The SEM schematic illustration is given in Fig. 2.7. Different electrons are generated from material specimens with support of beam of negative charge carriers by electron gun.

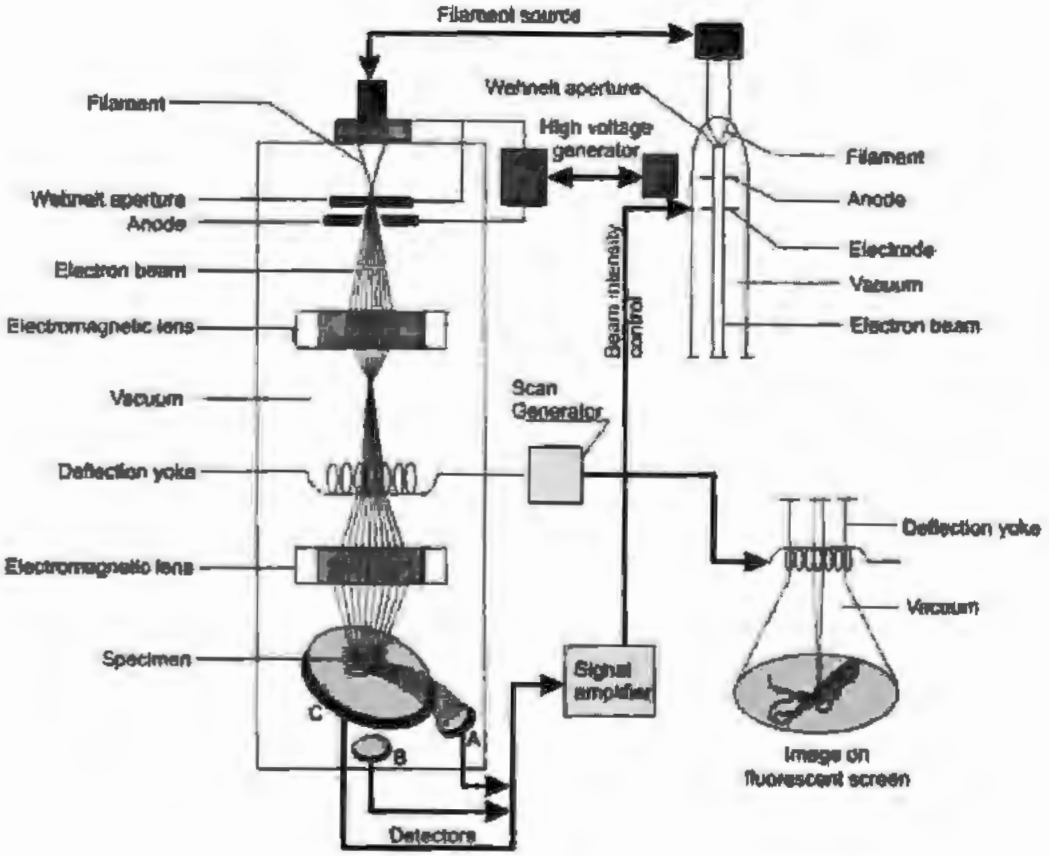

Fig. 2.7: SEM schematic illustration with its different parts [23].

Primary backscattered electron, auger electrons, secondary electrons along with X-rays are emitted from sample with beam of electrons. Information about chemical compositions and surface morphology can be obtained with these emitted signals produced by electron gun from samples. Interaction of electrons with materials and different types of electron along with X-rays emission is shown in Fig. 2.8. The scanning electron microscope carries large amount of kinetic energy and when the electrons are accelerated that produces various signals due to electron interaction with sample. X-rays in characteristic form are generated When beam of electrons slugs with inner core electrons of materials as result of removal of electrons from the surface. The characteristic X-rays and secondary negative charge carriers (electrons) are the main sources that give information about topography and morphology of the material [24, 25].

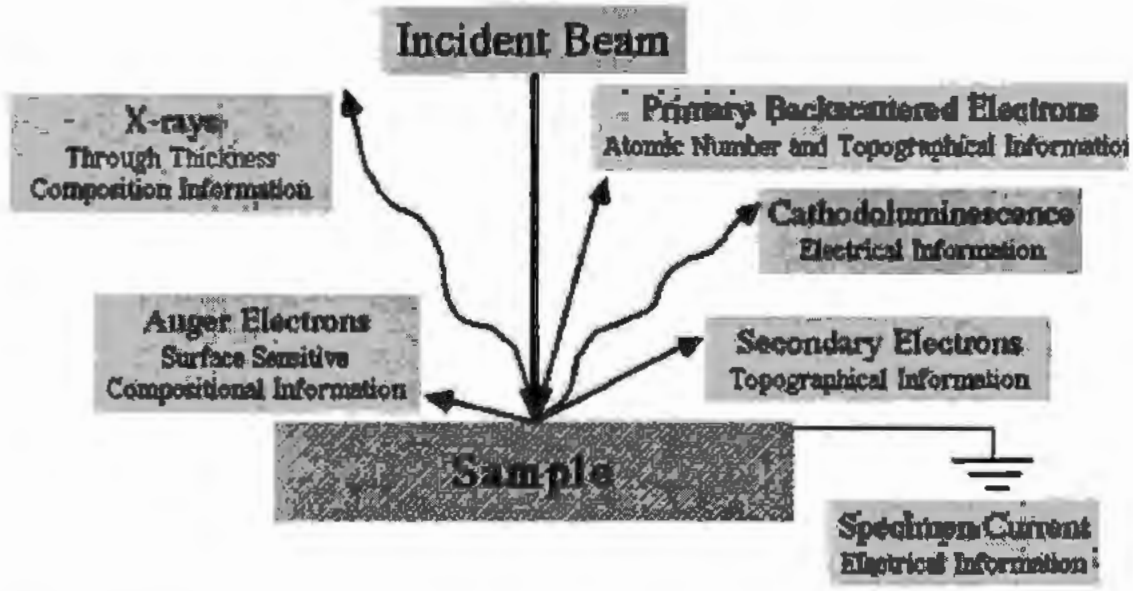

Fig. 2.8: Interaction of incident beam with sample and emission of electrons from surface [23].

To minimize the disturbance and interference generated by electron with surroundings, a vacuum pump is used in SEM. Primary electrons give allocations of various elements of materials in a sample, whereas secondary electrons detections give highly intensified image about 10 times to 500 K times. Environmental and regular SEMs are basic two types which are used for various field and materials. The examination of non-conducting materials is done with environmental SEM and regular SEM is used for the analysis of conductive materials. So, analysis of materials without conductive coating is only done by environmental SEM. The main purpose of coating on non-metallic materials during electron irradiation process is to evade accumulation of charges on the surface. Hence, coating is helpful in improvement in resolution and quality of the image for the materials [26].

2.2.3 Energy dispersive X-rays (EDX) analysis

Elemental composition of the material is studied by EDX that relies on the interactions between matter and electron beam. Its setup is mostly along with the SEM or TEM X-rays emerged from the material when energetic electrons beam particles hits with matter. In EDX investigation, eminent powerful electron beam is bombarded over specimen inside SEM. During this process, the highly energetic electrons knock-out numerous negative charge carriers (electrons) from interior shell and produce vacancies. These vacancies are occupied by outer shells electrons with

emission of X-ray photons called characteristics X-rays. These X-rays are ejected from the samples because of each element has its own specific energy due to its characteristic X-ray. In EDX, every energy level has particular characteristic spectra in an atom that shows elemental analysis of the material. The EDX spectra are corresponded to the specific energy level that display elemental information about maximum recorded X-rays. Every signal produced from an element resembles to unique peak in an atom. High intensity obtained by certain element of sample shows higher concentration of that element in spectra. Working principle of EDX is represented in Fig. 2.9.

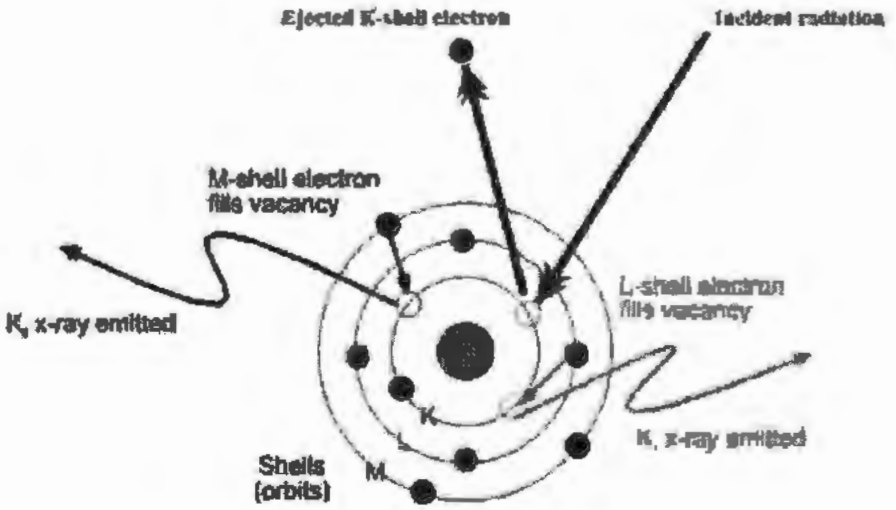

Fig. 2.9: Illustrative diagram of EDX inner shell transitions from an element.

2.2.4 Fourier transforms infrared (FTIR) spectroscopy

Absorption, emission and photoconductivity related spectrum of any material are determined by versatile technique known as FTIR. Atoms and molecules of atoms are always in persistent vibration as a result of bending, stretching and contractions of bonds even at low temperature. FTIR spectrometer is based on principle of Michelson interferometer that divides infrared radiation among different wavelength components. Basic principle of Michelson interferometer and illustrative diagram of FTIR apparatus are presented in Fig. 2.10. Radiations interact with atoms or molecules when radiations from FTIR apparatus fall on sample of material. Absorption peaks in a spectrum related to vibrational modes of materials are obtained due to superposition frequencies of infrared radiations and lattice vibrations. FTIR is useful techniques for investigation of possible correlation between lattice vibration and superconductivity. For

measurements of vibrational bands of superconductors by FTIR, a thin pallet is made by KBr powder with addition of small amount of nano-superconducting composite sample.

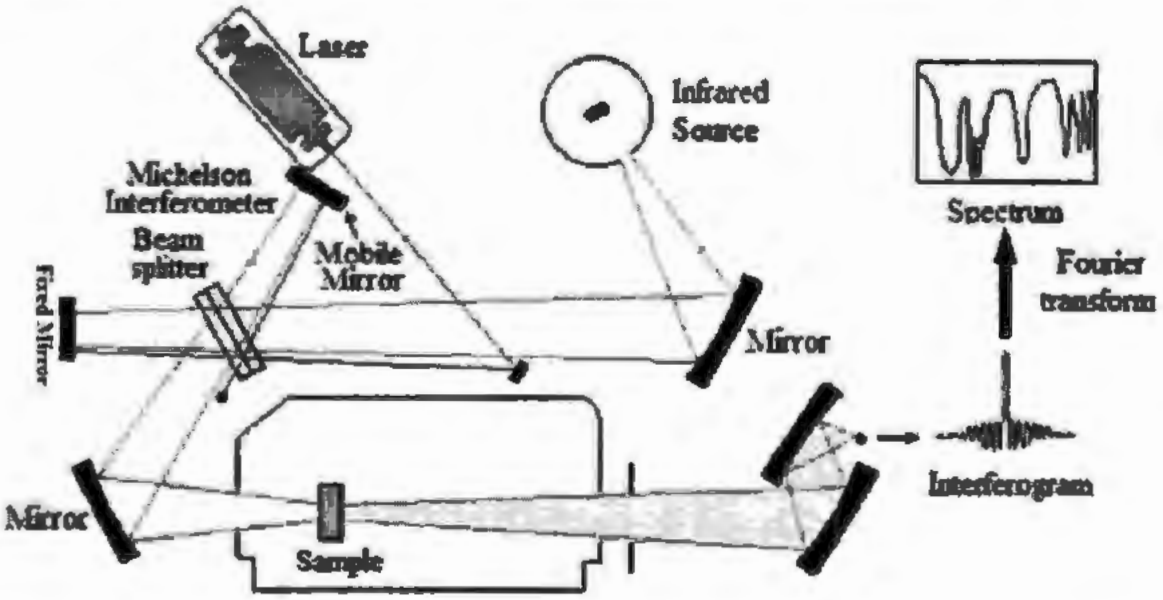

Fig. 2.10: Basic principle of Michelson interferometer and schematic illustration of modern FTIR spectrometer [27].

2.2.5 DC resistivity measurements

Critical temperatures or transition temperatures (zero critical temperature and onset critical temperature) are estimated via resistivity against temperature analysis. Four-probe physical property measurement system (PPMS) is utilized for R-T analysis of nanoparticles-superconducting composite with of 30 K to 250 K temperature ranges. For R-T measurement of nanoparticles-superconducting samples by PPMS at cryogenics temperature, liquid helium is used. Resistivity is found to be different for different material as it is dependent on nature of materials. Lattice vibration and electron-electron vibrations are main source of scattering of electrons for resistivity in materials [28]. Four equidistant junctions are made on rectangular bar shaped samples with helps of leads, fixed via silver paste in four probe techniques. These junctions are divided into two sets, one set for voltage and other set for current probes as shown in Fig.2.11. Potentiometer is inserted across voltage leads in order to measure potential drop due to establishment of electric field by constant current. Ohm law is used for calculation of resistivity of nanoparticle-superconducting composite and is given by;

$$\rho = \frac{VA}{IL} \text{----------(2.3)}$$

Where V= Potential drop, A= Area of pellets, I= Current and L= length of pellets.

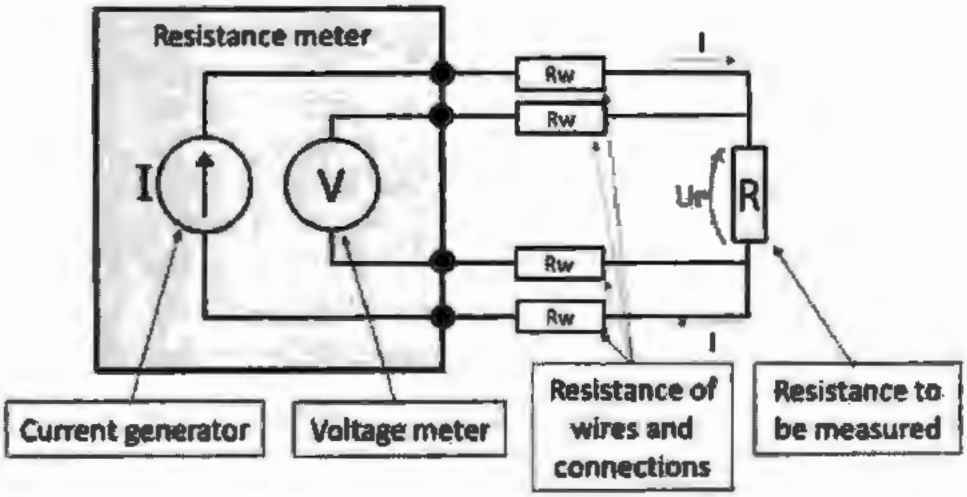

Fig. 2.11: Schematic diagram of R-T measurements of nanoparticles-superconductor composite by four probe technique.

Fig. 2.12: Experimental set up of modern quantum design PPMS [29].

We have investigated the R-T measurements of composites with application of external magnetic field in ranges from 0 to 8 T having minimal amount of 10 μA current by PPMS quantum design instrument. The heating rate was maintained in between 1 K per minute to 3 K per minutes during measurement for all samples. Modern set up of PPMS is shown in Fig. 2.12.

2.2.6 Current versus voltage (I-V) measurements

For electrical transport properties for superconducting materials, measurements of I_c are crucial and substantial. Maximum values of current that is passed through superconductors without affecting its critical state represent as critical current (I_c) and when this limit is exceeded, the material is transformed into normal conductor. I-V menstruations accomplished at constant 77 K temperature for all samples. Resistivity for superconducting materials is normally very small to be measured. Materials started to show resistance with increasing current as result of rising of potential drop across sample. So, values of J_c can be obtained by dividing I_c by cross-sectional area of sample.

2.3 References

[1] J. D. MacKenzie, "Glasses from melts and glasses from gels, a comparison", J. Non-Cryst. Solids, **48** (1982) 1.

[2] C. J. Brinker, D. E. Clark, and D. R. Ulrich, "Better ceramics through chemistry", North-Holland, New York (1984).

[3] C. N. R. Rao, "Chemistry of high temperature superconductors", World Scientific, Singapore (1991).

[4] C. N. R. Rao, "The blackett memorial Lecture, chemical insights into high-temperature superconductors", Phil. Trans. R. Soc. **336** (1991) 595.

[5] M. J. Parker, and R. Janes, The synthesis of cuprate superconductors via a dual-precipitation route", J. Mat. Sci. **28** (1993) 4515.

[6] A. M. M. Riveral, J. A. Gomez Cuaspud, C. A. Parra Vargas, and M. H. B. Ramirez, "Synthesis and characterization of $LaBa_2Cu_3O_{7-\delta}$ system by combustion technique", J. Supercond. Nov. Magn. **29** (2016) 1163.

[7] A. Palau, V. Rouco, R. F. Luccas, X. Obradors, and T. Puig, "Nanowall pinning for enhanced pinning force in YBCO films with nanofabricated structures", Physica C **506** (2014) 178.

[8] A. Chauhan, and P. Chauhan, "Powder XRD technique and its applications in science and technology", J. Anal. Bioanal. Tech. **5** (2014) 5.

[9] V. Guidi, M. A. Butturi, M. C. Carotta, B. Cavicchi, M. Ferroni, C. Malagu, G. Martinelli, D. Vincenzi, M. Sacerdoti, and M. Zen, "Gas sensing through thick film technology", Sens. Actu. B **84** (2002) 72.

[10] Y. Waseda, E. Matsubara and K. Shinoda, "X-Ray diffraction crystallography: Introduction, examples and solved problems", Springer (2011).

[11] I. Ivanisevic, R. B. Mcclurg, and P. J. Schields, "Uses of X-ray powder diffraction in the pharmaceutical industry: Pharmaceutical sciences encyclopedia: Drug discovery, development, and manufacturing", John Wiley & Sons, Inc., New Jersey (2010).

[12] A. Dey, A. K. Mukhopadhyay, S. Gangadharan, M. K. Sinha, and D. Basu, "Characterization of microplasma sprayed hydroxyapatite coating", J. Therm. Spray Tech. **18** (2009) 578.

[13] D. Ananias, F. A. A. Paz, L. D. Carlos, and J. Rocha, "Chiral microporous rare-earth silico-germanates: Synthesis, structure and photoluminescence properties", Micropor. Mesopor. Mat. **166** (2013) 50.

[14] M. Nicolae, I. Vilciu, and F. Zaman, "X-ray diffraction analysis of steel slag and blast furnace slag viewing their use for road construction", U. P. B. Sci. Bull., Series B **69** (2007) 99.

[15] L. J. Chyall, "Current applications of X-ray powder diffraction in the pharmaceutical industry", Amer. Pharmac. Rev. **15** (2012) 6.

[16] J. Singh, M. Srivastava, A. Roychoudhury, D. W. Lee, S. H. Lee, and B. D. Malhotra, "Bienzyme-functionalized monodispersed biocompatible cuprous oxide/chitosan nanocomposite platform for biomedical application", J. Phys. Chem. B **117** (2013) 141.

[17] R. Das, M. E. Ali, and S. B. A. Hamid, "Current applications of X-rays powder diffraction-A review", Rev. Adv. Mater. Sci. **38** (2014) 95.

[18] B. D. Cullity, "Elements of X-Ray diffraction", Addison-Wesley, Crop., Massachusetts (1978).

[19] C. Suryanarayana, and M. G. Norton, "X-ray diffraction a practical approach", Springer Science, New York (1998).

[20] R. Jenkins, "X-Ray techniques: Overview", Encycl. Analyt. Chem. (2000).

[21] Y. Leng, "Material characterization", John Wiley & Sons (2008).

[22] Klug, H. Philip, and L. E. Alexander, "X-ray diffraction procedures", New York: Wiley (1954).

[23] M. T. Postek, K. S. Howard, A. H. Johnson, and K. L. Mcmichael, "Scanning electron microscopy", Ladd Res. Ind., Inc. Williston (1980).

[24] D. C. Joy, and C. S. Joy, "Low voltage scanning electron microscopy", Micron 27 (1996) 247.

[25] J. I. Goldstein, D. E. Newbury, D. C. Joy, C. E. Lyman, P. Echlin, E. Lifshin, L. Sawyer, and J. R. Michael, "Scanning electron microscopy and X-ray microanalysis" Kluwer Academic/Plenum Publishers, 3rd Ed. New York (2003).

[26] H. Besler, "Scanning electron microscopy", Develop. Sedimen. 59 (2008) 153.

[27] P. R. Griffiths, "Fourier transform infrared spectroscopy", Plenum Press, New York (1975).

[28] H. Ibach, and H. Luth, "Solid state physics: An introduction to theory and experiment", Spinger-Verlag, Berlin (1991).

[29] W. Wang, H. Liu, R. Huang, Y. Zhao, C. Huang, S. Guo, Y. Shan, and L. Li, "Thermal expansion and magnetostriction measurements at cryogenic temperature using the strain gauge method", Front. Chem. 6 (2018) 72.

Chapter No. 3

$(Cu)_x$/(CuTl)-1223 Nanoparticles-Superconductor Composites

The effect of MNPs inclusion with different concentrations on superconducting and magneto-electrical properties of (CuTl)-1223 phase was investigated in this chapter. Cu NPs owing to their conducting character were intended to improve these properties of (CuTl)-1223 phase by healing of spaces among grain, void and pores. Our desire was to find an optimum level of these Cu NPs in order to get enhancement in superconducting and magneto-electrical properties without effecting crystal symmetry of this phase. The structural, morphogical, compositional, superconducting and magneto-electrical properties were analyzed by using different experimental techniques. Magnetization measurements (M versus T and M versus H) of nanoparticle-superconductor composites were performed in temperature range of 5 K to 300 K without field and 0.01 T field by PPMS.

3.2. Results and discussion

3.2.1 X-rays diffraction (XRD) analysis

Phase purity of Cu nanoparticles and nanoparticles superconductor composites were examined through XRD spectra. The XRD spectrum of Cu NPs is presented in Fig. 3.1. Average crystallite size of Cu NPs, calculated by Debye-Scherer's formula was found 20 nm. The XRD peaks found at 43.09°, 50.32° and 74.15° were indexed as (111), (200) and (220) planes according to the standard card JCPDS (Card No. 04-0836) indicating FCC crystal structure of the Cu NPs [1]. The X-ray diffraction scan for every sample was collected from 2θ = 2° to 65° ranges. The crystal symmetry, cell criterions and phase perfection were procured from XRD Scans. XRD scans of bulk (CuTl)-1223 superconductor by inclusion of Cu NPs with variation in contents (0, 1.0 and 3.0 wt. %) are represented by Fig. 3.2. The XRD analysis indicated that superconducting phase was accomplished and very small amount of other superconducting phases including (CuTl)-1234 and few other unknown impurities were displayed. The distinguished Bragg's peaks of XRD scans were registered in accordance with tetragonal symmetry of (CuTl)-1223 along with P4/mmm space group. These XRD scans showed the preservation of CuTl-1223 structure in spite of Cu NPs inclusion.

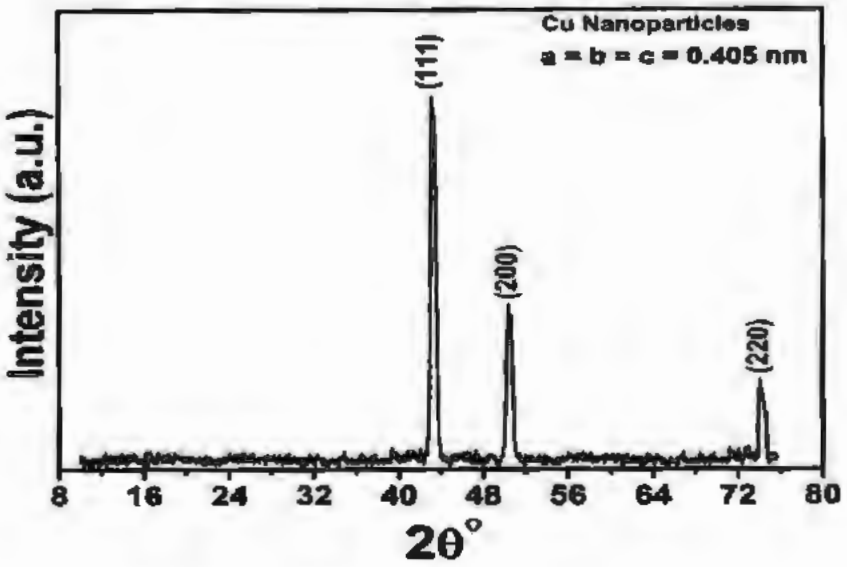

Fig. 3.1: The XRD spectrum of Cu nanoparticles

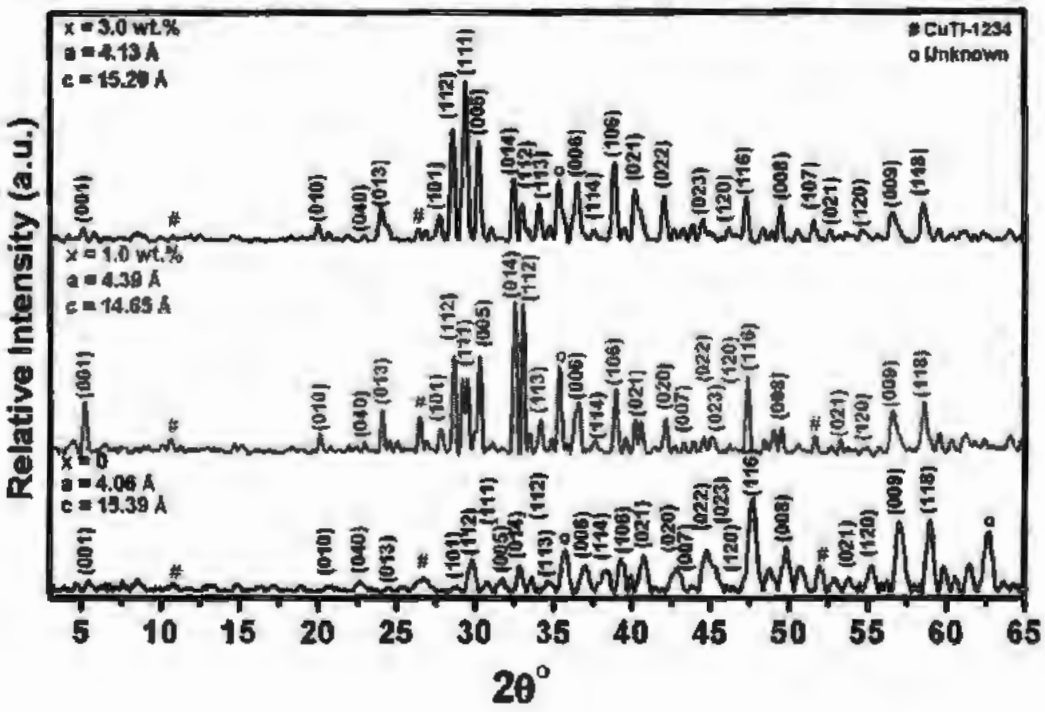

Fig. 3.2: XRD patterns of (Cu)$_x$/(CuTl-1223) nanoparticles-superconductor composites with x = 0, 1.0 wt. % and 3.0 wt. %.

Consequently, these NPs immersed among crystallite sites of (CuTl)-1223 superconductor. The occurrence of these NPs among grains can assist to strengthen voids to recover weak-links among grains along with superconducting volume fraction in order to enhance superconducting properties. These results indicated that Cu NPs had not embedded within unit cell of (CuTl)-1223 superconducting phase [2]. Inconsiderable digression along c-axis was noticed, which may be owing to some stresses, strain, variation in oxygen (O_δ) contents and distortion produced after inclusion of Cu NPs. Percentage volume fraction of these different phases was calculated by using relation [3];

$$\{(CuTl)\text{-}1223\}\ \% = \frac{\sum I(1223)}{\sum (I(1223)+I(1234)+I(unkown/other))} x100 \text{----------} (3.1a)$$

$$\{(CuTl)\text{-}1234\}\ \% = \frac{\sum I(1234)}{\sum (I(1223)+I(1234)+I(unkown/other))} x100 \text{----------} (3.1b)$$

$$\{(CuTl)\text{-}unkown/other\}\ \% = \frac{\sum I(unkown/other)}{\sum (I(1223)+I(1234)+I(unkown/other))} x100 \text{-----} (3.1c)$$

Since, I(1223) = XRD intensity peak of (CuTl)-1223, I(1234) = XRD intensity peak of (CuTl)-1234 and I(unknown/Other) = XRD intensity peak of other unknown phases accordingly. The estimated concerning percentage of every phase was indexed in Table.3.1.

Table 3.1. The lattice parameters and percentage volume fraction of CuTl-1223, CuTl-1234 and unknown/other phases of (x= 0, 1.0 and 3.0 wt. %)

Sample	(CuTl)-1223 Orthorhombic unit cell a (Å)	(CuTl)-1223 Orthorhombic unit cell c (Å)	Volume fraction of (CuTl)-1223 Phase Composition (%)	Volume fraction of (CuTl)-1234 Phase Composition (%)	Unknown/ Other Volume fraction (%)
x= 0	4.06	15.39	92.62	2.94	4.43
x=1	4.39	14.65	91.72	2.86	5.40
x=3	4.13	15.20	94.31	3.21	2.48

3.2.2 Scanning electron microscopy (SEM) and energy dispersive X-rays spectroscopy (EDX) Measurements

Morphology and compositional analysis were carried out by using SEM and EDX respectively. Typical SEM and EDX images of (CuTl)-1223 superconducting phase by Cu NPs insertion with 0 and 4.0 wt. % contents are shown in Fig. 3.3 (a-d). EDX was assured chemical composition of (CuTl)-1223 superconductor by Cu NPs inclusion with content variation of 0 and 4 wt. % as shown in the Fig. 3.3 (c, d). EDX peaks revealed the existence of numerous elements such as Ba, Ca, Tl Cu, C and O. The proportions of individual element for 0 and 4.0 wt. % of Cu NPs insertion is given in Table 3.2.

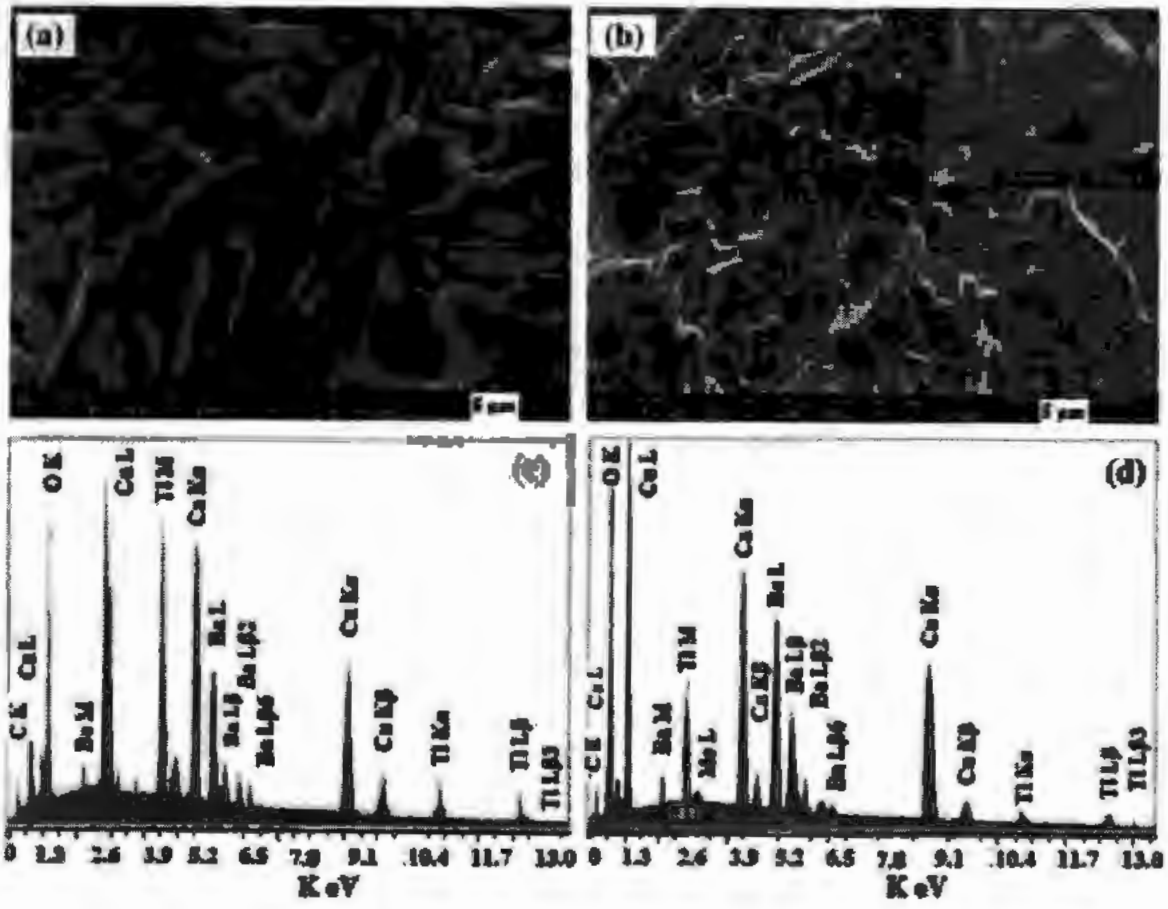

Fig.3.3 (a-d): Typical SEM and EDX images of (CuTl)-1223 superconductor with Cu NPs insertion with 0 and 4.0 wt. % respectively.

Table 3.2. The EDX quantified elemental analysis of (CuTl)-1223 superconductor by inclusion of Cu NPs with 0 and 4.0 wt. % respectively

x= 0				x= 4%			
Element	**Weight %**	**Atomic %**	**Error %**	**Element**	**Weight %**	**Atomic %**	**Error %**
C K	1	4.4	18.12	**C K**	1.66	6.4	14.08
O K	14.21	47.08	9.7	**O K**	16.34	47.29	9.35
Ca K	9.16	12.11	4.36	**Ca K**	9.78	11.3	3.6
Ba K	30.63	11.82	3.05	**Ba K**	28.75	9.69	2.58
Cu K	22.48	18.75	3.49	**Cu K**	30.33	22.1	2.99
Tl L	22.51	5.84	12.1	**Tl L**	12.16	2.75	15.16
Total	99.99	100		**Mo L**	0.97	0.45	13.19
				Total	99.99	99.98	

It was noticed that microstructures of samples manifested a unifying feature of randomly scattered plate like grains. The pores, voids and weak- links witnessed obviously prominent in SEM for pristine sample, on the other hand theses parameters were decreased after Cu NPs insertion. In upper- right corner of SEM image for x = 4 wt. %, the magnification was increased to 1 μm and we noticed that white spot, which were Cu NPs distributed on surface of grain. The improvement in connectivity among grains was accountable due to Cu NPs along with strengthen of pinning centers to embed the vortices. However for Cu NPs higher contents (i.e., x= 4.0 wt. %) placed on grain surface, superconducting properties were suppressed by phenomena like scattering, pair breaking [4].

3.2.3 Fourier transformation infrared (FTIR) Spectroscopy analysis

FTIR is very sensitive technique used to detect a trace amount of impurities along with functional groups in the material. The FTIR absorption spectra of (Cu)$_x$/CuTl-1223 composites (0 ~ 4.0 wt. %), in the wave number ranges of 400-700 cm^{-1} are shown in Fig.3.4.

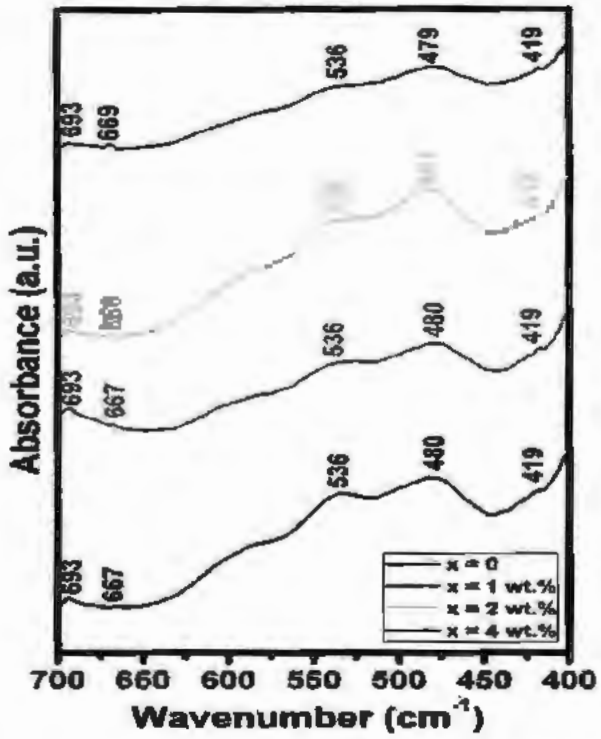

Fig.3. 4: FTIR absorption spectra regarding $(Cu)_x$/(CuTl)-1223 NPs-superconductor composites (0 ~ 4 wt. %).

The vibrational modes of apical, planner oxygen and delta oxygen (O_δ) are depicted in wave number ranges of 400 to 540, 541 to 600 and 670 to 700 cm^{-1} accordingly [5]. It can be witnessed that apical and planar oxygen modes remained unaltered by Cu NPs insertion in host superconducting phase. The invariant oxygen modes' position supports our claim that these NPs are distributed the spaces among grains rather incorporate in unit cell of host phase.

3.2.4 Electrical resistivity against temperature analysis

The electrical resistivity versus temperature criterions of $(Cu)_x$/(CuTl)-1223 (x = 0 ~ 4 wt. %) nanoparticles-superconductor composites in temperature range of 75 k to 300 K are displayed in Fig. 3. 5.

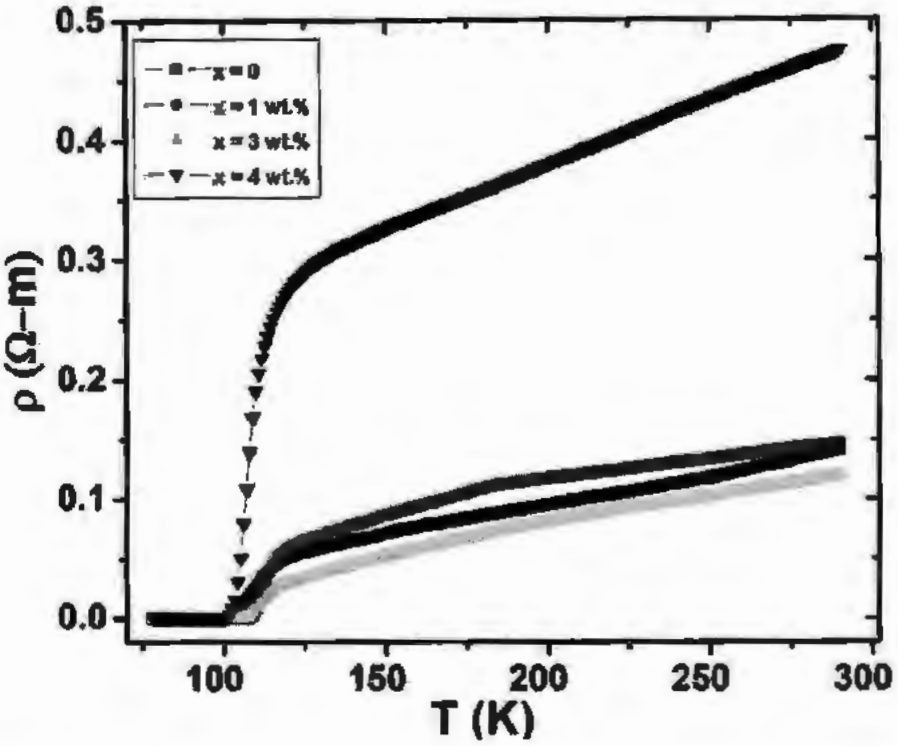

Fig. 3.5: The resistivity versus temperature measurements for (Cu)$_x$/(CuTl)-1223 nanoparticles-superconductor composites (0 ~ 4 wt. %).

As a whole improvement in zero critical temperature of (CuTl)-1223 superconductor was noticed after Cu NPs insertion till 1.0 wt. % optimum level. The increment in transition temperature may be assigned to improvement of connectivity among grains through pores and voids filling owing to conducting Cu NPs. It was expected that non-monotonic change of zero critical temperature was mostly due to non uniform scattering of Cu NPs among grains of host superconducting phase. The transition temperature width was estimated by $\Delta T_c = T_c^{onset} - T_{c(0)}$ and ΔT_c was found shorten for 1.0 wt. % of Cu NPs inclusion. A minimal value of ΔT_c was confirmed the improvement of connectivity among grains with Cu NPs insertion. Inter-grain connectivity was strengthened by reduction of ΔT_c for x= 1.0 wt. %, which was in accordance to results of XRD, SEM and EDX. Hole concentration (p) of (CuTl)-1223 superconductor by addition of Cu NPs was evaluated by an equation [6, 7];

$$p = 0.16 - \left(\frac{1 - \frac{T_c}{T_c^{max}}}{82.6} \right)^{1/2} \text{----------(3.2)}$$

Where T_c^{max}= 132 K is taken as highest temperature of (CuTl)-1223 phase. The doubled-y graphical representation between *p* and T_c (0) against NP contents (x) of (CuTl)-1223 superconductor is indicated by Fig.3.6. The values of *p* deviated from 0.1071 to 0.1130 with Cu NPs variation. The maximal value of *p* was observed to be 0.1130 for 1.0 wt. % and this sample as well revealed utmost superconducting transport properties in comparison with (CuTl)-1223 superconducting pristine sample. The values of $T_{c\,(0)}$, T_c^{onset}, ΔT_c and p are presented in Table 3.3. The utmost superconducting properties were achieved for 1.0 wt. % optimum level by Cu NPs insertion in host superconductor as noticed from Table 3.3 and Fig.3.6, which was in accordance to results of XRD, SEM and EDX. The initially increase in zero critical temperature and hole contents were mostly due to improve weak-links among the superconducting grains by healing up the voids and pores with inclusion of these NPs. The occurrence of these NPs between grain-boundaries can assist to strengthen voids to recover weak-links among grains along with superconducting volume fraction in order to enhance superconducting properties up to optimum value of 1 wt. %. In cuprates HTSCs, the zero critical temperature depends upon the carriers' density in copper oxide planes and these carriers depends upon the oxygen contents in charge reservoir layer. The decrease in hole concentrations and hence T_c was observed with increasing values of these NPs (2, 3 and 4 wt. %) as result of agglomerizations and segregation of these NPs among grains, which degraded the superconducting sample quality.

Table 3.3: The superconducting parameters of (Cu)$_x$/(CuTl)-1223 NPs-superconductor composites.

Cu NPs concentration	T_c(0) (Kelvin)	T_c^{onset} (Kelvin)	ΔT_c	Hole concentration
x=0	101	116.3	14.2	0.1075
x=1.0	108	116.0	8.0	0.1130
x=3.0	104	115.3	11.1	0.1105
x=4.0	102	114.0	12.5	0.1071

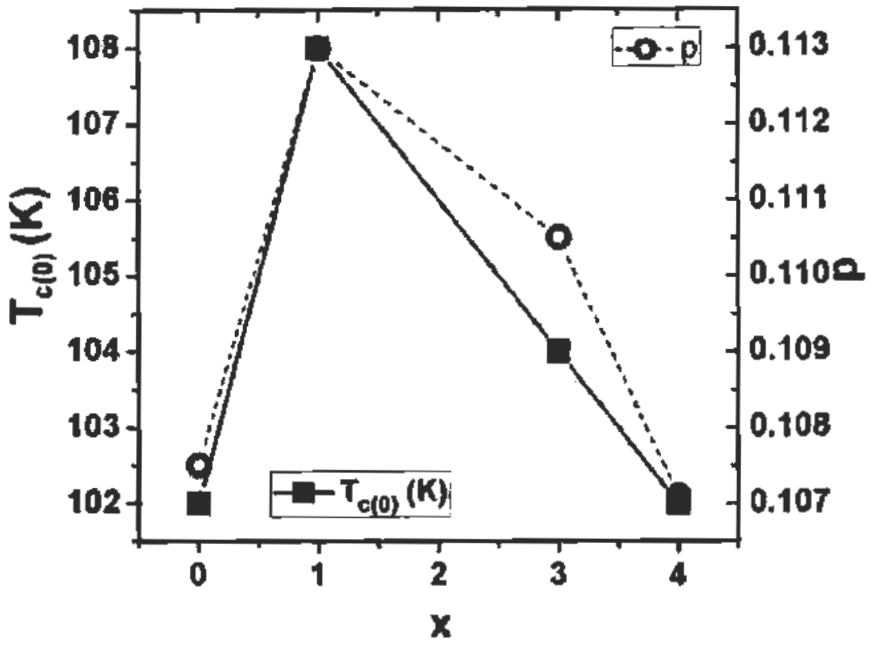

Fig.3.6: Variation of critical temperature and hole concentration against various contents (0 ~ 4 wt. %) of Cu NPs in (CuTl)-1223 superconductor.

The density of mobile charge carriers started to decrease after optimum level as result of suppression of superconducting volume fraction by phenomena of scattering and pair breaking.

3.2.5 Zero field cooled (ZFC) and field cooled (FC) versus temperature measurements

The magnetic moment against temperature from 5 K to 300 K of (Cu)$_x$/(CuTl)-1223; x = 0 ~ 4.0 wt.%, NPs-superconductor composites for zero-field-cooled (ZFC) and the field-cooled (FC) measurements are displayed in Fig. 3.7 (a-d). The diamagnetic transition temperature T_c^{onset} calculated from ZFC curves was found around 97 K, 112 K, 95 K, 98 K for x = 0 ~ 4 wt. % accordingly. The T_c^{onset} is temperature in M-T measurements where ZFC and FC curves merge with each other. The utmost improvement was witnessed in (CuTl)-1223 superconductor by addition of Cu NPs up to optimum level of 1.0 wt. %. The optimizations in T_c^{onset} can be rendered to refinement of inter-grains connectivity via filling up the pores and spaces with metallic Cu NPs.

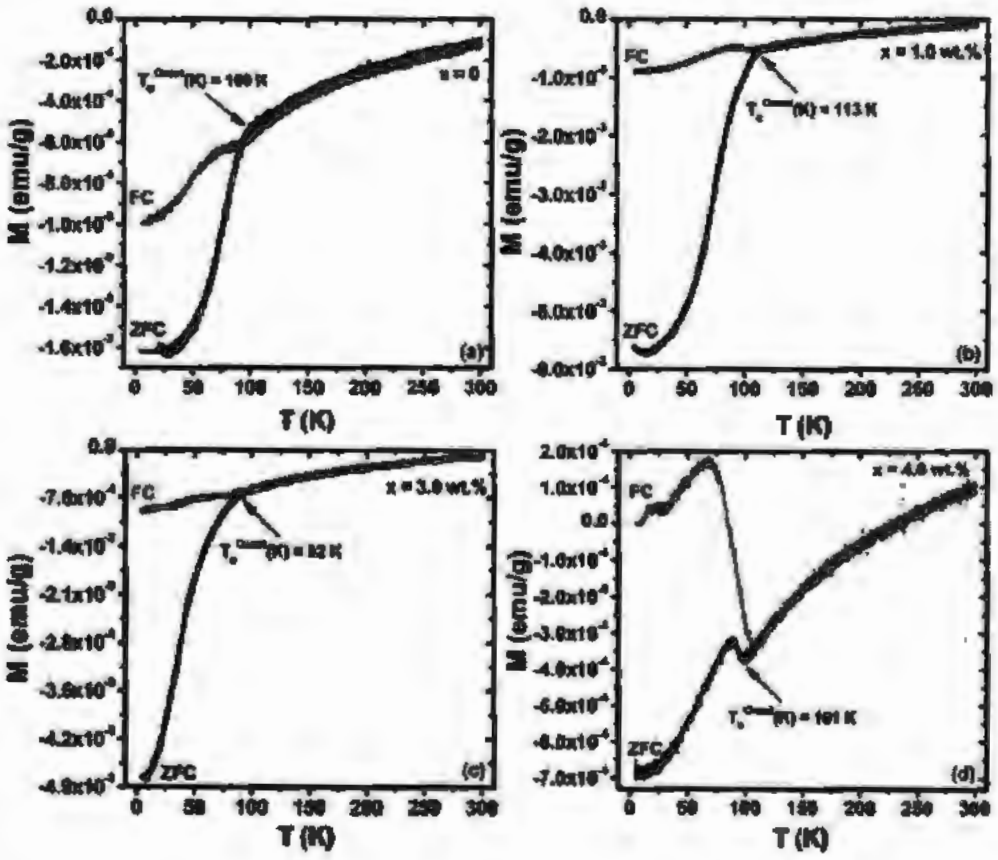

Fig. 3.7 (a-d): The ZFC and FC measurements of magnetic moment against temperature by inclusion of Cu NPs in (CuTl)-1223 superconductor with x = 0, 1.0, 3.0 and 4.0 wt. % respectively.

The resistivity of sample starts decreasing well before T_c^{onset} (K) [8-10]. The field cooled magnetization measurements were performed by 0.01 T strength of magnetic field and these measurements did not show any sign of Meissner signal remarkably. Where $M_{T^{onset}}$ and $M_{T_c(0)}$ are magnetizations measured at T_c^{onset}(K) and T_c (0) K , accordingly. The amplitude of diamagnetic signal (ADS) is examined roughly by esteem of ΔM. It is considered that ADS has positive correlation along with quantity of superconducting domains such that ADS reflects superconducting features of material [11]. The values of $\Delta M = |M_{T^{onset}} - M_{T_c(0)}|$ as estimated from ZFC curves by addition of Cu NPs in (CuTl)-1223 superconductor are presented in Table 3.4.

Table. 3.4. Amplitude of diamagnetic signal (ΔM) from ZFC curves by addition of different contents of Cu NPs in CuTl-1223superconductor.

Values of amplitude of diamagnetic signal (ΔM) for ZFC by addition of Cu NPs with concentration of 0 ~ 4.0 wt. % in CuTl-1223.			
Samples	**M $\{T_{c(Onset)}\}$**	**M $\{T_{c(0)}\}$**	**ΔM**
0	5.18×10^{-4}	1.60×10^{-3}	1.08×10^{-3}
1.0 wt. %	4.56×10^{-4}	5.56×10^{-3}	5.11×10^{-3}
3.0 wt. %	6.68×10^{-4}	4.57×10^{-3}	3.90×10^{-3}
4.0 wt. %	3.25×10^{-4}	6.80×10^{-4}	1.21×10^{-4}

The increase in values of ADS by addition of Cu NPs in CuTl-1223 superconductor as seen from above table was an indication of enhanced superconducting domains in a material. The optimization value of ΔM estimated by inclusion of Cu NPs with x = 1.0 wt. % in (CuTl)-1223 sample wt. % was conformation of maximum enhancement of superconducting domains.

3.2.6 Magnetic hysteresis (M-H) measurements

Magnetic hysteresis (M-H) curves at various temperatures particularly 10, 30, 60, 90, 200 and 300 K by inclusion of Cu NPs with different contents in (CuTl)-1223 are demonstrated in Fig. 3. 8 (a-d). The peculiar superconducting M-H features were witnessed only for 10, 60 and 90 K by Cu NPs addition in (CuTl)-1223 superconductor and beyond 90 K temperature, the superconducting material was shifted into ferromagnetic material. Magnetic hysteresis vanished entirely towards higher temperatures in all the samples. The declination of magnetization from linearity suggested the insertion of magnetic lines in superconducting materials and revealed the change of superconducting material to normal material state [12]. The values of lower critical field H_{c1} can be inferred from variation in magnetization at temperatures of 10 K, 30 K, 60 K and 90 K. To obtain more effective sigh of the onset of deviation from linearity by addition of Cu NPs with different concentration in (CuTl)-1223 superconductor, we plot M versus H graphs at various temperatures from 10 K to 90 K as represented by Fig. 3.9 (a-d). The inset of Fig 3.9 indicated the values of H_{c1} against temperature for Cu NPs in (CuTl)-1223 superconductor.

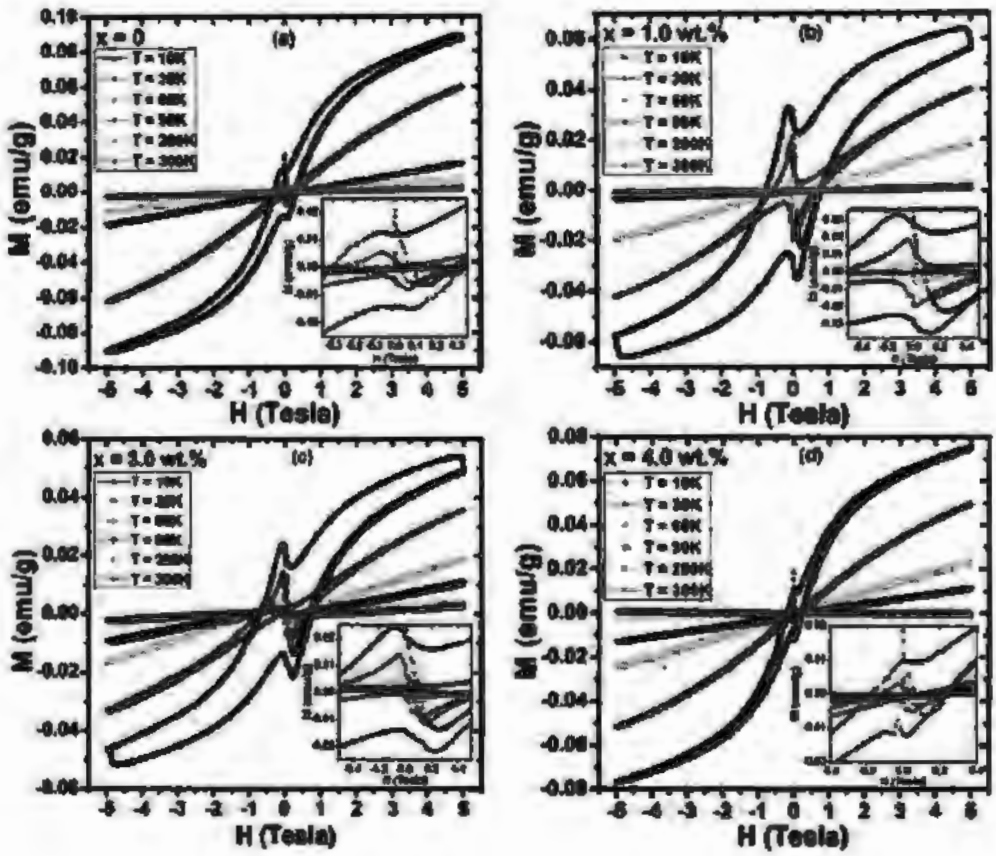

Fig. 3.8(a-d): Magnetic hysteresis (M versus H) measurements by Cu NPs addition in (CuTl)-1223 superconductor at various temperature of 10 K ~ 300 K with x = 0, 1.0, 3.0 and 4.0 wt.% respectively.

The values of lower critical field (H_{c1}) were reduced linearly with increase of functional temperatures. The utmost value of lower critical field by addition of Cu NPs in host superconducting matrix at very small temperature of 10 K were observed around 0.148 T, 0.20 T, 0.18 T, 0.127 T. The effect of Cu NPs in (CuTl)-1223 superconductor on lower critical field (H_{c1}) is shown in Fig. 3.9 (e). The highest value of H_{c1} was observed with optimum level of 1.0 wt. % by Cu NPs addition in CuTl-1223 superconducting matrix. The superconducting volume fraction initiated to suppress beyond optimum level of Cu NPs in host superconductor. The improvement in inter-grain connectivity and reduction in weak-links were caused by settled of Cu NPs at inter-granular spaces of (CuTl)-1223 matrix [13].

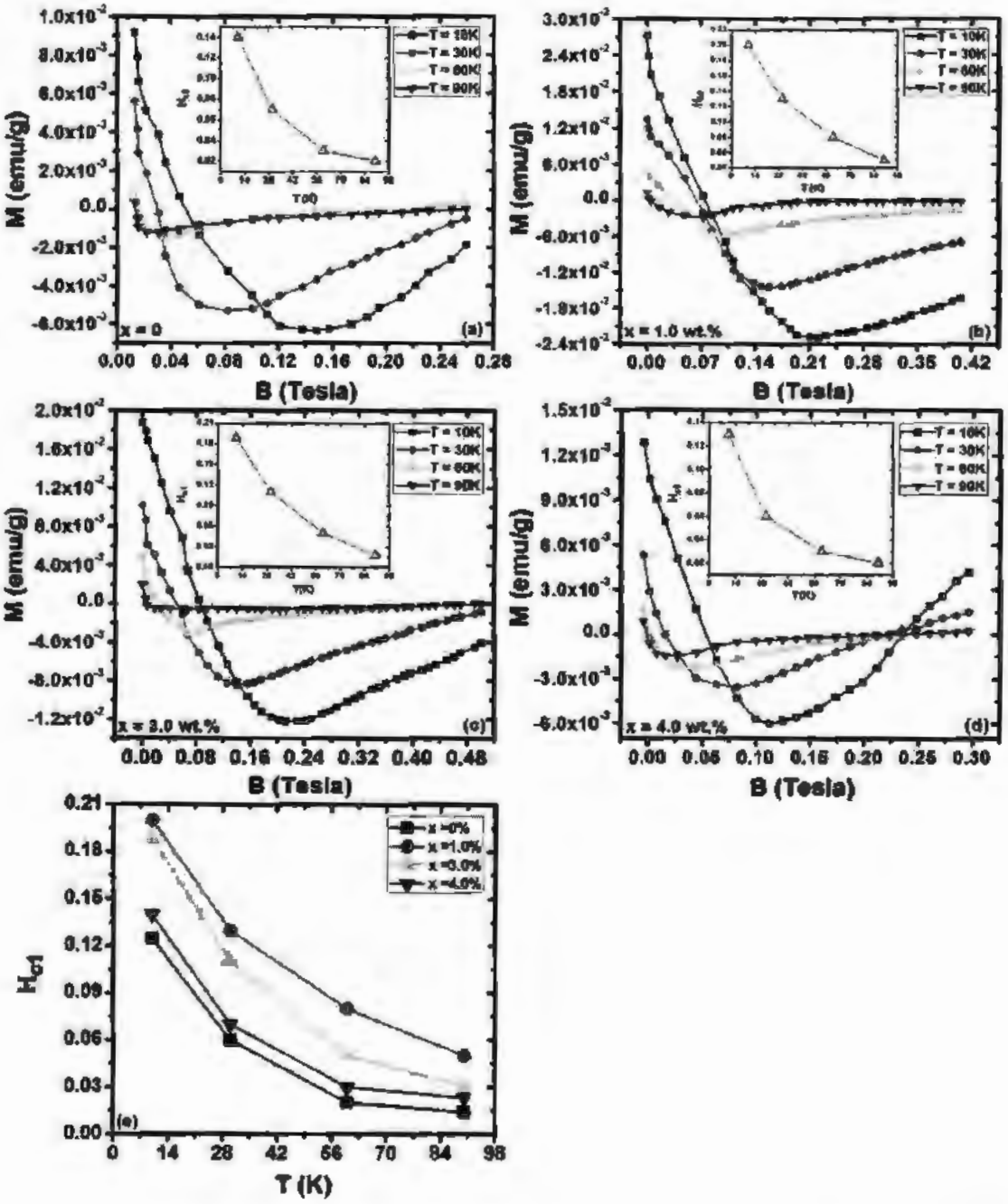

Fig. 3.9 (a-e). The magnetization versus applied field plots at temperature from 10 K to 90 K by addition of Cu NPs in (CuTl)-1223 superconducting matrix with x = 0, 1.0, 3.0 and 4.0 wt.% respectively and Fig. (e) Represents collective plots of H_{c1} against temperatures. Inset indicates the values of H_{c1} at different operating temperatures.

3.2.7 Critical current density (J_c) measurements

The field related critical current density J_c by addition of Cu NPs with different concentrations in (CuTl)-1223 superconductor is represented by Fig. 3.10 (a-e) and was calculated by using Bean's equation [14];

$$J_c = \frac{20\,\Delta M}{a\left(1-\frac{a}{3b}\right)} \qquad (3.3)$$

Where $\Delta M = M^+ - M^-$, and dimensions of the samples are represented by a, b such that (a > b). The variations in field dependent J_c calculated by Bean's equation by Cu NPs inclusion in (CuTl)-1223 samples are displayed by Fig. 3.10 (a-d). The field dependent measured values of J_c showed broadly increasing tendency by inclusion of Cu NPs in (CuTl)-1223 superconductor. The utmost value of J_c was varied from 2.4×10^2, 7.1×10^2, 4.6×10^2 to 3.2×10^2 A cm^{-2} at temperature of 10 K by various contents of Cu NPs in (CuTl)-1223 superconductor. The maximal value of critical current density was achieved with optimum level of 1.0 wt. % of Cu NPs addition in (CuTl)-1223 superconductor. The volume fraction and hence the infield superconducting transport properties of (CuTl)-1223 were suppressed beyond optimum level of Cu NPs addition. These Cu NPs as conducting medium were adjusted at grain-boundaries of (CuTl)-1223 superconductor and served as artificial efficient pinning centers, which can permit the movement of charge carriers [15, 16]. These consequences recommend that Cu NPs have remarkably enhanced number of pinning centers and these pinning centers acting as additionally phases in superconducting samples, which evolve the source of increment in infield J_c. Fig. 3.10 (e) represents the alteration of J_c against temperatures with different concentrations of Cu NPs in (CuTl)-1223 superconductor. The utmost enhancement of critical current density at all temperature was witnessed by an optimum level of 1.0 wt. % Cu NPs addition in (CuTl)-1223 superconductor. It was also witnessed that values of J_c were lessened by raising temperature for each samples, which indicated strong pinning at low temperatures. Magnetization provoked with pinning to decrease with increased of temperature. The vortex motion in the samples was increased of temperature, which lead to degradation of magnetic fluxes and resulted energy loss in host material. Consequently the decrement of infield J_c at higher temperatures was observed by addition of all concentrations of Cu NPs in (CuTl)-1223 superconductor due to vortex motion and energy dissipation.

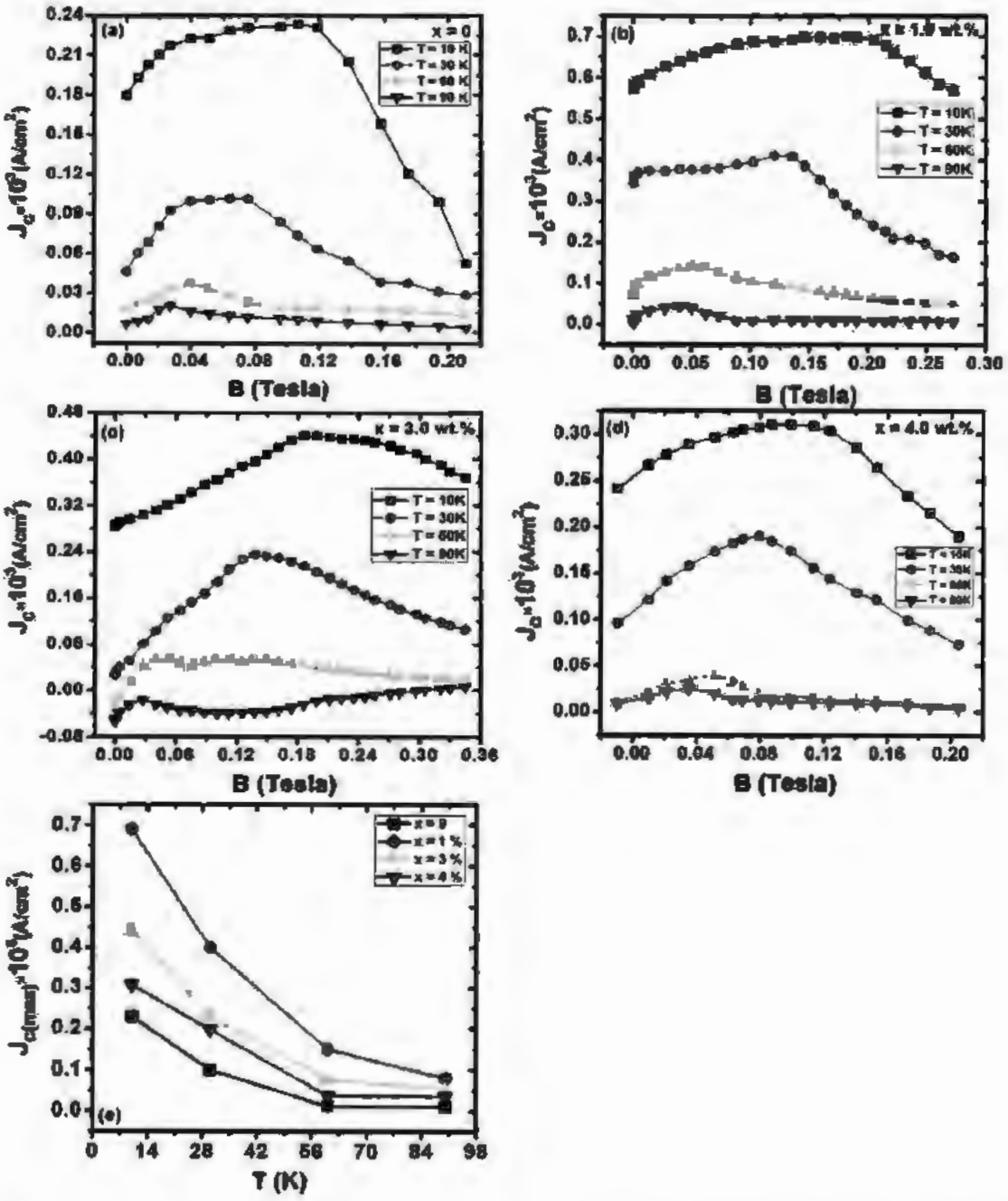

Fig. 3.10 (a-e). The alteration of magnetization J_c against temperature at 10, 30, 60, and 90 K by Cu NPs addition in (CuTl)-1223 superconductor with x = 0, 1.0, 3.0 and 4.0 wt.% respectively and (e) part represents the collective plots of J_c against temperatures for all concentration of Cu NPs.

3.3 References

[1] Y. Suresh, S. Annapurna, A. K. Singh, and G. Bhikshamaiah "Green synthesis and characterization of tea decoction stabilized copper nanoparticles", Int. J. Inno. Res. Sci. Eng. Technol. 3 (2014) 11265.

[2] A. Jabbar, I. Qasim, S. A. Khan, K. Nadeem, M. W. Rehman, M. Mumtaz and F. Zeb, "Highly Coercive cobalt ferrite nanoparticles-CuTl-1223 superconductor composites", J. Magn. Magn. Mater. 377 (2015) 6.

[3] S. A. Halim, S. A. Khawaldeh, S. B. Mohamed, H. Azhan, "Superconducting properties of $Bi_{2-x}Pb_xSr_2Ca_2Cu_3O_y$ system derived via sol-gel and solid state routes", Mater. Chem. Phys. 61 (1999) 9.

[4] J. M. Tarascon, Y. L. Page, P. Barboux, B. G. Bagley, L. H. Green, W. R. Mckinnon, G. W. Hull, M. Giroud and D. M. Hwang, "Crystal structure and physical properties of superconducting phase $Bi_4(Sr, Ca)_6Cu_4O_{6+x}$", Phys. Rev. B 37 (1988) 9382.

[5] Nawazish A. Khan, M. Mumtaz, K. Sabeeh, M. I. A. Khan, and M. Ahmad, "The study of phonon modes of $Cu_{1-x}Tl_xBa_2Ca_3Cu_4O_{12-y}$ superconductor thin films by FTIR absorption spectroscopy", Physica C 407 (2004) 103.

[6] A. Zelati, A. Amirabadizadeh, A. Kompany, H. Salamati, and J. Sonier, "Effects of Dy_2O_3 nanoparticle addition on structural and superconducting properties of BSCCO", Ind. J. Sci. Technol. 7 (2014) 123.

[7] O. Bilgili, Y. Selamet, and K. Kocabaş, "Effects of Li substitution in Bi-2223 superconductors", J. Supercond. Nov. Magn. 21 (2008) 439.

[8] R. S. Meena, A. Pal, S. Kumar, K. V. R. Rao, and V. P. S. Awan "Magneto-transport and magnetic susceptibility of $SmFeAsO_{1-x}F_x$(x= 0.0 and 0.20)", J. Supercond. Nov. Magn. 26 (2013) 2383.

[9] S. Fostner, A. Nande, R. M. A. Smith, and J. M. B. Van, "Percolating transport in superconducting nanoparticle films", J. Appl. Phys. 122 (2017) 223905.

[10] A. Masahiro, "Fluctuation and percolation effect of superconductivity in Nb3Ge Films", Jpn. J. Appl. Phys. **26** (1987) 3.

[11] G. Kmat, O. Kzılaslan, and M. A. Aksan, "Effect of the Er-substitution on critical current density in glass-ceramic $Bi_2Sr_2Ca_2$ $(Cu_{3-x}Er_x)O_{10+\delta}$ superconducting system", Ceram. Int. **13** (2016) 15072.

[12] A. G. Joshi, C. G. S. Pillai, P. Raj, and S. K. Malik, "Magnetization studies on superconducting MgB_2 lower and upper critical fields and critical current density", Solid Stat. Commun. **9** (2001) 445.

[13] P. Przyslupski, I. Komissarov, W. Paszkowicz, P. Dluzewski, R. Minikayev, and M. Sawicki, "Magnetic properties of $La_{0.67}Sr_{0.33}MnO_3/YBa_2Cu_3O_7$ superlattices", Phys. Rev. B **69** (2004) 134428.

[14] D. Song, S. Ishida, A. Iyo, M. Nakajima, J.Shioyama , M. Eisterer, and H. Eisoka, "Distinct doping dependence of critical temperature and critical current density in $Ba_{1-x}K_xFe_2AS_2$ superconductor", Sci. Rep. U. K. **6** (2016) 26671.

[15] P. Przyslupski, A. Tsarou, P. Dluzewski, W. Paszkowicz, R. Minikayev, K. Dybko , M. Sawicki, B. Dabrowski and C. Kimaball, "Interplay of superconductivity and ferromagnetism in $YBa_2Cu_3O_7/La_{1-x}Sr_xMnO_3$ heterostructures", Supercond. Sci. Technol. **19** (2006) S38.

[16] U. Tapal, C. Birlikseven, M. F. Yakinci, and T. Nurgaliev, "Analysis of the magneto-transport properties of superconducting/ferromagnetic $YBa_2Cu_3O_7/La_{0.7}Sr_{0.3}MnO_3$ bilayer thin film", J. Alloys Compd. **492** (2010) 8.

Chapter 4

(Ag)$_x$/CuTl-1223 Nanoparticles-Superconductor Composites

The field dependent superconducting transport properties of (CuTl)-1223 by inclusion of Ag NPs with concentrations of x= 0 ~ 4.0 wt. % nanoparticle superconductor composites have been studied. Ag nanoparticles with different concentrations were added to investigate different superconducting feathers of (CuTl)-1223 host matrix. Superconducting along with flux pinning properties are expected to enhance by metallic nature of Ag NPs in CuTl-1223 superconducting phase. Infield DC resistivity of composites was measured by PPMS with magnetic strength of 0~8T. Various superconducting parameters such as upper critical field (H_{c2}), transition width (ΔT_c) and coherence length {$\xi(0)$} were calculated by using Ginzburg- Landau (GL) formula, TAFF model and Werthmer-Helfand-Hohenberg (WHH) formula. The Arrhenius law was used for calculation of activation energy U_o.

4.2 Results and discussion

4.2.1 X-rays diffraction (XRD) analysis

Phase purity of Ag NPs and nanoparticles superconducting composites were examined by X-rays diffraction pattern. The XRD spectrum of Ag NPs is represented by Fig. 4.1. Average crystallite size of Ag NPs, calculated by Debye-Scherer's formula was found 17 nm. The XRD peaks found at 38°, 44.32°, 64.35° and 77.25° were indexed as (111), (200), (220) and(311) planes according to the standard card JCPDS (Card No. 04-0783) indicating FCC crystal structure of the Ag NPs [1]. Figure 4.2 represents the XRD spectra of Ag NPs addition with various contents (x = 0, 2.0 and 4.0 wt. %) in (CuTl)-1223 superconductor. Pronounced XRD peaks were labeled in accordance with tetragonal symmetry of P4/mmm space group for (CuTl)-1223 superconductor. The lattice parameter (a) was un-altered with Ag NPs inclusion, which showed that Ag NPs probably had not entered in unit cell of host material. The parameter 'c' was slightly varied with addition of Ag NPs in (CuTl)-1223 superconductor by virtue of stresses or strains. Fig. 4.2 represents low intensity perks of (CuTl)-1234, (CuTl)-1212superconductors and unknown impurities.

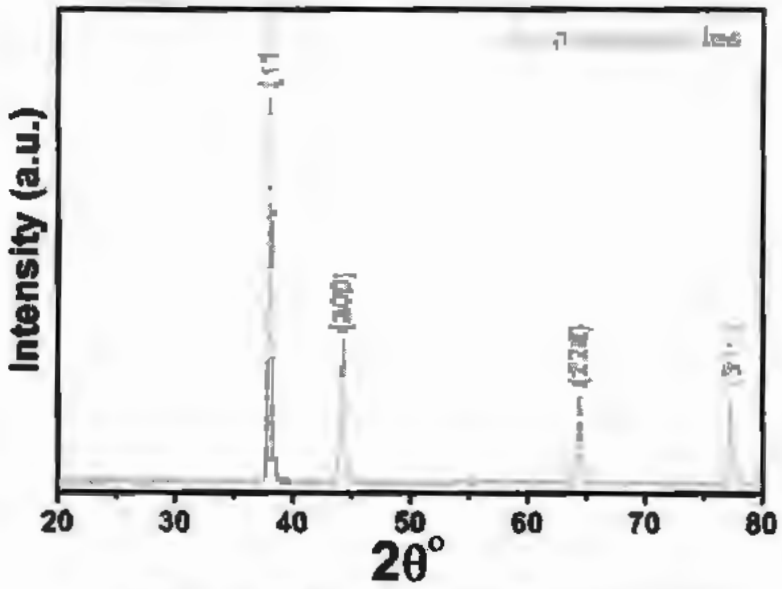

Fig. 4.1: The X-rays diffraction pattern of Ag NPs.

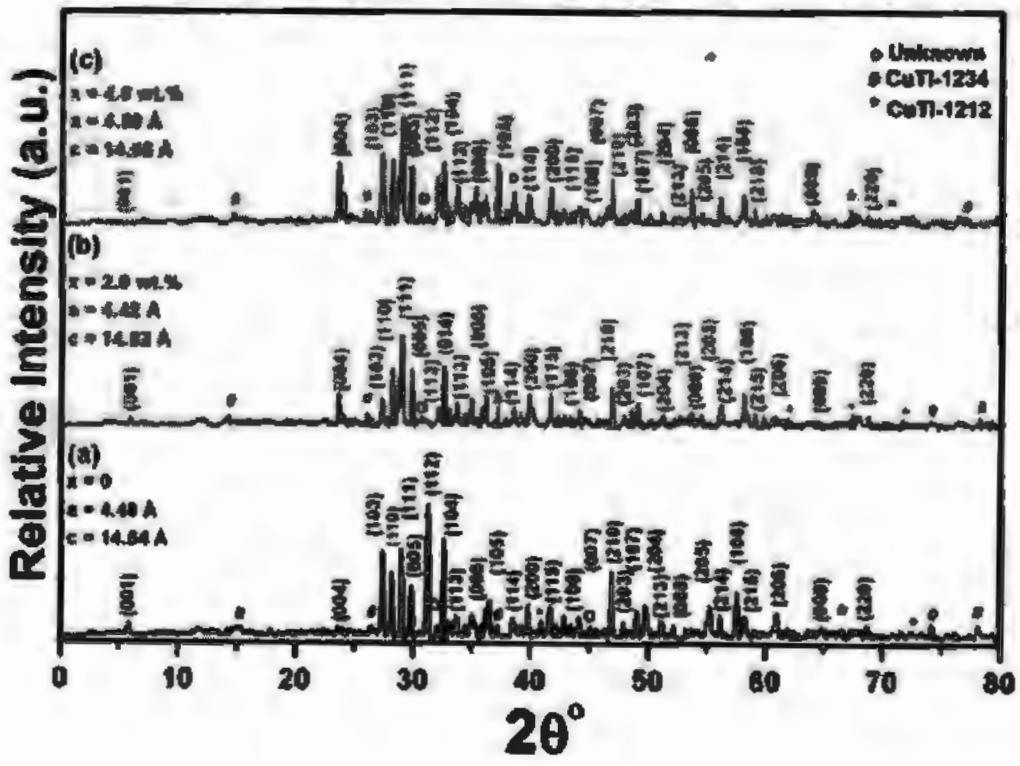

Fig. 4.2: XRD patterns of (CuTl)-1223 superconductor by inclusion of various contents (x = 0, 2 and 4 wt. %) of Ag NPs.

4.2.2 Scanning electron microscopy (SEM)

The surface morphology of $(Ag)_x$/(CuTl-1223) nanoparticles-superconductor composites was studied by scanning electron microscopy (SEM). Fig. 4.3 (a-c) indicates the SEM images of (CuTl)-1223 superconductor by Ag NPs inclusion using different concentrations such as 0, 2 and 4 wt. %. The gaps, voids were observed prominently at inter-granular spaces in pristine sample of CuTl-1223. The connectivity among grains of (CuTl)-1223 phase was amended by filling the voids and pores by various Ag NPs contents as shown in Fig. 4.3. The small grains amplified to larger grain size as result of activation energy supplied by reaction. These grains were observed to attach with surface by Ag NPs addition to host matrix.

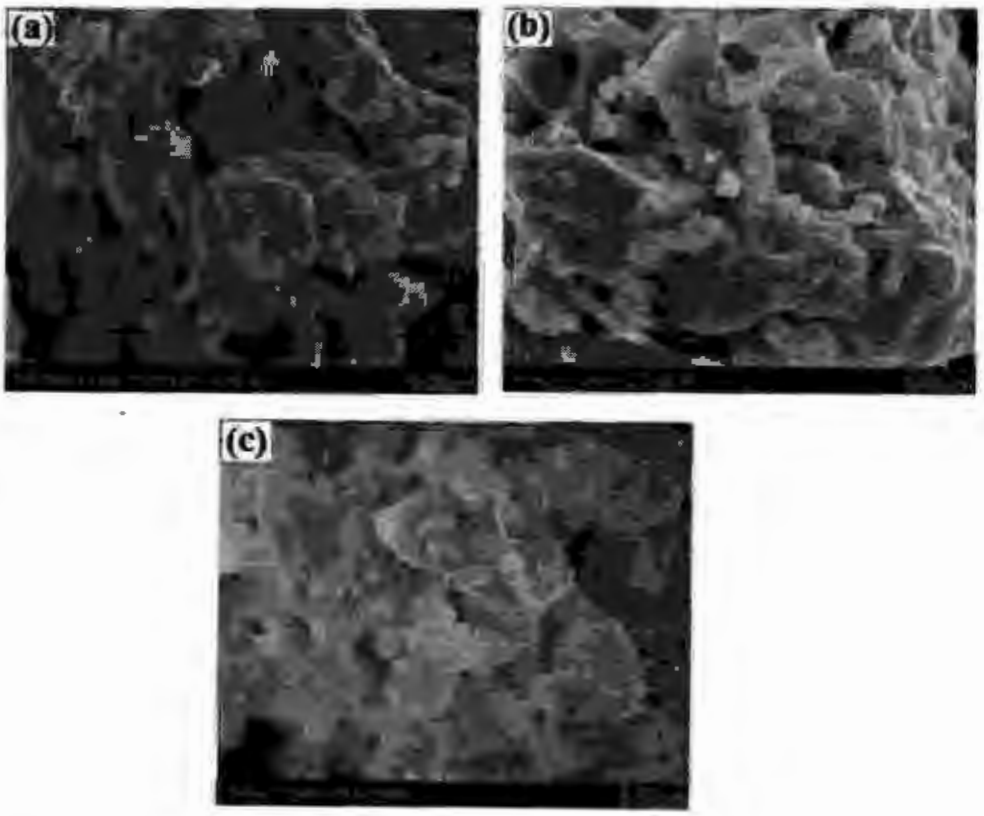

Fig. 4.3: The SEM images of (CuTl)-1223 superconductor by Ag NPs addition with various contents such as 0, 2.0 and 4.0 wt. %, represented by a, b, c respectively.

4.2.3 The Fourier transforms infrared (FTIR) and resistivity against temperature (R-T) Analysis

The vibrational bands of elements and various oxygen atoms present in unit cell can be verified by FTIR technique. The FTIR absorption spectra of (Ag)$_x$/CuTl-1223 composites in the range from 400-700 cm^{-1} with x = 0, 0.5, 1.0, 2.0 and 4.0 wt. %, are shown in Fig 4.4. The bands of apical oxygen atoms and CuO_2 planar oxygen atoms were observed at 400 to 540 cm^{-1} and 541 to 600 cm^{-1} correspondingly. The bonds related to charge reservoir layer affiliated with O_δ atom were positioned at 670 to 700 cm^{-1}. The small variation was observed in these bonds by stress and strain production during the inclusion of Ag NPs in CuTl-1223 superconductor. The FTIR results were good agreements to XRD and SEM results and indicated that Ag NPs had not incorporated to unit cell of host superconductor.

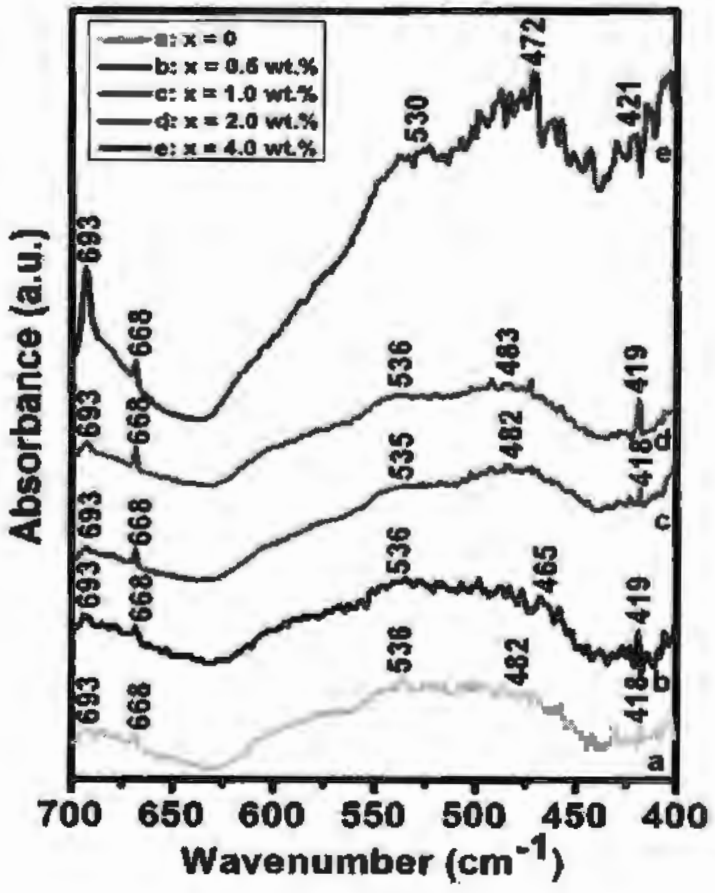

Fig. 4.4 (a-e): FTIR absorption spectra of (Ag)$_x$/CuTl-1223 composites with x = 0, 0.5, 1.0, 2.0 and 4.0 wt.% .

Figure 4.5 indicates the temperature based dc-resistivity with different applied magnetic fields (H = 0 ~ 8 T) of (CuTl)-1223 superconductor by inclusion of various contents (x = 0 and 2 wt. %) of Ag NPs. The offset critical temperature was suppressed while onset critical temperature remained almost unaffected with increasing strength of magnetic field for all contents of Ag NPs as claimed by other researches [2, 3]. These behaviors were ascribed by robust inter-grain pinning energy and seize motion of vortices near offset temperature [4]. The offset critical temperature was enhanced up to an optimum level of 2 wt. % with Ag NPs inclusion due to reformation of weak-links between grains by healing pores and voids. The superconducting parameters then suppressed beyond optimum level of Ag NPs due to decreasing superconducting volume fraction. The normal state resistivity (ρo) was lessened which was indication of connectivity improvement among grains due to reduction in porosity by Ag NPs inclusion in host phase. Refining of transition curves below T_c^{onset} was correlated with thermally activated flux flow (TAFF) under esteem of magnetic field.

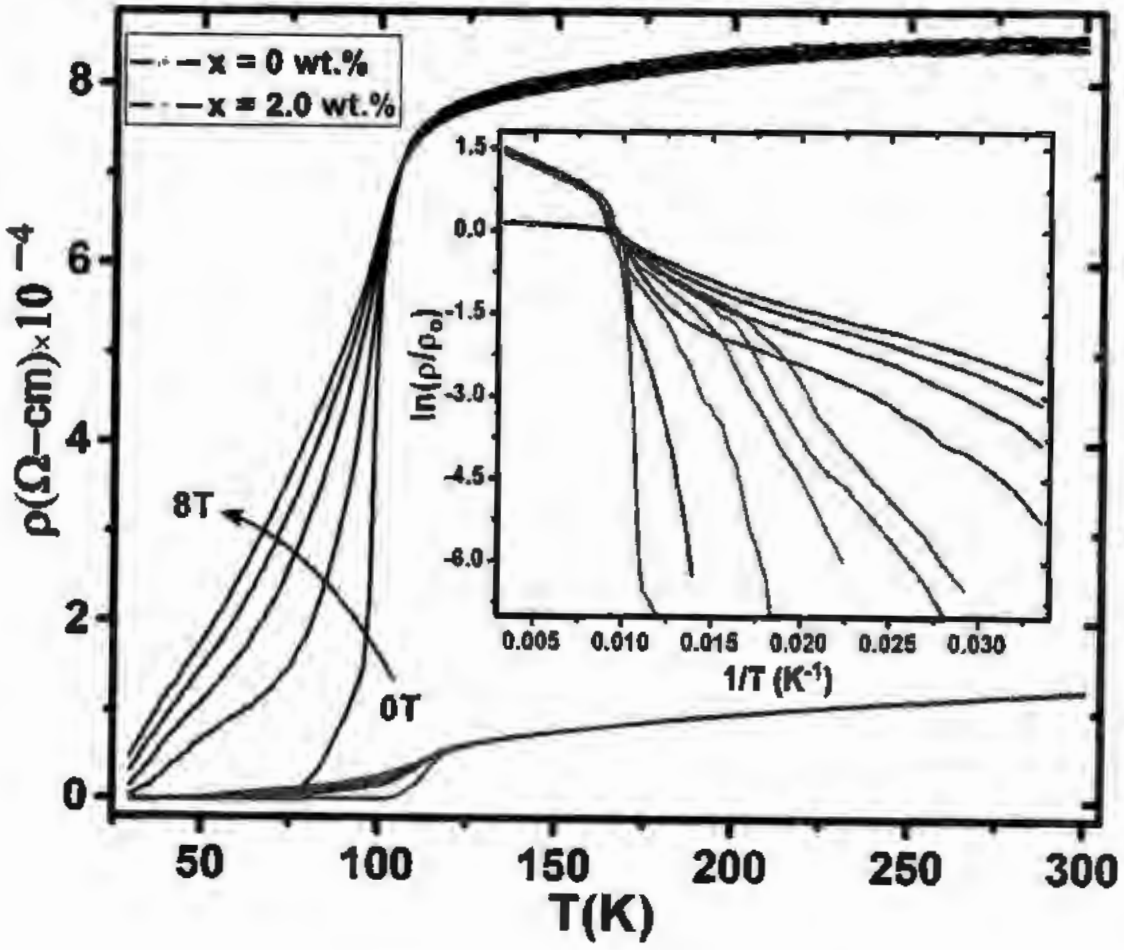

Fig. 4.5: Infield dc-resistivity against temperature of (CuTl)-1223 superconductor with addition of Ag NPs for 0 and 2.0 wt. % with application of field from 0 ~ 8T. The inset represents Arrhenius plot for activation energy and resistive transition.

4.2.4 Activation energy, upper critical magnetic field and transition width analysis

The various superconducting parameters such as activation energy (U_o), Transition width (ΔT_c) coherence length {$\xi(0)$} and upper critical magnetic field (H_{c2}) was calculated by thermally activated flux flow model. Activation energies were calculated at low temperature from linear part of Arrhenius plots of ln (ρ/ρ_o) against (1/T) as indicated in inset of Fig. 4.5. At low temperature in TAFF regime, the Arrhenius law was utilized to calculate current independent resistivity as given by Eq. 1.49. Fig.4.6 represents activation energy (U_o) against magnetic field H by inclusion of Ag NPs in host matrix.

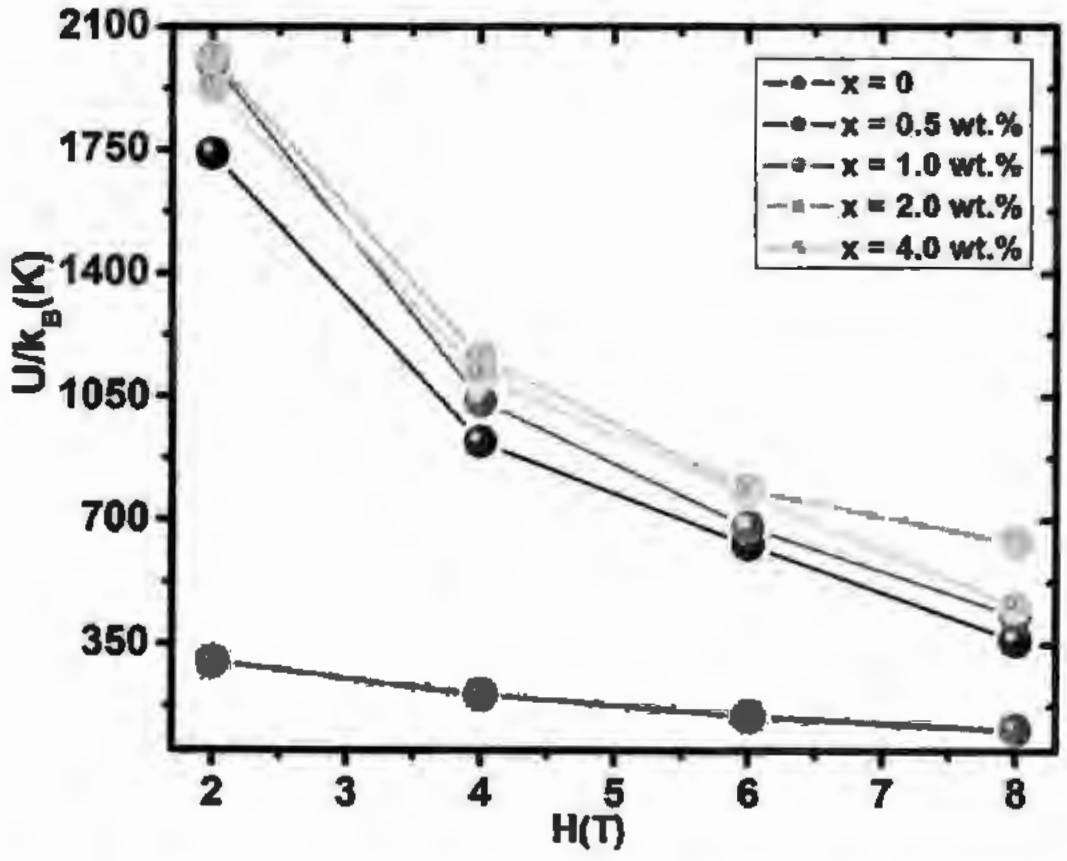

Fig. 4.6: The activation energy (U_o) against magnetic field (H) of (CuTl)-1223 superconductor by Ag NPs inclusion from 0 ~ 4.0 wt. % respectively. The activation energy was lessened

dramatically with the increasing magnetic field as clearly witnessed by Fig. 4.6. At start, the quickened decrease of activation energy could be due to demolition of weak-links among granular spaces. At large values of magnetic field, the drop in activation energy were not so quick due to grabbing of flux lines and departing inter-granular spaces relatively unaltered [5]. The activation energy also based on concentrations of nanostructures and observed optimum up to 2.0 wt. % for these Ag NPs. The transition width {$\Delta T = T_c^{onset} - T_c(0)$} against magnetic field of (CuTl)-1223 superconductor by addition of various contents (0 ~ 4.0 wt. %) of Ag NPs is represented by Fig. 4.7. The curves were plotted and fitted on basis of TAFF model, as given by Eq.1.51.

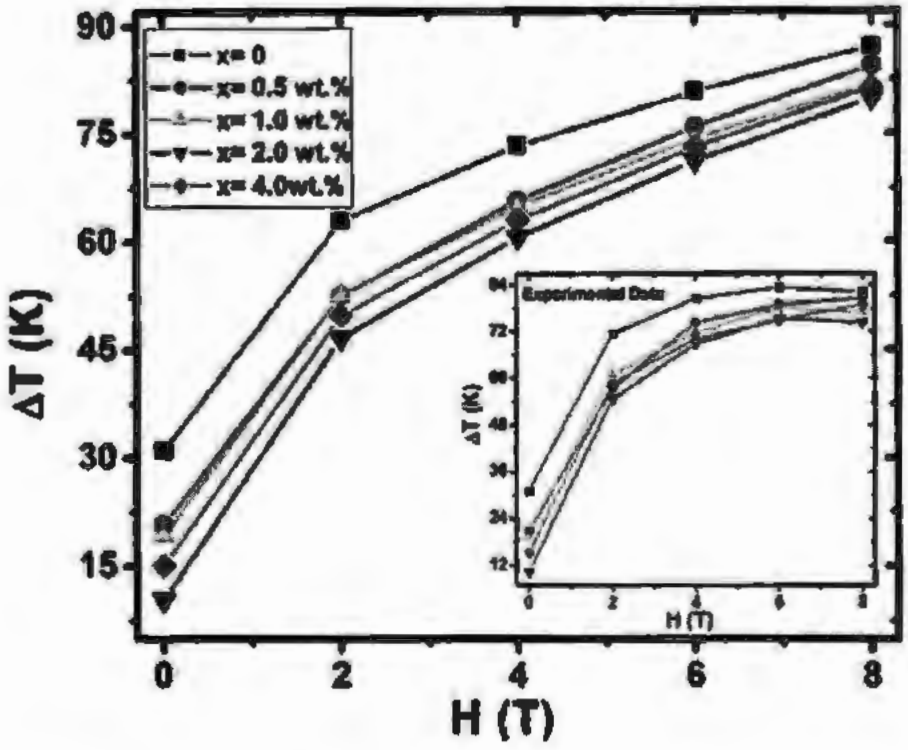

Fig. 4.7: Transition width ΔT against magnetic field of (CuTl)-1223 superconductor by varying contents (0 ~ 4.0 wt. %) of Ag NPs with fitted according to TAFF model. Inset indicates observed plot of ΔT against H.

Decrease in ΔT was observed with incorporation of Ag NPs in host matrix, indicating improvement in flux pinning strength due to improvement in activation energy. Upper critical field (H_{c2}) was approximated by 90 % of ρ_o and also was calculated by WHH formula, expressed as;

$$H_{c2}(0) = -0.693 \left(\frac{dH_{c2}}{dT}\right) T_c \text{ ----------(4.1)}$$

where $\frac{dHc2}{dT}$ is H_{c2} slope against T and T_c = Zero resistivity transition temperature [6-8]. Upper critical field versus temperature with different concentration (0 ~ 4.0 wt. %) of Ag NPs in (CuTl)-1223 and is represented by Fig. 4.8.

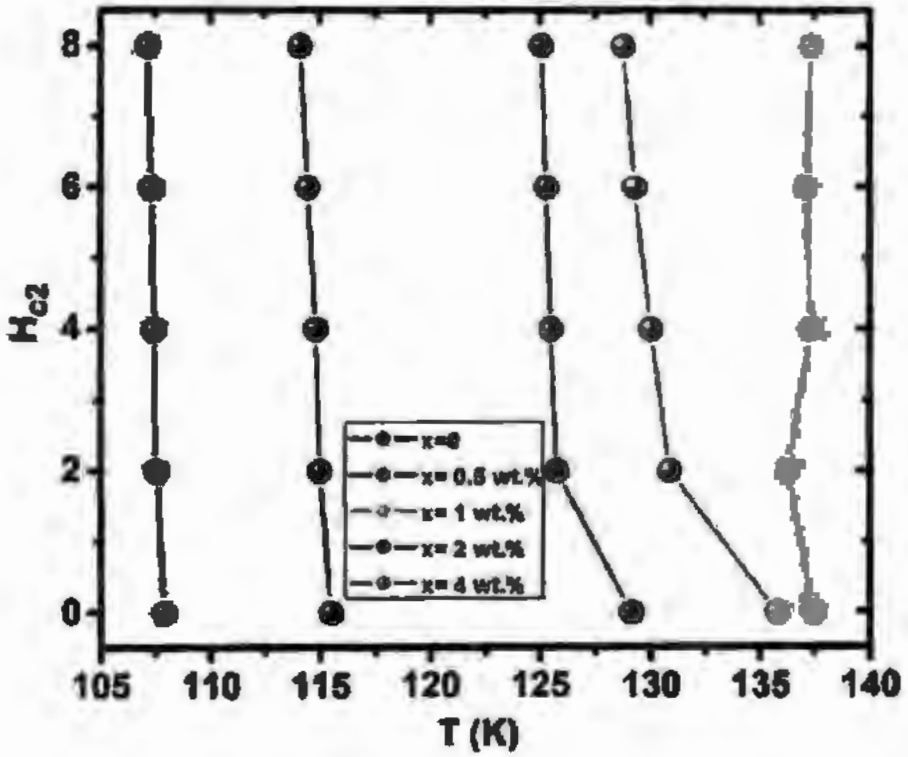

Fig. 4.8: Upper critical field against Temperature of (CuTl)-1223 superconductor with x= 0 ~ 4.0 wt. % Ag NPs addition.

Coherence length at T= 0 K was estimated by an equation given as;

$$\xi(0) = \sqrt{\frac{\phi_o}{2\pi H_{c2}(0)}} \text{ ----------(4.2)}$$

where Φ_o = quantum magnetic flux and have value 2.07×10^{-7} G/cm^2 [9]. Values of different superconducting parameters as function of Ag NPs contents are given in Table 4.1. The value of H_{c2} was increased while $\xi(0)$ was decreased with increasing contents of Ag NPs as represented by Fig.4.9, which indicated the increment in flux pinning properties of host matrix.

Table 4.1: Superconducting parameters of (CuTl)-1223 superconductor by varying contents (x= 0 ~ 4.0 wt. %) of Ag NPs.

'Ag' nanoparticles Content (wt %)	T_c (0) (K)	Slope (T/K)	H_{c2} (0) (T)	ξ (0) (Å)
0	73.23	−0.20	10.14	0.570
0.5	95.69	−0.191	12.66	0.510
1.0	98.73	−0.196	13.48	0.494
2.0	101.76	−0.235	16.61	0.445
4.0	91.23	−0.193	12.07	0.522

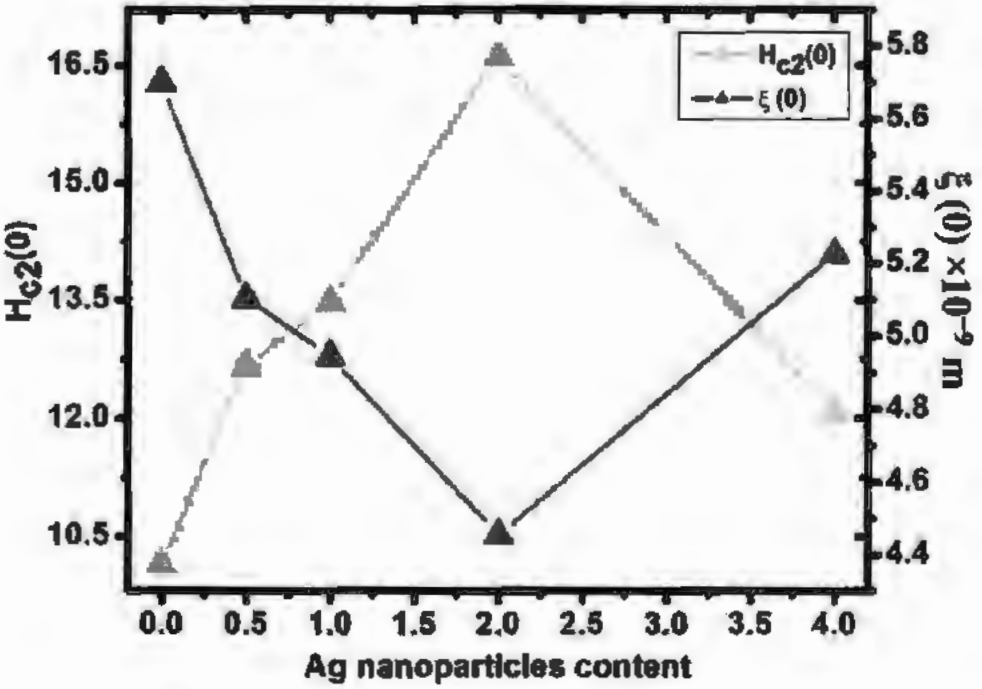

Fig. 4.9: The double plots of H_{c2} and ξ(0) with various contents of Ag NPs.

4.3 References

[1] K. M. M. Abou El-Nour, A. Eftaiha, A. Al-Warthan, and R. A. A. Ammar "Synthesis and applications of silver nanoparticles", Arab. J. Chem. 3 (2010) 135.

[2] D. Sharma, R. Kumar, and V. Awana, "Temperature and field dependence of thermally activated flux flow resistance in $Bi_2Sr_2CaCu_2O_{8+\delta}$ superconductor", Solid State Commun. **152** (2012) 941.

[3] S. Vinu, P. M. Sarun, R. Shabna, and U. Syamaprasad, "Analysis of thermo-magnetic fluctuations above the glass-transition temperature in $Bi_{1.6}Pb_{0.5}Sr_{2-x}$ $Eu_xCa_{1.1}Cu_{2.1}O_{8+\delta}$ ($0.000 \leq x \leq 0.180$) system", Solid State Sci. **11** (2009) 1530.

[4] R. Awad, N. Aly, I. Ibrahim, A. Abou-Aly, and A. Saad, "Effect of magnetic field on the electrical resistance of Tl-1223 doped by Zn and Ni", Physica B **307** (2001) 72.

[5] J. R. Castellanos, Y. Matsui, E. T. Muromachi, and M. Isobe, "Microstructural characterization of $GaSr_2Ca_2Cu_3O_{9+\delta}$, n=3 member of the homologous series of superconductors $GaSr_2Ca_{n-1}Cu_nO_{2n+3}$, Physica C **251** (1995) 279.

[6] S. R. Ghorbani, X. Wang, M. Shabazi, S. Dou, K. Choi, and C. Lin, "Flux pinning and vortex transitions in doped $BaFe_2As_2$ single crystals", Appl. Phys. Lett. **100** (2012) 072603.

[7] G. S. Thakur, J. Prakash, M. Kanagaraj, S. Arumugam, and A. K. Ganguli, "Enhancement in superconducting transition temperature (T_c) and upper critical field (H_{c2}) in new Yb-doped $Ce_{1-x}Yb_xO_{0.9}F_{0.1}$ FeAs superconductors", Physica C **480** (2012) 71.

[8] A. Yamamoto, J. Jaroszynski, C. Tarantini, L. Balicas, J. Jiang, A. Gurevich, D. Larbalestier, R. Jin, A. Sefat, and M. A. McGuire, "Small anisotropy, weak thermal fluctuations, and high field superconductivity in Co-doped iron pnictide Ba $(Fe_{1-x}Co_x)_2As_2$", Appl. Phys. Lett. **94** (2009) 062511.

[9] B. Maruszewski, A. Drzewiecki, and R. Starosta, "Anomalous features of the thermomagnetoelastic field in a vortex array in a superconductor: Propagation of love's waves", J. Therm. Stresses **30** (2007) 1049.

Chapter 5

(Au)$_x$/CuTl-1223 Nanoparticles-Superconductor Composites

Infield superconducting transport properties have been investigated by inclusion of gold (Au) nanoparticles with various concentrations (x= 0, 0.5, 1.0 and 1.5 wt. %) in CuTl-1223 superconductor. Phase purity and morphology were examined by XRD and SEM respectively. Infield properties have been studied by using four point probe technique without field and also with strength of magnetic field up to 7 T by virtue of quantum design PPMS. Vortex dynamics with inclusion of Au NPs in CuTl-1223 superconductor were investigated by analyzing the resistive transition in external applied magnetic field. Superconducting parameters such as activation energy (U_o), upper critical field (H_{c2}), coherence length {$\xi(0)$, transition width (ΔT_c), and critical current densities (J_c) were calculated by infield measurements with help of different models.

5.2 Results and discussion

5.2.1 X-rays diffraction (XRD) analysis

Phase purity of Au NPs and host matrix with these NPs were examined by XRD spectra. The XRD spectrum of Au NPs is represented by Fig. 5.1. Average crystallite size of Ag NPs,

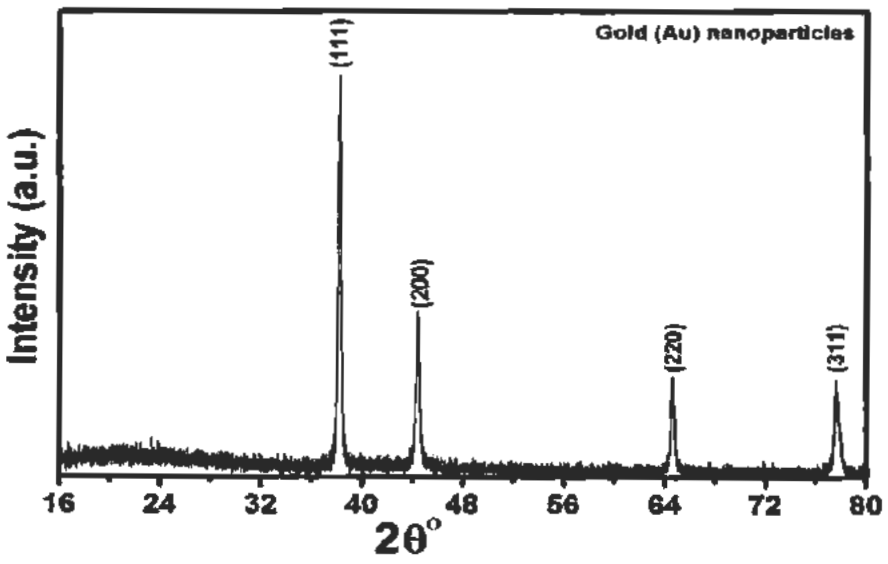

Fig. 5.1: XRD scan of Au NPs.

calculated by Debye-Scherer's formula was found 39 nm. The XRD peaks found at 38.28°, 44.32°, 64.72° and 77.65° were indexed as (111), (200), (220) and (311) planes according to the standard card JCPDS (Card No. 04-0784) indicating FCC crystal structure of the Au NPs [1]. The illustrative X-ray diffraction (XRD) scans of (CuTl)-1223 superconductor by various Au NPs (0 and 1.0 wt. %) insertion are represented by Fig. 5.2. These XRD scans were indexed according to tetragonal texture in accordance to P4/mmm symmetry. Most of diffraction peaks were well indexed in accordance with (CuTl)-1223 superconductor. The lattice parameters 'a' = 4.20 Å and 'c' = 15.31 Å, lattice parameters 'a' & 'c' = 4.19 Å, & 15.13 Å were observed for samples 0 and 1.0 wt. %, accordingly. A slight subside along c-axis was noticed in host (CuTl)-1223 superconducting phase, that can be most likely to oxygen contents modification or stresses and strains generated by Au NPs insertion. Some un-indexed diffraction peaks depict the existence of impurities and other superconducting phases.

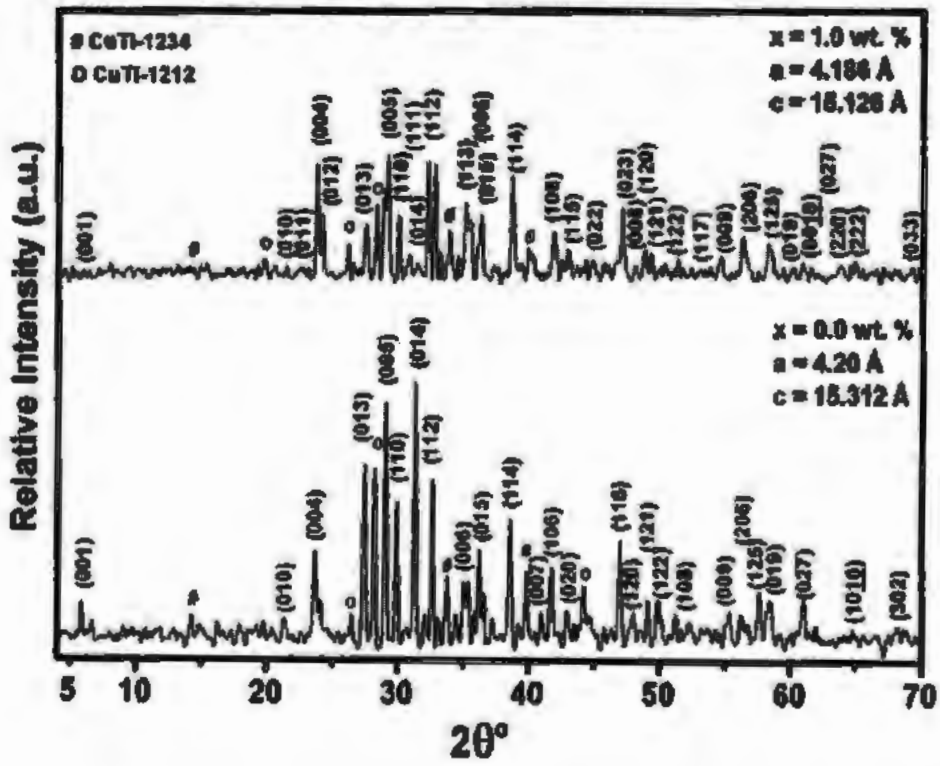

Fig. 5.2: The XRD scans of (CuTl)-1223 superconductor by inclusions of Au NPs with various contents of 0 and 1.0 wt. % respectively.

5.2.2 Surface morphology investigation via SEM

The surface formative analysis of Au NPs inclusion in CuTl-1223 superconductor was investigated by scanning electron microscope. The SEM counterparts of (CuTl)-1223 superconductor by addition of Au NPs with various contents of 0, 0.5, 1.0 and 1.5 wt. % are shown in Fig.5.3. The inter-granular connectivity and grain size were improved by addition of Au NPs in CuTl-1223 superconductor. The Voids and spaces between grains were reduced by addition of Au NPs.

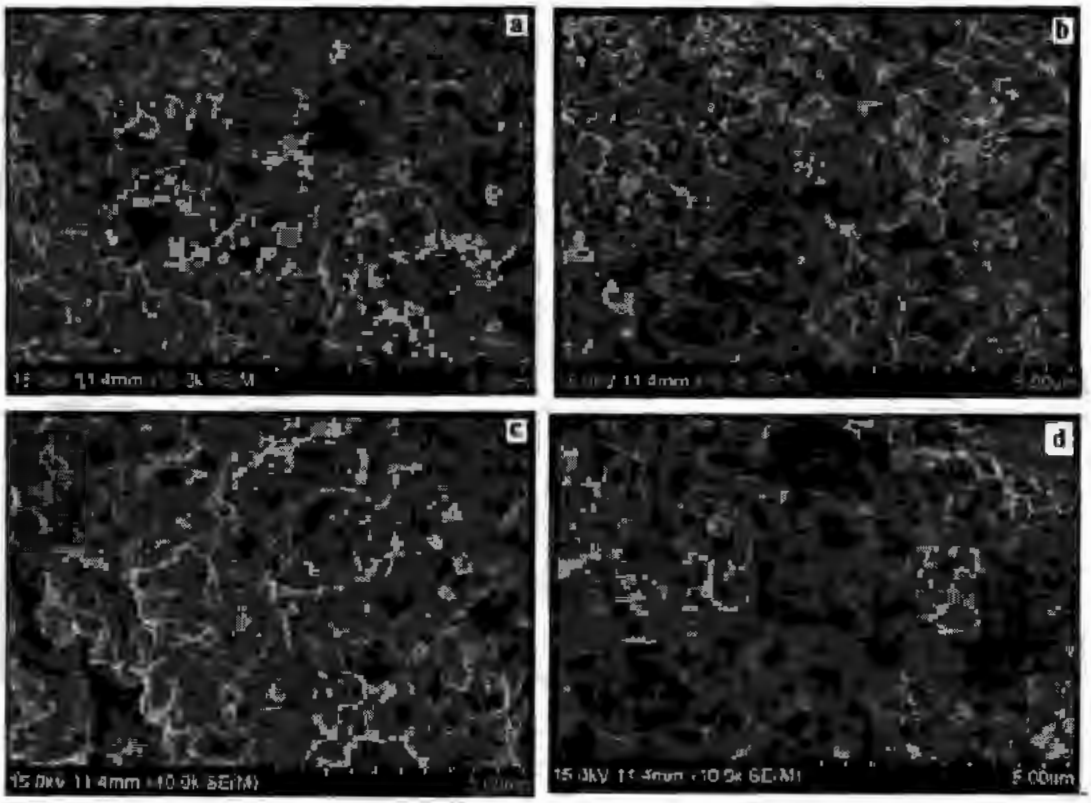

Fig. 5.3: The SEM counterparts of (CuTl)-1223 superconductor by Au NPs insertion with different contents of 0, 0.5, 1.0 and 1.5 wt. % respectively.

5.2.3 The analysis of Fourier transforms infrared spectroscopy

The FTIR spectra of Au NPs added CuTl-1223 superconductor in range of 400 to 700 cm^{-1} with $x = 0 \sim 1.5$ wt. % is represented by Fig.5.4. The bands in host unit cell affiliated with apical oxygen are observed in 400 to 540 cm^{-1} domain. The bands affiliated accompanying copper oxide planar oxygen atoms as well as charge reservoir layer are observed in domain of 541 to

600 and 670 to 700 cm^{-1} respectively. These bonds were slight shifted at different positions by addition of Au NPs in superconductor matrix. The variation in bonds was due to change of bond length as result of strain produced during inclusion of Au NPs in host superconductor.

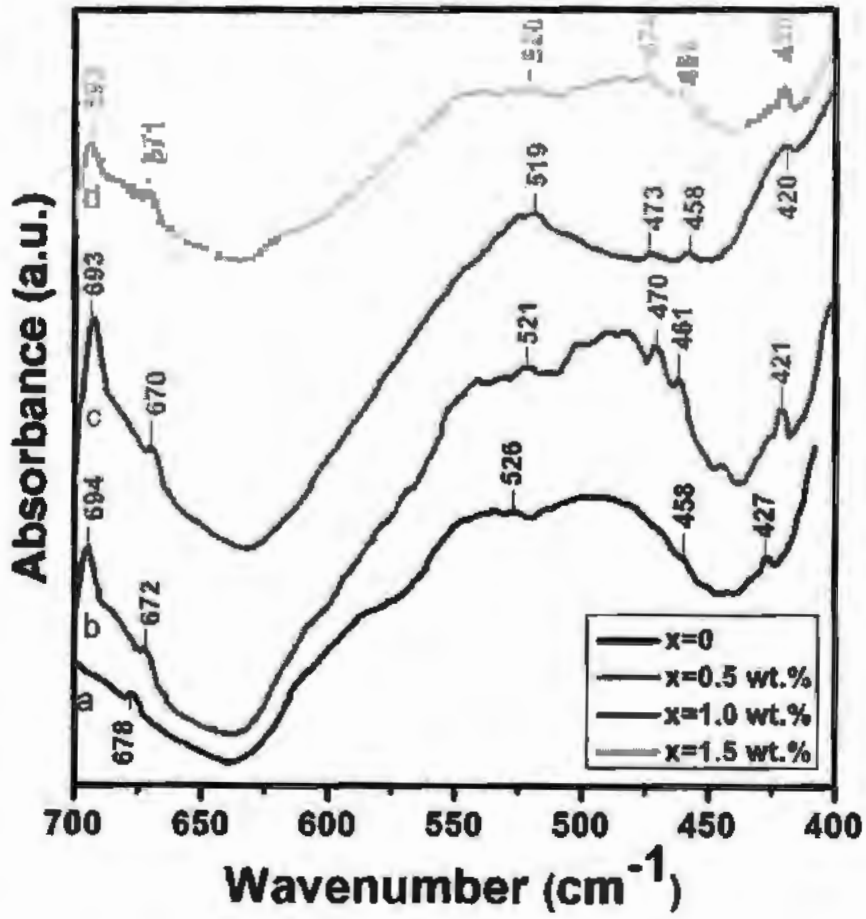

Fig. 5.4: The FTIR scans of (CuTl)-1223 superconductor by Au NPs insertion with various contents of 0, 0.5, 1.0 and 1.5 wt. % respectively.

5.2.4 Infield temperature dependent dc-resistivity and TAFF analysis

Temperature-dependence dc-resistivity measurements for (CuTl)-1223 superconductor were examined at wide range strength of magnetic fields till 7 T as shown in Fig. 5.5. The magnetic field affected regions among grains efficiently and delivered a branching effect close to the transition temperature (T_c). However, T_c^{onset} remained unaffected by increasing the external applied magnetic field. Primarily, an enhancement in T_c was witnessed by optimum 1.0 wt.%

insertion of Au NPs which could be due to refinement of weak- links among grains of superconductor by healing up voids and pores by inclusion of these NPs. The superconducting parameters were suppressed as result of superconducting volume fraction decrement beyond an optimum level of An NPs in host phase. The reduction of normal state resistivity (ρ_n) was an evidence of connectivity improvement among grains and reduction in porosity of host superconducting phase by Au NPs insertion. In thermally assisted flux flow regime, the Arrhenius law is utilized for estimation of activation energy (U_o) to prevail flux hoping. The current independent resistivity can be explained with Arrhenius law as given by Eq.1.49. The inset of Fig.5.5 is used to represent the ln (ρ/ρ_o) against 1/T plots of resistivity and utilized for activation energies (U_o) estimation from the linear parts of these plots at lower temperatures. The resistive transition broadening is provoked via energy losses, which can be explained by thermally assisted flux flow model (TAFF). The TAFF suggested that energy losses are directly proportional to thermal excitation of vortices [2, 3].

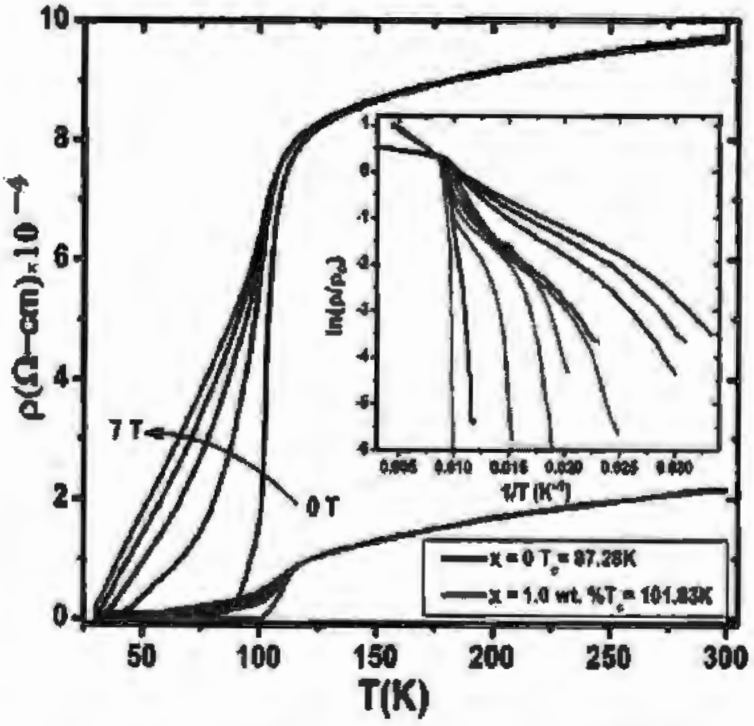

Fig. 5.5: Resistivity against temperature curves subjected to different applied magnetic field till 7 T for (CuTl)-1223 superconducting phase by insertion of Au NPs by various contents of 0 and

1.0 wt. %. The resistive transition Arrhenius plots and linear part of the low resistivity region that was utilized to get activation energy is shown in inset of that Fig.

5.2.5 The interpretation of transition width (ΔT) and activation energy (U_o)

The diversification in activation energy U_o against applied field H for (CuTl)-1223 superconducting matrix by various concentrations (0 ~ 1.5 wt. %) of Au NPs is shown in Fig. 5.6.

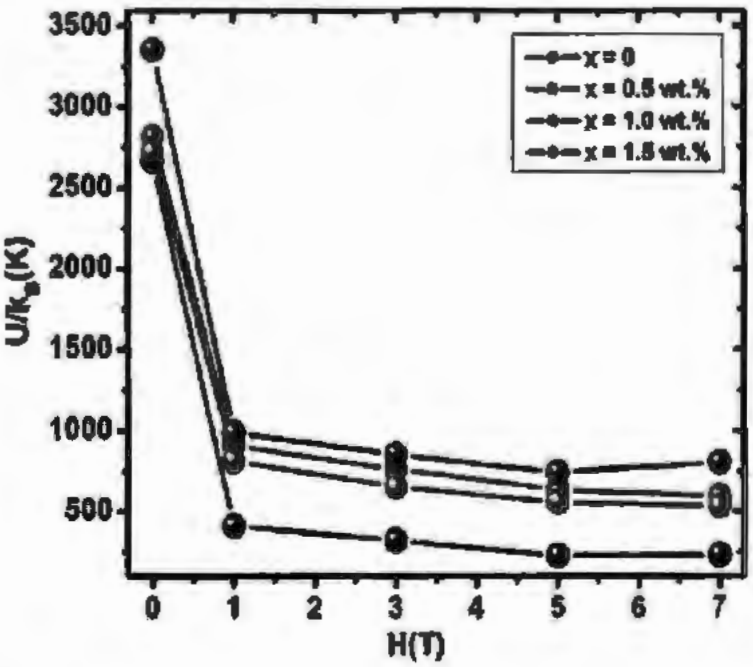

Fig. 5.6: The diversification in activation energy against applied field for (CuTl)-1223 superconductor with various contents of 0 ~ 1.5 wt. % for Au NPs insertion.

A declining tendency in U_o was noticed by increasing externally applied magnetic field that may be due to shorten of energy barriers. The U_o was found dependant on concentrations of Au NPs that was optimized for 1.0 wt. % as represented by Fig. 5. 6. Thermal activation of flux across pinning barriers induces loses of energy. The field dependent resistivity data were appraised with help of thermally activated flux flow model (TAFF), which could be utilized for estimation of shape and broadening of ΔT as given by Eq.1.51 and n is taken 2/3 in this equation [4]. The diversification of T with respect to applied magnetic field was estimated by $T = T_c^{onset} - T_c(0)$. Theoretically, fitted plot of ΔT against H in accordance with power law $U = \beta H^{-\alpha}$ is indicated by

Fig. 5.7. The parameter α deviates from 0.3627~ 0.3950, whereas unfitted scam is represented by inset of Fig. 5.7.

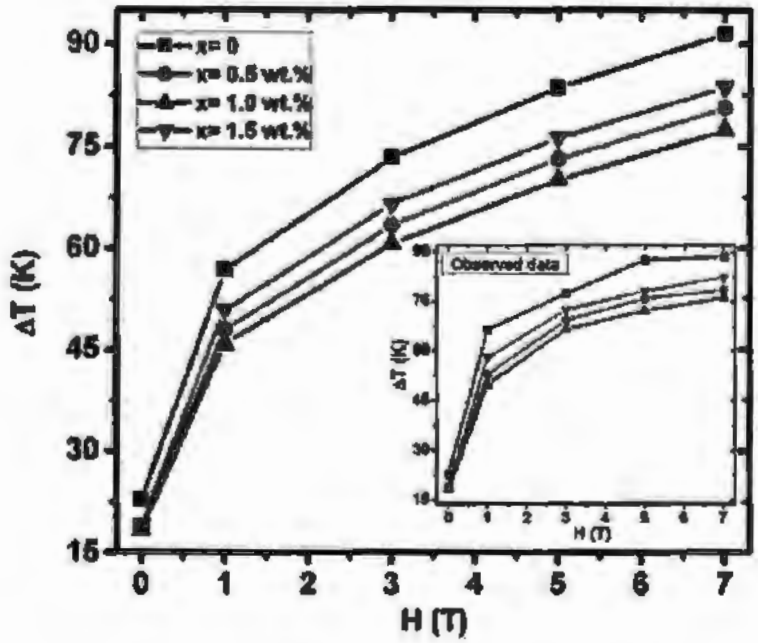

Fig. 5.7: Theoretically fitted plots of ΔT against various applied fields for (CuTl)-1223 superconducting phase with Au NPs insertion by varying contents of 0 ~ 1.5 wt. %. The observed plot of ΔT against H is represented in inset of above Fig.

The eminent enhancement of ΔT by increment of externally applied magnetic field might be as a result of haphazard orientations of grains. Weak- links among grains can be wrecked as result of increment in magnetic field [5]. Thermal fluctuations, applied field as well as dissipation phenomenon are key factors on which superconducting resistive broadening strongly depends.

5.2.6 Measurement of critical temperature with and without applied field

The variation of critical temperature versus applied external field of (CuTl)-1223 superconductor by insertion of Au NPs with various contents of 0 ~ 1.5 wt. % is represented by Fig.5.8. The zero critical temperature was lessened by increasing external applied while onset critical temperature was relatively unaffected by magnetic field for pristine and Au NPs insertion in host superconducting matrix. The transition broadening in superconductor was noticed by rising external applied field, which was ascribed to TAFF among (CuTl)-1223 superconductor [2].

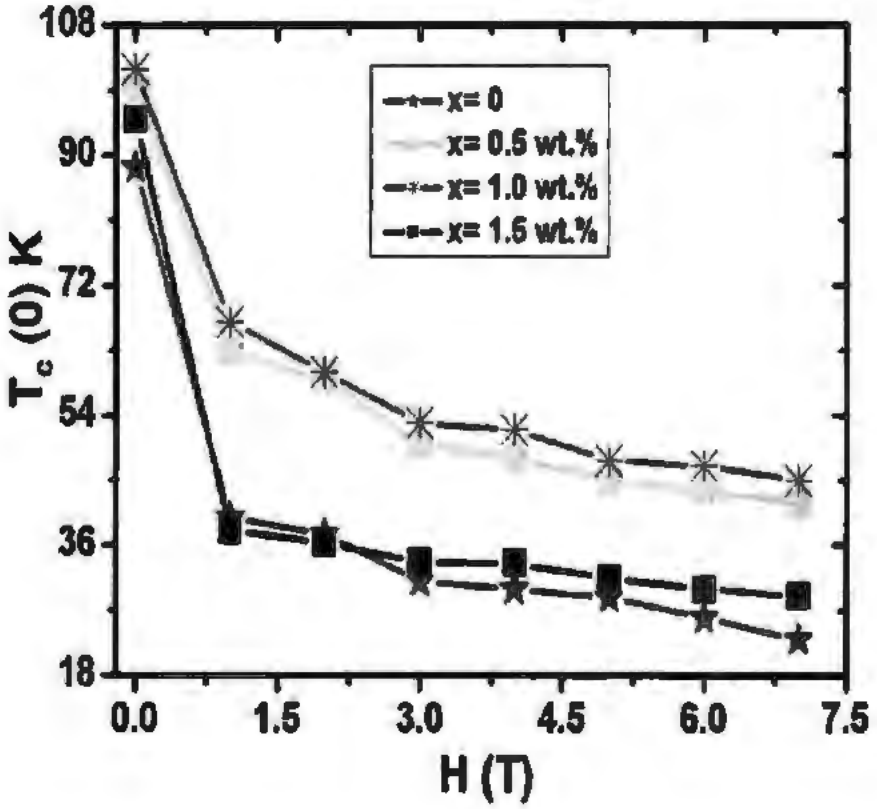

Fig. 5.8: Diversification of zero critical temperature against externally applied magnetic field of (CuTl)-1223 superconductor with various contents (0 ~ 1.5 wt. %) of Au NPs.

The alteration of zero critical temperature by concentrations of gold NPs is indicated by Fig. 5.9. The utmost enhancement in zero critical temperature was noticed in (CuTl)-1223 matrix by inclusion of 1.0 wt. % Au NPs, which predicted the optimum inclusion level in host superconductor composite [6, 7]. Filling up spaces among grains by gold NPs was major cause of increment in mechanism of superconductivity. Initially enhancement in T_c (0) was indication of improved weak-links of superconducting grains and was decreased beyond optimum level due to decrease of volume fraction by inclusion of Au NPs [6, 7]. Another reason in decreasing the values of T_c (0) was due to agglomerizations and segregation, caused the degradation the quality of samples.

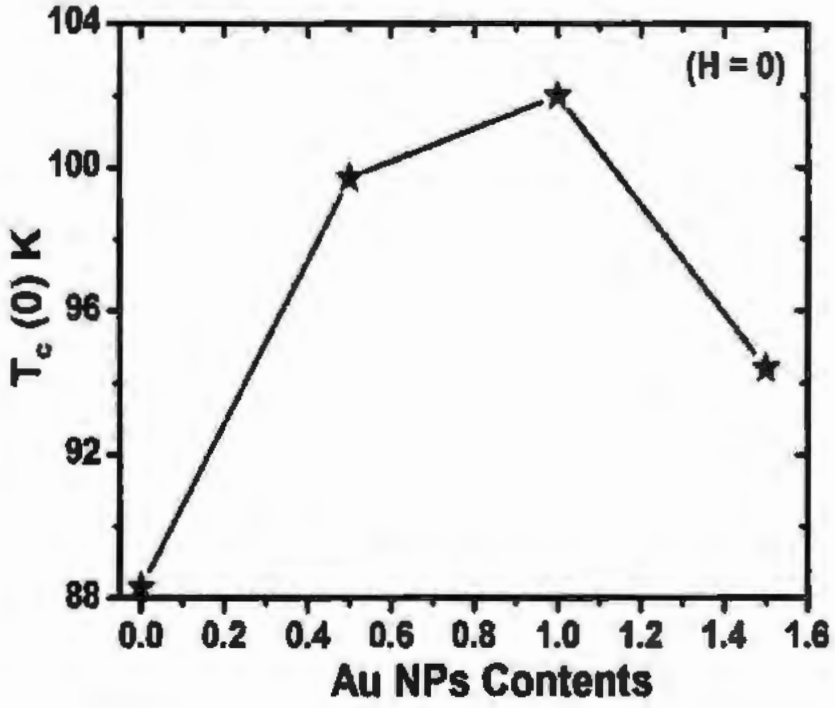

Fig. 5.9: Alteration of zero critical temperature against Au NPs concentrations in (CuTl)-1223 superconductor in absence of applied magnetic field.

5.2.7 Upper critical field (H_{c2}) versus temperature (T) analysis

The superconducting state of cuprate HTSCs alter to normal state at specific utmost values of externally applied field known as upper critical field (H_{c2}). The Werthamer-Helfand-Hohenberg (WHH) formula was used for estimation of upper critical field at 0 K as given by Eq.4.1. The diversification of H_{c2} against T in Kelvin of (CuTl)-1223 superconductor by Au NPs insertion with peculiar concentrations of 0 ~1.5 wt. % is represented by Fig. 5.10. The successive decrement in upper critical field by increment of temperature was noticed, which can be ascribed to thermal activated flux flow (TAFF) mechanism in these superconducting samples. Maximal improvement in the value of upper critical field was noticed in (CuTl)-1223 superconducting matrix by 1.0 wt. % Au NPs insertion. The increment in zero critical temperature and upper critical field pointed out that flux dynamics got decreased by insertion of Au NPs [8].

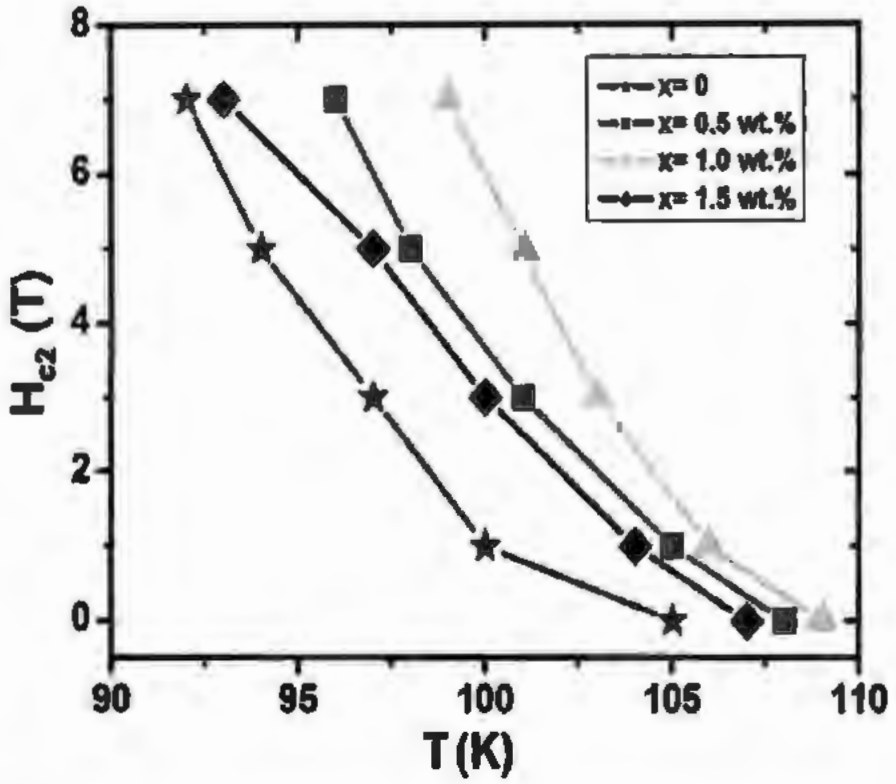

Fig. 5.10: The alteration in upper critical field against temperature of (CuTl)-1223 superconductor by Au NPs insertion with various contents (0 –1.5 wt. %).

5.2.8 The analysis of externally applied field (H) against coherence length (ξ)

The values of coherence length as calculated by Eq. 4.2 of (CuTl)-1223 superconductor by Au NPs insertion with different concentrations of x = 0 –1.5 wt. % and associated with externally applied magnetic field using graph as indicated by Fig. 5.11. Overall decrement in coherence length of (CuTl)-1223 superconductor was noticed by Au NPs insertion. The coherence length and radius of magnetic vortex are comparable in HTSCs. Thus, the suppression in coherence length by Au NPs insertion in (CuTl)-1223 superconductor under externally applied magnetic field and indicated that radii of magnetic vortices were decreased due to Lorentz force (F_L) [9].

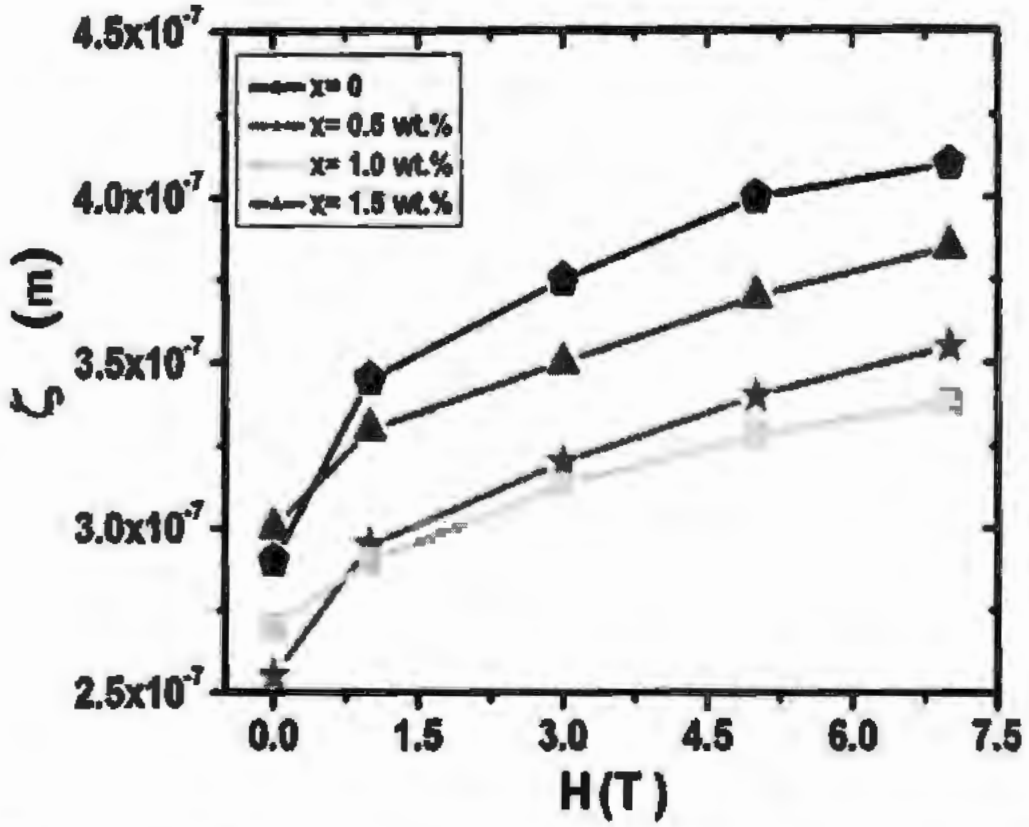

Fig. 5.11: Variation of $\xi(0)$ versus applied field for (CuTl)-1223 superconductor by insertion of Au NPs with variation of x = 0 – 1.5 wt. %.

The energy losses got reduced as result of reduction in Lorentz forces and suppression of flux dynamics. Hence it was concluded that depreciation in $\xi(0)$ was manifestation of improvement in flux pinning mechanism. The improvement of flux pinning mechanism was in pursuance of enhancement in zero critical temperature of host (CuTl)-1223 matrix by insertion of Au NPs.

5.2.9 Critical current density (J_c) analysis

The field dependent J_c is crucial parameter for flux pinning strength prediction in cuprate HTSCs in accordance to practical applications. The diversification in J_c against concentrations of Au NPs in (CuTl)-1223 superconductor without field and 0.5 T field is represented by Fig. 5.12. It was noticed that increment in values of J_c was observed in (CuTl)-1223 superconducting matrix with Au NPs inclusion. The magnetic field dependent sustainability of J_c affirmed the applicability of (CuTl)-1223 superconductor for practical applications. These investigations

revealed that Au NPs with suitable wt. % are feasible in various cuprate HTSCs for artificial flux pinning mechanism [10, 11].

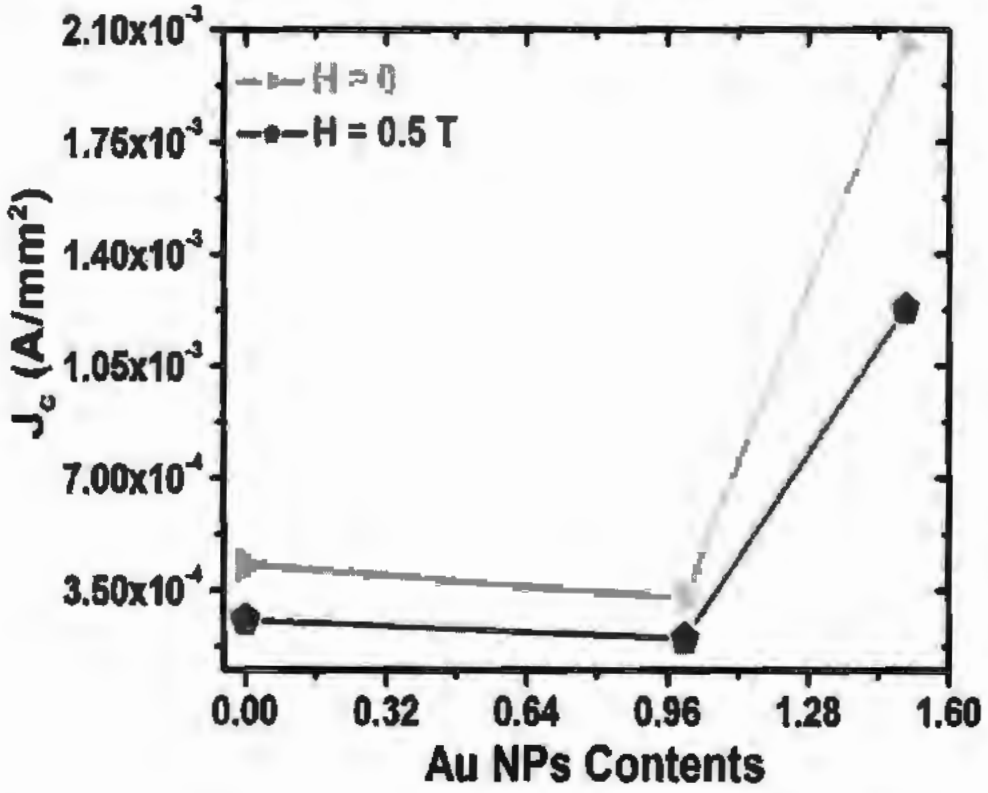

Fig. 5.12: The Jc variation against gold NPs concentrations in (CuTl)-1223 superconducting matrix without filed and 0.5 T field.

5.3 References

[1] S. Krishnamurthy, A. Esterle, N. C. Sharma and S. V. Sahi, "Yucca-derived synthesis of gold nano-material and their catalytic potential", Nanoscale Res. Lett. 9 (2014) 627.

[2] A. A. Khurram, S. Ahmad, and Nawazish. A. Khan, "Flux pinning in $Tl_{1-x}C_xBa_2Ca_3Cu_4O_{12-x}$ superconductor", Physica C 480 (2012) 19.

[3] N. H. Mohammed, A.I. Abou-Aly, I. H. Ibrahim, R. Awad and M. Rekaby, "Mechanical properties of $(Cu_{0.5}Tl_{0.5})$-1223 added by nano-SnO_2", J. Alloys Compd. 486 (2009) 733.

[4] W. Woch, R. Zalecki, A. Koodziejczyk, O. Heiml and G. Gritzner, "Temperature and field dependence of critical currents, resistances and irreversibility fields of a $(Tl_{0.6}Pb_{0.24}Bi_{0.16})(Ba_{0.1}Sr_{0.9})_2Ca_2Cu_3O_Y$ film on single crystalline lanthanum aluminate", Physica C 434 (2006) 17.

[5] A. I. Abou-Aly, S. Mahmoud, R. Awad, and M. Barakat, "Electrical resistivity and magnetoresistance studies of (Bi, Pb)-2223 phase substituted by Ru", J. Supercond. Nov. Magn. 23 (2010) 1575.

[6] Liaqat Ali, M. Mumtaz, and M. W. Rabbani, "Flux pinning with addition of gold nanoparticles in CuTl-1223 superconductor", J. Supercond. Nov. Magn. 30 (2017) 325.

[7] A. Jabbar, M. Mumtaz, and K. Nadeem, "Noble metals (Ag, Au) nanoparticles addition effects on superconducting properties of CuTl-1223 phase", Eur. Phys. J. Appl. Phys. 69 (2015) 30601.

[8] A. Kujur, and D. Behera, "Magneto-transport studies in (1-X) $YBa_2Cu_3O_{7-\delta}$+X $BaTiO_3$ superconductors", J. Magn, Magn. Mater. 377 (2015) 34.

[9] S. Celik, K. Ozturk, U. Cevik, and E. Yanmaz, "Investigation of the dependency of the upper critical magnetic field on the content x in $Y_{1-x}Yb_{x/2}Gd_{x/2}Ba_2Cu_3O_{7-y}$ superconducting structures", J. Alloys Compd. 460 (2008) 79.

[10] I. Dhingra, B. K. Das, and S. C. Kashyap, "Flux dynamics of YBCO/Ag composite", Bull. Matr. Sci. 17 (1994) 153.

[11] M. Waqee-ur-rehman, M. Mumtaz, I. Qasim, and K. Nadeem, "Infield response of (Co)$_x$/CuTl-1223 nanoparticles–superconductor composites", Cryogenics. 73 (2016) 68.

Chapter No. 6

CONCLUSIONS

Superconducting $(CuTl)_{0.5}Ca_2Ba_2Cu_3O_{10-\delta}$ (CuTl-1223) phase and metallic (i.e. Cu, Ag and Au) nanoparticles (MNPs) were successfully synthesized by sol-gel method and solid-sate reaction method, respectively. The different concentrations of these MNPs with different sizes were added in CuTl-1223 superconducting matrix to obtain $(D)_x$/(CuTl)-1223; (x = 0 ~ 4 wt.% and D = Cu, Ag and Au) nanoparticles-superconductor composites.

The following conclusions have been drawn from the experimental results presented in this dissertation;

- ✓ The crystalline structure of the host (CuTl)-1223 superconducting phase remained preserve as tetragonal with P4/mmm symmetry after the inclusion of MNPs, which confirmed about the occupancy of these MNPs at inter-granular spaces of the parent material. Slight variation in the lattice parameters was noticed owing to stresses and strains generated by inclusion of these MNPs at the grain-boundaries of (CuTl)-1223 superconductor. The SEM images of these composites also reflected the improvement in inter-grain connectivity and reduction in porosity after the inclusion of MNPs.
- ✓ The normal state resistivity {ρ (Ω-cm)} and broadening in superconducting resistive transition temperature (ΔT) was suppressed while superconducting critical parameters such as zero resistivity critical temperature (T_c) and critical current density (J_c) were enhanced by the inclusion of MNPs in CuTl-1223 superconducting phase.
- ✓ The lower critical magnetic field (H_{c1}) and the upper critical magnetic field (H_{c2}) were increased with the addition of MNPs up to certain optimal level in (CuTl)-1223 superconducting phase.
- ✓ Activation energy (U_o) was increased with the addition of MNPs up to certain optimum level in (CuTl)-1223 superconducting phase, while it was suppressed with increase of temperature due to damaging of weak-links.

From experimental measurements and theoretical analysis of the experimental data of $(D)_x$/(CuTl)-1223; (x = 0 ~ 4 wt.% and D = Cu, Ag and Au) nanoparticles-superconductor composites, it has been concluded that these MNPs are suitable candidates for the addition in

(CuTl)-1223 superconducting phase to improve its zero field and infield superconducting properties, which is the desire of modern age practical applications.

Published Articles

Cryogenics 105 (2020) 103021

Contents lists available at ScienceDirect

Cryogenics

journal homepage: www.elsevier.com/locate/cryogenics

AC-conduction mechanism via dielectric measurements of $(Cr)_x$/(CuTl)-1223 nanoparticles-superconductor composites

M. Mumtaz[a,*], Liaqat Ali[a], Mubasher[a], Ahmed Saleh[a], Y. Slimani[b], Irfan Qasim[c], Mehwish Hassan[d], Zubair Ahmad[e]

[a] Materials Research Laboratory, Department of Physics, Faculty of Basic and Applied Sciences (FBAS), International Islamic University (IIU) Islamabad 44000, Pakistan
[b] Department of Physics Research, Institute for Research & Medical Consultations (IRMC), Imam Abdulrahman Bin Faisal University, P.O. Box 1982, Dammam 31441, Saudi Arabia
[c] Department of Physics, Riphah International University, Islamabad, Pakistan
[d] Department of Sciences and Humanities, FAST, NUCES, Islamabad, Pakistan
[e] Ibn-e-Sina Institute of Technology, H-12/4 Islamabad, Pakistan

ARTICLE INFO

Keywords:
$(Cr)_x$/(CuTl)-1223 composites
Cr nanoparticles
(CuTl)-1223 superconducting phase
Grain-boundaries
Dielectric properties

ABSTRACT

Chemical sol-gel route was opted for synthesis of chromium (Cr) nanoparticles (NPs) and solid-state reaction method was used to synthesize the superconducting $(CuTl)_{0.5}Ba_2Ca_2Cu_3O_{10-\delta}$ ((CuTl)-1223) phase. The desired $(Cr)_x$/(CuTl)-1223; x = 0–2.0 wt% nanoparticles-superconductor composites were obtained by the incorporation of Cr NPs in the host superconducting (CuTl)-1223 matrix. The crystal structure along with the phase purity was explored by X-rays diffraction (XRD) and the transport properties were studied by the dc-resistivity and dielectric measurements of these composites. The crystal structure of these composites was found un-altered, which indicated the presence of Cr NPs at the inter-granular regions of the host CuTl-1223 superconducting matrix. The suppression in superconducting transport properties of CuTl-1223 superconducting phase could be associated to the reduction of superconducting volume fraction after the inclusion of Cr NPs. The effects of Cr NPs on the ac-conduction process in (CuTl)-1223 phase were investigated via frequency dependent dielectric measurements at different operating temperatures.

1. Introduction

Many superconducting ceramic materials showed high dielectric properties, which is the need of modern age for technological practical applications [1–4]. These materials are the best candidates in different fields due to high dielectric constants and versatile synthesis techniques. The materials with both high and low dielectric constants are crucial in different fields of electronic industry [4]. Capacitive elements in electronic circuits make use of high dielectric constant materials, while electronic insulation devices generally utilize low dielectric constant materials [4]. Materials with dielectric constant greater than 10^3 are known as colossal permittivity materials (CPMs) [5]. These CPMs with low dielectric loss can be considered as the best candidates for high energy-density storage applications [6,7]. Micro-cracks and inter-grain boundaries in polycrystalline superconducting ceramics are generally considered as dielectric media across which mobile charge carriers can be piled up and becomes the source of polarization in these materials [4]. Frequency and temperature are the crucial constraints in the study of ac-conduction process in superconducting materials [8,9].

The dielectric response of $GdBa_2Cu_{7-\delta}$ superconductor added with single-walled carbon nanotubes was investigated at temperature 77 K and frequency ranging from 100 KHz to 5 MHz [10]. An enhancement in dielectric properties was observed after the addition of single-walled carbon nanotubes up to 0.06 wt% as a result of maximum reduction in defects and improvement in inter-grains connections. Real part of dielectric constant was increased at lower frequency regime and it was decreased with further increase in frequency. Two dispersion peaks were observed in imaginary part of dielectric constant due to space or interfacial polarizations. Negative value in tangent loss was observed in some samples due to permanent shift of space charge in the presence of applied electric ac-field. The dielectric study of $Bi_{1.7}Pb_{0.3}Sr_2Ca_2Cu_3O_{10-\delta}$ (Bi, Pb)-2223 superconductor with different concentrations of gold (Au) nanoparticles were executed [11]. The highest values of dielectric constant as well as tangent loss were observed at lower frequencies and these parameters got reduced with further increase in the values of external frequency. The pristine (Bi, Pb)-2223 superconducting sample

* Corresponding author.
E-mail address: mmumtaz@iiu.edu.pk (M. Mumtaz).

https://doi.org/10.1016/j.cryogenics.2019.103021
Received 19 January 2019; Received in revised form 18 September 2019; Accepted 16 December 2019
Available online 17 December 2019
0011-2275/

Physica C: Superconductivity and its applications 559 (2019) 21–24

Contents lists available at ScienceDirect

Physica C: Superconductivity and its applications

journal homepage: www.elsevier.com/locate/physc

Infield superconductivity in Au nanoparticles added $Cu_{0.5}Tl_{0.5}Ba_2Ca_2Cu_3O_{10-\delta}$ phase

M. Mumtaz[a,*], Waqas Ahmad Khan[a], Liaqat Ali[a], M. Waqee-Ur-Rehman[a], K. Nadeem[b]

[a] Materials Research Laboratory, Department of Physics, Faculty of Basic and Applied Sciences (FBAS), International Islamic University (IIU) Islamabad 44000, Pakistan
[b] Nanomagnetism and Nanotechnology Laboratory, Department of Physics, Faculty of Basic and Applied Sciences (FBAS), International Islamic University (IIU) Islamabad 44000, Pakistan

ARTICLE INFO

Keywords:
$(Au)_x$/CuTl-1223 composites
Au nanoparticles
CuTl-1223 superconducting phase
Infield superconducting properties

ABSTRACT

Solid-state reaction method was used to synthesize $(Cu_{0.5}Tl_{0.5})Ba_2Ca_2Cu_3O_{10-\delta}$ (CuTl-1223) superconducting phase and gold (Au) nanoparticles were extracted from colloidal gold solution. The Au nanoparticles of 39 nm average in size were added in the host CuTl-1223 superconducting matrix to obtain $(Au)_x$/CuTl-1223; x = 0, 0.5, 1.0 and 1.5 wt.% nanoparticles-superconductor composites. Superconducting transport properties of $(Au)_x$/CuTl-1223 composites were explored by resistivity versus temperature (R–T) measurements in different external applied magnetic fields of H = 0–7 Tesla. Overall improvement in superconducting transport properties were observed after Au nanoparticles addition in CuTl-1223 superconducting matrix. The decrease in coherence length {$\xi(0)$} was attributed to the reduction of vortex core radius with addition of Au nanoparticles, which was gradually increased with increasing external applied magnetic field. The sustainability of superconductivity at high magnetic field in Au nanoparticles added CuTl-1223 superconductor can be attributed to the enhanced flux pinning ability of grains-boundaries due to the presence of Au nanoparticles there.

1. Introduction

$Cu_{1-x}Tl_xBa_2Ca_{n-1}Cu_nO_{2n+4-\delta}$ (CuTl-based) is the promising high temperature superconducting (HTSC) family due to ambient pressure synthesis with second highest superconducting properties in cuprates. $(Cu_{0.5}Tl_{0.5})Ba_2Ca_2Cu_3O_{10-\delta}$ (CuTl-1223) superconductor is one of the most attractive phase due to its highest values of superconducting parameters among the others phases of this CuTl-based HTSC family. The main tasks for the scientists working in the field of superconductivity is always to enhance the important superconducting parameters i.e. critical current density (J_c), critical temperature (T_c) and critical field (H_c), with the help of different methodologies [1–3]. The crystal structure, chemical composition, and morphology are the main targets to be focused to obtain the goal of improvements of superconducting parameters of the bulk HTSCs. The grains size and inter-grains coupling through weak-links are the main features of the bulk cuprate HTSCs morphology. Therefore, the inter-grains pores and voids in granular bulk cuprate HTSCs are of great importance to be addressed. The pores and voids in the granular bulk HTSCs have demerits along with some merits. These voids cause hurdle in inter-grains charge carriers' transportation and become the source of energy loss across these potential barriers. On the other hand, theses voids and spaces are the best flux pinning sites for the magnetic flux vortices in bulk cuprates. Therefore, it has become very important to explore the most suitable way, which could reduce the inter-grains weak connectivity and could improve the efficient flux pinning in the system. Different methods have been worked out to address this issue but embedding of nanostructures of suitable nature, shape and size in the bulk of HTSCs is found one of the most appropriate techniques [4–6]. The nanostructures of different materials, shapes and sizes such as $BaTiO_3$, Al_2O_3, $BaZrO_3$, $BaCeO_3$, ZrO_2, SiC, Sm_2O_3, Al_2O_3 and Cr_2O_3 nanoparticles were added in different bulk HTSCs like Bismuth-based, Yttrium-based etc., to enhance inter-grains coupling strength as well as to improve the flux pinning efficiency of host HTSCs matrices [7–16]. In vortex state of HTSCs, the flux pinning is the main motivation to avoid the energy dissipation due to vortex dynamics in the presence of magnetic field when Lorentz force dominates the flux pinning force [17,18].

In present research article, the effects of Au nanoparticles' addition on superconducting critical parameters such as H_c, J_c, T_c and ξ (0) of CuTl-1223 phase have been reported. The main motivation was to enhance the infield superconductivity of CuTl-1223 phase with addition of Au nanoparticles.

* Corresponding author.
E-mail address: mumtaz@iiu.edu.pk (M. Mumtaz).

https://doi.org/10.1016/j.physc.2019.01.010
Received 30 June 2018; Received in revised form 13 January 2019; Accepted 31 January 2019
Available online 01 February 2019
0921-4534/

J Supercond Nov Magn (2018) 31:561–567
DOI 10.1007/s10948-017-4229-8

Metallic Cu Nanoparticles Added to $Cu_{0.5}Tl_{0.5}Ba_2Ca_2Cu_3O_{10-\delta}$ Superconductor

Liaqat Ali[1] · M. Mumtaz[1] · Irfan Ali[1] · M. Waqee-ur-Rehman[1] · Abdul Jabbar[2]

Received: 28 April 2017 / Accepted: 28 June 2017 / Published online: 17 July 2017

Abstract Metallic copper (Cu) nanoparticles were added in appropriate ratios into the $Cu_{0.5}Tl_{0.5}Ba_2Ca_2Cu_3O_{10-\delta}$ (CuTl-1223) superconducting phase to obtain $(Cu)_x$/CuTl-1223 ($x = 0 \sim 4.0$ wt%) nanoparticle-superconductor composites. Structural, morphological, compositional, and superconducting transport properties were investigated by using different experimental characterization techniques. The crystal structure of the host CuTl-1223 phase remained unaltered (i.e. tetragonal) after addition of Cu nanoparticles, which gave a clue about the occupancy of these nanoparticles at the inter-crystallite sites. Grain morphology and inter-grain connectivity were improved after addition of these Cu nanoparticles being metallic in nature were supposed to be the best candidate for improvement of inter-grain connectivity and superconducting properties. Calculation of the superconducting volume fraction showed the dominance of the CuTl-1223 phase along with the presence of some other superconducting phases and unknown impurities. The optimum content level of Cu nanoparticles in the CuTl-1223 phase for maximum improvement of superconducting properties was 1.0 wt%.

Keywords $(Cu)_x$/CuTl-1223 composites · Crystal structure · Morphology · Superconducting properties

✉ M. Mumtaz
mmumtaz75@yahoo.com

[1] Materials Research Laboratory, Department of Physics, Faculty of Basic and Applied Sciences (FBAS), International Islamic University (IIU), Islamabad 44000, Pakistan

[2] Department of Physics, Ghazi University, Dera Ghazi Khan 32200, Pakistan

1 Introduction

The potential applications of high-temperature superconductors (HTSCs) have always been the aim of researchers since their discovery. Great efforts have been put into processing to optimize the macroscopic superconducting properties envisaging practical applications of bulk materials. Small imperfections at grain boundaries with spatial extensions of the order of the coherence length lead to a substantial weakening of inter-grain connectivity and suppression of transport properties. This way, the granularity of these materials limits their transport properties due to a current percolation problem, which strongly depends on the microstructures. The ambient pressure synthesis of different HTSC families lowers their superconducting properties due to the presence of inter-grain voids and pores. Different techniques have been used to overcome these problems such as high pressure synthesis and post-annealing, to enhance superconducting properties [1–4]. Addition of different nanoparticles in HTSCs is one of the easiest, effective, and novel techniques to address this issue. The nanoparticles heal up the inter-grain voids and pores with the virtue of which it may be expected that superconductivity will be enhanced. Controlled size, concentration, and distribution of nanostructures at grain boundaries of the bulk HTSCs are real challenges [5–10]. The nature of the different nanostructure is very important because different nanoparticles have different effects on various properties on HTSCs. High-pressure synthesis is not suitable at commercial level production of HTSCs, so we have chosen the CuTl-1223 phase of the HTSC family due to its synthesis at ambient pressure.

The CuTl-1223 phase with different concentrations of nano-Ag particles was investigated. Volume fraction, melting point, T_c, and J_c were found to be improved up to

Cryogenics 93 (2018) 5–10

Contents lists available at ScienceDirect

Cryogenics

journal homepage: www.elsevier.com/locate/cryogenics

Research paper

Magneto-transport properties of $(Cu)_x$/CuTl-1223 nanoparticles-superconductor composites

M. Mumtaz[a,*], M. Naveed[a], L. Ali[a], Abrar A. Khan[a], M. Imran[a], M. Waqee-Ur-Rehaman[a], M. Nasir Khan[b]

[a] Materials Research Laboratory, Department of Physics, FBAS, International Islamic University (IIU), Islamabad 44000, Pakistan
[b] Central Diagnostic Laboratory, Physics Division PINSTECH, Islamabad 45500, Pakistan

ARTICLE INFO

Keywords:
$(Cu)_x$/CuTl-1223 composites
Cu nanoparticles
CuTl-1223 superconducting phase
Magneto-transport properties
Flux pinning

ABSTRACT

Copper (Cu) nanoparticles and $Cu_{0.5}Tl_{0.5}Ba_2Ca_2Cu_3O_{10-\delta}$ (CuTl-1223) superconducting phase were synthesized by sol-gel and solid-state reaction, respectively. These metallic Cu nanoparticles were added in CuTl-1223 superconducting matrix to get $(Cu)_x$/CuTl-1223; x = 0–4.0 wt% nanoparticles-superconductor composites and their temperature dependent magneto-transport properties were studied. The zero-field-cooled (ZFC) and field-cooled (FC) temperature dependent magnetization (M-T) measurements of $(Cu)_x$/CuTl-1223 samples showed an increase in transition temperature and in amplitude of diamagnetic signal after the inclusion of Cu nanoparticles in the host CuTl-1223 matrix. The improvement in these magneto-transport properties can be attributed to the increase in number of efficient pinning centres in CuTl-1223 matrix after addition of Cu nanoparticles. Magnetization hysteresis (M-H) loops were obtained at various operating temperatures from which the magnetization critical current density (J_c) was estimated using Bean's critical state model. M-H loops indicated the combined superconducting and ferromagnetic behaviour up to 90 K in all $(Cu)_x$/CuTl-1223 samples. Improvement in J_c could also be due to increase in number of pinning centres with addition of Cu nanoparticles in CuTl-1223 matrix. Maximum improvement in magneto-transport properties of $(Cu)_x$/CuTl-1223 samples was observed for x = 1.0 wt%, which had specified the optimum content level of Cu nanoparticles in CuTl-1223 phase.

1. Introduction

With the discovery of high-temperature superconductors (HTSCs), substantial efforts have been made to improve their critical parameters through the development and use of diverse techniques [1]. $Cu_{0.5}Tl_{0.5}Ba_2Ca_2Cu_3O_{10-\delta}$ (CuTl-1223) is an attractive phase of CuTl-based HTSCs family due to its synthesis at ambient pressure and having higher values of critical superconducting parameters such as transition temperature (T_c), irreversibility field (H_{irr}), critical current density (J_c) etc [2–4]. High value of J_c is required for technological applications of HTSCs and for this purpose different techniques have been used. It was reported that the J_c is strongly dependent on the microstructure of HTSCs due to their highly anisotropic layered crystal structures. In order to improve the microstructure, various fabrication techniques have been tried to obtain highly oriented materials [6–11]. In external applied magnetic field, the vortex motion in HTSCs is the main source of energy dissipation and suppression of J_c [12–16]. One way to improve J_c is to introduce artificial pinning centres especially secondary phases or non-superconducting inclusions, which can act as isotropic and randomly dispersed artificial pinning centres [17–23]. Dislocations, stacking faults, twin boundaries and oxygen defects can also act as effective pinning centres. The most useful, effective and easy way to improve infield J_c as well as other superconducting critical parameters is to introduce additional artificial pinning centres by the inclusion of different nanostructures of different materials in bulk HTSCs [24,25].

In this paper, we reported the effects of metallic Cu nanoparticles addition on magneto-transport properties of CuTl-1223 superconducting phase. Series of $(Cu)_x$/CuTl-1223 samples were synthesized to find out the optimal concentration level of Cu nanoparticles to obtain the maximum improvement in superconducting magneto-transport properties without affecting the crystal structure of host CuTl-1223 phase.

2. Samples synthesis and experimental detail

Powders of Cu(CN), $Ca(NO_3)_2$ and $Ba(NO_3)_2$ were measured, mixed

* Corresponding author.
E-mail address: mmumtaz75@yahoo.com (M. Mumtaz).

https://doi.org/10.1016/j.cryogenics.2018.08.005
Received 6 January 2018; Received in revised form 5 February 2018; Accepted 15 August 2018
Available online 17 August 2018
0011-2275/

Physica C: Superconductivity and its applications 551 (2018) 19–24

Contents lists available at ScienceDirect

Physica C: Superconductivity and its applications

journal homepage: www.elsevier.com/locate/physc

Phase formation, activation energy and superconductivity of MgO nanoparticles added $(Cu_{0.5}Tl_{0.5})Ba_2Ca_2Cu_3O_{10-\delta}$ phase

M. Mumtaz*, Liaqat Ali, Iftikhar Ahmad

Materials Research Laboratory, Department of Physics, Faculty of Basic and Applied Sciences (FBAS), International Islamic University (IIU), Islamabad 44000, Pakistan

ARTICLE INFO

Keywords:
(MgO)x/(CuTl)-1223 composites
MgO nanoparticles
(CuTl)-1223 superconducting phase
Superconducting properties

ABSTRACT

A well-established solid-state reaction route was adopted for the synthesis of $(Cu_{0.5}Tl_{0.5})Ba_2Ca_2Cu_3O_{10-\delta}$ ((CuTl)-1223) superconducting phase and a well-known sol-gel method was used to prepare the magnesium oxide (MgO) nanoparticles. The different weight percentages of these MgO nanoparticles were mixed with (CuTl)-1223 superconductor to obtain $(MgO)_x/(CuTl)$-1223; $x = 0 - 5.0$ wt.% nanoparticles-superconductor composites. The phase formation, crystal structure, phase purity and morphology of MgO nanoparticles and $(MgO)_x/(CuTl)$-1223 composites were investigated by X-rays diffraction and scanning electron microscopy, respectively. Superconducting properties of $(MgO)_x/(CuTl)$-1223 composites were explored by resistivity versus temperature measurements. The holes' concentration, activation energy and zero resistivity critical temperature were suppressed while transition width was broadened, which can be attributed to the reduced superconducting volume fraction and enhanced number of scattering centers with increasing contents of insulating MgO nanoparticles in the host (CuTl)-1223 superconducting phase.

1. Introduction

The high temperature superconductors (HTSCs) have been focused by the scientists since the discovery due to the use of these materials in different very important technological applications. The HTSCs have been synthesized at high pressure as well as at ambient pressure. The high-pressure synthesis of HTSCs at the commercial scale is a big hurdle. Therefore, we have preferred to synthesize our HTSCs samples at ambient pressure. We have selected $(Cu_{0.5}Tl_{0.5})Ba_2Ca_2Cu_3O_{10-\delta}$ phase of $Cu_{0.5}Tl_{0.5}Ba_2Ca_{n-1}Cu_nO_{2n+4-\delta}$; $n = 2, 3...$, HTSCs family due to higher values of its superconducting critical parameters [1–5]. The carriers' density and the number of CuO_2 planes of cuprates are the important parameters, which can control the superconducting transport properties of the material [6]. The performance of bulk HTSCs materials can be affected by the presence of cracks, voids, pores and other microdefects [7]. The different techniques such as synthesis conditions and post annealing have been exercised to overcome these problems. In addition to these techniques, the simplest and effective one is the inclusion of different nanostructures such as nanoparticles, nanorods, and nanotubes in HTSCs matrices [8–10]. But still in this technique, the major issue is the uniform distribution of nanostructures over the grain-boundaries and the control of size and shape of nanostructures to observe the same effect throughout the bulk HTSCs samples [11–13]. The different contents of 20 nm and 40 nm size MgO nanoparticles were added in $(Bi_{1.6}Pb_{0.4}Sr_2Ca_2Cu_3O_{10})$/Ag tapes and electrical transport properties were investigated [14]. The critical current density (J_c) was improved up to certain content level of MgO nanoparticles. Relatively larger improvement in J_c was observed with the inclusion of 20 nm rather than 40 nm MgO nanoparticles in $(Bi_{1.6}Pb_{0.4}Sr_2Ca_2Cu_3O_{10})$/Ag tapes. Therefore, the smaller size and low contents of MgO nanoparticles was found best for flux pinning in $(Bi_{1.6}Pb_{0.4}Sr_2Ca_2Cu_3O_{10})$/Ag tapes. The effect of MgO nanoparticles addition on the phase formation and the superconducting transport properties of Bi2223 phase was investigated [15]. It was observed that the MgO nanoparticles present at the grain-boundaries acted as barriers and hindered the grain growth of the host Bi2223 phase. It was also reported that there was no chemical reaction occured between MgO nanoparticles and Bi2223 superconducting phase. It was also noticed that MgO nanoparticles were not doped in to the crystal structure of Bi2223 superconductor. The maximum supercurrent density was found in the sample with 15 wt.% of MgO nanoparticles. The excessive addition of MgO nanoparticles induced large agglomeration among the grains of the host Bi2223 matrix, which deteriorated the quality of the samples. The ultra-fine MgO nanoparticles obtained by the combustion of pure Mg element were added in Bi-2212/Ag tapes [16]. The addition of MgO nanoparticles in Bi-2212/Ag tapes has improved the infield superconducting transport properties by acting as additional artificial flux pinning centers. The microstructure and infield J_c of Bi-2212/Ag tapes were

* Corresponding author.
E-mail addresses: mmumtaz75@yahoo.com, mmumtaz@iiu.edu.pk (M. Mumtaz).

https://doi.org/10.1016/j.physc.2018.05.006
Received 12 April 2018; Received in revised form 3 May 2018; Accepted 15 May 2018
Available online 17 May 2018
0921-4534/

Ceramics International 42 (2016) 11193–11200

Contents lists available at ScienceDirect

Ceramics International

journal homepage: www.elsevier.com/locate/ceramint

Tuning of dielectric properties of $(ZnO)_x$-(CuTl-1223) nanoparticles-superconductor composites

M. Mumtaz [a,*], Liaqat Ali [a], Abdul Jabbar [c], M.W. Rabbani [a], M. Naveed [a], M. Imran [a], Badshah Amin [a], M. Nasir Khan [b], M. Usman Sajid [b]

[a] Materials Research Laboratory, Department of Physics, FBAS, International Islamic University (IIU), Islamabad 44000, Pakistan
[b] Central Diagnostic Laboratory, Physics Division PINSTECH, P.O. Nilore, Islamabad 45500, Pakistan
[c] Department of Physics, Ghazi University, Dera Ghazi Khan 32200, Pakistan

ARTICLE INFO

Article history:
Received 14 November 2015
Received in revised form
6 April 2016
Accepted 6 April 2016
Available online 7 April 2016

Keywords:
$(ZnO)_x$-(CuTl-1223) nanoparticles-superconductor composites
Structural characteristics
Superconducting properties
Dielectric properties

ABSTRACT

Zinc oxide (ZnO) nanoparticles and $Cu_{0.5}Tl_{0.5}Ba_2Ca_2Cu_3O_{10-\delta}$ (CuTl-1223) superconducting phase were prepared separately by sol-gel and solid-state reaction, respectively. ZnO nanoparticles were mixed with CuTl-1223 to get $(ZnO)_x$-(CuTl-1223); x=0, 0.5, 1.0 and 1.5 wt% nanoparticles-superconductor composites, which were characterized by different experimental techniques. There was no change observed in crystal structure of host CuTl-1223 phase after addition of ZnO nanoparticles, which provide a clue about the occupancy of these nanoparticles at the grains-boundaries. The inclusion of ZnO nanoparticles was found to reduce the voids and to improve the inter-grains connectivity in the host CuTl-1223 phase. The zero resistance critical temperature [$T_{c(R=0)}$(K)] was increased by increasing wt% addition of ZnO nanoparticles in CuTl-1223 matrix. The dielectric properties of these samples i.e. dielectric constants (ε; ε'), and dielectric loss (tan δ), were determined by experimentally measuring the capacitance (C) and conductance (G) as a function of frequency at different operating temperatures. The values of dielectric parameters were decreased with the increase of frequency and become constant at certain higher frequency values, while the values of these parameters were increased with the increase of operating temperature values. So, we can tune the dielectric properties of CuTl-1223 superconducting phase by varying the content of ZnO nanoparticles, frequency and operating temperature.

1. Introduction

The materials with giant dielectric constants can play a significant role for microelectronics growth due to desire of smaller and robust devices such as capacitor and memory devices [1]. High values of dielectric constants have also been observed in high temperature superconductors (HTSCs) [1–3]. There are four primary mechanisms of polarization in materials on basis of the frequency of external applied ac-field. Ions and electronic clouds of atoms can be shifted from their equilibrium positions, which can be observed in electronic polarization (α_e). This type of polarization has been observed in solids at very high frequencies of the order of 10^{15} Hz (i.e. in ultraviolet optical range). Atomic and ionic polarization (α_a), which can be originated from combined displacement of ionic charge and electronic charge distribution. This type of polarization can be observed at frequencies in the range of 10^{10} to 10^{13} Hz (i.e. in infrared optical range). Dipolar or oriental polarization (α_o) can occur in the range of frequencies from 10^3 to 10^6 Hz (i.e. in sub-infrared optical range). This type of polarization can normally be observed at lower frequencies due to shorter relaxation times. Interfacial polarization (α_i) is more sensitive in low frequency range of 10^3 Hz and may extend to few kHz [4–8]. A short-range motion of charges in all these polarizations contributes to the total polarization of the material. The dielectric properties of $Cu_{0.5}Tl_{0.5}Ba_2Ca_4Cu_3O_{12-\delta}$ (CuTl-1234) superconductor were investigated in frequency range from 10 kHz to 10 MHz at different operating temperatures from 78 K to 290 K and negative capacitance (NC) was observed. M. Mumtaz et al. [9] compared the dielectric constants of CuTl-1234 phase with those of Tl-2212 and Tl-2223 phases. They observed larger dielectric constant of double layered Tl-based HTSCs as compared to single layered CuTl-based HTSCs. The dielectric properties of $(CuO, CaO_2$ and $BaO)_y$/CuTl-1223; y=0, 5, 10, and 15 wt% nanoparticles-superconductor composites were also studied in frequency range from 10 kHz to 10 MHZ at different operating temperatures from 78 K to 300 K. The decrease in dielectric constant and increase in ac-conductivity was found at all operating temperatures with minimum frequency of 10 KHz [10]. It was observed a gradual

* Corresponding author.
E-mail address: mmumtaz75@yahoo.com (M. Mumtaz).

http://dx.doi.org/10.1016/j.ceramint.2016.04.025
0272-8842/

J Supercond Nov Magn (2018) 31:1315–1321
DOI 10.1007/s10948-017-4355-3

Study of $(DNPs)_x$/CuTl-1223 Nanoparticle-Superconductor Composites

M. Mumtaz[1] · Zafar Iqbal[2] · M. Raza Hussain[2] · Liaqat Ali[1] · M. Waqee-ur-Rehman[1] · M. Saqib[2]

Received: 3 September 2017 / Accepted: 13 September 2017 / Published online: 20 September 2017

Abstract Sol-gel and solid-state reaction methods were used to synthesize diamond nanoparticles (DNPs) and $(DNPs)_x$/CuTl-1223 (x = 0, 0.25, 0.50, and 1.00 wt.%) nanoparticle-superconductor composites, respectively. Effects of these DNPs on structural, morphological, compositional, and transport properties of CuTl-1223 superconducting phase were investigated by different experimental techniques such as X-ray diffraction (XRD), energy dispersive X-ray (EDX) spectroscopy, scanning electron microscopy (SEM), and resistivity versus temperature (R-T) measurements. The unchanged crystal structure and stoichiometry of host CuTl-1223 superconducting matrix with addition of DNPs gave evidence about the dispersion of nanoparticles at the grain boundaries of the host matrix, which may heal up the inter-granular voids and pores resulting in enhanced inter-grain connectivity. Critical transition temperature T_c (0) and hole concentration of CuTl-1223 superconductor were observed to be increased with addition of DNPs up to a certain optimum value (i.e. x = 0.5 wt.%).

Keywords $(DNPs)_x$/CuTl-1223 nanoparticle-superconductor composites · Diamonds nanoparticles · Superconducting properties

✉ M. Mumtaz
mmumtaz75@yahoo.com

[1] Materials Research Laboratory, Department of Physics, Faculty of Basic and Applied Sciences (FBAS), International Islamic University (IIU), Islamabad 44000, Pakistan

[2] Department of Physics, Riphah International University, I-14 Islamabad, Pakistan

1 Introduction

High-pressure synthesis imposes limitations to the use of high-temperature superconductors (HTSCs) at commercial level. $Cu_{0.5}Tl_{0.5}Ba_2Ca_{n-1}Cu_nO_{2n+4-\delta}$ (CuTl-12(n–1)n); n = 2, 3, 4, ... superconducting family is of great interest for researchers due to its easy synthesis both at ambient and high pressure. $(Cu_{0.5}Tl_{0.5})Ba_2Ca_2Cu_3O_{10-\delta}$(CuTl-1223) is the most attractive phase of CuTl-based superconducting family due to low anisotropy, high critical current density (J_c), and high critical transition temperature (T_c) [1–3]. The cuprate HTSCs are granular in nature and exhibit weak inter-grain connectivity, which limits their performance [4, 5]. Besides the demerits of inter-grain voids and pores present in cuprate superconductors, they have some merits also, just like these spaces serve as natural flux pinning centers when external magnetic field is applied. So, it is important to address the inter-gain weak linkages by keeping it in mind that improvement in inter-grain connectivity should not suppress the flux pinning ability of the superconducting matrix. One of the most effective methods in this regard is to embed nanoparticles at grain boundaries, which could enhance the grains connectivity and also act as effective artificial pinning centers [6–11].

Nanostructures of different materials such as diamond, SiC, SiO_2, and CNTs were added to $YBa_2Cu_3O_{7-\delta}$ cuprate superconductor, and their effects were investigated [12–15]. Critical current densities and pinning energies were enhanced with doping of different concentration of these nanostructures. Critical temperature was increased significantly with addition of CNTs while a small suppression was observed in case of carbon and SiC nanostructures. The effects of CNTs' addition in Bi-2223 and CuTl-1223 superconducting matrices were also explored [16, 17]. It was observed that superconducting volume fraction and cell

Surfaces and Interfaces 13 (2018) 196–204

Contents lists available at ScienceDirect

Surfaces and Interfaces

journal homepage: www.elsevier.com/locate/surfin

Study of uncoated and silica-coated hematite (α-Fe_2O_3) nanoparticles

Mustehsin Ali, Usama Tehseen, M. Alí, I. Ali, M. Mumtaz*

Materials Research Laboratory, Department of Physics, Faculty of Basic and Applied Sciences (FBAS), International Islamic University (IIU), Islamabad 44000, Pakistan

ARTICLE INFO

Keywords
α-Fe_2O_3 nanoparticles
Silica coating
Optical properties
Dielectric properties

ABSTRACT

The effect of silica (SiO_2) matrix with different concentrations (i.e. x = 0, 20, 40 and 60 wt.%) on structural, morphological, optical and dielectric properties of hematite (α-Fe_2O_3) nanoparticles was investigated. The uncoated and silica-coated α-Fe_2O_3 nanoparticles were characterized by X-ray diffraction (XRD), scanning electron microscopy (SEM), diffuse reflectance spectroscopy (DRS), Fourier transform infrared (FTIR) spectroscopy. The frequency dependent dielectric properties of uncoated and silica-coated α-Fe_2O_3 nanoparticles were also investigated by LCR meter. The size of α-Fe_2O_3 nanoparticles was reduced from 18.60 nm to 16.71 nm with increasing percentage of silica matrix. The crystallinity of α-Fe_2O_3 nanoparticles was suppressed with increasing contents of silica due to reduced particle size and amorphous nature of silica matrix. Scanning electron microscopy (SEM) revealed spherically shaped α-Fe_2O_3 nanoparticles. In FTIR spectra, different bonds of hematite nanoparticles, Si—OH and Si—O—Si were observed at 418 and 624, 659 and 1136 cm^{-1}, respectively. The direct band gap was increased from 1.91 eV to 1.95 eV and the in-direct band gap was decreased from 1.37 eV to 1.32 eV with the increase concentration of silica. It was found that silica coating has prominent effects on structural, optical and dielectric properties of α-Fe_2O_3 nanoparticles.

1. Introduction

Iron oxide nanoparticles are abundantly present on earth with sixteen different forms [1]. These iron oxide nanoparticles got so much attention of scientists and engineers over last few decades due to their supreme and unique electric and magnetic properties. These magnetic nanoparticles have different important properties such as high magnetic susceptibility ($\chi > 0$), high coercivity (H_c ~ 300 Oe) and low Curie temperature (T_c = 928 K) [2]. These magnetic nanoparticles are being widely used in various applications such as data storage, magnetic fluids, biotechnology, catalysis, biomedicine, hyperthermia, magnetic resonance imaging (MRI), magnetic optical devices, drug delivery, lithium ion batteries, separation and purification of biomolecular field, water purification, life sciences as well as engineering fields [3–11]. We have preferred hematite nanoparticles among iron oxide nanoparticles due their better conductivity, band gap and magnetic effects than other forms of iron oxide nanoparticles. New phenomena have been observed in these nanoparticles due to change of electric and magnetic properties, when size of these nanoparticles is decreased to few nanometers. Hematite nanoparticles exhibit novel properties like giant magneto-resistance, coercivity, etc., which make them promising to their bulk counterpart [12–18]. High surface to volume ratio, greater exchange of ions, surface roughness and breaking of symmetry are some causes, which make hematite nanoparticles different from their bulk materials. Hematite nanoparticles exhibit three critical temperature regimes like Neel, blocking and Morin temperatures [19–22]. Neel transition is observed normally at T_N = 960 K and hematite show weak ferromagnetism below Neel temperature to Morin temperature T_M = 263 K, due to slight spin outside basal plane [23]. Antiferromagnetic ordering is observed below Morin temperature due to spin rotations. The synthesis of hematite nanoparticles with required crystal structure and controlled properties is still a big challenge. Hematite nanoparticles are normally coated with chemically stable shell of silica in order to protect from thermal and chemical oxidation and to get desired properties of these nanoparticles [24]. Silica is being widely used as a matrix for magnetic nanoparticles to avoid from agglomerations. More over silica is used to increase chemical and thermal stabilities from seeping in an acid environment. Kopanja et al. synthesized hematite nanoparticles by using silica matrix and studied different properties of silica-coated nanoparticles [2]. They observed an improvement in magnetic properties due to increase in surface spins. Ziyadi et al. prepared hematite nano-fiber using silica shell [25]. They observed high magnetization (14 emu/g in case of sample with SiO_2 and 20 emu/g in case of pure sample) and low coercivity (390 Oe in case of sample with SiO_2 and 400 Oe in case of pure sample) in these nanoparticles due to silica coating. Tadic et al. observed that silica

* Corresponding author.
E-mail address: mmumtaz@iiu.edu.pk. (M. Mumtaz).

https://doi.org/10.1016/j.surfin.2018.09.001
Received 23 March 2018; Received in revised form 24 September 2018; Accepted 30 September 2018
Available online 03 October 2018

J Supercond Nov Magn (2017) 30:2741–2749
DOI 10.1007/s10948-017-4124-3

Improvement in Superconducting Properties of $Cu_{0.5}Tl_{0.5}Ba_2Ca_2Cu_3O_{10-\delta}$ Phase by Addition of γ-Fe_2O_3 Nanoparticles

M. Mumtaz[1] · Liaqat Ali[1] · M. Waqee-ur-Rehman[1] · K. Nadeem[2] · G. Hussain[1] · G. Abbas[1] · Bilal Majeed[1]

Received: 21 March 2017 / Accepted: 11 April 2017 / Published online: 24 April 2017

Abstract Maghemite (γ-Fe_2O_3) nanoparticles and the $(Cu_{0.5}Tl_{0.5})Ba_2Ca_2Cu_3O_{10-\delta}$ (CuTl-1223) superconducting phase were prepared separately by sol–gel and solid-state reactions, respectively. γ-Fe_2O_3 nanoparticles were added into the CuTl-1223 superconducting phase to get $(\gamma$-$Fe_2O_3)_x$/CuTl-1223, where $x = 0 \sim 1.25$ wt.% nanoparticle-superconductor composites. The structural, morphological, and superconducting transport properties of these composites were investigated by using different experimental techniques. X-ray diffraction (XRD) of these composites revealed that γ-Fe_2O_3 nanoparticles have not changed the crystal structure of the host CuTl-1223 superconducting phase, which has indicated the occupancy of these nanoparticles at grain-boundaries. The grain morphology was improved due to change in reaction thermodynamics with addition of these magnetic nanoparticles. Superconducting transport parameters of the CuTl-1223 phase were enhanced up to a certain optimum level of γ-Fe_2O_3 nanoparticle content (i.e. $x = 0.50$ wt.%) followed by systematic suppression. Different microscopic superconducting parameters were deduced from resistivity versus temperature experimentaldata of $(\gamma$-$Fe_2O_3)_x$/CuTl-1223, where $x = 0 \sim 1.25$ wt.% composites by using different theoretical models.

Keywords $(\gamma$-$Fe_2O_3)_x$/CuTl-1223 composites · Crystal structure · Morphology · Superconducting properties

1 Introduction

High-temperature superconductors (HTSCs) are still extensively characterized in order to understand the mechanism of high-T_c superconductivity. Among the HTSCs, the $(Cu_{0.5}Tl_{0.5})Ba_2Ca_2Cu_3O_{10-\delta}$ (CuTl-1223) phase has the highest critical parameters such as T_c, J_{cs} and J_c after Hg-based superconductors [1, 2]. The synthesis of CuTl-based superconductors at ambient pressure makes this phase a potential candidate among different superconductors [3, 4]. But these materials in bulk form have a large number of micro-defects, inter-grain voids, and pores which highly affect the performance of these materials [5, 6]. In order to enhance the superconducting properties of cuprate HTSCs, different techniques, such as chemical doping and ion irradiation, were utilized, but the inclusion of different nanostructures at the grain boundaries to heal up inter-grain voids, cracks, and pores was found to be very useful [7, 8]. However, the selection of nanostructures with appropriate sizes, their uniform distribution, and their nature are the real challenges in this area of research [9–12]. Thermodynamic fluctuations play a key role in affecting the superconductivity of HTSCs. Vortex motion in the presence of applied magnetic field is another characteristic parameter, which highly affects the overall superconductivity of a given material. Infield transport superconducting properties

✉ M. Mumtaz
mmumtaz75@yahoo.com

[1] Materials Research Laboratory, Department of Physics, Faculty of Basic and Applied Sciences (FBAS), International Islamic University (IIU), Islamabad 44000, Pakistan

[2] Nanomagnetism and Nanotechnology Laboratory, Department of Physics, Faculty of Basic and Applied Sciences (FBAS), International Islamic University (IIU), Islamabad 44000, Pakistan

Progress in Natural Science: Materials International 27 (2017) 487–490

Contents lists available at ScienceDirect

Progress in Natural Science: Materials International

journal homepage: www.elsevier.com/locate/pnsmi

Original Research

Infield superconducting properties of nano-sized Ag added $Cu_{0.5}Tl_{0.5}Ba_2Ca_2Cu_3O_{10-\delta}$

M.W. Rabbani[a], Liaqat Ali[a], M. Mumtaz[a,*], Iftikhar Hussain Gul[b]

[a] Materials Research Laboratory, Department of Physics, FBAS, International Islamic University (IIU), Islamabad 44000, Pakistan
[b] Department of Material s Engineering (MS), Thermal Transport Laboratory (TTL), School of Chemical and Materials Engineering (SCME), National University of Science and Technology (NUST), H-12 Islamabad, Pakistan

ARTICLE INFO

Keywords:
$(Ag)_x$/CuTl-1223 composites
Activation energy
Transition width
Flux pinning
Critical field

ABSTRACT

Infield superconducting properties of $(Ag)_x$/CuTl-1223; (x = 0, 0.5, 1.0, 2.0 and 4.0 wt %) nanoparticles-superconductor composites were investigated under different applied magnetic field up to H = 8 T. The increase in critical temperature ($T_c(0)$) and decrease in normal state resistivity (ρ_n) were observed with increasing contents of Ag nanoparticles in CuTl-1223 superconducting matrix. The value of T_c^{onset} (K) remained almost unaffected by applying external magnetic field, but a decreasing trend in T_c (0) was observed by increasing the value of external applied magnetic field. The transition region below T_c^{onset} (K) showed Arrhenius behavior due to thermally activated flow of magnetic vortices. Enhancement in flux flow activation energy (U_o) and suppression in transition width (ΔT) of CuTl-1223 phase with addition of Ag nanoparticles showed the improvement in flux pinning strength of superconductor.

1. Introduction

The high temperature superconductors (HTSCs) are extensively studied due to large number of technological applications. But their practical applications are strongly affected by various constraints; destruction of superconducting state in presence of applied external magnetic field is one of them [1]. The existence of vortex state in HTSCs makes them different from conventional low temperature superconductors. The vortex is simply described as a line of magnetic flux surrounded by whirlpools of electric current [2].

The vortex dynamics is extensively studied to estimate the energy loss in HTSCs in the presence of external magnetic field. The gradual decrease in diamagnetic behavior of superconductors, penetration of external flux lines takes place in the form of Abrikosov vortices. The Lorentz force ($f_L = \frac{1}{c}(j \times \Phi_o)$) experienced by vortices, when superconductor is subjected to electric current, which has a key role in flux dynamics and energy dissipation. We can divide energy dissipation in two distinguishable regimes named as flux creep and free flux flow (FFF). Flux creep gets activated when $U_o >> k_BT$ while in contrast FFF occurs when $U_o \sim k_BT$ [3–5]. Both of these regimes are normally useful in case of low temperature superconductors (LTSCs), while the thermally activated flux flow (TAFF) introduced a new aspect of HTSCs [6,7]. So, overall vortex dynamics in HTSCs gives useful information about critical magnetic field (T_c (0)), critical filed (H_c), critical current density (J_c), and activation energy (U_o). Moreover, two important phases according to (TAFF) model are solid vortex-lattice phase which exists in the region of lower critical field (H_{c1}), while the second is liquid vortex phase which exists below the upper critical field (H_{c2}) region. In liquid vortex lattice, the vortices begin to penetrate and upper critical field (H_{c2}) can be marked by the total loss of superconductivity due to overlapping of vortices. Theoretical models and experimental techniques have been extensively used to study the vortex dynamics in HTSCs [8–10].

Only a few number of research groups attempted to enhance intergrain coupling and flux pinning capability of CuTl based HTSCs by the inclusion of various nanostructures [11–15]. In this research article, we presented the effect of addition of Ag nanoparticles on flux pinning ability of CuTl-1223 superconducting matrix. We calculated superconducting parameters such as U_o, H_{c2}, $H_{c2}(0)$ and $\xi(0)$ by using TAFF model, Werthamer-Helfand-Hohenberg (WHH) and Ginzburg-Landau (GL) formulas.

2. Experimental details

$(Ag)_x$/CuTl-1223; x = 0, 0.5, 1.0, 2.0, and 4.0 wt % nanoparticles-superconductor composites were synthesized by solid-state reaction

Peer review under responsibility of Chinese Materials Research Society.

* Corresponding author.
E-mail address: mumtaz75@yahoo.com (M. Mumtaz).

http://dx.doi.org/10.1016/j.pnsc.2017.06.011
Received 21 November 2016; Received in revised form 7 June 2017; Accepted 14 June 2017
Available online 03 August 2017

Journal of Magnetism and Magnetic Materials 429 (2017) 270–275

Contents lists available at ScienceDirect

Journal of Magnetism and Magnetic Materials

journal homepage: www.elsevier.com/locate/jmmm

Surface spins disorder in uncoated and SiO_2 coated maghemite nanoparticles

F. Zeb[a], K. Nadeem[a,*], S. Kamran Ali Shah[a], M. Kamran[a], I. Hussain Gul[b], L. Ali[c]

[a] Nanosciences and Technology Laboratory, International Islamic University, H-10, 44000 Islamabad, Pakistan
[b] School of Chemical & Materials Engineering, National University of Sciences and Technology (NUST), E-12, 44000 Islamabad, Pakistan
[c] Materials Research Laboratory, International Islamic University, H-10, 44000 Islamabad, Pakistan

ARTICLE INFO

Keywords:
Magnetic nanoparticles
Maghemite
Surface functionalization
Silica coating

ABSTRACT

We studied the surface spins disorder in uncoated and silica (SiO_2) coated maghemite (γ-Fe_2O_3) nanoparticles using temperature and time dependent magnetization. The average crystallite size for SiO_2 coated and uncoated nanoparticles was about 12 and 29 nm, respectively. Scanning electron microscopy (SEM) showed that the nanoparticles are spherical in shape and well separated. Temperature scans of zero field cooled (ZFC)/field cooled (FC) magnetization measurements showed lower average blocking temperature (T_B) for SiO_2 coated maghemite nanoparticles as compared to uncoated nanoparticles. The saturation magnetization (M_s) of SiO_2 coated maghemite nanoparticles was also lower than the uncoated nanoparticles and is attributed to smaller average crystallite size of SiO_2 coated nanoparticles. For saturation magnetization vs. temperature data, Bloch's law ($M(T) = M(0).(1 - BT^b)$) was fitted well for both uncoated and SiO_2 coated nanoparticles and yields: B $=3\times10^{-7}$ K^{-b}, b=2.22 and B=0.0127 K^{-b}, b=0.57 for uncoated and SiO_2 coated nanoparticles, respectively. Higher value of B for SiO_2 coated nanoparticles depicts decrease in exchange coupling due to enhanced surface spins disorder (broken surface bonds) as compared to uncoated nanoparticles. The Bloch's exponent b was decreased for SiO_2 coated nanoparticles which is due to their smaller average crystallite size or finite size effects. Furthermore, a sharp increase of coercivity at low temperatures ($\lesssim$25 K) was observed for SiO_2 coated nanoparticles which is also due to contribution of increased surface anisotropy or frozen surface spins in these smaller nanoparticles. The FC magnetic relaxation data was fitted to stretched exponential law which revealed slower magnetic relaxation for SiO_2 coated nanoparticles. All these measurements revealed smaller average crystallite size and enhanced surface spins disorder in SiO_2 coated nanoparticles than in uncoated γ-Fe_2O_3 nanoparticles.

1. Introduction

Iron oxide nanoparticles have been extensively studied over the last few decades and continue to maintain interest due to their potential use in wide range of disciplines including magnetic fluids, catalysis, biotechnology, biomedicine, magnetic resonance imaging, magneto optical devices, data storage, and environmental remediation [1,2]. Among the three main oxides of iron namely maghemite (γ-Fe_2O_3), magnetite (Fe_3O_4) and hematite (α-Fe_2O_3), γ-Fe_2O_3 nanoparticles (NPs) have become one of the most promising candidates for many applications due to their non-toxicity, biocompatibility, eco-friendly performance, relatively low cost thermal and chemical stability. Their properties depend upon configuration, annealing temperature, particle size, and doped materials. Bulk γ-Fe_2O_3 is a ferrimagnetic material at room temperature with a Curie temperature (T_c) of 928 K and has spinel structure similar to magnetite but with vacancies in the cation sublattice. Two-thirds of the sites are filled with Fe (III) ions arranged regularly, with two filled sites being followed by one vacant site [3–7]. Haneda and Morrish [8] found that the degree of vacancy ordering decreases with decreasing particle size, with no vacancy ordering in maghemite nanoparticles smaller than about 20 nm. Maghemite nanoparticles also exhibits spin-glass state due to the presence of vacancies, interactions among spins located on tetrahedral and octahedral sites and broken bonds on the nanoparticle's surface [9].

Iron oxide nanoparticles have high surface energy as a result they tend to aggregate so as to minimize the surface energy. Therefore providing proper surface coating and developing some effective protection strategy to keep the stability of magnetic iron oxide nanoparticles is very important for practical applications. It includes coating with surfactants, polymers, and biomolecules, or coating with an inorganic

* Corresponding author.
E-mail address: knadeem@iiu.edu.pk (K. Nadeem).

http://dx.doi.org/10.1016/j.jmmm.2017.01.040
Received 8 July 2016; Received in revised form 21 December 2016; Accepted 11 January 2017
Available online 16 January 2017
0304-8853/

J Supercond Nov Magn (2016) 29:1181–1186
DOI 10.1007/s10948-016-3393-6

Tuning of Dielectric Parameters of $(NiFe_2O_4)_x$/CuTl-1223 Nano-superconductor Composites by Temperature and Frequency

M. Mumtaz[1] · Liaqat Ali[1] · M. Nasir Khan[2] · M. Usman Sajid[2]

Received: 17 October 2015 / Accepted: 6 January 2016 / Published online: 20 January 2016

Abstract Nickel ferrite ($NiFe_2O_4$) nanoparticles and $Cu_{0.5}Tl_{0.5}Ba_2Ca_2Cu_3O_{10-\delta}$ (CuTl-1223) superconductor were prepared separately and then mixed in an appropriate ratios at the final stage to obtain $(NiFe_2O_4)_x$/CuTl-1223 ($x = 0$, 0.5, and 1.0 wt%) nano-superconductor composites. There was no significant change observed in crystal structure of the host CuTl-1223 superconducting matrix after the addition of $NiFe_2O_4$ nanoparticles. The value of zero-resistivity critical temperature ($T_{c(R=0)}$ (K)) was decreased with increasing content of these nanoparticles in these composites. Maximum values of dielectric loss tangent ($\tan\delta$) at lowest possible frequency of 40 Hz were increased with the increase of operating temperature, while its values were decreased and become almost zero at higher frequencies for all these samples at all operating temperatures. A peak in dielectric loss tangent was shifted towards lower frequency values with the addition of these nanoparticles in CuTl-1223 superconducting matrix. The dielectric loss tangent peak was also shifted towards lower frequency values in all these samples with increasing operating temperature, which shows the relaxator-like behavior in these samples. The dielectric parameters of these composites can be tuned by frequency, operating temperatures, and nature and content of these nanoparticles.

Keywords $(NiFe_2O_4)_x$/CuTl-1223 nano-superconductor composites · Structural properties · Superconducting properties · Dielectric properties

1 Introduction

It is well known that there are four primary mechanisms of polarization in materials:

i Electronic polarization (α_e), which can be observed at very high frequencies of the order of 10^{15} Hz (i.e., in ultraviolet optical range),
ii Atomic and ionic polarization (α_a), which takes place at the frequencies in the range of 10^{10} to 10^{13} Hz (i.e., in the infrared optical range),
iii Dipolar or oriental polarization (α_o), which occurs in the range of frequencies from 10^3 to 10^9 Hz (i.e., in the sub-infrared optical range), and
iv Interfacial polarization (α_i), which is more sensitive in the low-frequency range of 10^3 Hz and may extend to a few kilohertz range [1–6].

The short-range motion of carriers in the above mentioned mechanisms contribute to the total polarization. The interfacial and dipolar or oriental polarizations mostly contribute to the dielectric parameters of these composites. Dielectric parameters become saturated at high frequencies at all operating temperatures [1]. The mobile charge carriers are accumulated at the barrier creating localized polarization [6]. The exploration of dielectric parameters over the broad spectrum of temperature and frequency is very significant [7]. Dielectric parameters can be adjusted by varying the nanoparticle contents in $(NiFe_2O_4)_x$/CuTl-1223 composites that manage the carrier density in these materials [8–12].

✉ M. Mumtaz
mmumtaz75@yahoo.com

1 Materials Research Laboratory, Department of Physics FBAS, International Islamic University (IIU), Islamabad 44000, Pakistan

2 Central Diagnostic Laboratory, Physics Division PINSTECH, P.O. Nilore, Islamabad 45500, Pakistan

J Supercond Nov Magn
DOI 10.1007/s10948-016-3724-7

Flux Pinning with Addition of Gold Nanoparticles in CuTl-1223 Superconductor

Liaqat Ali[1] · M. Mumtaz[1] · M. W. Rabbani[1]

Received: 6 July 2016 / Accepted: 13 August 2016

Abstract We investigated the effects of gold (Au) nanoparticles on flux pinning in $Cu_{0.5}Tl_{0.5}Ba_2Ca_2Cu_3O_{10-\delta}$ (CuTl-1223) superconductor by infield temperature-dependent dc-resistivity measurements. The values of T_c^{onset} (K) remained almost unaffected by applying external magnetic field on $(Au)_x$/CuTl-1223; ($x = 0$~1.5 wt.%) composites samples. But a decreasing trend in $T_c(0)$ and increasing trend in resistive broadening (ΔT) by increasing external applied magnetic field were reduced after addition of Au nanoparticles in CuTl-1223 superconducting matrix. The activation energy (U_0) was calculated according to thermally activated flux flow (TAFF) model by using the Arrhenius Law. The increase in $T_c(0)$, U_o, and upper critical field (H_{c2}) indicates a strong flux pinning after the inclusion of Au nanoparticles and found optimum for $x = 1.0$ wt.%.

Keywords $(Au)_x$/CuTl-1223 composites · Activation energy · Flux pinning · Critical field

1 Introduction

One of the most vexing hindrances has been the obliteration of superconducting state under the influence of external applied magnetic field, which is very crucial for many envision applications of superconducters [1]. Weak flux pinning in bulk high-temperature superconductors (HTSCs) with external applied magnetic field is the major cause of decline in critical superconducting parameters like critical temperature (T_c), critical field (H_c), and critical current density (J_c) [2–4].

The main source to understand the vortex hopping and its interaction with structural defects in type II superconductors is the study of vortex dynamics. The observations show that when the magnitude of the external applied magnetic field increases from certain critical values, the Meissener effect starts to decrease and magnetic field lines start to penetrate inside the superconducting material in the form of Abrikosov vortices. The agency for vortex movement is the Lorentz force $f_L = 1/c(j \times \Phi_o)$, which causes the energy dissipation and thermal fluctuations in superconducting material [5, 6]. Thermal fluctuations boost up due to large anisotropy and presence of crystal imperfections. The discernible regimes of energy dissipation are flux creep and flux flow. When the pinning forces are dominated, then flux creep is activated ($U_o >> k_BT$) and when Lorentz forces are dominated ($U_o \sim k_BT$) then flux flow occurs [6–8]. The required activation energy for flux motion can be estimated from dc-resistivity measurements [9, 10]. The important superconducting properties like T_c, J_c, U_o, vortex flow, quantized flux, etc., can be investigated through informative vortex dynamics.

Different experimental techniques have been used to avoid the vortex motion and to improve the infield superconducting properties of HTSCs but only few groups have attempted to improve the flux pinning and inter-grains coupling by the inclusion of different nanostructures in bulk HTSCs [1–14]. In the present work, we have tried to explore the vortex dynamics by analyzing the resistive

✉ M. Mumtaz
mmumtaz75@yahoo.com

[1] Materials Research Laboratory, Department of Physics FBAS, International Islamic University (IIU), Islamabad 44000, Pakistan

Published online: 05 September 2016

Journal of Advanced Ceramics
2016, 5(2): 159–166
DOI: 10.1007/s40145-016-0183-1

ISSN 2226-4108
CN 10-1154/TQ

Dielectric properties of $(Zn)_x$/CuTl-1223 nanoparticle–superconductor composites

M. MUMTAZ[a,*], Liaqat ALI[a], Shoaib AZEEM[a], Saad ULLAH[a], G. HUSSAIN[a], M. W. RABBANI[a], Abdul JABBAR[b], K. NADEEM[a]

[a]*Materials Research Laboratory, Department of Physics, FBAS, International Islamic University (IIU), Islamabad 44000, Pakistan*
[b]*Department of Physics, Ghazi University, Dera Ghazi Khan 32200, Pakistan*

Received: January 25, 2016; Revised: March 11, 2016; Accepted: March 16, 2016

Abstract: Zinc (Zn) nanoparticles and $(Cu_{0.5}Tl_{0.5})Ba_2Ca_2Cu_3O_{10-\delta}$ (CuTl-1223) superconducting phase were prepared separately by sol–gel and solid-state reaction methods, respectively. Zn nanoparticles were added in CuTl-1223 superconducting matrix with different weight percentage during the final sintering process to obtain $(Zn)_x$/CuTl-1223 (x=0–4 wt%) nanoparticle–superconductor composites. The effect of Zn nanoparticles on structural, morphological, superconducting, and dielectric properties of CuTl-1223 phase was investigated. The addition of these Zn nanoparticles has not affected the crystal structure of host CuTl-1223 superconducting phase. Superconducting properties were enhanced after the addition of Zn nanoparticles up to certain optimum content (i.e., x = 1 wt%), which were due to improved inter-grain connectivity by healing up of micro-cracks and reduction of defects like oxygen deficiencies, etc. The activation energy (U) was increased after the addition of Zn nanoparticles in CuTl-1223 phase. The dielectric properties of these samples (i.e., dielectric constant, dielectric loss) were determined by experimentally measured capacitance (C) and conductance (G) as a function of frequency at room temperature. The addition of metallic Zn nanoparticles in CuTl-1223 matrix has overall suppressed the dielectric parameters of $(Zn)_x$/CuTl-1223 nanoparticle–superconductor composites. The metallic Zn nanoparticles played a significant role in inter-grain couplings by filling the voids and pores.

Keywords: $(Zn)_x$/CuTl-1223 nanoparticle–superconductor composites; dielectric properties; activation energy

1 Introduction

One of the most eminent phase of $(Cu_{1-x}Tl_x)Ba_2Ca_{n-1}Cu_nO_{2n+4-\delta}$ (n = 2, 3, 4, ···) high temperature superconducting family is $(Cu_{0.5}Tl_{0.5})Ba_2Ca_2Cu_3O_{10-\delta}$ (CuTl-1223) [1]. CuTl-1223 superconducting phase has long coherence length along c-axis (ξ_{gc}) [2], low superconducting anisotropy ($\gamma = \xi_{gab}/\xi_{gc}$) [3], small penetration depth (λ), high zero resistivity critical temperature ($T_c(0)$), high irreversibility field (H_{irr}), and high critical current density (J_c) [4,5]. The performance of bulk high temperature superconductors can be severely affected by inter-grain voids, micro-cracks, and pores [6–8]. Different strategies have been exercised to minimize the voids and pores in

* Corresponding author.
E-mail: mmumtaz75@yahoo.com

Journal of Non-Crystalline Solids 404 (2014) 72–77

Contents lists available at ScienceDirect

Journal of Non-Crystalline Solids

journal homepage: www.elsevier.com/locate/jnoncrysol

Effect of silica coating on the structural, dielectric, and magnetic properties of maghemite nanoparticles

K. Nadeem [a,b,*], L. Ali [a], I. Gul [c], S. Rizwan [d], M. Mumtaz [a]

[a] Materials Research Laboratory, Department of Physics, International Islamic University, H-10, Islamabad, Pakistan
[b] Beijing National Laboratory for Condensed Matter Physics, Institute of Physics, Chinese Academy of Sciences, P.O. Box 603, Beijing 100190, China
[c] Thermal Transport Laboratory, School of Chemical and Materials Engineering (SCME), National University of Sciences and Technology (NUST), H-12 Campus, Islamabad, Pakistan
[d] Department of Electronics and Key Laboratory for the Physics and Chemistry of Nanodevices, Peking University, Beijing 100871, China

ARTICLE INFO

Article history:
Received 20 May 2014
Received in revised form 17 July 2014
Accepted 27 July 2014
Available online xxxx

Keywords:
Nanoparticles;
Dielectrics; magnetic properties;
Maghemite

ABSTRACT

Influence of silica (SiO_2) coating concentration (x) = 0, 15, 30, 45, and 60% on structural, dielectric, and magnetic properties of maghemite nanoparticles has been studied. X-ray diffraction analysis confirmed the cubic inverse spinel structure for the samples with $x = 0$, 15 and 30%, while $x = 45$ and 60% samples show amorphous behavior. Both average crystallite size and lattice constant were decreased with SiO_2 concentration. Scanning electron microscopy images showed that the nanoparticles are spherical in shape and self-organized in leaf-like shape. Fourier transform infrared spectroscopy analysis confirmed the formation of maghemite and SiO_2 phases for all the samples. At higher SiO_2 concentration, vibrational bands of maghemite were suppressed and some bands overlapped with the SiO_2 bands. Dielectric parameters such as dielectric constant and loss tangent were decreased with increasing frequency and became constant at higher frequencies. However, ac conductivity showed an opposite trend with higher values at higher frequencies. Dielectric properties have been explained using Koop's and Maxwell–Wagner models. Nanoparticles with $x = 30\%$ SiO_2 concentration showed the highest dielectric constant with reduced magnetization. Dielectric properties also showed non-monotonic dependency on the SiO_2 concentration. Bare nanoparticles got high saturation magnetization close to bulk value due to larger average crystallite size while, nanoparticles with higher SiO_2 concentration exhibited smaller magnetization and higher coercivity which is attributed to their smaller average crystallite size. In summary, SiO_2 concentration has significant effects on the structural, dielectric, and magnetic properties of maghemite nanoparticles and can be used to get suitable ferrite/SiO_2 nanocomposites for different applications.

1. Introduction

Iron-oxide spinel ferrite nanoparticles and their composites are interesting materials due to their potential application [1]. Structural and physical properties of the nanoparticles can be controlled by different parameters such as synthesis methods, chemical composition, surface coating and reaction temperature [2–4]. Iron-oxide nanoparticles are ferrites with different phases depending upon the annealing temperature [5]. Oxygen or hydroxide ions play an important role for the formation of structure in iron-oxide nanoparticles. Different phases of iron-oxide nanoparticles have different physical properties [6,7]. Maghemite (γ-Fe_2O_3) nanoparticles are ferrimagnetic in nature and can be used for remote sensing, in catalysis, for storage devices, as MRI contrast agent and targeted drug delivery [8–10]. Maghemite has spinel ferrite structure with two possible lattice sites such as tetrahedral and octahedral [11,12]. Maghemite and magnetite have the same structure with deficit of Fe^{+2} ions in maghemite with formula $(Fe_8^{+3})_A[Fe_{40/3}^{+3}\Delta_{8/3}]_BO_{32}$, where A and B represent tetrahedral and octahedral lattice sites, respectively, and Δ represents vacancies at the octahedral lattice sites [12]. Maghemite nanoparticles are very sensitive to the annealing temperature and can change their phase within small temperature range e.g., maghemite to hematite phase transition usually occurs between 400 °C and 500 °C due to change of oxidation state of the system [13].

At nanoscale, ferrite properties depend upon synthesis techniques, chemical composition, annealing time, annealing temperature, particle size, and doped material. Also the interparticle interactions between the magnetic nanoparticles can modify their individual magnetic behavior. Bare magnetic nanoparticles usually show agglomeration and must be coated with non-magnetic material to avoid interparticle interactions [14,15]. Different techniques have been used for coating nanoparticles to increase their stability and functionality [16,17]. Non-magnetic SiO_2 is an important compound used for coating purposes to prevent agglomeration, improve chemical stability of the nanoparticles and biologically friendly for targeted drug delivery [18]. The SiO_2 coating also plays an important role to get chemically functionalized surface of magnetic iron-oxide nanoparticles. However, SiO_2 can

* Corresponding author. Tel.: +92 51 9019714.
E-mail address: kashif.nadeem@iiu.edu.pk (K. Nadeem).

http://dx.doi.org/10.1016/j.jnoncrysol.2014.07.036
0022-3093/

Turnitin Originality Report

Thesis by Liaqat Ali

From FinalThesis (Repository)

- Processed on 23-Sep-2019 17:05 PKT
- ID: 1178231518
- Word Count: 19867

Similarity Index
13%
Similarity by Source

Internet Sources:
2%
Publications:
10%
Student Papers:
6%

23/9/19.
Prof. SYED SALMAN HUSSAIN
Assistant Professor
Department of Physics
International Islamic University
Islamabad

sources:

1 1% match (publications)
M. Mumtaz, M. Naveed, L. Ali, Abrar A. Khan, M. Imran, M. Waqas-Ur-Rahaman, M. Nasir Khan. "Magneto-Transport Properties of (Cu)x/CuTl-1223 Nanoparticles-Superconductor Composites", Cryogenics, 2018

2 1% match (publications)
Liaqat Ali, M. Mumtaz, Irfan Ali, M. Waqas-ur-Rehman, Abdul Jabbar. "Metallic Cu Nanoparticles Added to Cu0.5Tl0.5Ba2Ca2Cu3O10−δ Superconductor", Journal of Superconductivity and Novel Magnetism, 2017

3 1% match (student papers from 07-Apr-2016)
Class: Repository
Assignment: FinalThesis
Paper ID: 655764177

4 1% match (publications)
Liaqat Ali, M. Mumtaz, M. W. Rabbani. "Flux Pinning with Addition of Gold Nanoparticles in CuTl-1223 Superconductor", Journal of Superconductivity and Novel Magnetism, 2016

5 1% match (publications)
M.W. Rabbani, Liaqat Ali, M. Mumtaz, Iftikhar Hussain Gul. "Infield superconducting properties of nano-sized Ag added Cu 0.5 Tl 0.5 Ba 2 Ca 2 Cu 3 O 10−δ", Progress in Natural Science: Materials International, 2017

6 < 1% match (publications)
Wesche, Rainer. "Superconducting Properties of Cuprate High-Tc Superconductors", Physical Properties of High-Temperature Superconductors, 2015.

7 < 1% match (publications)
M. Mumtaz, Waqas Ahmad Khan, Liaqat Ali, M. Waqas-Ur-Rehman, K. Nadeem. "Infield Superconductivity in Au Nanoparticles Added Cu0.5Tl0.5Ba2Ca2Cu3O10-δ Phase", Physica C: Superconductivity and its Applications, 2019

8 < 1% match (publications)
Abdul Mouzzikhir. "High-Temperature Superconductivity in Cuprates", Springer Nature, 2002

9 < 1% match (publications)
Abdul Jabbar, Irfan Qasim, Shahid A. Khan, K. Nadeem, M. Waqas-ur-Rehman, M. Mumtaz, F. Zeb. "Highly coercive cobalt ferrite nanoparticles-CuTl-1223 superconductor composites", Journal of Magnetism and Magnetic Materials, 2015

10 < 1% match (publications)
Springer Series in Materials Science, 2016

11 < 1% match (publications)